



MASARYK UNIVERSITY

FACULTY OF SCIENCE

DEPARTMENT OF CHEMISTRY



Capillary Electrophoresis:

A well-established method with a modern twist

Markéta Vaculovičová

Habilitation Thesis

Brno 2017

Motto: “There are only two options, either it will work or it won’t “

Acknowledgments:

At this place, I would like to thank to my husband Tom for his support and help.

I would like to thank also to Prof. Vojtech Adam for or the chance he gave me and for his kind attitude during all these years.

Luckily, I got the chance to work with many brilliant coworkers, colleagues and students. Above all I would like to name Prof. Jan Preisler and Prof. Mirek Macka. I have learnt a lot from all of them.

I am grateful to all members of my group, my former and current students and my closest associates for their contribution to the papers discussed in this work. Namely, I would like to thank Luky Nejd, Týnka Šmerková, Dave Hynek, and Simča Dostálová.

Last but not least, I am thankful to my family and friends.

Markéta Vaculovičová

Brno, November 2017

Abstract:

This habilitation thesis is a commented collection of 11 selected peer-reviewed scientific papers that deals with combination of nanomaterials with powerful and well-established analytical method – capillary electrophoresis (CE). Such combination is beneficial for both of these sides since CE is able to characterize properties of nanomaterials in terms of size, charge or interaction with other compounds and on the other hand, nanomaterials are applicable for improvement of CE performance both separation resolution as well as detection sensitivity.

Abstrakt:

Tato habilitační práce je komentovaným souborem 11 vybraných recenzovaných publikací zaměřených na kombinaci výhod nanomateriálů se schopnostmi vysoce účinné analytické metody – kapilární elektroforézy (CE). Toto spojení oboustranně výhodné, protože CE umožňuje charakterizovat nanomateriály z pohledu velikosti, náboje nebo interakcí s jinými molekulami a na druhou stranu, nanomateriály lze využít pro zlepšení vlastností CE jak z pohledu zlepšení separačního rozlišení tak zvýšení detekční citlivosti.

Key words: nanotechnologies, nanomaterials, nanoparticles, separation techniques

Table of Contents:

| | | |
|----------|---|-----------|
| 1 | INTRODUCTION | 6 |
| 1.1 | STRUCTURE OF THE THESIS | 7 |
| 1.2 | PERSONAL COMMENTARY | 7 |
| 1.3 | AUTHOR'S CONTRIBUTION | 8 |
| 2 | NANOTECHNOLOGIES, NANOMATERIALS AND NANOMEDICINE | 12 |
| 2.1 | NANOTECHNOLOGIES | 12 |
| 2.2 | NANOMATERIALS | 12 |
| 2.2.1 | <i>Metal Nanoparticles</i> | 13 |
| 2.2.2 | <i>Semiconductor Nanocrystals</i> | 14 |
| 2.2.3 | <i>Carbon nanomaterials</i> | 15 |
| 2.3 | NANOMEDICINE | 16 |
| 3 | CAPILLARY ELECTROPHORESIS IN NANOMEDICINE | 19 |
| 3.1 | CARGO ENCAPSULATION | 19 |
| 3.2 | CONJUGATION TO TARGETING LIGANDS | 20 |
| 4 | MONITORING OF THE INTERACTION BETWEEN NANOPARTICLES AND BIOMOLECULES | 21 |
| 4.1 | AFFINITY INTERACTION | 21 |
| 4.2 | NON-SPECIFIC INTERACTION | 21 |
| 5 | CE FOR NANOMATERIALS AND NANOMATERIALS FOR CE | 22 |
| 5.1 | SAMPLE PRETREATMENT BY NANOMATERIALS | 22 |
| 5.2 | CHARACTERIZATION OF NANOPARTICLES BY CE | 23 |
| 5.3 | SEPARATION IMPROVEMENT | 24 |
| 5.4 | ENHANCEMENT OF DETECTION SENSITIVITY | 25 |
| 6 | IN-CAPILLARY QUANTUM DOT SYNTHESIS | 27 |
| 6.1 | ORGANOMETALLIC SYNTHESIS OF QUANTUM DOTS | 27 |
| 6.2 | AQUEOUS SYNTHESIS OF QUANTUM DOTS | 27 |
| 6.3 | THE OTHER WAYS OF SYNTHESIS | 28 |
| 6.4 | UV IRRADIATION IN-CAPILLARY SYNTHESIS OF QUANTUM DOTS | 28 |
| 7 | CONCLUSION | 29 |
| 8 | REFERENCES: | 30 |
| 9 | ARTICLES | 35 |

1 Introduction

Nanotechnology is a quickly developing area of science. Due to an outstanding lecture given by Richard P. Feynman in 1959, giving the vision that science and technology can be based on nanoscale, this year can be marked as turning-point in scientific history. However, already Michael Faraday in 1857, observed characteristic behavior of gold nanoparticles in aqueous solution. Yet, the oldest known application of nanomaterials would probably be the creation of Lycurgus Cup (5th - 4th century B.C.). Such cup was made from so-called “gold-ruby glass” contained gold nanoparticles (5-60 nm) causing the color change based on the way of illumination. The glass appeared green in reflected light and red when light was transmitted from inside.

The thigh connections between nanotechnology and physical chemistry can be found through such great names as Albert Einstein with his Brownian motion theory and/or Nobel prized Jean-Baptiste Perrin.

Nowadays, nanoparticles can be found everywhere from computers through house facades coatings to clothing and cosmetics. They have their place in medicine as well as in agriculture. Their benefits are indisputable including the advantages provided for improvement of conventional, well-established methods and techniques. In the future, however, the excessive use of nanomaterials may become problematic. Therefore, powerful procedures have to be implemented, not only for the detailed characterization of the properties of the produced nanoparticles but also for their sensitive detection in the environment.

There is always more than one point of view. Therefore, this thesis is trying to look at the symbiosis of nanomaterials and capillary electrophoresis from two perspectives – analysis and characterization of nanomaterials and their exploitation for improved performance of a well-known method.

1.1 Structure of the thesis

The thesis is presented as a collection of selected peer-reviewed scientific papers published between years 2011 and 2017. Since all discussed publications are attached, in following text I am discussing only main achievements and general conclusions. The included articles are referred to as “**article X**”

1.2 Personal commentary

During my PhD studies I was introduced to the field of electromigration techniques, especially capillary electrophoresis. I realized that this family of methods is extremely powerful when used properly (as every method). Its flexibility allows for its application for analysis of analytes ranging from ions and small molecules through smaller or bigger biomolecules including large proteins and nucleic acids to cellular compartments, viruses, whole cells (both prokaryotic and eukaryotic), and even nano- and microparticles.

However, I have realized that even though the method is so powerful, there are still some instrumental improvements, which can be done to enable even broader flexibility and applicability. These improvements include combination of detection modalities as well as development of alternative light sources for fluorescence detection. Some of these shortcomings were addressed in publications included in my PhD thesis [1-4] and even though my current work is based on these publications and I still draw information and knowledge from what I have learnt during the my PhD studies, I have realized that present trend of nanotechnologies, nanomaterials, and nanomedicine together with abilities of capillary electrophoresis may create an efficient combination benefiting both sides.

First, capillary electrophoresis may provide excellent way of nanoparticle characterization, synthesis quality control, and batch-to-batch preparation check-up including polydispersity monitoring and interaction determination. Second, nanomaterials not only due to their large surface area, but also due to the optical and electronic properties may benefit to capillary electrophoresis by improving/enhancing the separation resolution as well as detection sensitivity either as stationary/pseudo-stationary phases or labels enabling fluorescent, chemiluminescent or electrochemical detection. Finally, the in-

capillary environment is even suitable for low-volume nanoparticle preparation with on-line characterization for green-chemistry applications.

My postdoctoral work at both Dublin City University as well as at Mendel University in Brno was focused on development and application of capillary electrophoretic method. Through this work, I was able to build a scientific group (Laboratory of Bioanalysis and Imaging) at the Department of Chemistry and Biochemistry of Mendel University in Brno currently accommodating 2 postdoctoral researchers, 2 PhD students, 1 Master and 7 Bachelor students.

1.3 Author's contribution

Currently, under my ORCID (0000-0002-6771-1304) combining my maiden name (Ryvolova) and married name (Vaculovicova), one can find 98 hits at Web of Science database including 60 journal articles, 14 reviews, 21 conference proceedings and 1 editorial material. From these I have chosen 7 experimental articles and 4 reviews that I believe present pieces in the puzzle aiming at mapping the benefits of utilization of capillary electrophoresis for investigation in the field of nanotechnologies or nanomedicine.

The following summary is giving an overview of my contribution to the selected works with special attention to amount of performed experiments, supervision of students, definition of research direction, and my contribution to manuscript preparation.

1) Stanisavljevic M, Krizkova S, **Vaculovicova M**, Kizek R, Adam V. Quantum dots-fluorescence resonance energy transfer-based nano-sensors and their application. Biosens Bioelectron 2015;74:562-574.

Experimental work/Literature analysis 30%

Manuscript preparation 30%

Supervision 100%

Research direction 90%

2) Dostalova S, Cerna T, Hynek D, Koudelkova Z, Vaculovic T, Kopel P, Hrabeta J, Heger Z, **Vaculovicova M**, Eckschlager T, Stiborova M, Adam V. Site-directed conjugation of antibodies to apoferritin nanocarrier for targeted drug delivery to prostate cancer cells. ACS Appl Mater Interfaces 2016;8(23):14430-14441.

Experimental work/Literature analysis 30%

Manuscript preparation 30%

Supervision 50%

Research direction 70%

3) Dostalova S, Vasickova K, Hynek D, Krizkova S, Richtera L, **Vaculovicova M**, Eckschlager T, Stiborova M, Heger Z, Adam V. Apoferritin as an ubiquitous nanocarrier with excellent shelf life. Int J Nanomed 2017;12:2265-2278.

Experimental work/Literature analysis 30%

Manuscript preparation 30%

Supervision 30%

Research direction 30%

4) Konecna R, Nguyen HV, Stanisavljevic M, Blazkova I, Krizkova S, **Vaculovicova M**, Stiborova M, Eckschlager T, Zitka O, Adam V, Kizek R. Doxorubicin Encapsulation Investigated by Capillary Electrophoresis with Laser-Induced Fluorescence Detection. Chromatographia 2014 Nov;77(21-22):1469-1476.

Experimental work/Literature analysis 50%

Manuscript preparation 80%

Supervision 80%

Research direction 70%

5) Janu L, Stanisavljevic M, Krizkova S, Sobrova P, **Vaculovicova M**, Kizek R, Adam V. Electrophoretic study of peptide-mediated quantum dot-human immunoglobulin bioconjugation. Electrophoresis 2013;34(18):2725-2732.

Experimental work/Literature analysis 30%

Manuscript preparation 90%

Supervision 50%

Research direction 60%

6) **Ryvolova M**, Chomoucka J, Janu L, Drbohlavova J, Adam V, Hubalek J, Kizek R. Biotin-modified glutathione as a functionalized coating for bioconjugation of CdTe-based quantum dots. *Electrophoresis* 2011 Jun;32(13):1619-1622.

Experimental work/Literature analysis 60%

Manuscript preparation 80%

Supervision 50%

Research direction 50%

7) Stanislavljevic M, Chomoucka J, Dostalova S, Krizkova S, **Vaculovicova M**, Adam V, Kizek R. Interactions between CdTe quantum dots and DNA revealed by capillary electrophoresis with laser-induced fluorescence detection. *Electrophoresis* 2014;35(18):2587-2592.

Experimental work/Literature analysis 60%

Manuscript preparation 40%

Supervision 80%

Research direction 90%

8) Adam V, **Vaculovicova M**. Nanomaterials for sample pretreatment prior to capillary electrophoretic analysis. *Analyst* 2017;142(6):849-857.

Experimental work/Literature analysis 100%

Manuscript preparation 90%

Supervision 80%

Research direction 90%

9) Adam V, **Vaculovicova M**. Capillary electrophoresis and nanomaterials - Part I: Capillary electrophoresis of nanomaterials. *Electrophoresis* 2017 Oct;38(19):2389-2404.

Experimental work/Literature analysis 100%

Manuscript preparation 90%

Supervision 80%

Research direction 90%

10) Adam V, **Vaculovicova M**. CE and nanomaterials – Part II: Nanomaterials in CE. *Electrophoresis* 2017 Oct;38(19):2405-2430.

Experimental work/Literature analysis 100%

Manuscript preparation 90%

Supervision 80%

Research direction 90%

11) Nejd l, Zitka J, Mravec F, Milosavljevic V, Zitka O, Kopel P, Adam V, Vaculovicova M. Real-time monitoring of the UV-induced formation of quantum dots on a milliliter, microliter, and nanoliter scale. *Microchim Acta* 2017;184(5):1489-1497.

Experimental work/Literature analysis 10%

Manuscript preparation 80%

Supervision 80%

Research direction 50%

List of abbreviations:

ACE – affinity capillary electrophoresis

CE – capillary electrophoresis

EDC – N-(3-dimethylaminopropyl)-N-ethylcarbodiimide hydrochloride

Fab – antigen-binding region of antibody

Fc – region of antibody ensuring the communication with the other components of the immune system

FRET – Förster resonance energy transfer

QDs – quantum dots

2 Nanotechnologies, nanomaterials and nanomedicine

2.1 Nanotechnologies

The term “Nanotechnology” was used in 1974 by Taniguchi and since that time it is used for the scientific field where sizes from 0.1 to 100 nm play a crucial role. In the nano range, gravity presents less an issue, however the strength of materials is more important and also quantum size effect matters. The unique optical, electronic, thermal features and chemical properties of nanomaterials as well as the ability to be chemically modified are coming from their small dimensions and high ratios of surface to volume. Therefore, nanomaterials found their applications in numerous scientific areas including physics and engineering, however lately also in natural sciences including chemistry, biology and medicine. Although nanomaterials are affecting various scientific fields, they are approached differently. From the chemistry point of view, this field has historically been related with colloids, micelles and/or polymers - typically, very large molecules, or molecular aggregates. More recently, structures such as fullerenes, nanofibers, and semiconductor quantum dots have been included in the group of particularly interesting classes of nanostructures. In physics and electrical engineering, nanoscience is usually related to quantum behavior and electrons and photons. Biology and biochemistry are also interested in nanostructures as cell compartments; number of interesting biological structures such as DNA, subcellular organelles and/or viruses can be labeled as nanostructures [5-7].

2.2 Nanomaterials

“Nanomaterials” is a general name covering a large collection of compounds. Commonly accepted definition is that a nanomaterial is “any material that has an average particle size of between 1 and 100 nanometers.” Meanwhile, the definition given by The European Commission states that nanomaterial as “a natural, incidental or manufactured material containing particles, in an unbound state or as an aggregate or as an agglomerate and where, for 50% or more of the particles in the number size distribution, one or more external dimensions is in the size range 1 nm–100 nm.”[8]

Firm following of such definitions permits the use of the term nanomaterials also to a wide range of biomolecules such as proteins or nucleic acids. For instance, the albumin molecule is approximately 7 nm in size [9] and such protein fits the definition of nanomaterial. However, it is not typically comprised into this group.

Simultaneously, some materials bigger than 100 nm, might also be included into the nanomaterial group due to their properties significantly different from properties of bulk materials. For all these reasons, the definition given in the work by Buzea et al. may be more appropriate [10]. The authors state that majority of the important properties of nano begin to be apparent already in structures smaller than 1 μm (however some exceptions do exist).

In general, nanomaterials cover materials of different natures and enormously varied properties. Based on their specific properties, the materials as metallic and metal oxide nanoparticles, semiconductor nanocrystals (quantum dots [11]), carbon nanomaterials (nanodiamonds, fullerenes, graphene, carbon nanotubes) [12, 13], and polymeric nanomaterials (e.g., chitosan, latex, polystyrene, dendrimers) can be distinguished [14, 15]. Based on shapes, dots, wires, tubes, ribbons, nanosheet, etc. may be identified. Among key properties belong optical/fluorescent (e.g., quantum dots), electronic (e.g., fullerenes), magnetic (e.g., metallic nanomaterials), and biological (e.g., liposomes).

2.2.1 Metal Nanoparticles

Undoubtedly, the biggest and most variable group of nanomaterials is the set of metal nanoparticles. Metal- and metal-oxide nanoparticles are applicable as catalysts, sensors, (opto)electronic materials, and for environmental remediation.

Noble metals such as gold and silver are the most often used for generating nanoparticles. Gold nanoparticles have been known about for 2500 years. The generation of spherical gold nanoparticles is usually done *via* the citrate reduction method reported by Turkevitch in 1951 [16]. The size distribution of the gold nanoparticles is controllable by temperature, gold to citrate ratio, and the order in which reagents are added. Among other methods belong the seeding technique [17], the two-phase reaction method [18], and an approach employing inverse micelles [19] and dendrimers [20].

Silver-based nanomaterials are attracting attention due to its characteristic properties, such as chemical stability, catalytic activity, and good conductivity. Silver compounds including nanoparticles are used also due to their antimicrobial properties. Chemical reduction is the most commonly employed procedure for the synthesis of stable, colloidal suspension either in water or organic solvents. Commonly used reductants include borohydride, citrate, ascorbate, and elemental hydrogen [21].

Other noble metals such as platinum [22, 23], palladium [24-26], rhodium [27, 28], and/or osmium [29-31] have also been described.

2.2.2 Semiconductor Nanocrystals

Semiconductor nanoparticles exhibit namely optical properties strongly associated with the size and shape. These properties differ considerably from the bulk semiconductor material. The shapes vary from nanorods, nanowires, and nanotubes to the currently very popular quantum dots (QDs).

QDs have gained enormous popularity in the past two decades [32, 33]. Arising from the quantum confinement of electrons and holes within the nanostructure, the fluorescence of QDs is incomparable with organic fluorophores. In comparison with organic fluorescent dyes and fluorescent proteins, QDs have molar extinction coefficients that are 10–50 folds greater than those of conventional dyes, making them brighter and therefore applicable for *in vivo* conditions. The long lifetime of 10 – 40 ns enhances the option of absorption at lower wavelengths. Further, notable advantage is the high quantum yield from 40% to 90% and the fact they are resistant to the influence of the ambient light (photobleaching) and/or chemical degradation

Besides, QDs emission wavelengths are size-tunable over almost whole range of spectra [34] and the emission wavelength can even reach the near-infrared region (650 nm to 950 nm). Large Stokes shift of QDs (300 – 400 nm) and ability of multiplex detection enable imaging and/or monitoring several molecular targets simultaneously as well as elimination of background autofluorescence, which limits *in vivo* fluorescence imaging modalities. Since their introduction into biological imaging in 1998, enormous interest on the aqueous synthesis [35, 36], characterization [37-40], and bioconjugation of QDs [35, 41, 42] was attracted.

In **article 1** of this thesis, a summary of utilization of quantum dots as sensors in Förster resonance energy transfer (FRET) applications is given.

FRET is a process during which the donor is excited by the external light source and the emitted fluorescence is transferred to the acceptor leading to the emission of the light with higher wavelength (emission of the acceptor). In the review, also systems using the quenching mechanisms are included. In such case the acceptor returns after excitation to its ground state *via* non-radiative decay pathways. In general, FRET is applicable for a number of purposes including investigation of structural changes caused by alterations in the molecular environment (e.g. temperature, pH, etc.) and/or exploration of molecular interactions (i.e. aggregation or digestion).

2.2.3 Carbon nanomaterials

Especially due to its low toxicity for living organisms, nowadays carbon and carbon-based materials are extensively investigated. Graphite attractively lies in the fact that it consists of a flat single layer of carbon atoms organized into a two-dimensional (2D) honeycomb structure - graphene. It can be wrapped up into 0D fullerenes, rolled into 1D nanotubes, or stacked into 3D graphite. [43]

Fullerenes are arranged as a closed network of fused hexagons and pentagons. The smallest stable and therefore most abundant fullerene is the buckminsterfullerene C₆₀. [44] Fullerenes display antiviral and antioxidant properties and because of the hollow cavity inside the molecule, they serve as gene and drug carriers [45]. The lipophilic properties are helpful for interactions with many enzymes or enable the intercalation into biological membranes. Therefore, antibacterial activity of several derivatives may be observed [46].

Carbon nanotubes are well-ordered, hollow fiber-like nanomaterials consisting of tubes of sp²-hybridized carbon atoms [47]. The distortion of graphene into a cylinder noticeably complicates the orbital overlapping, thus leading to carbon atoms wound around in a helical mode. Moreover, a number of morphologies can occur among carbon nanotubes. These are known as “hollow tube,” “bamboo” and “herringbone” [48].

2.3 Nanomedicine

During the past years, substantial efforts have been driven towards the development of effective therapeutic substances. However, current anti-tumor therapy possesses limited safety and efficacy. Common conventional anticancer drugs display a narrow therapeutic window because of the random distribution in the body. Non-specific distribution causes cytotoxicity to healthy cells causing severe side effects to the patients. The non-specific toxicity of anti-tumor drugs also restricts the applicable dose and thus lowers the therapeutic value.

Nanoparticle-based drug carriers are colloidal systems acting as drug vehicles in the form of nanospheres or nanocapsules [49]. Nanoparticle carriers belong most often to the group of iron oxides, gold, biodegradable polymers, dendrimers, liposomes, viral capsids [50-52] and/or proteins [53]. The formulation of the drug encapsulated in the nanocarrier provides increased biocompatibility, which increases the applicability in clinical practice. These types of drugs already used in the clinical practice include liposomal doxorubicin and albumin-conjugate of paclitaxel [54].

Among the key properties of perfect nanocarrier is its size. The largest nanocarriers are liposomes with their diameter of 80-200 nm [55], polymer-based particles (40-100 nm) [56] or micelles (20-60 nm) [57] and the smallest ones are dendrimers (smaller than 10 nm) [58]. The size of nanocarrier should be uniform and enable the surface modification with targeting molecules [59]. The use of suitable nanocarriers can significantly decrease the undesired side effects, improve biocompatibility, specificity, stability and water solubility [60].

The size of the nanocarrier should be low enough to be able to enter the cells, but high enough to avoid early removal from the body by renal clearance [61]. Furthermore, the production should be simple and easy, capacity of encapsulation should be high and drug release mechanism should be reliable to prevent undesired drug release but guarantee the delivery into the target cells [62].

Even though, nanocarriers based on inorganic compounds/particles are easier for preparation, they often cause an immune response of the organism or are even toxic to

healthy cells. On the other hand, biomolecule-based nanocarriers can be found in human body and therefore are more suitable [63]. Among such carriers belongs protein called ferritin, which ensures the storage and transfer of iron ions [64]. After iron removal, hollow cavity - apoferritin - is created [65]. Such cavity is ideal for drug transport mainly due to the fact that the protein disassembles its structure in low pH environment. Such environment can be found inside the cancer cells. Therefore, the effect of the carried drug on the healthy cells is not as dramatic as on the diseased ones. Moreover, the encapsulation of drugs in apoferritin does not require any modification of either drug or carrier molecules because it employs an apoferritin behavior in surrounding environment [66]. The cell entry is done *via* specific receptors, found on most body cells. However, this natural ability of cell targeting and ferritin incorporation can be more enhanced by targeting moieties (e.g. antibodies [67]).

In **article 2** of this thesis, targeted drug delivery system consisting of protein nanocarrier (apoferritin), gold nanoparticles and antibodies was developed and characterized it according to its long-term stability (**article 3**). The scheme of the developed targeted nanocarrier is shown in Figure 1.

The apoferritin from horse spleen was used as a carrier of doxorubicin, which is an effective anti-tumor drug with severe cardiotoxicity limiting its therapeutic dose. Therefore, the protection of healthy tissues is highly required. The drug was encapsulated into the protein cage, which was surface-modified by gold nanoparticles providing the affinity to thiol groups of cysteine in the sequence of a heptapeptide (HWRGWVC). This peptide was derived from the protein G, which exhibits a high affinity to the Fc fragment of antibodies, which leads to the site-directed orientation of the antibody on the surface of the apoferritin surface.

The conjugation of prostate specific membrane antigen antibodies and apoferritin was used to target the prostate cancer cells (LNCaP) and HUVEC cells were used as a non-targeted control. The encapsulation of doxorubicin in apoferritin with subsequent modification by antibodies did not lead to lowering of doxorubicin toxicity for target prostate cancer cells. On the other hand, nonmalignant cells were protected against the

toxic effect of free doxorubicin. Moreover, the presented nanocarrier showed excellent hemocompatibility.

Subsequently, detail study of the long-term stability of the developed nanocarrier under various storage conditions was performed (**article 3**). The nanocarrier was prepared in two solvents (water and phosphate buffer), and stored for 12 weeks at -20 °C, 4 °C, 20 °C, and 37 °C in dark and at 4 °C and 20 °C under ambient light. The parameters such as optical properties; the amount of prematurely released drug molecules; size, shape, ζ -potential, and the ability to internalize into cancer cells and deliver the drug to nuclei were tested. It was found out that the optimal storage conditions were 4 °C in dark and in water. A very good stability for over 12 weeks was observed.

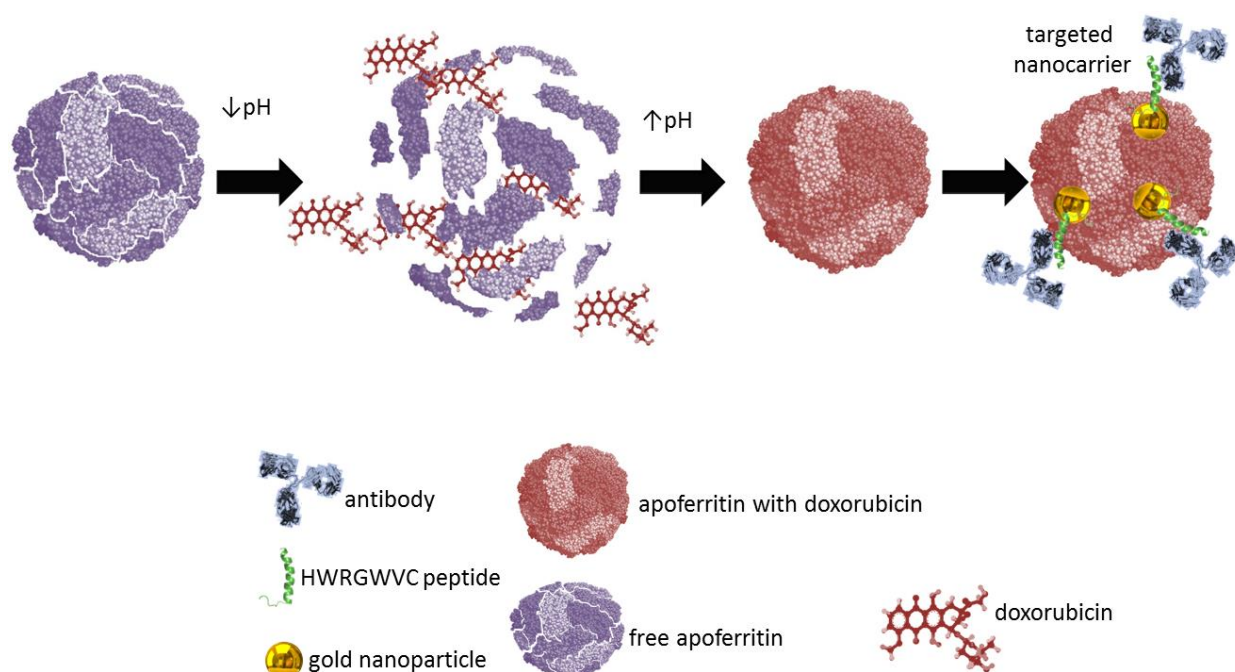


Figure 1: Scheme of the targeted apoferritin-based nanocarrier for doxorubicin transport

3 Capillary electrophoresis in nanomedicine

Since the transfer of electrophoresis into the narrow capillaries by Jorgenson and Lukacs in 1981 [68], the technique has rapidly developed into a versatile analytical tool. Classical capillary electrophoretic (CE) separation takes place in a fused silica capillary with internal diameter of 20-100 μm , where the voltage of up to ± 30 kV is applied. It is separating molecules based on their mobilities in the electric field. Its main advantages include high separation efficiency, short time of analysis and low consumption of chemicals.

Besides monitoring of properties of analytes such as size, charge, and/or surface modification, etc., CE is able to monitor the interactions between molecules. An entire field has appeared known as “affinity capillary electrophoresis” (ACE) [69, 70]. Although many interactions are being investigated and employed, the term ACE appears to be more or less reserved for stronger interactions with specific stoichiometries.

Nanomaterial surfaces can be easily modified and functionalized by many molecules that may enter into interactions with molecules of interest. In this case, CE can work in several ways: 1) monitoring the direct interaction between the nanomaterial and analyte (the signal is provided by both the analyte and nanoparticle), 2) monitoring the interaction between two analytes mediated by the nanomaterial (the signal is provided by the analytes themselves, not by the nanomaterial), and 3) monitoring the interaction between two analytes reported by a change in the signal of the nanoparticle.

3.1 Cargo encapsulation

The aim of the **article 4** of this thesis was to study the encapsulation of doxorubicin into the cavity of apoferritin nanotransporter and to investigate the behavior of doxorubicin in CE using electrolytes with different pH values with purpose of exploration of release of the drug from the apoferritin cage by changing pH. It can be summarized that decreasing the pH of doxorubicin-carrying apoferritin to 3 caused the presence of a single peak with migration time matching to the doxorubicin at the same conditions. Therefore, the release of the drug was confirmed. Further, the properties of doxorubicin using capillary electrophoresis with laser-induced fluorescence detection were investigated. The intrinsic

fluorescence of the drug enabled to monitor the behavior of doxorubicin in the presence of several compounds quenching the fluorescence.

3.2 Conjugation to targeting ligands

To improve the targeted drug delivery, the conjugation of the nanotransporter with a selective targeting ligand is recommended. For such conjugation, antibodies, targeting peptides (e.g. RGD peptide, etc.), or small molecules (e.g. folic acid, etc.), nanocarriers can be used to specifically target the diseased cells [20–23]. The coupling can be done by covalent bond, physical or hydrophobic adsorption. Commonly, cross-linking through an *N*-(3-dimethylaminopropyl)-*N*-ethylcarbodiimide hydrochloride (EDC)/*N*-hydroxysuccinimide reaction is used. In the EDC coupling, there is an unwanted option that the antigen binding sites of antibodies are blocked by the nonselective formation of amide bonds close to a Fab (antigen-binding fragment) area of the antibody. For this reason, alternative ways are searched.

Therefore the **article 5** of this thesis presents capillary electrophoretic investigation of the nanostructure conjugation with antibody with the aim of sterically-specific orientation to ensure the activity of the antigen-binding fragment of the antibody remains unchanged. This approach was employed in the designing of the above mentioned drug nanocarrier (doxorubicin-carrying apoferritin).

In the article, a new strategy of the coupling of CdTe QDs with human immunoglobulin using a specially designed heptapeptide was presented. The heptapeptide with a sequence of HWRGWVC was prepared and characterized by mass spectrometry, liquid chromatography, and capillary electrophoresis. Subsequently, the peptide was used as a stabilizing compound for QDs. The coupling QDs capped *via* this peptide with immunoglobulin was studied by capillary electrophoresis and magnetic immunoextraction coupled with differential pulse voltammetry. Finally, the prepared conjugates were used for fluorescent detection using immobilized goat antihuman immunoglobulin antibody.

4 Monitoring of the interaction between nanoparticles and biomolecules

4.1 Affinity interaction

Besides the affinity interaction between Fc fragment of antibody and HWRGWVC peptide, other affinity-exhibiting pairs are applicable. The (strept)avidin–biotin interaction is considered as the strongest non-covalent interaction with dissociation constant $K_d = 4 \times 10^{-14}$ M. (Strept)avidin-biotin complex is rapidly formed and it is resistant to many extreme conditions (extreme pH values, temperature and even to denaturing agent). Due to strong and reliable affinity (strept)avidin-biotin interaction is often used in diagnostics application. In most of the assays when interaction is applied, streptavidin is coupled to solid phase, such as QDs, magnetic particles, microtitration wellplate and surfaces while biotin is conjugated to the molecule of the interest (e.g. protein, etc.).

However, in the **article 6**, different approach was taken. Biotin-conjugated glutathione was prepared and used as a coating for CdTe QDs. Such coating connected the ability of the biotin to bind avidin, streptavidin and/or neutravidin with the fluorescent properties of the QDs creating specific, high-affinity fluorescent label. The results obtained by the capillary electrophoretic analysis of the prepared probe showed that biotinylated glutathione is suitable coating for the elegant synthesis of thiol capped QDs. Obtained QDs were of good properties for fluorimetric detection and moreover, it was demonstrated that capillary electrophoresis is an efficient method for separation of the glutathione and biotinylated glutathione excess from the quantum dots stabilized with biotinylated glutathione. Moreover, the functionality was verified by interaction with avidin.

4.2 Non-specific interaction

In some cases, not only the covalent labeling or affinity-based conjugation is required, but also non-specific interaction based on structural properties of the analyte and probe may be of an interest. However, it should be highlighted that not only intentional coupling of nanoparticles with biomolecules may occur, but due to the constantly increasing use of nanomaterials, the undesired interactions may happen. Therefore, both of these possibilities (intentional and unintentional interaction) should be taken into an account.

One of the possible targets is the genetic information of the cell. Possible interaction between DNA and nanomaterials is probably ensured by electrostatic binding in major groove of double stranded DNA (dsDNA) and incorporation between base pairs.

The aim of work presented in **article 7** was aqueous synthesis of CdTe QDs capped with glutathione of the specific 2 nm size for monitoring of the interaction based on QDs size fitting into the major groove of the DNA double helix. Characterization of the nanoparticles has confirmed desired size of 2 nm. The interaction between QDs and DNA have been studied, through time and different concentration interaction with double stranded genomic chicken DNA (dsDNA), ssDNA and 500 base pair long DNA fragment. The comparison of the interaction between ssDNA and dsDNA has confirmed that dsDNA is needed for complex creation because peak complex was not observed in the case of ssDNA interaction with QDs. Interaction with 500 base pairs long DNA fragment has shown the same tendency of creating complex as with genomic DNA. The presence of the QDs in the structure of DNA was observed with gel electrophoresis after ethidium bromide staining. Observed interaction relies on possible similarity between size of quantum dots and major groove of the DNA (aprox. 2.1 nm).

5 CE for nanomaterials and nanomaterials for CE

5.1 Sample pretreatment by nanomaterials

CE can be coupled with many detection techniques. Each of them has its own advantages as well as disadvantages in terms of sensitivity, selectivity, and/or versatility. On-capillary as well as off-capillary detection modes are available. On-capillary detection is a nondestructive strategy minimizing the band broadening and enabling the employment of several detectors simultaneously (either consecutively or at the same detection point, however the off-capillary methods may provide additional information such as molecular mass. Photometric (or absorbance) detection is outstanding because of its versatility and due to this reason it is the most commonly used technique. However, the internal diameter of the capillary (generally tens of μm) defines the light path length. Therefore, relatively high analyte concentrations are necessary. Otherwise, extended path length flow cells (bubble cell, Z-cell), or preconcentration techniques are required to reach satisfactory

results. Moreover, several cleaning steps are usually needed in case of biological matrices significantly interfering with electrophoretic analysis. Sample pretreatment and preconcentration can be done either electrophoretically or chromatographically. Electrophoretic strategies are based on un-matching electrophoretic mobilities of the components or on their behavior in presence of (pseudo)stationary phase. On the contrary, chromatographic methods rely on compound sorption on a solid-phase material. These techniques take advantage from loading of multiple capillary volumes of sample subsequently eluted in a minute volume of solvent.

For extraction, isolation or preconcentration purposes, nanomaterials are offering appreciated high surface-to-volume ratios. As an example may serve the comparison of surface area of carbon microparticles with 60 μm in diameter of (0.01 mm^2) and the surface area of carbon nanoparticles with 60 nm in diameter (11.3 mm^2). Besides the increase in the surface area, the reactivity increases approximately 1000 \times . Not only the surface area, but also the chemical affinity may be beneficial.

For example, gold nanoparticles deliver outstanding isolation power because of the high affinity for thiols. Similarly, magnetic separation is a method using magnetism for the effective separation mediated by paramagnetic and superparamagnetic particles. This technique relies on the option of surface modification of magnetic nanoparticles to facilitate immunoextraction. Such particles may be modified by either antibodies for targeted capture of the analyte of interest or by oligonucleotide chains having sequences complementary to the desired nucleic acid. Magnetic particles can be immobilized using a magnetic field while interfering compounds are removed from the solution [71]. The above mentioned preconcentration techniques can be combined with CE in an off-line, at-line, on-line, or in-line mode.

The summary of the work combining the nanomaterial-based sample pretreatment (preconcentration) followed by CE analysis is the goal of the **article 8** of this thesis.

5.2 Characterization of nanoparticles by CE

Despite of all the advances in nanomaterial synthesis, problem in terms of batch-to-batch repeatability still persists. Moreover, sometimes, tools for characterization of nanomaterial

composition and properties are missing. Even in the same lot, the polydispersity of the particles and the inconsistency of the properties may present problem for satisfactory application. Therefore, it is not surprising that various methods of synthesis and characterization of the nanomaterials have been developed. From these methods, capillary electrophoresis has its unreplaceable position due to many advantages discussed. CE is the easy to use and low cost technique for studying nanoparticles parameters, such as their size, surface chemistry, and interaction abilities. Based on the literature search, it can be concluded that electromigration techniques represent a family of effective methods for nanomaterial characterization, evaluation, and investigation. In the future, manufacturing of portable or even hand-held CE-based instruments for *in situ* characterization of produced nanomaterials, as well as incorporating of CE into some industrial devices for high-throughput production of nanomaterials as quality control may emerge this field even further.

The overview of application of CE for separation and characterization of nanoparticles is given in **article 9** of this thesis.

5.3 Separation improvement

Even though, the development of miniaturized devices using microfluidic chips presented a great boom at the end of last century, nowadays, an increasing number of researchers perform CE separations in short capillaries (units of centimeters) instead of microfluidic chips [72, 73]. In such capillaries, fast and efficient separations take place without more or less difficult chip preparation requiring expensive facilities (e.g. clean rooms and lithography). In comparison to microchip-based rapid CE, short capillary-based high-speed CE take advantage of simple structure, easy fabrication, and low costs.

The shortcoming, however, is in lowered resolution linked with short separation length. This obstacle can be overcome either by injection of very low sample volumes (picoliters) or by extra selectivity coming from an added (pseudo)stationary phase of various nature (e.g. micelles, nanoparticles, nanostructures, etc.). Such solution significantly eliminates the adsorption on the capillary wall [74-77]. Nanomaterials have been proven to be effective (pseudo)stationary phase due to their beneficial properties, such as large surface/volume ratio and simple functionalization. Among often used

nanomaterials belong carbon nanotubes [78]. But, also other structures including nanoparticles [79, 80], nanofibres [81] and/or nanorods [82, 83] have been used. On the other hand, interaction of analyte with immobilized nanostructures such as monoliths, nanopillars, bound nanoparticles and/or other nanomaterials is also applicable. All of these types have already been employed in coupling with CE. Immobilized nanomaterials, either deposited on capillary wall as a thin layer coating or filled into the capillary, are frequently utilized as stationary phases for capillary electrochromatographic mode of separation. Equally, (pseudo)stationary phases enable a broad range of functionalities providing a number of interactions [84].

5.4 Enhancement of detection sensitivity

Laser-induced fluorescence detection is the most sensitive optical detection modality connected with microcolumn separations. Picomolar detection limits [85] and good detection selectivity enables analysis of samples in rather complex matrices. Concurrently, this selectivity could be perceived as a limitation due to the fact that majority of analytes does not fluoresce and derivatization by some fluorescent label is desirable.

Such photoluminescent labels may be not only organic fluorophores or fluorescent proteins but also QDs [86-89]. However, besides photoluminescence detection, chemiluminescence and electrochemiluminescence detection are also benefiting from properties of nanomaterials [90]. Undesired background signals are eliminated which leads to improved sensitivity. Furthermore, the instrumentation is simplified by absence of certain optical components such as excitation sources or optical filters. Metal nanomaterials (such as gold, silver, platinum, semiconductors, and magnetic) are in chemiluminescence and electrochemiluminescence detection applicable as catalysts, fluorophores, or energy acceptors [91].

Potentiometric, amperometric and conductometric are three of the most commonly used types of electrochemical detection in CE. Compared to the optical detection modes is that the electrochemical detection is mostly performed by off-column, end-capillary, and therefore, in destructive arrangement. The main roles of nanoparticles cover biomolecule immobilization, catalysis of reactions, improvement of electrode-analyte electron transfer, analyte labelling, and even use as a reactant [92].

It is highly unlikely that nanomaterials will wholly substitute such well-established approaches as organic dyes for fluorescent labeling. However, nanomaterials offer new options for a broad range of applications. The electrochemical detection particularly benefits from use of nanomaterials that enable increasingly sensitive detection.

The abilities of nanomaterials to improve the performance of CE analysis in terms of both separation resolution as well as detection sensitivity are summarized in the **article 10** of this thesis (Figure 2)

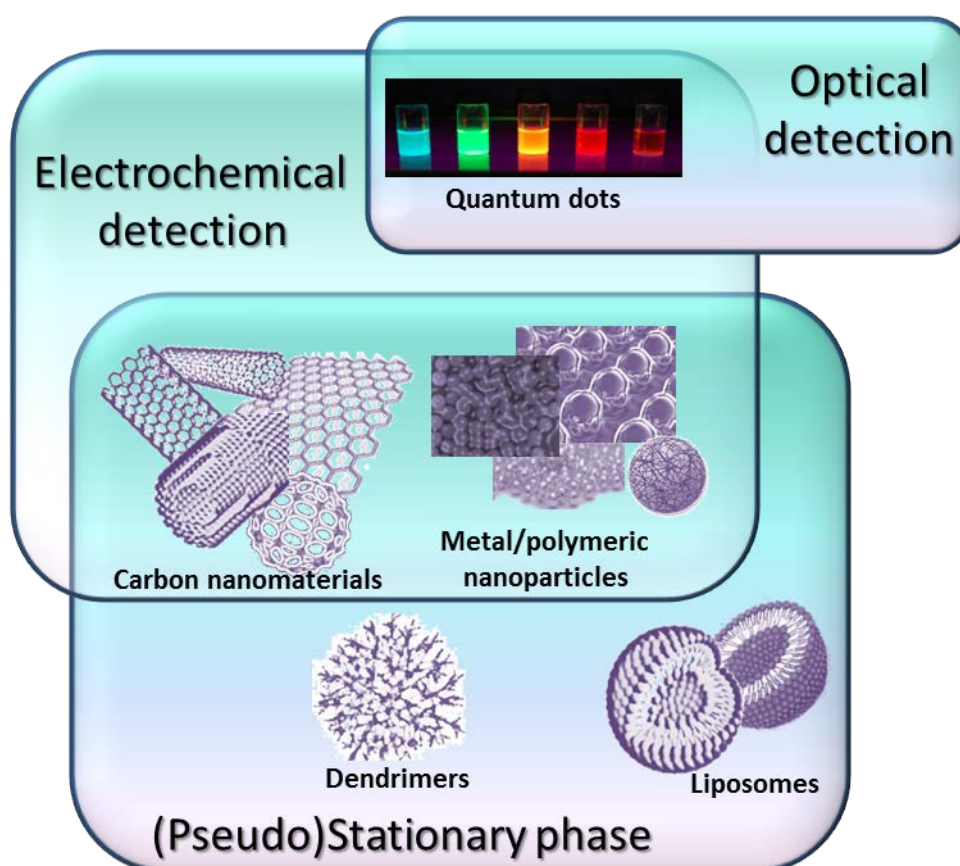


Figure 2: Summary of application of nanomaterials for improvement of CE performance

6 In-capillary quantum dot synthesis

6.1 Organometallic synthesis of quantum dots

Organometallic synthesis is still the most popular method of quantum dot preparation. It was introduced by Murray et al. in 1993 and involves very high temperature, toxic precursors, organic solvents and surfactants. However resulting quantum dots are highly monodisperse, size-tunable and surface coated. Usually the precursors are loaded into the flask with organic solvents trioctylphosphine (TOP) and its oxide (TOPO). The reaction is performed under an inert atmosphere and at 230-260 °C for nanocrystals growth. Final hydrophobic quantum dots have to be subsequently modified for water-solubility and biocompatibility. Nevertheless problems of the reproducibility, lack of the control and the overall costs of the procedure are its major disadvantages.

6.2 Aqueous synthesis of quantum dots

The second most often used synthesis method for direct producing stable and biocompatible aqueous solution of QDs is aqueous synthesis. Reactions are performed in three-necked flask with reflux condenser. Heavy metal precursors are easily dissolved in water; while chalcogens precursors can be bought as commercial solid powder. Metal salts dissolution in water occurs in the presence of capping agents (usually thiols, e.g. 2-mercaptoethanol, 2-thioglycerol, thioglycolic acid). The thiols control the QDs synthesis kinetics, passivate surface, provide stability, solubility and surface functionality of the QDs. This method is considered more environment-friendly and less expensive than organometallic, easy with high reproducibility, but comparing to the organometallic procedure lower quantum yields and higher polydispersity is observed. Disadvantages of the aqueous synthesis including a long reaction time (hours and/or days) have been overcome by employing microwave irradiation. High-quality quantum dots with enhanced quantum yield are produced. Generally, CdTe, CdSe, CdS, Zn_{1-x}Cd_xS and ZnSe QDs are synthesized by microwave irradiation.

6.3 The other ways of synthesis

Above mentioned methods are very effective in production of highly fluorescent QDs but usage of toxic chemicals limits their application in clinical practice. Therefore, more eco-friendly paths of QDs synthesis have been investigated using the principles of „green chemistry“ such as use of biocompatible and non-toxic solvents, precursors, and stabilizers such as bovine serum albumin as a capping agent.

Also, biosynthesis is new area of synthesis method and involves biological organisms and their metabolic pathways in preparation of QDs of desired composition, size, shape and functionality. Microbial synthesis is done either intracellular or extracellular and each of these QDs has their specific characteristics and is naturally capped with the proteins from the system with good stability and compatibility for any biological application. However, challenges such as improving size and shape control, obtaining larger amount of QDs and detail explanation of the synthesis mechanisms have to overcome.

6.4 UV irradiation in-capillary synthesis of quantum dots

In the **article 11** included in this thesis, a detail investigation of the inexpensive, low-temperature, and rapid preparation of aqueous QDs by UV illumination is reported. The influence of UV irradiation (at 254 nm and 250 nm) and temperature on the solutions of precursors were described. Optimal results were achieved with a solution of precursors composed by cadmium, selenium and mercaptosuccinic acid (quantum yield of 13.5%). Furthermore, the synthesis and observation of the formation of QDs in quantities from sub-mg to sub-ng was carried out. The smallest concentration being 258 pg in volume of 4 nL. The growth of QDs was observed in real time by photometry, fluorimetry and dynamic light scattering. Among biggest advantages of the presented method belong the simplicity, controllability, and low costs. The presented procedure can be integrated with miniaturized analytical systems or other instrumentation.

7 Conclusion

Undoubtedly, nanomaterials are exceptionally valuable tool not only improving highly the selectivity and effectivity of analyte isolation methods, increasing the ability of separation techniques to distinguish closely-structured molecules but also and improving greatly the abilities of detectors. Among numerous of crucial features of devices used for clinical purposes belong simplicity of application and robustness. Although, the great benefits of capillary electrophoresis are indisputable, robustness and repeatability of analyses belong to the weak points. Therefore, use of CE in clinical practice is limited to DNA sequencer. Therefore, employment of nanomaterials in CE might open new insight due to lower detection limits on one side and enhance the separation efficacy on the other side. Nevertheless, this is at the beginning and waiting for exploration.

Nanomaterials such as liposomes and dendrimers are able to advance the separation part of the CE analysis and QDs can significantly improve the detection part. Nevertheless, some types of nanomaterials such as carbon nanotubes or metal nanoparticles can improve both. Simultaneously, CE is an effective technique for characterization of nanomaterials, evaluation and/or investigation.

The relationship of CE and nanotechnology is advantageous not only for analytical chemists and material scientists, but also for biochemists and molecular biologists, because it leads to the advance of new, more effective, and more sensitive approaches.

The combination with the ease of miniaturization is offering opportunities for portable and point-of-care applicable devices suitable for personalized diagnostics. Moreover, the improved separation power of electrophoretic analysis promises effective analyses of complex biological samples.

8 References:

- [1] Johns, C., Breadmore, M. C., Macka, M., Ryvolova, M., Haddad, P. R., *Electrophoresis* 2009, 30, S53-S67.
- [2] Ryvolova, M., Preisler, J., Brabazon, D., Macka, M., *Trac-Trends Anal. Chem.* 2010, 29, 339-353.
- [3] Ryvolova, M., Preisler, J., Foret, F., Hauser, P. C., *et al.*, *Anal. Chem.* 2010, 82, 129-135.
- [4] Vaculovicova, M., Akther, M., Maaskant, P., Brabazon, D., Macka, M., *Anal. Chim. Acta* 2015, 871, 85-92.
- [5] Whitesides, G. M., *Small* 2005, 1, 172-179.
- [6] Drbohlavova, J., Chomoucka, J., Hrdy, R., Prasek, J., *et al.*, *Int. J. Electrochem. Sci.* 2012, 7, 1424-1432.
- [7] Drbohlavova, J., Vorozhtsova, M., Hrdy, R., Kizek, R., *et al.*, *Nanoscale Res. Lett.* 2012, 7, 1-4.
- [8] http://ec.europa.eu/environment/chemicals/nanotech/faq/definition_en.htm.
- [9] Armstrong, J. K., Wenby, R. B., Meiselman, H. J., Fisher, T. C., *Biophys. J.* 2004, 87, 4259-4270.
- [10] Buzea, C., Pacheco, II, Robbie, K., *Biointerphases* 2007, 2, MR17-MR71.
- [11] Alivisatos, A. P., *Science* 1996, 271, 933-937.
- [12] Shenderova, O. A., Zhirnov, V. V., Brenner, D. W., *Crit. Rev. Solid State Mat. Sci.* 2002, 27, 227-356.
- [13] Guldi, D. M., Rahman, A., Sgobba, V., Ehli, C., *Chem. Soc. Rev.* 2006, 35, 471-487.
- [14] Paul, D. R., Robeson, L. M., *Polymer* 2008, 49, 3187-3204.
- [15] Balazs, A. C., Emrick, T., Russell, T. P., *Science* 2006, 314, 1107-1110.
- [16] Turkevich, J., Stevenson, P. C., Hillier, J., *Dis. Farad. Soc.* 1951, 55-75.
- [17] Murphy, C. J., San, T. K., Gole, A. M., Orendorff, C. J., *et al.*, *J. Phys. Chem. B* 2005, 109, 13857-13870.
- [18] Daniel, M. C., Astruc, D., *Chem. Rev.* 2004, 104, 293-346.

- [19] Pileni, M. P., *Nat. Mater.* 2003, 2, 145-150.
- [20] Scott, R. W. J., Wilson, O. M., Crooks, R. M., *J. Phys. Chem. B* 2005, 109, 692-704.
- [21] Sharma, V. K., Yngard, R. A., Lin, Y., *Adv. Colloid Interface Sci.* 2009, 145, 83-96.
- [22] Peng, Z. M., Yang, H., *Nano Today* 2009, 4, 143-164.
- [23] Ahmadi, T. S., Wang, Z. L., Green, T. C., Henglein, A., ElSayed, M. A., *Science* 1996, 272, 1924-1926.
- [24] Cheong, S. S., Watt, J. D., Tilley, R. D., *Nanoscale* 2010, 2, 2045-2053.
- [25] Kim, S. W., Park, J., Jang, Y., Chung, Y., *et al.*, *Nano Lett.* 2003, 3, 1289-1291.
- [26] Teranishi, T., Miyake, M., *Chem. Mat.* 1998, 10, 594-600.
- [27] Hoefelmeyer, J. D., Niesz, K., Somorjai, G. A., Tilley, T. D., *Nano Lett.* 2005, 5, 435-438.
- [28] Mu, X. D., Meng, J. Q., Li, Z. C., Kou, Y., *J. Am. Chem. Soc.* 2005, 127, 9694-9695.
- [29] Kramer, J., Redel, E., Thomann, R., Janiak, C., *Organometallics* 2008, 27, 1976-1978.
- [30] Li, C. X., Leong, W. K., Zhong, Z. Y., *J. Organomet. Chem.* 2009, 694, 2315-2318.
- [31] Reetz, M. T., Lopez, M., Grunert, W., Vogel, W., Mahlendorf, F., *J. Phys. Chem. B* 2003, 107, 7414-7419.
- [32] Medintz, I. L., Uyeda, H. T., Goldman, E. R., Mattoussi, H., *Nat. Mater.* 2005, 4, 435-446.
- [33] Michalet, X., Pinaud, F. F., Bentolila, L. A., Tsay, J. M., *et al.*, *Science* 2005, 307, 538-544.
- [34] Stewart, D. T. R., Celiz, M. D., Vicente, G., Colon, L. A., Aga, D. S., *Trac-Trends Anal. Chem.* 2011, 30, 113-122.
- [35] Geszke-Moritz, M., Moritz, M., *Mater. Sci. Eng. C-Mater. Biol. Appl.* 2013, 33, 1008-1021.
- [36] Valizadeh, A., Mikaeili, H., Samiei, M., Farkhani, S. M., *et al.*, *Nanoscale Res. Lett.* 2012, 7.
- [37] Drbohlavova, J., Adam, V., Kizek, R., Hubalek, J., *Int. J. Mol. Sci.* 2009, 10, 656-673.
- [38] Morris-Cohen, A. J., Malicki, M., Peterson, M. D., Slavin, J. W. J., Weiss, E. A., *Chem. Mat.* 2013, 25, 1155-1165.

- [39] Kadkhodazadeh, S., *Micron* 2013, *44*, 75-92.
- [40] Riley, E. A., Hess, C. M., Reid, P. J., *Int. J. Mol. Sci.* 2012, *13*, 12487-12518.
- [41] Petryayeva, E., Algar, W. R., Medintz, I. L., *Appl. Spectrosc.* 2013, *67*, 215-252.
- [42] Wang, Y. C., Hu, R., Lin, G. M., Roy, I., Yong, K. T., *ACS Appl. Mater. Interfaces* 2013, *5*, 2786-2799.
- [43] Geim, A. K., Novoselov, K. S., *Nat. Mater.* 2007, *6*, 183-191.
- [44] Buhl, M., Hirsch, A., *Chem. Rev.* 2001, *101*, 1153-1183.
- [45] Bakry, R., Vallant, R. M., Najam-Ul-Haq, M., Rainer, M., *et al.*, *Int. J. Nanomed.* 2007, *2*, 639-649.
- [46] Bosi, S., Da Ros, T., Castellano, S., Banfi, E., Prato, M., *Bioorg. Med. Chem. Lett.* 2000, *10*, 1043-1045.
- [47] Iijima, S., *Nature* 1991, *354*, 56-58.
- [48] Yang, W. R., Ratinac, K. R., Ringer, S. P., Thordarson, P., *et al.*, *Angew. Chem.-Int. Edit.* 2010, *49*, 2114-2138.
- [49] Juillerat-Jeanneret, L., *Drug Discov. Today* 2008, *13*, 1099-1106.
- [50] Gu, F. X., Karnik, R., Wang, A. Z., Alexis, F., *et al.*, *Nano Today* 2007, *2*, 14-21.
- [51] Cho, K. J., Wang, X., Nie, S. M., Chen, Z., Shin, D. M., *Clin. Cancer Res.* 2008, *14*, 1310-1316.
- [52] Mishra, B., Patel, B. B., Tiwari, S., *Nanomed.-Nanotechnol. Biol. Med.* 2010, *6*, 9-24.
- [53] Dostalova, S., Cerna, T., Hynek, D., Koudelkova, Z., *et al.*, *ACS Appl. Mater. Interfaces* 2016, *8*, 14430-14441.
- [54] Haley, B., Frenkel, E., *Urol. Oncol.-Semin. Orig. Investig.* 2008, *26*, 57-64.
- [55] Vaz, G. C., Bahia, A., Muller-Ribeiro, F. C. D., Xavier, C. H., *et al.*, *Neuroscience* 2015, *285*, 60-69.
- [56] Cernat, A., Bodoki, E., Farcau, C., Astilean, S., *et al.*, *J. Nanosci. Nanotechnol.* 2015, *15*, 3359-3364.
- [57] Zhang, H. Q., Zhao, L. L., Chu, L. J., Han, X., Zhai, G. X., *J. Colloid Interface Sci.* 2014, *434*, 40-47.

- [58] Alanagh, H. R., Khosroshahi, M. E., Tajabadi, M., Keshvari, H., *J. Supercond. Nov. Magn* 2014, 27, 2337-2345.
- [59] Svenson, S., *Mol. Pharm.* 2013, 10, 848-856.
- [60] Kratz, F., Warnecke, A., *J. Control. Release* 2012, 164, 221-235.
- [61] Allen, T. M., Cullis, P. R., *Science* 2004, 303, 1818-1822.
- [62] Sumer, B., Gao, J. M., *Nanomedicine* 2008, 3, 137-140.
- [63] Panyam, J., Labhasetwar, V., *Adv. Drug Deliv. Rev.* 2003, 55, 329-347.
- [64] Smith, J. L., *Crit. Rev. Microbiol.* 2004, 30, 173-185.
- [65] Kopp, R., Vogt, A., Maass, G., *Nature* 1964, 202, 1211-1212.
- [66] Kilic, M. A., Ozlu, E., Calis, S., *J. Biomed. Nanotechnol.* 2012, 8, 508-514.
- [67] Lu, W., Xiong, C. Y., Zhang, R., Shi, L. F., *et al.*, *J. Control. Release* 2012, 161, 959-966.
- [68] Jorgenson, J. W., Lukacs, K. D., *Anal. Chem.* 1981, 53, 1298-1302.
- [69] Colton, I. J., Carbeck, J. D., Rao, J., Whitesides, G. M., *Electrophoresis* 1998, 19, 367-382.
- [70] Shimura, K., Kasai, K., *Anal. Biochem.* 1997, 251, 1-16.
- [71] Adam, V., Vaculovicova, M., *Electrophoresis* 2017, *in press*.
- [72] Wang, W., Ma, L. H., Yao, F. Z., Lin, X. L., Xu, K. X., *Electrophoresis* 2015, 36, 335-340.
- [73] Lin, Q. H., Cheng, Y. Q., Dong, Y. N., Zhu, Y., *et al.*, *Electrophoresis* 2011, 32, 2898-2903.
- [74] Duan, A. H., Xie, S. M., Yuan, L. M., *Trac-Trends Anal. Chem.* 2011, 30, 484-491.
- [75] Terabe, S., *Annual Review of Analytical Chemistry*, Annual Reviews, Palo Alto 2009, pp. 99-120.
- [76] Hajba, L., Guttman, A., *Trac-Trends Anal. Chem.* 2017, 90, 38-44.
- [77] Gonzalez-Curbelo, M. A., Varela-Martinez, D. A., Socas-Rodriguez, B., Hernandez-Borges, J., *Electrophoresis* 2017, 38, 2431-2446.
- [78] Ravelo-Perez, L. M., Herrera-Herrera, A. V., Hernandez-Borges, J., Rodriguez-Delgado, M. A., *J. Chromatogr. A* 2010, 1217, 2618-2641.

- [79] Peng, Y., Xie, Y., Luo, J., Nie, L., *et al.*, *Anal. Chim. Acta* 2010, *674*, 190-200.
- [80] Guihen, E., *Electrophoresis* 2017, *38*, 2184-2192.
- [81] Chigome, S., Darko, G., Torto, N., *Analyst* 2011, *136*, 2879-2889.
- [82] Wang, D., Wang, Q. T., Zhang, Z. M., Chen, G. N., *Analyst* 2012, *137*, 476-480.
- [83] Wang, D., Zhang, Z. M., Luo, L., Li, T. M., *et al.*, *Nanotechnology* 2009, *20*.
- [84] Adam, V., Vaculovicova, M., *Analyst* 2017, *142*, 849-857.
- [85] Swinney, K., Bornhop, D. J., *Electrophoresis* 2000, *21*, 1239-1250.
- [86] Chen, Q. D., Zhao, W. F., Fung, Y. S., *Electrophoresis* 2011, *32*, 1252-1257.
- [87] Bai, Y., Du, F. Y., Yang, Y. Y., Liu, H. W., *J. Sep. Sci.* 2011, *34*, 2893-2900.
- [88] Guo, D. S., Chen, G. H., Tong, M. Z., Wu, C. Q., *et al.*, *Chin. J. Anal. Chem.* 2012, *40*, 1379-1384.
- [89] Qiu, L., Bi, Y. H., Wang, C. L., Li, J. Y., *et al.*, *Int. J. Mol. Sci.* 2014, *15*, 1804-1811.
- [90] Yao, J., Li, L., Li, P. F., Yang, M., *Nanoscale* 2017, *9*, 13364-13383.
- [91] Giokas, D. L., Vlessidis, A. G., Tsogas, G. Z., Evmiridis, N. P., *Trac-Trends Anal. Chem.* 2010, *29*, 1113-1126.
- [92] Luo, X. L., Morrin, A., Killard, A. J., Smyth, M. R., *Electroanalysis* 2006, *18*, 319-326.

9 Articles

Article 1

Stanisavljevic M, Krizkova S, Vaculovicova M, Kizek R, Adam V. Quantum dots-fluorescence resonance energy transfer-based nano-sensors and their application. Biosens Bioelectron 2015;74:562-574.



Quantum dots-fluorescence resonance energy transfer-based nanosensors and their application



Maja Stanisavljevic^a, Sona Krizkova^{a,b}, Marketa Vaculovicova^{a,b}, Rene Kizek^{a,b}, Vojtech Adam^{a,b,*}

^a Department of Chemistry and Biochemistry, Mendel University in Brno, Zemedelska 1, CZ-613 00 Brno, Czech Republic

^b Central European Institute of Technology, Brno University of Technology, Technicka 3058/10, CZ-616 00 Brno, Czech Republic

ARTICLE INFO

Article history:

Received 30 April 2015

Received in revised form

26 June 2015

Accepted 29 June 2015

Available online 3 July 2015

Keywords:

Quantum dots

Fluorescence resonance energy transfer

Sensor

Nucleic acid

Enzyme

ABSTRACT

Fluorescence resonance energy transfer (FRET) in combination with quantum dots (QDs) and their superior properties has enabled designing of the new and improved sensors. In this review, the latest novelties in development and application of FRET nanosensors employing QDs are presented. QDs offer several advantages over organic dyes – broad excitation spectra, narrow defined tunable emission peak, longer fluorescence lifetime, resistance to photobleaching and 10–100 times higher molar extinction coefficient. These properties of QDs allow multicolor QDs to be excited from one source by common fluorescent dyes without emission signal overlap and results in brighter probes comparing to conventional fluorophores. Due to these benefits, QD-FRET-based nanosensors gained a wide spread popularity in a variety of scientific areas. These sensors are most frequently applied in the domain of the nucleic acid and enzyme activity detection. Other applications are detection of peptides and low-molecular compounds, environmental pollutants, viruses, microorganisms and their toxins, QD-FRET-based immunoassays, and pH sensors.

© 2015 Elsevier B.V. All rights reserved.

Contents

| | |
|--|-----|
| 1. Introduction | 563 |
| 2. FRET basics | 563 |
| 3. Quantum dots as new fluorophores | 564 |
| 4. QD-FRET-based sensor | 565 |
| 4.1. QD-FRET sensors for nucleic acid | 565 |
| 4.1.1. Hybridization sensors | 565 |
| 4.1.2. Immobilized QDs for nucleic acid detection assays | 566 |
| 4.2. QD-FRET sensors for enzymatic activities | 567 |
| 4.2.1. Immobilized QDs for enzymes activities – chip and paper-based sensors | 567 |
| 4.3. QD-FRET-based immunoassays and organic compounds detection | 568 |
| 4.4. QD-FRET sensors for small molecules | 569 |
| 4.5. QD-FRET sensors for heavy metals detection | 569 |
| 4.6. Sensors for detection of microorganisms and their toxins | 570 |
| 4.7. Detection of viruses via QD-FRET-based sensors | 571 |
| 5. Summary and conclusions | 572 |
| 6. Future perspectives | 572 |
| Acknowledgments | 572 |
| Appendix A. Supplementary material | 572 |
| References | 572 |

* Corresponding author at: Department of Chemistry and Biochemistry, Mendel University in Brno, Zemedelska 1, CZ-613 00 Brno, Czech Republic.
Fax: +420 5 4521 2044.

E-mail address: vojtech.adam@mendelu.cz (V. Adam).

<http://dx.doi.org/10.1016/j.bios.2015.06.076>

0956-5663/© 2015 Elsevier B.V. All rights reserved.

1. Introduction

Nanotechnology—the development of materials at the nanoscale—is one of the most prominent advancing technologies today. Novel nanomaterials have found their place in improvement of biosensors including well-known and widespread technologies. Biosensors classification is done according to multiple criteria like transduction mechanism and/or biorecognition principles (Rodríguez-Mozaz et al., 2004). In our focus will be biosensors with optical transduction mechanism or precisely speaking, based on fluorescence.

Fluorescence is a physical phenomenon described for the first time by Sir David Brewster on the chlorophyll (Brewster 1834) and quinine by Sir John Herschel (Herschel and W, 1845). Further fluorescence-based technique, which rises great interest, is Förster resonance energy transfer (FRET) as a specific mechanism of energy transfer between two molecules, called fluorophores, which can be easily excited with photon.

As a number of other areas, also FRET-based sensors have been affected by nanotechnology development. Nanoscale materials with their uniqueness have become a new challenge for biosensors designing. In this review, we will give an insight into the development of FRET-based nanosensors after new nanomaterials have been implemented into sensor designing process.

2. FRET basics

FRET is an acronym for Förster resonance energy transfer named according to its discoverer German scientist Theodor Förster (Förster, 1948). In the presence of two fluorophores, the energy donor and acceptor, FRET will occur. Detailed explanation of the fluorescence and FRET has been published in the past (Selvin, 2000; Shanker and Bane, 2008; Uhl et al., 2011).

FRET involves non-radiative transfer of energy between donor and acceptor fluorophores, also called FRET pairs. Energy transfer between FRET pair is the result of long-range dipole–dipole interaction between them and does not include a photon emission.

FRET will occur when overlap of the emission spectrum of the

donor and absorption spectrum of the acceptor is bigger than 30% and the distance is less than 10 nm (Elangovan et al., 2002). The distance between FRET pair is not only defining whether FRET occurs or not, but the efficiency of energy transfer has the same dependence of the distance and mathematically is expressed with the following equation:

$$E = R_0^6 / (R_0^6 + r^6)$$

where E is efficiency of energy transfer, R_0 is Förster distance (the distance at which energy efficiency is 50%) and r is the donor–acceptor distance.

Other properties, though not less important, include quantum yield (QY) and fluorescence lifetime of the fluorophores. Larger QY means approaching to the unity and displaying the brighter emission and represents number of emitted photons relative to the number of absorbed ones. The more photons are emitted from the donor, the better energy transfer will occur. Fluorescence lifetime, on the other hand, defines an average time that molecule spends in the excited state before relaxation. Both of these properties are dependent on rates of radiative and non-radiative decay because they are tightly connected to depopulation of excited state which determinate fluorescent characteristic of the fluorophores (Lakowicz, 1999; Uhl et al., 2011).

FRET can be detected by monitoring the acceptor fluorescence and/or the acceptor quenching (Fig. 1). In FRET system, quenching will be observed when the acceptor belongs to the family of molecules called quenchers which after excitation are returned to their ground state via non-radiative decay pathways (Leriche et al., 2012). In general, FRET is applicable for a number of purposes at the molecular level including monitoring of structural changes caused by changes in the molecular environment (i.e. temperature, ionic strength, etc.) and/or monitoring of interactions between molecules (i.e. aggregation or cleavage) (Fig. 2).

Due to aforementioned conditions, that fluorophores have to achieve it is obvious that designing FRET encounter a lot of limitations and shortcomings. To overcome them besides improvement of existing fluorophores, new nanomaterials have been explored and used for the sensing.

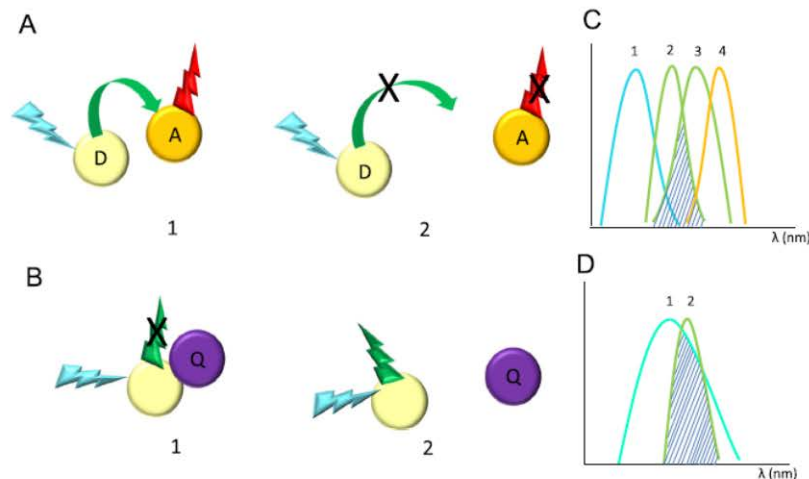


Fig. 1. (A) Basic principle of FRET: Excitation light is absorbed by donor (D), transferred by non-radiative transfer to acceptor (A) and emitted (top); in case of long distance between D and A, FRET does not occur (bottom). (B) In presence of quencher (Q), the emission of the fluorophore is not detected (top), after cleavage of Q the emission is restored (bottom). (C) Spectral characteristics of donor acceptor FRET pair: 1 - Absorption spectrum of donor, 2 - emission spectrum of donor, 3 - absorption spectrum of acceptor, 4 - emission spectrum of acceptor (hatched maked area is the spectral overlap); (D) Spectral characteristics of fluorophore-quencher FRET pair: 1 - Absorption spectrum of quencher, 2 - emission spectrum of fluorophore (hatched maked area is the spectral overlap).

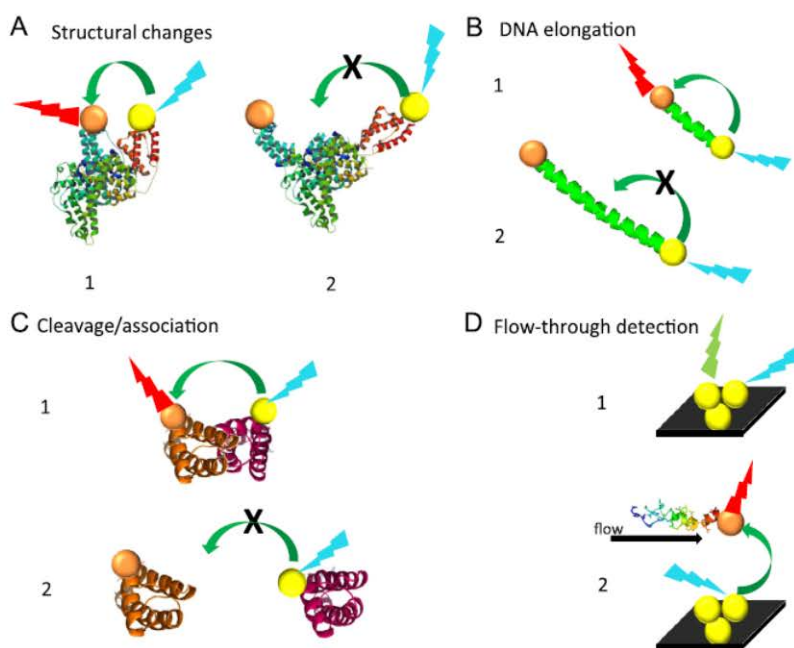


Fig. 2. Applications of FRET: (A) Structural changes monitoring: 1 – FRET occurs when two fluorescently labeled parts of the molecules are properly folded, 2 – unfolding of the molecule by external impacts (i.e. temperature, chemical environment, etc.) causes quenching of the FRET; (B) DNA elongation: 1 – FRET occurs when the chain is short enough, 2 – elongation of the strand causes the FRET quenching; (C) Monitoring of cleavage: 1 – FRET occurs when molecule is intact and two labeled parts are in proximity, 2 – when molecule is cleaved, FRET is quenched. (alternatively, association of two molecules is monitored by FRET generation upon interaction); (D) Flow through detection: 1 – emission wavelength of the immobilized fluorophore is detected, 2 – when acceptor labeled molecule is passing by, FRET occurs and acceptor emission wavelength is detected.

3. Quantum dots as new fluorophores

Regarding FRET, one of the most interesting nanomaterials are nanoparticles, especially quantum dots (QDs). QDs are semiconductors made out of the elements from groups II and VI or groups III and V in periodic table. They are known for their small size (1–10 nm) and size-dependent optical and electronic properties caused by quantum confinement (Adams and Barbante, 2013). They offer several advantages over organic dyes; some of them will be discussed according to FRET desirable characteristics and are presented in the Table 1.

QDs have one unique characteristic incomparable with organic fluorophores; the ability of tuning the emission range as a result of core size regulation during synthesis follows quantum confinement. QDs broad excitation spectra and narrow defined emission peak allow multicolor QDs to be excited from one source without emission signal overlap (Alivisatos et al., 2005; Probst et al., 2013),

also 10–100 times higher molar extinction coefficient than fluorophores results in brighter probes comparing the conventional fluorophores (Sun and Goldys 2008; Yu et al., 2003). This induces large Stokes shift (difference between peak absorption and peak emission wavelengths) of QDs in a range of 300–400 nm as well valuable for multiplexing purposes (Fu et al., 2005). These advantages enable imaging and/or tracking multiple molecular targets at the same time as well as elimination of background autofluorescence, which can emerge in biological samples. Therefore, fluorescence lifetime plays an important role and QDs, with lifetime of 20–50 ns, have superiority over fluorophores with few-nanosecond fluorescence lifetime, as well as size-tunable absorption and emission spectra (Walling et al., 2009). Further notable advantage is the high QY ranging from 40% to 90% and due to their inorganic core; they are highly resistant to the photobleaching and/or chemical degradation (Zrazhevskiy et al., 2010).

QDs are not flawless, they suffer of luminescence intermittency

Table 1
Short summary of characteristics comparison between QDs and organic fluorophores.

| Property | Quantum dots | Fluorophores | Ref. |
|------------------------------|--|---|--|
| Absorption spectra | Broad spectra, possible excitation with UV light | In general narrow, but variable | (Alivisatos et al., 2005; Probst et al., 2013) |
| Emission spectra | Narrow, in band width 20–40 nm | Broad, asymmetric and tailed | (Alivisatos et al., 2005; Probst et al., 2013) |
| Stokes shift | 300–400 nm | Less than 100 nm | (Fu et al., 2005) |
| Quantum yield | 40–90%, depending on buffer and surface modification | Variable, depends on the chosen fluorophore | (Zrazhevskiy et al., 2010) |
| Fluorescence lifetime | 20–50 ns | Few nanoseconds | (Walling et al., 2009) |
| Photostability | Strong resistance to photobleaching | Variable, depends on the chosen fluorophore | (Zrazhevskiy et al., 2010) |
| Molar extinction coefficient | 10–100 times larger than of fluorophores | < 200,000 M ⁻¹ cm ⁻¹ | (Sun and Goldys 2008; Yu et al., 2003) |

known as blinking, which can cause problems in applications and usually have been overcome by shell engineering and/or decreasing the excitation intensity (Li et al., 2013; Stopel et al., 2013), and then their inorganic nature and insolubility has been successfully mitigated by different coating and capping agents. QDs are an order of magnitude bigger than organic dyes, which represents a problem if the probe size is important (Walling et al., 2009). Further as shortcomings, their synthesis costs and toxicity of the precursors are usually stated. Overall QDs toxicity remains a subject of discussions although possible solutions are given by development of alternative ways of synthesis such as “green synthesis” (Ahmed et al., 2014; Beri and Khanna, 2011; Huang et al., 2013a) or biosynthesis (Bao et al., 2010; Huang et al., 2012; Sturzenbaum et al., 2013).

4. QD-FRET-based sensor

Due to the numerous benefits, QD-FRET-based sensors gained a wide spread popularity in a variety of scientific areas. The main fields and representative examples are discussed in the following text. The overall summary of applications is given in Fig. 3.

4.1. QD-FRET sensors for nucleic acid

4.1.1. Hybridization sensors

A very first QD-FRET-based sensor for the detection of DNA which can be found in the literature was designed by Zhang et al. (Zhang et al., 2005). This FRET system consisted of streptavidin-modified CdSe/ZnS QDs with photoluminescence emission at 605 nm (QD605) as energy donor and organic fluorophore Cy5 as energy acceptor. The sandwich hybrid was formed by binding complementary Cy5-labeled reporter probe and biotinylated capture probe with targeted DNA and hybrid was driven toward QDs surface via strong streptavidin-biotin affinity. It has been established that 54 hybrids could be self-assembled on an individual QD causing significant increase of the FRET efficiency and providing achievement of 4.8 fM as limit of detection (LOD), which was improvement comparing to the 0.48 pM obtained from molecular beacon. Designed sensor has been combined with an

oligonucleotide ligation assay and applied for detection of a point mutation characteristic for ovarian tumors. Further, Chen et al. have successfully combined QD-FRET and single molecule detection for targeting DNA directly in solution and without prior separation or amplification (Chen and Leong, 2006). Later, for improving detection sensitivity of previously formed QD-FRET-based DNA sensor (Zhang et al., 2005) Zhang et al. have conducted detection under the capillary microfluidic flow. The new conditions have shown significant improvement related to FRET efficiency, photobleaching prevention, higher sensitivity and lower sample consumption (~5 orders of magnitude less). Observed improvement of the FRET efficiency is caused by DNA deformation in the capillary (Zhang and Johnson, 2006).

Problem of the non-specific adsorption of DNA on the QDs is common in nucleic acid sensors design and Zhou et al. have offered a solution in 11-mercaptoundecyl tri(ethylene glycol) alcohol (EG₃OH)/11-mercaptoundecyl tri(ethylene glycol) acetic acid (EG₃COOH)-capped QDs. The EG₃ group provided surface stabilization as well as prevention of non-specific DNA adsorption. Target DNA was covalently attached to the (EG₃OH)/(EG₃COOH)-capped QDs through carboxyl-to-amine crosslinker and was used as energy donor while Alexa 594 (A594) labeled complementary DNA was energy acceptor in the designed system. Further they have shown that target DNA attached to (EG₃OH)/(EG₃COOH)-capped QDs could be used for detection of non-labeled complementary DNA by introduction of a dsDNA intercalating dye, such as ethidium bromide (EB). During the hybridization process, EB was intercalated into the double-strand hybrid and upon QD excitation, FRET occurred between QD and EB. Authors have successfully designed system suitable for the detection of labeled as well as non-labeled DNA with sensitivity of 1 nM measured on a conventional fluorimeter (Zhou et al., 2008). Further Algar et al. likewise (Zhou et al., 2008) have designed system with two different color QDs as donors and EB as energy acceptor showing that EB can be used even for multiple detections of DNA. QD-FRET-based sensors for simultaneous detection of two different targeted DNA is formed of green mercaptoacetic acid (MAA) capped CdSe/ZnS QDs and sequences of spinal muscular atrophy labeled with Cy3 for detection of this genetic disorder and red MAA-capped CdSe/ZnS QDs with A647-labeled target sequence for detection of *E. coli* (Algar and Krull, 2007). Peng et al. used the simplicity of the electrostatic attraction to bring the donor and acceptor into the proximity enabling FRET. They have used cationic polymer, poly(diallyldimethylammonium chloride) as an electrostatic linker between blue thioglycolic acid (TGA)-capped CdTe QDs and Cy3-labeled single stranded DNA (Cy3-ssDNA) as energy donor and acceptor, respectively. In the presence of the sample DNA and after hybridization decrease of QD/Cy3-ssDNA photoluminescence was observed, due to more rigid structure of dsDNA which increases donor-acceptor distance (Peng et al., 2007). Still decreased photoluminescence was observed due to aggregation of QDs caused by hybridization. Lee et al. have used positively charged dihydroliopic acid (DHLA)-2,2'-(ethylenedioxy)bis(ethylamine)-derived ligand and polyethylene glycol-modified CdSe/ZnS QDs for formation of an electrostatic complex with negatively charged ssDNA labeled with fluorescent dye TAMRA without the QDs aggregation, which was not observed in the case of Peng et al. study. QDs aggregation was not possible due to charge neutralization after hybridization, (Lee et al., 2009).

Mainly in the QD-dye FRET systems QDs, as energy donors, contribute to the increase of dye's fluorescence used for detection but in the sensor designed by Mao et al. QDs were used for dye's fluorescence quenching and its recovery was used for detection. This characteristic behavior was observed when CdS QDs interacted with acridine orange (AO), a DNA intercalating dye. However, in the presence of calf thymus DNA (ctDNA), ctDNA and AO



Fig. 3. Summary of application fields of QD-FRET sensors.

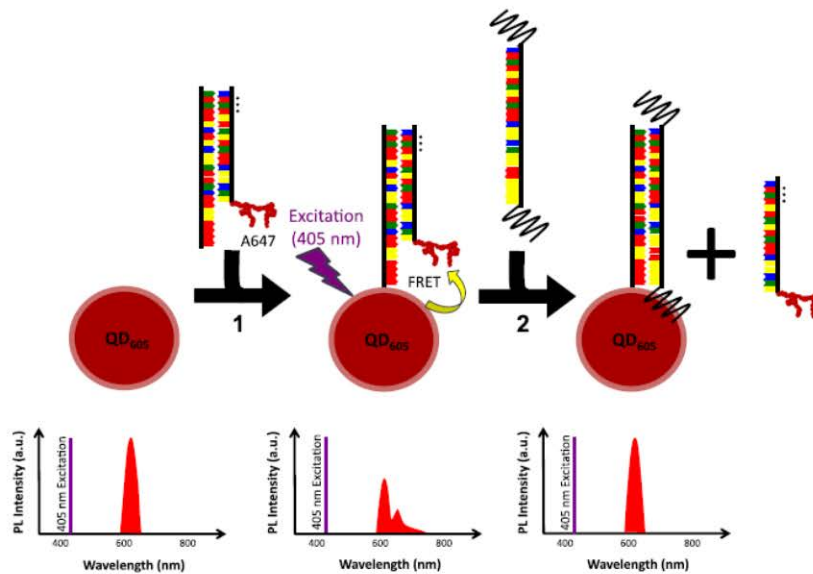


Fig. 4. Competitive displacement-based QD-FRET assay for intracellular detection of target DNA. System designed consisted of (1) CdSe/ZnS QD₆₀₅ and A647-labeled dsDNA containing mismatching bases (marked with asterisks) as energy donor and acceptor with visible high photoluminescence of QDs, (2) streptavidin–biotin linkage between QDs and A647-labeled dsDNA followed, upon excitation with QDs photoluminescence quenching and (3) detachment of the single strand with designed mismatches of dsDNA in the presence of the fully complementary target ssDNA visible by QDs photoluminescence recovery. Reprinted from (Vannoy et al., 2013) with permission from Elsevier.

created a binary ion-association of AO-ctDNA resulting in AO fluorescence recovery. Further QD-AO interaction was prevented by electrostatic repulsion between ctDNA and QDs (Mao et al., 2008). In existing sensors, a chemical conjugation between targeted nucleic acid and labeling dye always occurs, but there are environments, such as intracellular, where chemical interaction is impossible. Vannoy et al. were focused on designing the sensor, which would enable detection of nucleic acid in these conditions. They proposed a competitive displacement-based assay. The system consisted of CdSe/ZnS QD₆₀₅ conjugated to the A647-labeled dsDNA via streptavidin–biotin linkage resulting in QDs photoluminescence quenching. The dsDNA was formed of the ssDNA probe hybridized with 18-mer long reporter with three base-pair mismatches and was labeled with A647 (Fig. 4). The presence of the 98-mer ssDNA fully complementary to the ssDNA probe caused displacement of the 18-mer reporter with mismatching base pairs and recovery of the QDs photoluminescence (Vannoy et al., 2013). DNA-triggered dye transfer designed by Michaelis et al. has offered a good solution for spectral cross-talk between QDs and dyes as well as lack of the needed distance. Sensor consisted of 3'-thiolated oligonucleotide labeled with a cyanine dye (donor) and oligonucleotide attached to the QD surface via streptavidin–biotin affinity at its 3'-end and at 5'-end to the cysteine moiety (acceptor). In the presence of a complementary nucleic acid, after the hybridization, transfer of the linked fluorophore from the oligonucleotide dye donor to the oligonucleotide dye acceptor occurred via a native chemical ligation-type mechanism providing bigger proximity between QD and dye. System was successfully applied on the DNA-analogous peptide nucleic acids which bound complementary DNA and RNA strands with improved affinity (Michaelis et al., 2014).

4.1.2. Immobilized QDs for nucleic acid detection assays

Algar et al. have presented an interesting work by designing

several QD-FRET-based sensors for nucleic acid hybridization with immobilized QDs as energy donors. Mercaptopropionic acid (MPA) modified CdSe/ZnS QDs conjugated with oligonucleotide probe were immobilized on fused-silica optical fibers modified with multidentate thiol ligands. A layer of denatured bovine serum albumin prevented possible non-specific adsorption of the Cy5-labeled target on the interface active sites. After introduction of the Cy5-labeled target DNA, hybridization occurred, providing proximity between QDs and Cy5 required for FRET. Found LOD was 5 nM for designed system (Algar and Krull, 2009). Further, the same group has reported and discussed several multiplex assays for simultaneous detection of two or more target sequences. They have designed multiplex assay consisting of green MPA-capped CdSe/ZnS QDs–Cy3 and red MPA-capped CdSe/ZnS QDs–A647 as FRET pairs. For multiplexing, two different color QDs were co-immobilized in mixed films and in this assay single nucleotide polymorphisms discrimination with contrast ratios as high as 31:1 was possible (Algar and Krull, 2009). The same approach of two color QDs co-immobilized was used for detection of three different nucleic acids (Algar and Krull, 2010). The authors have shown that multiplexing is possible even using single color QDs immobilized on optical fibers as energy donor to two, Cy3 and Rhodamine Red-X, energy acceptors (Algar and Krull, 2010). Consequently, an idea of using immobilized QD-FRET probes was applied in chips. Chen et al. have constructed solid-phase nucleic acid hybridization assay using immobilized QDs within microfluidic channels. Immobilization of QDs inside the channels was done via hybridization of the complementary oligonucleotides assembled on the QDs surface and located on a glass surface inside the microfluidic channels. The second oligonucleotide sequence attached to QDs was available for hybridization with targeted Cy3-labeled DNA driven through channels electrokinetically, which enabled FRET (Chen et al., 2011).

Similarly Traver et al. have designed on-chip QD-FRET-based

assay for detection of transduction of nucleic acids. Streptavidin-modified green CdSe/ZnS QDs were immobilized into the microfluidic channels on the biotinylated polydimethylsiloxane (PDMS)-glass via streptavidin–biotin affinity and energy acceptor Cy3 was conjugated to target oligonucleotide sequence. Achieved LOD of the probe was in the range of femtomole (Tavares et al., 2012). Later on, this work was expanded on designing multiplex detection of nucleic acids in microfluidic channels (Noor et al., 2013). The most recent reported novelty in QD-FRET-based detection of nucleic acid is paper-based solid-phase assay and multicolor paper-based solid-phase assay reported by Noor et al. Paper surface has been modified with imidazole ligands for immobilization of glutathione (GSH)-capped QDs with oligonucleotide probe self-assembled on their surface as energy donors and Cy3 has been used as energy acceptors (Noor and Krull, 2013). For multicolor assay, green and red-emitting GSH-capped QDs with appropriate oligonucleotide sequence for target DNA detection were immobilized on the paper surface, and Cy3 and A647 were used as their FRET pair (Noor and Krull, 2013). In both cases, selectivity of nucleic acid hybridization was demonstrated by single-nucleotide polymorphism detection, reaching LOD in the range of femtomole. Similarly Petryayeva et al. have modified polystyrene microplate with multidentate imidazole-based surface ligands for immobilization of green- and red-emitting QD donors. Two different oligonucleotide probe sequences were assembled on QDs surface via hybridization with target oligonucleotides. QDs were paired with Cy3 and A647 acceptor dyes, respectively, creating two FRET-based detection channels. Established LOD was 4 nM for both assays, with green- and red-emitting QDs (Petryayeva et al., 2013).

4.2. QD-FRET sensors for enzymatic activities

Enzymes are involved in the thousands of metabolic processes. Proteases, which catalyze hydrolysis of proteins into smaller peptides and/or amino acids, are ubiquitous in all normal metabolic processes but as well as in diseases, such as viral infections (Meeprasert et al., 2014), AIDS (Pokorna et al., 2009) and in malignant progression like tumor angiogenesis, invasion and metastasis (Flores-Resendiz et al., 2009). Designing QD-FRET-based sensors for activity monitoring of proteases such as trypsin, caspase, HIV protease and others have attracted a lot of attention recently due to their diagnostic importance. However, such design is not so straightforward and includes several very important and complicated steps such as engineering of the linking protease-specific peptide or finding appropriate energy donors and acceptors.

4.2.1. Immobilized QDs for enzymes activities – chip and paper-based sensors

Since QD-FRET-based systems have the potential to be used in diagnostics and therapy, several chip-based QD-FRET sensors have been reported along with immobilization of QDs into the surface, which prevents their aggregation. For the detection of the MMP-7 activity, streptavidin-coated QD525 have been immobilized on the amine-reactive glass surface and QDs photoluminescence was quenched with TAMRA attached to biotinylated MMP-7 degradable peptide (RPLALWRSK). Fifty peptide molecules were attached per one QD and the designed chip-based assay was able to detect MMP-7 enzyme activity at concentration of approximately 100 ng/mL (Kim et al., 2007). The Medintz group has demonstrated monitoring of trypsin activity on electroluminescent (EL)-charged-coupled device (CCD)-microchip platform using QD bioconjugated with a trypsin substrate dye-labeled peptide (Fig. 5) (Medintz et al., 2006). The 16-well microchip was designed and linking peptide consisted of two segments: (1) a polyhistidine segment for self-assembly on the DHLA-PEG₆₀₀-capped QDs,

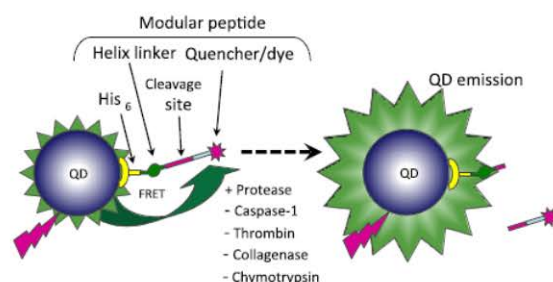


Fig. 5. QD-FRET sensor for detection of the enzymes activity. N-terminal hexahistidine (His₆) sequence for easier attachment to the DHLA-capped QDs as energy donors, while on C-terminal on the cysteine residues was used for dye attachment followed by helix linker for providing peptide rigidity, next part is cleavage site which was specific to the protease, caspase-1, thrombin, collagenase and chymotrypsin as enzyme of interest and on C-terminal site-specific location (cysteine thiol) for dye attachment. Cy3 and QXL™520 were used in this sensor for QDs photoluminescence quenching. In the presence of the enzyme, cleavage occurred rambling QD and dyes which prevented FRET enabling QDs photoluminescence recovery. Adapted by permission from Macmillan Publishers Ltd.: Nature Materials (Medintz et al. 2006) copyright 2006.

(2) enzyme cleavage site and cysteine residue for Cy3 attachment as acceptor dye. System had an optimal QD: Cy3-peptide ratio of 1:2 and was used for trypsin proteolytic activity and trypsin inhibition monitoring. The EL-CCD combined the spatial detection of CCD with the simple illumination by EL strips to measure fluorescence from chips. The results were compared to the conventional fluorescent plate reader measurements showing that used volumes were more than an order of magnitude lower comparing to the conventional method though LOD of trypsin (6.2 nM) has remained the same (Sapsford et al., 2009). Also, a microbiochip has been designed by Lee et al. using specific micro-electro-mechanical system. The design of the chip was based on microbead probes, where microbeads together with donor and acceptor fixed on their surface were injected into microchip and captured by micropillars in reaction chamber. Streptavidin-modified QDs were used for coupling with MMP-7 degradable peptide labeled by TAMRA quenching dye as FRET pair with the ratio of 1:20, which resulted in 90% of QDs photoluminescence quenching. Microbeads-QDs linkage was based on the streptavidin–biotin affinity. The microbiochip successfully measured QDs photoluminescence recovery in the presence of the MMP-7 after 50 min of reaction at 37 °C and LOD was 1 μg/mL. Besides reducing of reagents volume, main advantages of this microbiochip were easy handling and mass production potential due to its simple structure. Similarly, as for nucleic acid detection the most recent reported novelty in QD-FRET-based detection and monitoring of enzyme activity is paper-based assay, firstly reported by Algar group. Cellulose fibers in the paper were modified with bidentate thiol surface ligand on which CdSeS/ZnS QDs capped with DHLA or GSH can readily immobilize. After immobilization, QDs were assembled with Alexa Fluor 555-labeled peptide substrates for proteases (trypsin, chymotrypsin and enterokinase). Enzyme specific peptides have been engineered with His₆, cysteine bonding segments and enzyme-characteristic cleavage site. A portable USB spectrometer with violet LED as an excitation source, digital camera, webcam and an iPhone were sufficient for analysis on the basis of a red/green color intensity ratio in enzyme concentration 1–2 nM (Petryayeva and Algar, 2013). In order to minimize the unusually high analysis costs, due to sophisticated instrumentation, the same authors have shown that even smartphone camera can be used as photoluminescence detector as well as multiplexed protease sensing is possible and easily detectable (Fig. 6) (Kim et al., 2014). Later, they have

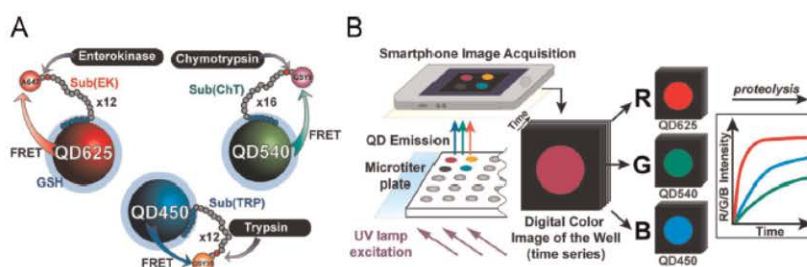


Fig. 6. Multiplexed QD-FRET assays for the detection of proteolytic activity using a smartphone. (A) Design of the assay with three color QDs as energy donors and QSY35, QSY9 or A647 as energy acceptors, which are used for labeling of the peptide with enzyme-specific cleavage site. (B) Detection of the photoluminescence recovery as a result of proteolytic activity via smartphone camera and hand-held UV lamp as excitation source. Reprinted with permission from (Kim et al., 2014). Copyright 2014 American Chemical Society.

reported work with immobilized QDs and different amounts of dye-labeled peptide for trypsin activity measurement, which had bright luminescence under ultraviolet illumination making QDs photoluminescence emission visible by eye (Kim et al., 2014).

4.3. QD-FRET-based immunoassays and organic compounds detection

Immunoassays are biochemical tests based on the antibody-antigen methodology. QDs in combination with FRET were used for designing immunoassays for variety of samples and compounds. One of the first published reports, which used FRET and QDs in immunoassay has been reported by Goldman et al. for TNT detection. Sensor consisted of anti-TNT specific antibody fragments attached to DHLA-CdTe-ZnS QDs via metal-affinity coordination. Black Hole Quencher-10-labeled TNT analogue was coupled to the antibody binding site and it quenched photoluminescence of the QDs. In the presence of TNT, dye-labeled analogue is displaced and photoluminescence is recovered. LOD was 20 ng/mL of TNT (Goldman et al., 2005). Several years later, another QD-FRET-based sensor for TNT has been reported. A hybrid system was based on the QDs photoluminescence quenched by the gold nanorods with LOD of 0.1 nM (Xia et al., 2011). Further two immunoassays are probably the most known QD-FRET-based sensor and they have been designed for maltose detection. The detection is based on β -cyclodextrin displacement as maltose analogue. First, sensor consists of multiple copies of *Escherichia coli* maltose-binding protein (MBP) bound to QDs by a C-terminal oligohistidine segment and plays a role of the sugar receptors. β -cyclodextrin-QSY⁹ dark quencher conjugate was bound to MBP saccharide binding site for QDs photoluminescence quenching. Displacement of the β -cyclodextrin was caused in the presence of the maltose, which was detected as photoluminescence recovery of QDs strongly dependent on maltose concentration. The second sensor uses a fluorescent dye as acceptor instead of QSY⁹ dark quencher. In this case, MBP-QD photoluminescence was quenched in two steps. First, energy was transferred from QDs to Cy3-labeled MBP and then to Cy3.5-labeled cyclodextrin (Medintz et al., 2003). In addition, a displacement mechanism was used for the glucose detection by Tang et al. Authors have designed a nanobiosensor in which glucose was detected upon fluorescence recovery. Sensor consisted of QDs as energy donors conjugated to a sugar-binding lectin concanavalin A (ConA) and glucose analogue, thiolated P-cyclodextrins (beta-SH-CDs) assembled on the surface of gold nanoparticles (AuNPs) as quenching acceptor. Fluorescence recovery was observed in the presence of glucose due to displacement of AuNPs-beta-CDs segment from ConA binding sites. Sensor had a high sensitivity with LOD of 50 nM and showed very good selectivity toward glucose in the presence of other sugars or serum biomolecules (Tang et al., 2008). Another nanosensor designed for

glucose detection was based upon observation of fluorescence inhibition and the authors have introduced binding site pre-blocking glucose assay protocol, as a part of the detection system. In the system, green QDs conjugated with ConA were used as energy donor and red QDs-NH₂-glu as acceptor. The authors have used ConA specificity for sugars and pre-bound glucose into the QD-ConA acceptor, which disabled attachment of the QDs-NH₂-glu acceptor blocking the resonance energy transfer between green and red QDs. The more glucose was bound into the binding sites of the ConA, the lower the conjugation with the red QDs-NH₂-glu was and photoluminescence of the green QDs was not quenched (Hu et al., 2012). Recently, a FRET-based aptamer biosensor for insulin was reported. FRET system was built between near-infrared QDs (NIR-QDs) and oxidized carbon nanoparticles as the energy donor and acceptor, respectively (Wang et al., 2014b). For achieving good FRET efficiency, the distance between QDs and antibody binding site is very important, as well as the number and location of the acceptor molecules. Molecules used for QDs surface modification sometimes enlarge the distance between the donor and the acceptor molecules causing a decrease in the FRET efficiency. To overcome this problem, Nikiforov et al. have designed a QD-FRET-based immunoassay, in which QDs surface was modified with haptens such as biotin, fluorescein and cortisol. The synthesis of hapten-QDs conjugates was very straightforward and based on the mixing of amine-labeled QDs with an excess of the N-hydroxysuccinimide esters of biotin and fluorescein. In the case of cortisol, a carbodiimide-activated carboxylic acid derivative of the hormone has been used. The binding of hapten-QDs to Alexa Fluor-labeled streptavidin, anti-biotin, anti-fluorescein or anti-cortisol antibody formed a FRET system and achieved LOD for fluorescein and cortisol that was 25 nM and 2 nM for biotin (Nikiforov and Beechem, 2006). Wei et al. have used QDs in the open sandwich fluoroimmunoassay (OsFIA) and estrogen was used as a model sample. In the sensor, CdSe-ZnS QDs attached to the hinge area of anti-estrogen receptor β (anti-ER- β) monoclonal antibody was used as energy donor and anti-ER polyclonal antibody was labeled with the energy acceptors-Alexa Fluor 568 or Alexa Fluor 633. After 30 min of incubation with estrogen receptor β (ER- β) antigen, FRET could be measured with LOD of 0.05 nM. OsFIA offers a simpler way of detection than ELISA (Wei et al., 2006). Another hormone QD-FRET sensor was reported for estradiol. It was FRET-based aptasensor using QDs bioconjugated as a nano-bioprobe and a high-affinity, high-specificity fluorescence-labeled anti-17 beta-estradiol aptamer as a bio-recognition molecule. LOD was 0.22 nM and probe showed really high estradiol specificity and sensitivity against potentially interfering endocrine-disrupting compounds or other chemicals (Long et al., 2014).

4.4. QD-FRET sensors for small molecules

Besides large biomolecules such as proteins or nucleic acids, also small molecules are extremely important either as compounds essential for life or as toxic and harmful species. In both cases, they have to be sensitively detected and identified. Even for these purposes, QD-based FRET can be applied (Esteve-Turrillas and Abad-Fuentes, 2013).

One of the most commonly determined analytes is currently glucose due to the widespread of type 2 diabetes. This disease affects more than 370 million people (Kahn et al., 2014) and therefore the need for proper diagnostics and treatment is urgent. In the area of QD-based FRET, number of studies have been published (Duong and Il Rhee 2007; Gill et al., 2008; Hu et al., 2012; Huang et al., 2013c). Very recently, a simple and ultrasensitive platform for the detection of glucose and hydrogen peroxide based on fluorescence resonance energy transfer between carbon quantum dots and polyaniline was described (Zhang et al., 2015). By this method, detection of glucose down to submicromolar levels was achieved and moreover, it was found that traces of hydrogen peroxide can be detected in a range of 0.5–50 μM .

Among other important molecules detectable by QD-based FRET belong vitamins such as ascorbic acid (Huang et al., 2014), cobalamin (Gore et al., 2014; Vaishnavi and Renganathan, 2013) and/or biotin (Mattsson et al., 2015) also amino acids (Heger et al., 2015; Tirado-Guizar et al., 2014), glutathione (Shi et al., 2014) and adenosine triphosphate (Chen et al., 2008; Revesz et al., 2007).

Finally, substances that may cause pollution are numerous, some of them are directly connected to human activities, such as agriculture, and/or mining industry, and therefore monitoring is required. Few QD-FRET based nanosensor have been reported for some of the pollutants. Sensor for the detection of residues from organophosphorus pesticides was based on the simple ligand replacement on the QDs surface, which resulted in turning off the FRET. CdTe QDs were quenched by bidentate ligand dithizone (DZ) attached on the surface due to FRET and presence of organophosphorothioate pesticides replaced DZ ligands on the QDs surface by the hydrolyzation of the organophosphorothioate and photoluminescence recovery occurred. Model pesticide was chlorpyrifos and system achieved LOD of 0.1 nM. Organophosphorothioates were successfully detected in apples (Zhang et al., 2010). Glyphosate is a broad-spectrum herbicide brought up to the market in the 70's of the last century by Monsanto Corporation. QD-FRET based glyphosate sensor was designed with the negatively charged TGA capped CdTe-QDs as energy donor and positively charged gold nanoparticles stabilized with cysteamine (CS-AuNPs) as energy acceptor. Electrostatic interaction approximated FRET pair resulting in the QDs fluorescence quenching. Glyphosate interaction with the FRET system induced aggregation of the CS-AuNPs due to electrostatic interaction and fluorescence recovery has been observed. The detection limit for glyphosate in the apples was 9.8 ng/kg (Guo et al., 2014). Octachlorostyrene (OCS) was never used as a commercial product but it can be produced during magnesium production, incineration, combustion processes involving chlorinated compounds and others. It is characterized as persistent, bioaccumulative and toxic compound, involved in the mutagenicity/genotoxicity and carcinogenicity in humans. OCS detection FRET system was built in a microtitration plate and contained several steps. Laboratory produced anti-OCS antibody were adsorbed on a microtiter plate and competitive immunoreaction occurred between rhodamine B-labeled OCS (RB-OCS) and OCS. Afterwards separated solution was mixed with TGA capped CdTe QDs and based on the electrostatic interaction between CdTe QDs donor and RB-OCS acceptor FRET occurred and increasing of the fluorescence emission of the rhodamine B was observed with corresponding decreasing of the QDs photoluminescence (Wang et al., 2014a).

4.5. QD-FRET sensors for heavy metals detection

One of the biggest problems of today's society is environmental pollution with heavy metals. FRET-based nanosensors enhanced with QDs as novel fluorophores had been successfully applied for heavy metals as prominent sensing tool. As well as in the others QDs-based nanosensors, interaction between QDs and metal ions is detected as photoluminescence enhancement or quenching caused by direct physical adsorption or chelating metal-ions on the QDs surface or more often is used interaction between metal-ions and QDs functionalized with metal-ion selective receptors. For direct interaction, several pathways have been described as probable reaction mechanisms, but it is not possible to clearly determine which one had happened or if several pathways had been combined (Wu et al., 2014). On the other hand, functionalization of the QDs reduces direct metal-ion attack and application of the QDs encapsulated with materials such as polymers reduce non-specific interactions. Hereafter, QDs-FRET-based nanosensor for most common pollutant, such as Hg(II), which belongs to one of the most toxic and dangerous pollutants, will be described. QD-FRET-based sensor designed by Li et al. for Hg(II) detection used TGA-capped CdTe QDs and butyl-rhodamine-B dye in Tris-HCl buffer with addition of the cetyltrimethylammoniumbromide in order to bring the electronegative QDs and dye closer for better FRET efficiency. In the presence of Hg(II), photoluminescence quenching of TGA-CdTe QDs and corresponding fluorescence enhancement of the butyl-rhodamine-B was observed. QDs photoluminescence has been quenched because of mercury affinity toward telluride, which caused Cd(II) ion displacements from the QDs surface. Reached LOD was 20.3 μM (Li et al., 2008). Since mercury has a bio-accumulative nature, an intracellular detection might be needed and FRET ratiometric approach is a good solution, especially with long lifetime material like QDs whose emission will last longer than background autofluorescence. A system with polymer-encapsulated CdSe/ZnS QDs and thiosemicarbazide-functionalized rhodamine-B, which is capable of non-specific adsorption on the QDs surface, as energy donor and acceptor was designed by Page et al. Detection was followed by ring-opening reaction at thiosemicarbazide-functionalized rhodamine-B and rise of absorption peak at 550 nm, which overlapped with emission maxima of the QDs and FRET occurred. Measured LOD was 79 ppb (Page et al., 2011). Follow, Liu et al. designed QDs-FRET ratiometric fluorescence sensors for detection of Hg(II) in water, which involved CdTe QDs encapsulated into silica particles and rhodamine-B as FRET pair (Liu et al., 2012). Hu et al. have used N-acetyl-L-cysteine (NAC) functionalized QDs and rhodamine-6 G derivative-mercury conjugate as FRET pair for ratiometric FRET sensor. NAC stabilized QDs and gave much brighter emission than typical TGA and/or MPA stabilizers, as well as it has good affinity toward mercury ions. Sensor was employed for intracellular colorimetric imaging in live HeLa cells (Hu et al., 2013).

Mainly, QDs are used as a donor in FRET systems and the system in which they are used as acceptor are rare. In such system, TGA-CdTe QDs and fluorescent brightener were used in concentration ratio 10:1 and as acceptor and donor respectively. Detection of Hg(II) ions was followed by QDs photoluminescence quenching due to strong absorption of Hg(II) to the carboxyl group on the QD surface (Tao et al., 2014). Among common, bio-accumulative and persistent pollutant also belongs lead. Therefore, several QD-FRET-based sensor for detection are reported in the literature. CdTe QDs capped with cysteamine have been used as energy donors while surface of gold nanoparticles modified with 11-mercaptopundecanoic acid (MUA-AuNP) have been used as energy acceptors. Lead ions have been detected according to the QDs photoluminescence recovery with LOD 30 ppb. Supposed interaction that led to photoluminescence recovery is the aggregation of

MUA-AuNP in the presence of lead (Wang and Guo, 2009). Similarly, Zhao et al. have reported lead detection with the system of dithizone (Dz) functionalized CdSe/CdS QDs, where Dz quenched QDs photoluminescence. The recovery of photoluminescence has been observed in the presence of the lead ions caused by removal of Dz from QDs surface due to its strong affinity to lead ions. LOD was 0.006 nM and probe has shown satisfactory results with real environmental samples (Zhao et al., 2013). Very interesting approach was published by Wu et al. showing the design of QD-DNAzyme nanosensor in which fluorescence recovery of QDs is consequence of DNAzyme cleavage in the presence of the heavy metals, Pb(II) and Cu(II) were used as models. The carboxyl-silane-modified QDs have been linked to DNAzyme through the zero-length crosslinker EDC and sulfo-NHS. The achieved LOD for Pb(II) and Cu(II) were 0.2 and 0.5 nM, respectively. Using different colors of QDs, Pb(II) and Cu(II) ions were successfully recognized within the mixture without any signal interference (Wu et al., 2010). Further, different systems for Cu(II) ions were designed. Ganguly et al. have used salen-coupled CdSe/ZnS QDs through condensation reaction between surface amine and salicylic aldehyde. In the presence of Cu(II) salen will exhibit photoluminescence quenching. Model has been applied for Fe(II) ions detection as well (Ganguly et al., 2010). Further, for Cu(II) ions, a sensor using MPA-CdTe QDs as energy acceptor and green luminescent monodisperse phenol formaldehyde resin nanoparticles (PFR NPs) as energy donors was built. In the system of QD-PFR NPs, red color of QDs has been observed, but in the presence of Cu(II) ions, FRET has been disrupted and QDs photoluminescence has been quenched while green color of PFR NPs has arose visible by naked eye within 1 min (Yang et al., 2011). Besides mercury, cadmium and lead, also others pollutants such as zinc and potassium have been subjected to the detection. Ruedas-Rama et al. have designed an interesting QD-FRET-based sensor for Zn(II) and Mn(II) ions sensing with 2-carboxyl-2-hydroxy-5-sulfoformazylbenzene (Zincon) modified QDs. System has shown different behavior in the presence of these two metals. In case of Zn(II), Zn(II)-Zincon absorption spectra overlaps with the emission of QDs thereby photoluminescence quenching is observed. On the other hand, in the presence of Mn(II) and its binding to Zincon, enhancement of the photoluminescence intensity is observed as a result of deactivation of the quenching

interaction between Zincon and QDs (Fig. 7) (Ruedas-Rama and Hall, 2009). Chen et al. developed a crownether(15-crown-5)-functionalized dual QDs system for potassium detection. CdSe/ZnS QDs of two different colors were used, QD545, as energy donor and QD635, as energy acceptor. When potassium has bound, aggregation of the QDs has occurred due to shortening of the distance between them causing QD545 quenching and QD635 fluorescence increase (Chen et al., 2006). CdTe-AuNPs quenching system has been designed for sensing of fluoride (F^-) anion. CdTe-AuNPs have bound through formation of cyclic boronate esters, whose integration with F^- formed trifluoroborate and have disassembled CdTe from AuNPs. The linkage breaking has resulted in the fluorescence recovery of QDs and LOD for F^- has been measured at the concentration of 50 nM (Xue et al., 2012).

4.6. Sensors for detection of microorganisms and their toxins

A majority of microorganisms are harmless to humans, however some microorganisms are/or their toxins can be very dangerous, causing serious diseases; therefore their rapid and sensitive detection is needed. In this section, a short insight in QDs-FRET-based nanosensors designed for detection of different microorganism and toxins will be given. These nanosensors employ previously introduced mechanisms of the hybridization and antibody-antigen interaction to provide appropriate proximity of the donor and acceptor for FRET as well as activity of the proteases.

Kattke et al. have developed QD-FRET-based immunoassays for spores in the solution of *Aspergillus amstelodami*, presented in the Fig. 8. Detection system has been formed by anti-*Aspergillus* antibody conjugated to the amine-derivatized (PEG)-coated CdSe/ZnS QDs through succinimidyl-4-[N-maleimidomethyl]cyclohexane-1-carboxylate (SMCC) crosslinker and black hole quencher (BHQ3)-labeled mold analytes that had a lower affinity for the antibody than *A. amstelodami*. Fluorescence recovery was observed in the presence of *A. amstelodami* due to black hole quencher-labeled mold analytes displacement. The immunoassay has detected concentrations as low as 10^3 spores/mL in five minutes or less (Kattke et al., 2011). The toxic shock syndrome toxin-1 (TSST-1)-producing *Staphylococcus aureus* has been successfully detected by FRET system with CdSe-ZnS QDs as donor and BHQ3 as acceptor.

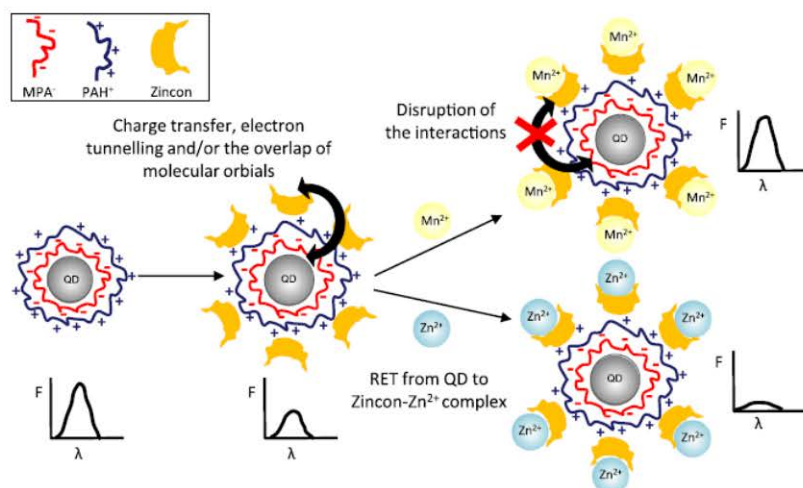


Fig. 7. QD-FRET sensor for detection of Zn(II) and Mn(II) ions. In designed system, MPA-capped QDs were modified with poly(allylamine hydrochloride) (PAH⁺) was chosen for achieving positive charge on the QDs surface used for electrostatic binding of the Zincon. System has exhibited QDs photoluminescence quenching due to metal-ion disruption of the QD-Zincon system caused by formation of the Zincon-metal complex and QDs photoluminescence enhancement due to RET and/or FRET in the detection of the Zn(II) and Mn(II) ions, respectively. Reproduced from (Ruedas-Rama and Hall 2009) with permission of The Royal Society of Chemistry.

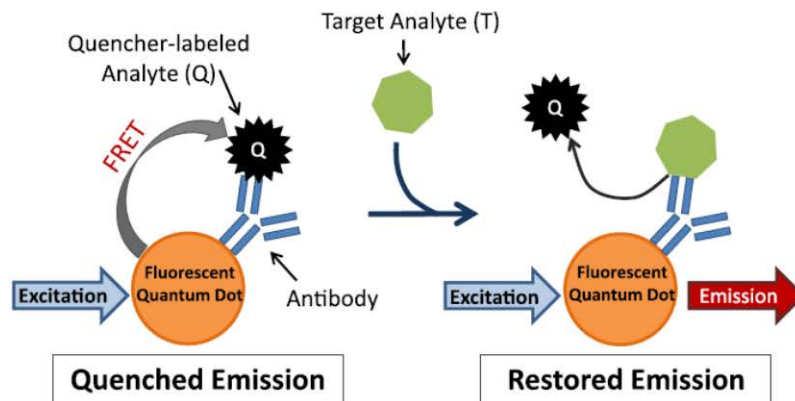


Fig. 8. Schematic presentation of the QD-FRET-based immunoassays for spores of the *Aspergillus amstelodami*. Amine-derivatized (PEG)-coated CdSe/ZnS QDs were linked to the anti-*Aspergillus* antibody via SMCC crosslinker, which interacted with BHQ-3-labeled mold analytes with lower affinity than *A. amstelodami* spores. As a result, QDs photoluminescence was quenched but in the presence of the *A. amstelodami* spores lower affinity mold analytes will be displaced recovering photoluminescence as detection signal. Reprinted with permission from (Kattke et al., 2011).

QD-DNA probe was prepared by conjugation of the carboxyl-modified QD and the amino-modified DNA with the EDC in ratio 1:40, respectively. Photoluminescence quenching has been observed after DNA hybridization between matching ssDNA-modified donor and acceptor. In the presence of targeted DNA the photoluminescence recovery was observed due to BHQ-3-labeled ssDNA detachment from the probe. Recovered QDs photoluminescence has been linearly dependent on the concentration of target DNA and LOD was 0.2 μM (Wang et al., 2011). QD-FRET-based sensors relied on the DNA hybridization process for providing the donor-acceptor proximity between QDs and graphene oxide (GO) has been applied for *Listeria monocytogenes* detection, a foodborne pathogen. Method consisted of a multiplex linear-after-the-exponential PCR amplification, DNA hybridization, and QD-GO signal detection. QD525 and QD605 have been conjugated to the ssDNA amplification products of the *iap* and *hlyA* genes, respectively due to streptavidin-biotin interaction. The photoluminescence recovery has been observed in the presence of the targeted DNA. Genomic DNA from *L. monocytogenes* can be detected as low as 100 fg/ μL (Liao et al., 2014). Similarly, the FRET between QDs and quenchers has been developed for *Listeria monocytogenes*, *Bacillus thuringiensis*, and *Salmonella typhimurium* detection designed by Burris et al. (2013). A very simple and rapid QD-FRET-based nanosensor has been designed for *Helicobacter pylori* by Shanesaz et al. Two oligonucleotides probes were differently labeled, one with TGA-capped CdTe QDs and the other with TAMRA. 210 bp PCR product of urease gene of bacterium *H. pylori* was used as complementary DNA. Complementary DNA hybridized with oligonucleotides probes brought closer QDs and TAMRA and enabled FRET. The LOD was estimated as 4.5 nM (Shanesaz et al., 2013). Several QD-FRET-based nanosensors for bacteria toxins have been reported. Botulinum neurotoxins (BoNTs) are proteins produced by the *Clostridium botulinum*. BoNTs are one of the strongest and most dangerous natural toxins known to human and could cause poisonings with fatal outcomes, therefore rapid and sensitive detection of the toxins is needed. QD-FRET-based nanosensors were based on observing activity of light chain protease of the BoNT serotype A (LcA). The authors designed LcA peptide substrate consisting central LcA recognition/cleavage region with C-terminal cysteine residue labeled with Cy3 acceptor dye and N-terminal oligohistidine for self-assembly with PEGylated or DHLA-capped CdSe/ZnS QDs. In the presence of BoNT LcA the created QD-LcApep-Cy3 quenching system exhibited

fluorescence recovery as a result of LcApep cleavage. Obtained LOD was 350 pM for LcA (Sapsford et al., 2011).

Staphylococcal enterotoxin B (SEB) is one of the toxins produced by *Staphylococcus aureus* and is commonly associated with food poisoning. Detection system for SEB was based on FRET between two different QDs, QD₅₂₃ and QD₆₀₁, which were bioconjugated to anti-SEB antibody and SEB respectively according to the carbodiimide protocol. Mutual affinity of anti-SEB antibody and SEB enabled efficient FRET between QDs, where fluorescence quenching was observed at QD₅₂₃ (energy donor) and fluorescence enhancement at QD₆₀₁ (energy acceptor) (Vinayaka and Thakur, 2013). Aflatoxins are group of secondary metabolites produced mainly by the fungi of *Aspergillus flavus* and *Aspergillus parasiticus*. They are harmful to human, poultry and livestock health. QD-FRET-based competitive immunoassay for aflatoxin B1 detection was designed by Zekavatin et al. CdTe QDs conjugation with anti-aflatoxin B1 antibody and Rhodamine123-labeled aflatoxin B1-albumin both done by EDC-sulfo NHS methodology, were used as energy donor and acceptor. The proximity of the QDs and the Rhodamine123 provided by labeled-aflatoxin B1-albumine enabled FRET and strong Rhodamine123 fluorescence emission was observed. Aflatoxin B1 was detected according the reduction of the Rhodamine123 fluorescence due to competitive replacement of the labeled-aflatoxin B1-albumine with aflatoxin B1. Achieved LOD was 2×10^{-11} M (Zekavati et al., 2013). Another sensor for aflatoxin B1 in rice grain was formed by using hapten-labeled green QDs as energy donor and monoclonal antibody-labeled red QDs as energy acceptor. Achieved LOD was 0.13 pM in rice extracts (Xu et al., 2014).

4.7. Detection of viruses via QD-FRET-based sensors

Viruses are small infectious agents that require a host organism for living and replicating. Most of the viruses have either RNA or DNA as their genetic material, they undergo the genetic mutation very quickly, and due to that, they stand as an unsolved diagnostics and therapeutic problem. Rapid, inexpensive and sensitive virus detection methods are still under investigation. Similarly to QD-FRET-based bacteria detection, in the most of the cases viral nucleic acids been used for hybridization assays as well as antigen-antibody affinity for building immunoassays as mechanism, which will enable FRET follow their detection. For Porcine Reproductive and Respiratory Syndrome Virus (PRRSV) two different

QD-FRET-based sensors have been proposed. An anti-PRRSV monoclonal antibody labeled with Alexa Fluor 546 (A546) fluorescent dye was attached to the commercially protein-modified green QDs as first FRET system, in the second one the same dye-labeled anti-PRRSV monoclonal antibody was used and coupled with protein A-modified gold nanoparticles. In the presence of the antigen, antibody-antigen reaction will occur causing conformational change within the antibody structure bringing closer FRET pair and increasing FRET efficiency. For QDs-based sensor, less energy has been transferred from QDs to the A546, increasing QDs photoluminescence and decreasing A546 fluorescence. For gold nanoparticle-based sensor, this has caused the decrease in the quenching effect. Both sensors were able to rapidly and effectively detect PRRSV in solution with LOD 3 particles/ μl (Stringer et al., 2008). Further, for hepatitis B virus (HBV) sensor has been reported consisting of MPA-capped CdSe/ZnS QDs conjugated with amine-modified 15-mer oligonucleotides via carbodiimide chemistry along with Cy5 dye used for labeling of the target DNAs. Bringing QD-Cy5 FRET pair together by sandwiched hybridization fluorescence emission of the Cy5 was observed. Non-complementary and unbound DNAs did not produce any FRET signal because they could not hybridize with the QD-DNA conjugate. Applicability of the nanosensor was also demonstrated in the detection of synthetic 30-mer oligonucleotide targets derived from the HBV with a sensitivity of 4.0 nM by using a multilabel counter (Wang et al., 2010). Relaying on the same procedure another HBV sensor was designed with the usage of 6-carboxy-X-rhodamine fluorophore as energy acceptor (Huang et al., 2013b). FRET technique was applied for H5N1 avian influenza virus detection as well. FRET system consisted of CdTe QDs conjugated with ssDNA via EDC/NHS linkage as energy donor and oxidized carbon nanotubes (oxCNT) were used as fluorescence quenchers. Upon the recognition of the target, efficient competitive binding toward QD-ssDNA occurred and resulted in the oxCNT removal from the system and photoluminescence recovery. Registered LOD was 9.39 nM (Tian et al., 2012). Moreover, a nucleic acid sandwich QD-FRET-based hybridization assay was used for H5N1 virus detection where 16-mer oligonucleotide was attached to QD655 via sulfosuccinimide crosslinker in the molar ratio of 10:1 (probe-to-QD) and 18-mer oligonucleotides was attached to Alexa Fluor 660 (A660) dye. Since these oligonucleotides recognize two separate but adjacent regions of the H5 sequences, sandwich hybridization assay was applied. In the presence of label-free hemagglutinin H5, A660 dye emission was increased as consequence of FRET (Chou and Huang 2012).

Human Enterovirus 71 (EV71) and Coxsackie virus B3 (CVB3) immunoassays were proposed based on the energy transfer between two colored QDs and graphene oxide as energy donors and acceptors. Streptavidin-modified green CdSe/ZnS QDs were attached to biotinylated EV71 antibody and streptavidin-modified red CdSe/ZnS QD were attached to biotinylated CVB3 antibody and in both cases GO was used as quenching acceptor. The QD-Ab-GO complex was broken up in the presence of the targeted EV71 and CVB3 followed by photoluminescence recovery of QDs. Achieved LOD for EV71 and CVB3 were 0.42 and 0.39 ng/mL, respectively (Chen et al., 2012). QDs-FRET-based sensors are also applied in the detection of viruses like necrotic yellow vein virus (BNYVV); a plant virus, which is responsible for most destructive disease in sugar beet, called rhizomania transmitted by protozoan *Polymyxabetae* (Keskin). BNYVV sensor was proposed by Safarpour et al. and FRET occurred between TGA-capped CdTe QDs conjugated with anti-glutathione-S-transferase antibody (anti-GST) via electrostatic interaction as energy donor and fluorescent dye rhodamine attached to GST as energy acceptor (Safarpour et al., 2012).

5. Summary and conclusions

FRET has gained a huge importance in different research fields and improved detection sensitivity in various analytical techniques since its first description. As it is presented in this review, FRET in combination with QDs and their superior properties, such as long fluorescence lifetime and resistance to photobleaching, has enabled designing of the new and improved sensors. QD-FRET-based sensor are giving a great contribution to the miniaturization of the sensors. Moreover, QDs immobilization to the inexpensive materials and employing phone cameras as detectors leads toward cheaper detections possibilities, which is a solid proof of their immense potential to be affordable and perhaps applied in everyday life in the future.

6. Future perspectives

We suggest that FRET-based biosensors could be a key for point-of-care diagnostics, which has to be low cost, easy-to-use (color change) and sensitive. Besides this *in vitro* diagnostics, there is an ocean of fields in *in vivo* diagnostics, where FRET would find a good place including tracking of the target molecules, studying of changes in biochemical pathways and cell structures.

Acknowledgments

Financial support from the European funds Project CZ.1.07/2.3.00/30.0039 is highly acknowledged.

Appendix A. Supplementary material

Supplementary data associated with this article can be found in the online version at <http://dx.doi.org/10.1016/j.bios.2015.06.076>.

References

- Adams, F.C., Barbante, C., 2013. Nanoscience, nanotechnology and spectrometry. *Spectrochim. Acta B* 86, 3–13.
- Ahmed, M., Guleria, A., Rath, M.C., Singh, A.K., Adhikari, S., Sarkar, S.K., 2014. Facile and green synthesis of CdSe quantum dots in protein matrix: tuning of morphology and optical properties. *J. Nanosci. Nanotechnol.* 14, 5730–5742.
- Algar, W.R., Krull, U.J., 2007. Towards multi-colour strategies for the detection of oligonucleotide hybridization using quantum dots as energy donors in fluorescence resonance energy transfer (FRET). *Anal. Chim. Acta* 581, 193–201.
- Algar, W.R., Krull, U.J., 2009. Toward a multiplexed solid-phase nucleic acid hybridization assay using quantum dots as donors in fluorescence resonance energy transfer. *Anal. Chem.* 81, 4113–4120.
- Algar, W.R., Krull, U.J., 2010. Multiplexed interfacial transduction of nucleic acid hybridization using a single color of immobilized quantum dot donor and two acceptors in fluorescence resonance energy transfer. *Anal. Chem.* 82, 400–405.
- Alivisatos, A.P., Gu, W.W., Larabell, C., 2005. Quantum dots as cellular probes. *Annu. Rev. Biomed. Eng.* 7, 55–76.
- Bao, H.F., Hao, N., Yang, Y.X., Zhao, D.Y., 2010. Biosynthesis of biocompatible cadmium telluride quantum dots using yeast cells. *Nano Res.* 3, 481–489.
- Beri, R.K., Khanna, P.K., 2011. “Green” synthesis of cadmium selenide nanocrystals: the scope of 1,2,3-selendiazoles in the synthesis of magic-size nanocrystals and quantum dots. *J. Nanosci. Nanotechnol.* 11, 5137–5142.
- Brewster, D., 1834. XIX. On the colours of natural bodies. *Earth Environ. Sci. Transac. R. Soc. Edinb.* 12, 538–545.
- Burris, K.P., Wu, T.C., Vasudev, M., Strosio, M.A., Millwood, R.J., Stewart, C.N., 2013. Mega-nano detection of foodborne pathogens and transgenes using molecular beacon and semiconductor quantum dot technologies. *IEEE Trans. Nanobiosci.* 12, 233–238.
- Duong, H.D., Il Rhee, J., 2007. Use of CdSe/ZnS core-shell quantum dots as energy transfer donors in sensing glucose. *Talanta* 73, 899–905.
- Elangovan, M., Day, R.N., Periasamy, A., 2002. Nanosecond fluorescence resonance energy transfer-fluorescence lifetime imaging microscopy to localize the protein interactions in a single living cell. *J. Microsc.* 205, 3–14.
- Esteve-Turrillas, F.A., Abad-Fuentes, A., 2013. Applications of quantum dots as

- probes in immunosensing of small-sized analytes. *Biosens. Bioelectron.* 41, 12–29.
- Flores-Resendiz, D., Castellanos-Juarez, E., Benitez-Bribiesca, L., 2009. Proteases in cancer progression. *Gac. Med. Mex.* 145, 131–142.
- Förster, T., 1948. Zwischenmolekulare Energiewanderung und Fluoreszenz. *Ann. Phys.* 437, 55–75.
- Fu, A.H., Gu, W.W., Larabell, C., Alivisatos, A.P., 2005. Semiconductor nanocrystals for biological imaging. *Curr. Opin. Neurobiol.* 15, 568–575.
- Ganguly, R., Wang, S.H., Huang, D.J., 2010. Salen derivatives functionalized CdSe-ZnS quantum dots as fluorescent probes for selective Cu(II) and Fe(II) sensing. *Nanosci. Nanotechnol. Lett.* 2, 208–212.
- Gill, R., Bahshi, L., Freeman, R., Willner, I., 2008. Optical detection of glucose and acetylcholine esterase inhibitors by H2O2-sensitive CdSe/ZnS quantum dots. *Angew. Chem. Int. Ed.* 47, 1676–1679.
- Goldman, E.R., Medintz, I.L., Whitley, J.L., Hayhurst, A., Clapp, A.R., Uyeda, H.T., Deschamps, J.R., Lassman, M.E., Mattoussi, H., 2005. A hybrid quantum dot-antibody fragment fluorescence resonance energy transfer-based TNT sensor. *J. Am. Chem. Soc.* 127, 6744–6751.
- Gore, A.H., Kale, M.B., Anbhule, P.V., Patil, S.R., Kolekar, G.B., 2014. A novel FRET probe for selective and sensitive determination of vitamin B-12 by functionalized CdS QDs in aqueous media: applications to pharmaceutical and biomedical analysis. *RSC Adv.* 4, 683–692.
- Guo, J.J., Zhang, Y., Luo, Y.L., Shen, F., Sun, C.Y., 2014. Efficient fluorescence resonance energy transfer between oppositely charged CdTe quantum dots and gold nanoparticles for turn-on fluorescence detection of glyphosate. *Talanta* 125, 385–392.
- Heger, Z., Cernei, N., Krizkova, S., Masarik, M., Kopel, P., Hodek, P., Zitka, O., Adam, V., Kizek, R., 2015. Paramagnetic Nanoparticles as a Platform for FRET-Based Sarcosine Picomolar Detection. *Sci. Rep.* 5, 1–7.
- Herschel, J. W., F., 1845. On a case of superficial colour presented by a homogeneous liquid internally colourless. *Phil. Trans. R. Soc. Lond.* 135, 143–145.
- Hu, B., Hu, L.L., Chen, M.L., Wang, J.H., 2013. A FRET ratiometric fluorescence sensing system for mercury detection and intracellular colorimetric imaging in live HeLa cells. *Biosens. Bioelectron.* 49, 499–505.
- Hu, B., Zhang, L.P., Chen, M.L., Wang, J.H., 2012. The inhibition of fluorescence resonance energy transfer between quantum dots for glucose assay. *Biosens. Bioelectron.* 32, 82–88.
- Huang, H.Q., He, M.X., Wang, W.X., Liu, J.L., Mi, C.C., Xu, S.K., 2012. Biosynthesis of CdS quantum dots in *Saccharomyces cerevisiae* and spectroscopic characterization. *Spectrosc. Spectr. Anal.* 32, 1090–1093.
- Huang, P.C., Jiang, Q., Yu, P., Yang, L.F., Mao, L.Q., 2013a. Alkaline post-treatment of Cd(II)-glutathione coordination polymers: toward green synthesis of water-soluble and cytocompatible CdS quantum dots with tunable optical properties. *ACS Appl. Mater. Interfaces* 5, 5239–5246.
- Huang, S., Qiu, H.N., Xiao, Q., Huang, C.S., Su, W., Hu, B.Q., 2013b. A simple QD-FRET bioprobe for sensitive and specific detection of hepatitis B virus DNA. *J. Fluoresc.* 23, 1089–1098.
- Huang, S., Zhu, F.W., Xiao, Q., Su, W., Sheng, J.R., Huang, C.S., Hu, B.Q., 2014. A CdTe/CdS/ZnS core/shell/shell QDs-based “OFF-ON” fluorescent biosensor for sensitive and specific determination of L-ascorbic acid. *RSC Adv.* 4, 46751–46761.
- Huang, X.Y., Wang, J.J., Liu, H., Lan, T., Ren, J.C., 2013c. Quantum dot-based FRET for sensitive determination of hydrogen peroxide and glucose using tyramide reaction. *Talanta* 106, 79–84.
- Chen, C.Y., Cheng, C.T., Lai, C.W., Wu, P.W., Wu, K.C., Chou, P.T., Chou, Y.H., Chiu, H.T., 2006. Potassium ion recognition by 15-crown-5 functionalized CdSe/ZnS quantum dots in H₂O. *Chem. Commun.* 42, 263–265.
- Chen, H.H., Leong, K.W., 2006. Quantum-dots-FRET nanosensors for detecting unamplified nucleic acids by single molecule detection. *Nanomedicine* 1, 119–122.
- Chen, L., Algar, W.R., Tavares, A.J., Krull, U.J., 2011. Toward a solid-phase nucleic acid hybridization assay within microfluidic channels using immobilized quantum dots as donors in fluorescence resonance energy transfer. *Anal. Bioanal. Chem.* 399, 133–141.
- Chen, L., Zhang, X.W., Zhou, G.H., Xiang, X., Ji, X.H., Zheng, Z.H., He, Z.K., Wang, H.Z., 2012. Simultaneous determination of human enterovirus 71 and coxsackievirus B3 by dual-color quantum dots and homogeneous immunoassay. *Anal. Chem.* 84, 3200–3207.
- Chen, Z., Li, G., Zhang, L., Jiang, J.F., Li, Z., Peng, Z.H., Deng, L., 2008. A new method for the detection of ATP using a quantum-dot-tagged aptamer. *Anal. Bioanal. Chem.* 392, 1185–1188.
- Chou, C.C., Huang, Y.H., 2012. Nucleic acid sandwich hybridization assay with quantum dot-induced fluorescence resonance energy transfer for pathogen detection. *Sensors* 12, 16660–16672.
- Kahn, S.E., Cooper, M.E., Del Prato, S., 2014. Pathophysiology and treatment of type 2 diabetes: perspectives on the past, present, and future. *Lancet* 383, 1068–1083.
- Kattke, M.D., Gao, E.J., Sapsford, K.E., Stephenson, L.D., Kumar, A., 2011. FRET-based quantum dot immunoassay for rapid and sensitive detection of *aspergillus amstelodami*. *Sensors* 11, 6396–6410.
- Kim, H., Petryayeva, E., Algar, W.R., 2014. Enhancement of quantum dot forster resonance energy transfer within paper matrices and application to proteolytic assays. *IEEE J. Sel. Top. Quantum Electron.* 20, 1–20.
- Kim, Y.P., Oh, Y.H., Oh, E., Kim, H.S., 2007. Chip-based protease assay using fluorescence resonance energy transfer between quantum dots and fluorophores. *BioChip J.* 1, 228–233.
- Lakowicz, J., 1999. *Principles of Fluorescence Spectroscopy*. Kluwer Academic/Plenum Publishers, New York, Boston, Dordrecht, London, Moscow.
- Lee, J., Choi, Y., Kim, J., Park, E., Song, R., 2009. Positively charged compact quantum dot-dna complexes for detection of nucleic acids. *ChemPhysChem* 10, 806–811.
- Leriche, G., Budin, G., Darwich, Z., Weltin, D., Mely, Y., Klymchenko, A.S., Wagner, A., 2012. A FRET-based probe with a chemically deactivatable quencher. *Chem. Commun.* 48, 3224–3226.
- Li, J., Mei, F., Li, W.Y., He, X.W., Zhang, Y.K., 2008. Study on the fluorescence resonance energy transfer between CdTe QDs and butyl-rhodamine B in the presence of CTMAB and its application on the detection of Hg(II). *Spectrochim. Acta Part A-Mol. Biomol. Spectrosc.* 70, 811–817.
- Li, L., Tian, G.J., Luo, Y., Brismar, H., Fu, Y., 2013. Blinking, flickering, and correlation in fluorescence of single colloidal CdSe quantum dots with different shells under different excitations. *J. Phys. Chem. C* 117, 4844–4851.
- Liao, Y.H., Zhou, X.M., Xing, D., 2014. Quantum dots and graphene oxide fluorescent switch based multivariate testing strategy for reliable detection of listeria monocytogenes. *ACS Appl. Mater. Interfaces* 6, 9988–9996.
- Liu, B.Y., Zeng, F., Wu, G.F., Wu, S.Z., 2012. Nanoparticles as scaffolds for FRET-based ratiometric detection of mercury ions in water with QDs as donors. *Analyst* 137, 3717–3724.
- Long, F., Shi, H.C., Wang, H.C., 2014. Fluorescence resonance energy transfer based aptasensor for the sensitive and selective detection of 17 beta-estradiol using a quantum dot-bioconjugate as a nano-bioprobe. *RSC Adv.* 4, 2935–2941.
- Mao, J., Lai, S.J., Chang, X.J., Liu, W.S., 2008. Interaction among cadmium sulfide nanoparticles, acridine orange, and deoxyribonucleic acid in fluorescence spectra and a method for deoxyribonucleic acid determination. *J. Fluoresc.* 18, 727–732.
- Mattsson, L., Wegner, K.D., Hildebrandt, N., Soukka, T., 2015. Upconverting nanoparticle to quantum dot FRET for homogeneous double-nano biosensors. *RSC Adv.* 5, 13270–13277.
- Medintz, I.L., Clapp, A.R., Mattoussi, H., Goldman, E.R., Fisher, B., Mauro, J.M., 2003. Self-assembled nanoscale biosensors based on quantum dot FRET donors. *Nat. Mater.* 2, 630–638.
- Medintz, I.L., Clapp, A.R., Brunel, F.M., Teiefenbrunn, T., Uyeda, H.T., Chang, E.L., Deschamps, J.R., Dawson, P.E., Mattoussi, H., 2006. Proteolytic activity monitored by fluorescence resonance energy transfer through quantum-dot-peptide conjugates. *Nat. Mater.* 5, 581–589.
- Meeprasert, A., Hannongbua, S., Rungrotmongkol, T., 2014. Key binding and susceptibility of NS3/4A serine protease inhibitors against hepatitis C virus. *J. Chem. Inf. Model.* 54, 1208–1217.
- Michaels, J., van Noort, G.J.V., Seitz, O., 2014. DNA-triggered dye transfer on a quantum dot. *Bioconjug. Chem.* 25, 18–23.
- Nikiforov, T.T., Beechem, J.M., 2006. Development of homogeneous binding assays based on fluorescence resonance energy transfer between quantum dots and Alexa Fluor fluorophores. *Anal. Biochem.* 357, 68–76.
- Noor, M.O., Krull, U.J., 2013. Paper-based solid-phase multiplexed nucleic acid hybridization assay with tunable dynamic range using immobilized quantum dots as donors in fluorescence resonance energy transfer. *Anal. Chem.* 85, 7502–7511.
- Noor, M.O., Shahmuryan, A., Krull, U.J., 2013. Paper-based solid-phase nucleic acid hybridization assay using immobilized quantum dots as donors in fluorescence resonance energy transfer. *Anal. Chem.* 85, 1860–1867.
- Page, L.E., Zhang, X., Jawaid, A.M., Snee, P.T., 2011. Detection of toxic mercury ions using a ratiometric CdSe/ZnS nanocrystal sensor. *Chem. Commun.* 47, 7773–7775.
- Peng, H., Zhang, L.J., Kjallman, T.H.M., Soeller, C., Travas-Sejdic, J., 2007. DNA hybridization detection with blue luminescent quantum dots and dye-labeled single-stranded DNA. *J. Am. Chem. Soc.* 129, 3048–3049.
- Petryayeva, E., Algar, W.R., 2013. Proteolytic assays on quantum-dot-modified paper substrates using simple optical readout platforms. *Anal. Chem.* 85, 8817–8825.
- Petryayeva, E., Algar, W.R., Krull, U.J., 2013. Adapting fluorescence resonance energy transfer with quantum dot donors for solid-phase hybridization assays in microtiter plate format. *Langmuir* 29, 977–987.
- Pokorna, J., Machala, L., Rezacova, P., Konvalinka, J., 2009. Current and novel inhibitors of HIV protease. *Viruses-Basel* 1, 1209–1239.
- Probst, C.E., Zrazhevskiy, P., Bagalkot, V., Gao, X.H., 2013. Quantum dots as a platform for nanoparticle drug delivery vehicle design. *Adv. Drug Deliv. Rev.* 65, 703–718.
- Revesz, E., Lai, E.P.C., DeRosa, M.C., 2007. Towards a FRET-based ATP biosensor using quantum dot/aptamer-based complexes. *J. Biomol. Struct. Dyn.* 24, 645.
- Rodriguez-Mozaz, S., Marco, M.P., de Alda, M.J.L., Barcelo, D., 2004. Biosensors for environmental applications: future development trends. *Pure Appl. Chem.* 76, 723–752.
- Ruedas-Rama, M.J., Hall, E.A.H., 2009. Multiplexed energy transfer mechanisms in a dual-function quantum dot for zinc and manganese. *Analyst* 134, 159–169.
- Safarpour, H., Safarnejad, M.R., Tabatabaei, M., Mohsenifar, A., Rad, F., Basirat, M., Shahryari, F., Hasanzadeh, F., 2012. Development of a quantum dots FRET-based biosensor for efficient detection of *Polymyxa betae*. *Can. J. Plant Pathol.-Rev. Can. Phytopathol.* 34, 507–515.
- Sapsford, K.E., Farrell, D., Sun, S., Rasooly, A., Mattoussi, H., Medintz, I.L., 2009. Monitoring of enzymatic proteolysis on an electroluminescent-CCD microchip platform using quantum dot-peptide substrates. *Sens. Actuatur B-Chem.* 139, 13–21.
- Sapsford, K.E., Granek, J., Deschamps, J.R., Boeneman, K., Blanco-Canosa, J.B., Dawson, P.E., Susumu, K., Stewart, M.H., Medintz, I.L., 2011. Monitoring botulinum neurotoxin activity with peptide-functionalized quantum dot resonance energy transfer sensors. *ACS Nano* 5, 2687–2699.
- Selvin, P.R., 2000. The renaissance of fluorescence resonance energy transfer. *Nat.*

- Struct. Biol. 7, 730–734.
- Shanehsaz, M., Mohsenifar, A., Hasannia, S., Pirooznia, N., Samaei, Y., Shamsipur, M., 2013. Detection of *Helicobacter pylori* with a nanobiosensor based on fluorescence resonance energy transfer using CdTe quantum dots. *Microchim. Acta* 180, 195–202.
- Shanker, N., Bane, S.L., 2008. Basic aspects of absorption and fluorescence spectroscopy and resonance energy transfer methods. In: Correia, J.J., Detrich, H.W. (Eds.), *Biophysical Tools for Biologists: Vol 1 in Vitro Techniques*. Elsevier Academic Press Inc, San Diego, pp. 213–242.
- Shi, Y.P., Pan, Y., Zhang, H., Zhang, Z.M., Li, M.J., Yi, C.Q., Yang, M.S., 2014. A dual-mode nanosensor based on carbon quantum dots and gold nanoparticles for discriminative detection of glutathione in human plasma. *Biosens. Bioelectron.* 56, 39–45.
- Stoppel, M.H.W., Prangma, J.C., Blum, C., Subramaniam, V., 2013. Blinking statistics of colloidal quantum dots at different excitation wavelengths. *RSC Adv.* 3, 17440–17445.
- Stringer, R.C., Schommer, S., Hoehn, D., Grant, S.A., 2008. Development of an optical biosensor using gold nanoparticles and quantum dots for the detection of porcine reproductive and respiratory syndrome virus. *Sens. Actuator B-Chem.* 134, 427–431.
- Sturzenbaum, S.R., Hockner, M., Panneerselvam, A., Levitt, J., Bouillard, J.S., Taniguchi, S., Dailey, L.A., Khanbeigi, R.A., Rosca, E.V., Thanou, M., Suhling, K., Zayats, A.V., Green, M., 2013. Biosynthesis of luminescent quantum dots in an earthworm. *Nat. Nanotechnol.* 8, 57–60.
- Sun, J.J., Goldys, E.M., 2008. Linear absorption and molar extinction coefficients in direct semiconductor quantum dots. *J. Phys. Chem. C* 112, 9261–9266.
- Tang, B., Cao, L.H., Xu, K.H., Zhuo, L.H., Ge, J.H., Li, Q.F., Yu, L.J., 2008. A new nanobiosensor for glucose with high sensitivity and selectivity in serum based on fluorescence resonance energy transfer (FRET) between CdTe quantum dots and an nanoparticles. *Chem.-Eur. J* 14, 3637–3644.
- Tao, H.L., Liao, X.F., Xu, M.Z., Li, S.H., Zhong, F.X., Yi, Z.S., 2014. Determination of trace Hg²⁺ ions based on the fluorescence resonance energy transfer between fluorescent brightener and CdTe quantum dots. *J. Lumines* 146, 376–381.
- Tavares, A.J., Noor, M.O., Vannoy, C.H., Algar, W.R., Krull, U.J., 2012. On-chip transduction of nucleic acid hybridization using spatial profiles of immobilized quantum dots and fluorescence resonance energy transfer. *Anal. Chem.* 84, 312–319.
- Tian, J.P., Zhao, H.M., Liu, M., Chen, Y.Q., Quan, X., 2012. Detection of influenza A virus based on fluorescence resonance energy transfer from quantum dots to carbon nanotubes. *Anal. Chim. Acta* 723, 83–87.
- Tirado-Guizar, A., Pina-Luis, G., Paraguay-Delgado, F., Ramirez-Herrera, D., 2014. Size-dependent enhanced energy transfer from tryptophan to CdSe/mercaptotripropionic acid quantum dots: a new fluorescence resonance energy transfer nanosensor. *Sci. Adv. Mater.* 6, 492–499.
- Uhl, J.R., Tang, Y.W., Cockerill, E.R., 2011. Fluorescence Resonance Energy Transfer, *Amer. Soc. Microbiology*.
- Vaishnavi, E., Renganathan, R., 2013. CdTe quantum dot as a fluorescence probe for vitamin B-12 in dosage form. *Spectrochim. Acta Part. A-Mol. Biomol. Spectrosc.* 115, 603–609.
- Vannoy, C.H., Chong, L., Le, C., Krull, U.J., 2013. A competitive displacement assay with quantum dots as fluorescence resonance energy transfer donors. *Anal. Chim. Acta* 759, 92–99.
- Vinayaka, A.C., Thakur, M.S., 2013. Facile synthesis and photophysical characterization of luminescent CdTe quantum dots for Forster resonance energy transfer based immunosensing of staphylococcal enterotoxin B. *Luminescence* 28, 827–835.
- Walling, M.A., Novak, J.A., Shepard, J.R.E., 2009. Quantum dots for live cell and in vivo imaging. *Int. J. Mol. Sci* 10, 441–491.
- Wang, D., Chen, H., Li, H., He, Q.Z., Ding, X.H., Deng, L., 2011. Detection of staphylococcus aureus carrying the gene for toxic shock syndrome toxin 1 by quantum-dot-probe complexes. *J. Fluoresc.* 21, 1525–1530.
- Wang, X., Guo, X.Q., 2009. Ultrasensitive Pb(2+) detection based on fluorescence resonance energy transfer (FRET) between quantum dots and gold nanoparticles. *Analyst* 134, 1348–1354.
- Wang, X., Lou, X.H., Wang, Y., Guo, Q.C., Fang, Z., Zhong, X.H., Mao, H.J., Jin, Q.H., Wu, L., Zhao, H., Zhao, J.L., 2010. QDs-DNA nanosensor for the detection of hepatitis B virus DNA and the single-base mutants. *Biosens. Bioelectron.* 25, 1934–1940.
- Wang, X., Sheng, P.T., Zhou, L.P., Tong, X., Shi, L., Cai, Q.Y., 2014a. Fluorescence immunoassay of octachlorostyrene based on Forster resonance energy transfer between CdTe quantum dots and rhodamine B. *Biosens. Bioelectron.* 60, 52–56.
- Wang, Y.H., Gao, D.Y., Zhang, P.F., Gong, P., Chen, C., Gao, G.H., Cai, L.T., 2014b. A near infrared fluorescence resonance energy transfer based aptamer biosensor for insulin detection in human plasma. *Chem. Commun.* 50, 811–813.
- Wei, O.D., Lee, M., Yu, X., Lee, E.K., Seong, G.H., Choo, J., Cho, Y.W., 2006. Development of an open sandwich fluoroimmunoassay based on fluorescence resonance energy transfer. *Anal. Biochem.* 358, 31–37.
- Wu, C.S., Oo, M.K.K., Fan, X.D., 2010. Highly sensitive multiplexed heavy metal detection using quantum-dot-labeled DNAs. *ACS Nano* 4, 5897–5904.
- Wu, P., Zhao, T., Wang, S.L., Hou, X.D., 2014. Semiconductor quantum dots-based metal ion probes. *Nanoscale* 6, 43–64.
- Xia, Y.S., Song, L., Zhu, C.Q., 2011. Turn-on and near-infrared fluorescent sensing for 2,4,6-trinitrotoluene based on hybrid (gold nanorod)-(quantum dots) assembly. *Anal. Chem.* 83, 1401–1407.
- Xu, W., Xiong, Y.H., Lai, W.H., Xu, Y., Li, C.M., Xie, M.Y., 2014. A homogeneous immunosensor for AFB₁ detection based on FRET between different-sized quantum dots. *Biosens. Bioelectron.* 56, 144–150.
- Xue, M., Wang, X., Duan, L.L., Gao, W., Ji, L.F., Tang, B., 2012. A new nanoprobe based on FRET between functional quantum dots and gold nanoparticles for fluoride anion and its applications for biological imaging. *Biosens. Bioelectron.* 36, 168–173.
- Yang, P., Zhao, Y., Lu, Y., Xu, Q.Z., Xu, X.W., Dong, L., Yu, S.H., 2011. Phenol formaldehyde resin nanoparticles loaded with CdTe quantum dots: a fluorescence resonance energy transfer probe for optical visual detection of copper(II) ions. *ACS Nano* 5, 2147–2154.
- Yu, W.W., Qu, L.H., Guo, W.Z., Peng, X.G., 2003. Experimental determination of the extinction coefficient of CdTe, CdSe, and CdS nanocrystals. *Chem. Mater.* 15, 2854–2860.
- Zekavati, R., Safi, S., Hashemi, S.J., Rahmani-Cherati, T., Tabatabaei, M., Mohsenifar, A., Bayat, M., 2013. Highly sensitive FRET-based fluorescence immunoassay for aflatoxin B1 using cadmium telluride quantum dots. *Microchim. Acta* 180, 1217–1223.
- Zhang, C.Y., Johnson, L.W., 2006. Quantum dot-based fluorescence resonance energy transfer with improved FRET efficiency in capillary flows. *Anal. Chem.* 78, 5532–5537.
- Zhang, C.Y., Yeh, H.C., Kuroki, M.T., Wang, T.H., 2005. Single-quantum-dot-based DNA nanosensor. *Nat. Mater.* 4, 826–831.
- Zhang, K., Mei, Q.S., Guan, G.J., Liu, B.H., Wang, S.H., Zhang, Z.P., 2010. Ligand replacement-induced fluorescence switch of quantum dots for ultrasensitive detection of organophosphorothioate pesticides. *Anal. Chem.* 82, 9579–9586.
- Zhang, Y.M., Yang, X.J., Gao, Z.Q., 2015. In situ polymerization of aniline on carbon quantum dots: a new platform for ultrasensitive detection of glucose and hydrogen peroxide. *RSC Adv.* 5, 21675–21680.
- Zhao, Q., Rong, X.L., Ma, H.B., Tao, G.H., 2013. Dithizone functionalized CdSe/CdS quantum dots as turn-on fluorescent probe for ultrasensitive detection of lead ion. *J. Hazard. Mater.* 250, 45–52.
- Zhou, D.J., Ying, L.M., Hong, X., Hall, E.A., Abell, C., Klenerman, D., 2008. A compact functional quantum dot-DNA conjugate: preparation, hybridization, and specific label-free DNA detection. *Langmuir* 24, 1659–1664.
- Zrazhevskiy, P., Sena, M., Gao, X.H., 2010. Designing multifunctional quantum dots for bioimaging, detection, and drug delivery. *Chem. Soc. Rev.* 39, 4326–4354.

Article 2

Dostalova S, Cerna T, Hynek D, Koudelkova Z, Vaculovic T, Kopel P, Hrabeta J, Heger Z, **Vaculovicova M**, Eckschlager T, Stiborova M, Adam V. Site-directed conjugation of antibodies to apoferritin nanocarrier for targeted drug delivery to prostate cancer cells. ACS Appl Mater Interfaces 2016;8(23):14430-14441.

Site-Directed Conjugation of Antibodies to Apoferritin Nanocarrier for Targeted Drug Delivery to Prostate Cancer Cells

Simona Dostalova,^{†,‡} Tereza Cerna,^{§,||} David Hynek,^{†,‡} Zuzana Koudelkova,^{†,‡} Tomas Vaculovic,[‡] Pavel Kopel,^{†,‡} Jan Hrabeta,[§] Zbynek Heger,^{†,‡} Marketa Vaculovicova,^{†,‡} Tomas Eckschlager,[§] Marie Stiborova,^{||} and Vojtech Adam^{*,†,‡}

[†]Department of Chemistry and Biochemistry, Mendel University in Brno, Zemedelska 1, Brno CZ-613 00, Czech Republic

[‡]Central European Institute of Technology, Brno University of Technology, Purkynova 123, Brno CZ-612 00, Czech Republic

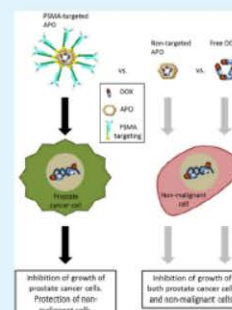
[§]Department of Pediatric Hematology and Oncology, Second Faculty of Medicine, Charles University in Prague and University Hospital Motol, V Uvalu 84/1, Prague 5 CZ-150 06, Czech Republic

^{||}Department of Biochemistry, Faculty of Science, Charles University in Prague, Hlavova 2030/8, Prague 2 CZ-128 43, Czech Republic

^{*}Department of Chemistry, Faculty of Science, Masaryk University, Kotlarska 2, Brno CZ-611 37, Czech Republic

ABSTRACT: Herein, we describe a novel approach for targeting of ubiquitous protein apoferritin (APO)-encapsulating doxorubicin (DOX) to prostate cancer using antibodies against prostate-specific membrane antigen (PSMA). The conjugation of anti-PSMA antibodies and APO was carried out using HWRGWVC heptapeptide, providing their site-directed orientation. The prostate-cancer-targeted and nontargeted nanocarriers were tested using LNCaP and HUVEC cell lines. A total of 90% of LNCaP cells died after treatment with DOX (0.25 μM) or DOX in nontargeted and prostate-cancer-targeted APO, proving that the encapsulated DOX toxicity for LNCaP cells remained the same. Free DOX showed higher toxicity for nonmalignant cells, whereas the toxicity was lower after treatment with the same dosage of APO-encapsulated DOX (APODOX) and even more in prostate-cancer-targeted APODOX. Hemolytic assay revealed exceptional hemocompatibility of the entire nanocarrier. The APO encapsulation mechanism ensures applicability using a wide variety of chemotherapeutic drugs, and the presented surface modification enables targeting to various tumors.

KEYWORDS: antibodies, apoferritin, doxorubicin, nanomedicine, targeted drug delivery



1. INTRODUCTION

Using nanomedical approaches for personalized medicine, it is possible to target multiple disease markers and deliver multiple therapeutic agents at once, as required for heterogeneous diseases such as cancer.¹ Conventional cancer treatment is often based on small differences between nonmalignant and cancer cells; thus, the toxicity to nonmalignant cells is enormous, resulting in a significant reduction of therapeutic index of cytostatics. To overcome this phenomenon, therapeutic agents can be protected against unwanted interactions by nanocarriers.¹ Nanocarriers enable delivery of poorly water-soluble drugs² or control the drug release,³ and the advantage of the nanocarrier's small size is employed. Nanoparticles below 100 nm in diameter can utilize the enhanced permeability and retention (EPR) effect in tumors, so they can easily get into irregularly dilated and leaky tumor blood vessels with relatively large pores. Moreover, nanocarriers over 10 nm in size can avoid renal clearance and extravasation from normal blood vessels.⁴

A wide variety of materials, either organic or inorganic, can be used for creating a nanocarrier.⁴ This includes carbon nanotubes,⁵ liposomes,⁶ fullerenes,⁷ micelles,⁵ nanospheres,⁶ emulsions,⁸ or dendrimers.⁵ We recently developed a method using 480 kDa protein apoferritin (APO) as a nanocarrier for

doxorubicin (DOX).^{9,10} APO contains a cage with internal diameter of 8 nm and external diameter of 12 nm in which drug can be enclosed.¹¹ APO may also improve selectivity for cells expressing transferrin receptors (TfR1) that are overexpressed in a number of tumors.¹²

Moreover, to enhance the specificity, targeting peptides or antibodies can be attached to nanocarrier, reducing the amount of drug administered in patient's blood circulation and minimizing the toxicity and side effects.¹ The attachment of antibodies to the nanocarrier surface can be realized by covalent coupling, physical and/or hydrophobic adsorption,¹³ or the frequently used affinity of biotin to streptavidin/avidin.¹⁴ However, this results in creating relatively large nanoparticles where it is not possible to control the site-directed orientation of antibody and where the antibody can contain multiple biotinylated sites. To eliminate these problems, a linker between the antibody and the nanocarrier can be used, ensuring the site-directed orientation.¹³

Received: April 11, 2016

Accepted: May 24, 2016

Published: May 24, 2016

DOX is an anthracycline drug inhibiting the synthesis of nucleic acids,¹⁵ and it is used in the treatment of diverse malignant tumors (e.g., breast or small cell lung cancer).¹⁶ Its fluorescent properties allow easy visualization.⁹ However, this cytostatic drug exhibits some severe side effects, such as cardiotoxicity¹⁷ that can be reduced by its enclosing in nanocarrier such as APO.^{9,10}

In this study, antibody-targeted, APO-mediated, and pH-triggered transport of cytostatic drug DOX was studied using the fluorescent properties of DOX. We present utilization of a site-directed conjugation of antibodies using a combination of advanced nanotechnologies and a short heptapeptide linker. To ensure the specificity, we have exploited anti-PSMA (prostate-specific membrane antigen) antibodies. The functional modification of APO surface with anti-PSMA antibodies was observed using transmission electron microscopy (TEM) and an ELISA-like method. The presented approach significantly impacts the geometry of the resulting delivery system and its biological activity. The influence of targeted and nontargeted APO with encapsulated DOX (APODOX) on nonmalignant and prostate cancer cells was studied using proliferation, spreading, and cell attachment kinetics. Although we have exploited the prostate cancer model for testing, we anticipate that our system is versatile and can be exploited for any cancer disease with known overexpressed transmembrane antigens.

2. METHODS

2.1. Chemicals. All chemicals of ACS purity were obtained from Sigma-Aldrich (St. Louis, MO, USA).

2.2. Encapsulation of DOX into APO. A 200 μL aliquot of 1 $\text{mg}\cdot\text{mL}^{-1}$ DOX was added to 20 μL of 50 $\text{mg}\cdot\text{mL}^{-1}$ horse spleen APO (Sigma-Aldrich, St. Louis, MO, USA) and 100 μL of water. A 2.5 μL aliquot of 1 M hydrochloric acid was added to decrease the solution pH (WTW inoLab, Weilheim, Germany) and dissociate the APO. The solution was mixed for 15 min. Then, 2.5 μL of 1 M sodium hydroxide was added to increase the pH and encapsulate the DOX inside APO (creating APODOX). The mixture was kept at 20 $^{\circ}\text{C}$ for 15 min and then rinsed twice with water using Amicon Ultra-0.5 mL 3 K (Merck Millipore, Billerica, MA, USA). Absorbance and emission spectra of APODOX were subsequently measured using Tecan Infinite 200 PRO (Tecan, Männedorf, Switzerland, excitation wavelength 480 nm and emission wavelengths 515–815 nm).

2.3. Modification of APODOX Surface with Gold. The surface of APODOX was modified either with gold nanoparticles or gold(III) chloride hydrate (HAu). The preparation of gold nanoparticles (AuNP) was as follows: A 0.25 mL aliquot of trisodium citrate (26.5 $\text{mg}\cdot\text{mL}^{-1}$) was added to 10 mL of 1 mM gold(III) chloride hydrate and shaken on an Orbital Shaker (Biosan, Riga, Latvia) at 20 $^{\circ}\text{C}$ for 1 h. The resulting AuNP were 1.4 nm in diameter.

To APODOX, 25 μL of 1 mM solution of AuNP (creating APODOX-Nano) or 200 μL of 1 mM HAu was added (followed with 3 mg of reducing agent NaBH_4 , thus synthesizing AuNP on APO surface, creating APODOX-HAu), and the mixture was shaken at 20 $^{\circ}\text{C}$ for 12 h. The resulting product was rinsed twice with water on Amicon Ultra-0.5 mL 3 K.

2.4. Gel Electrophoresis. APODOX modified with AuNP and HAu were run on 6% nondenaturing PAGE (polyacrylamide gel electrophoresis) using a continuous buffer system. Nondenaturing PAGE gels were prepared and run using 60 mM HEPES with 40 mM imidazole, pH 7.4, buffer systems as described by Kilic et al.¹⁸ The samples were loaded with a loading buffer in 2:1 ratio (50% glycerol). The electrophoretic apparatus was kept at 6 $^{\circ}\text{C}$ to avoid overheating the gels. The DOX was visualized at 312 nm, and the gels were stained with coomassie blue according to Krizkova et al.¹⁹

2.5. Determination of Gold. Mineralized samples of gel were filled up to 10 mL with ultrapure water and analyzed by means of quadrupole inductively coupled plasma mass spectrometer (ICP-MS) Agilent 7500

CE (Agilent, Santa Clara, CA, USA) which is equipped with collision–reaction cell for suppressing polyatomic interferences. Optimization of ICP-MS parameters was performed with respect to maximum S/N ratio of signal of ^{197}Au isotope and minimum oxide formation. Optimized parameters are summarized in Table 1.

Table 1. ICP-MS Parameters Used

| parameter (unit) | value |
|---|-------|
| radio-frequency power (W) | 1500 |
| plasma gas (Ar) ($\text{L}\cdot\text{min}^{-1}$) | 15 |
| sheath gas (Ar) ($\text{L}\cdot\text{min}^{-1}$) | 0.84 |
| carrier gas (Ar) ($\text{L}\cdot\text{min}^{-1}$) | 0.21 |
| He in collision–reaction cell ($\text{mL}\cdot\text{min}^{-1}$) | 2.5 |

Mineralized sample was nebulized into ICP-MS via double-pass Scott spray chamber with Babington nebulizer. The sample uptake was 0.1 $\text{mL}\cdot\text{s}^{-1}$. For suppressing variation of plasma condition and sample uptake, the internal standard was used (water solution containing 100 $\text{ng}\cdot\text{mL}^{-1}$ Tl). The matrix effect was compensated using matrix-matched calibration solutions containing the same amount of acids as well as the mineralized samples. The concentration of ^{197}Au in calibration solution was 0, 0.5, 2.0, and 10 $\text{ng}\cdot\text{mL}^{-1}$.

2.6. Creation of Targeted Nanocarrier. APODOX or APODOX modified with gold (125 μg) was conjugated with 625 ng of HWRGWVC (HWR) peptide (Clonestar Peptide Services, s.r.o., Brno, Czech Republic) at appropriate temperature (20 or 45 $^{\circ}\text{C}$) and 400 rpm for 1 h. Unbound HWR peptide was removed by filtration using Amicon Ultra-0.5 mL 3K at 20 $^{\circ}\text{C}$ and 6000 g for 15 min. A 7 ng aliquot of human IgG antibodies (Sigma-Aldrich, St. Louis, MO, USA) or 17.5 ng aliquot of mouse monoclonal anti-PSMA antibodies (Abcam, Cambridge, UK) was added to the samples and incubated at 20 $^{\circ}\text{C}$ and 600 rpm for 1 h, creating targeted APODOX-Nano-HWR-IgG or APODOX-anti-PSMA, respectively.

2.7. Characterization of Created Nanocarrier. The technique of negative staining was used for the visualization of samples using transmission electron microscopy. For this purpose, organotin compound Nano-W (Nanoprobes, USA) was utilized. Samples ($\sim 4 \mu\text{L}$) were deposited onto 400-mesh copper grids coated with a continuous carbon layer. Dried grids were imaged by a Tecnai F20 microscope (FEI, OR, USA) at 80 000 \times magnification.

The surface zeta potential of the presented nano carrier was measured using the Zetasizer Nano ZS instrument (Malvern Instruments Ltd., Worcestershire, UK). The size of the created nanocarrier was evaluated from TEM images.

FT-IR spectra were collected using a Nicolet iS10 FT-IR spectrometer with diamond attenuated total reflectance (ATR) attachment (Thermo Electron Inc., San Jose, WI, USA). The sample solution was supplied dropwise (5 μL) on the diamond crystal of the ATR cell, and thin film was measured after spontaneous evaporation of the solvent. Infrared spectra were recorded from 4000 to 650 cm^{-1} at a resolution of 2 cm^{-1} . Each spectrum was acquired by adding together 64 interferograms. Spectra were acquired at room temperature (22 $^{\circ}\text{C}$) for each sample. The OMNIC software was used for IR spectra recording and JDXview v0.2 software was used for further spectra evaluation.

The drug release kinetics from APODOX and APODOX-anti-PSMA were evaluated using the Ringer's solution as the imitation of human plasma prepared according to Williams et al.²⁰ and the intracellular fluid according to Corazzari et al.²¹ Samples were incubated for 24 h at 37 $^{\circ}\text{C}$, collected at various time points, and free DOX was removed by filtration using Amicon Ultra-0.5 mL 3K at 20 $^{\circ}\text{C}$ and 6000 g for 15 min.

2.8. ELISA-Like Method for Determination of Individual Components' Influence on Nanocarrier Geometry. A microtiter plate Nunc Maxisorp (Thermo-Fisher Scientific Inc., Waltham, MA, USA) was coated with 50 μL of goat anti-human IgG antibodies diluted with carbonate buffer according to ref 20 to the desired concentration (0.5 or 2 $\mu\text{g}\cdot\text{mL}^{-1}$). The coating was performed at 37 $^{\circ}\text{C}$ for 2 h. The unbound antibodies were removed, and the well surface was blocked with 50 μL of 1% BSA in phosphate-buffered saline (PBS), pH 7.4,

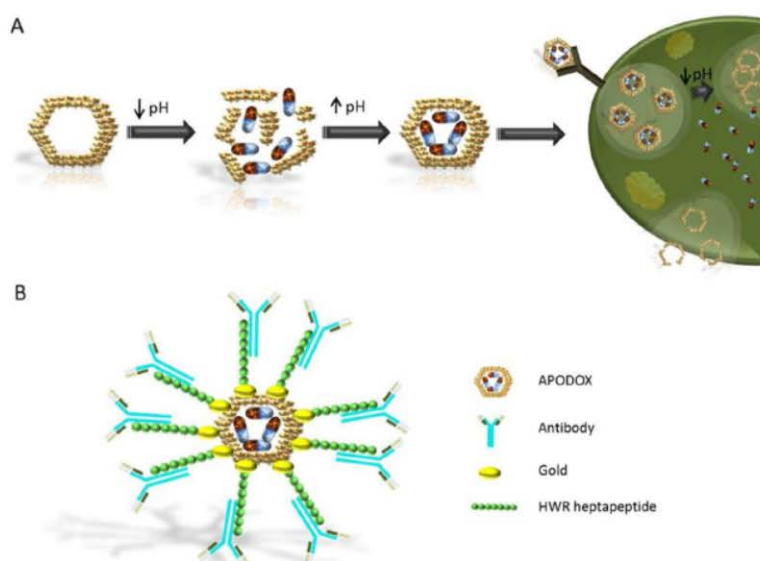


Figure 1. Layout of nanocarrier. (A) Mechanism of pH-dependent drug encapsulation into APO based on pH changes and release from APO during acidification in endosomes. (B) Design of nanocarrier modified with antibodies via specific peptide linker derived from immunoglobulin-binding protein A.

according to ref 20 at 37 °C for 1 h. The wells were washed with 50 μL of PBS-T (PBS with Tween 20). A 50 μL aliquot of nanocarrier was added to each well and incubated at 37 °C for 1 h. Wells were washed with 50 μL of PBS, and to enhance the fluorescent signal, samples were acidified with 2 μL of 1 M HCl (pH 2.8).

2.9. Influence of Nanocarrier on Nonmalignant and Prostate Cancer Cell Lines. Human umbilical vein endothelial cells (HUVEC) were cultured in EBM-2 medium (Lonza, Basel, Switzerland) and Earle's Medium 199 (1 \times) without L-glutamine (GE Healthcare, South Logan, UT, USA) in 1:1 ratio supplemented with 10% fetal bovine serum (Gibco, Gaithersburg, MD, USA), 2 mM L-glutamine (PAA, Vienna, Austria), 100 $\mu\text{g}\cdot\text{mL}^{-1}$ heparin (Sigma-Aldrich, St. Louis, MO, USA), and 50 $\mu\text{g}\cdot\text{mL}^{-1}$ endothelial cell growth supplement (ECGS, Sigma-Aldrich). Human prostate adenocarcinoma derived cell line LNCaP was maintained with RPMI Medium 1640 (1 \times) with GlutaMAX (Gibco) supplemented with 10% fetal bovine serum. Cells were incubated with 5% CO_2 in the air at 37 °C.

Quantitative expression of PSMA on LNCaP and HUVEC cell lines was investigated by flow cytometry. A total of 5×10^5 HUVEC or LNCaP cells were transferred in FACS tubes. Cells were resuspended in 50 μL of PBS and incubated with monoclonal anti-GCPII/-PSMA antibody conjugated to Alexa Fluor 488 (clone GCP-05) (Exbio, Prague, Czech Republic) at 25 °C for 15 min in the dark. Cells were then washed, resuspended in 200 μL of PBS, and immediately analyzed using a BD LSR II flow cytometer (BD Biosciences, Franklin Lakes, NJ, USA).

xCELLigence RTCA DP instrument (Roche Diagnostics GmbH, Basel, Switzerland) was used to evaluate the in vitro cytotoxicity of APODOX, APODOX-anti-PSMA, and free DOX. The background impedance signal was measured using 100 μL of cell culture media with cytostatics. Then, 1.5×10^4 HUVEC or LNCaP cells were seeded in each well of 16-well E-plates (Roche Diagnostics GmbH), followed by incubation at 37 °C with 5% CO_2 . Final concentrations of APODOX, APODOX-anti-PSMA, and DOX were 0.50 μM for HUVEC and 0.25 μM for LNCaP in a 200 μL total volume in each well. Proliferation, spreading, and cell attachment kinetics were monitored every 30 s for first 10 min, then every 30 min for 72 h. Experiments were performed in three independent repetitions. After 72 h of treatment, the cells were stained using the CellEvent Caspase-3/7 Green Flow Cytometry Assay Kit (Thermo Fisher Scientific) according to the manufacturer's protocol

and visualized using the Countess II FL Automated Cell Counter (Thermo Fisher Scientific).

2.10. Red Blood Cell Hemolysis Test. Hemolytic assay was done to check the hemolytic activity of APODOX and APODOX-anti-PSMA on human erythrocytes. Plasma from the fresh blood sample collected from a human donor was removed by multiple washings with 150 mM sodium chloride and centrifugation at 5000 rpm for 5 min. Then, different concentrations of APODOX and APODOX-anti-PSMA (0.25–50 μM) in PBS pH 7.4 were mixed with the RBC and incubated for 1 h at 37 °C. PBS and 0.1% Triton X-100 was used as negative and positive controls, respectively. After completion of the incubation period, the cells were centrifuged, and the absorbance of the supernatant containing lysed erythrocytes was measured at 540 nm. The percentage of hemolysis was determined by the following equation:

$$\% \text{ Hemolysis} = \left[\frac{(A_t - A_c)}{(A_{100\%} - A_c)} \right] \times 100$$

where A_t is the absorbance of the supernatant from samples incubated with the particles, A_c is the absorbance of the supernatant from negative control (PBS), and $A_{100\%}$ is the absorbance of the positive control supernatant (completely lysed RBC incubated in the presence of 0.1% Triton X-100).²²

3. RESULTS

3.1. Layout of Nanocarrier. The drug encapsulation/release in/from APO is pH-dependent. Acidification of APO leads to disassembly into 24 single subunits.²³ After mixing the subunits with DOX and subsequent increase of the pH to physiological conditions, the APO structure is reassembled, and DOX molecules are encapsulated within the cavity.¹⁸ After entering the intracellular region, APODOX is engulfed by lysosomes. Lysosomal acidification significantly contributes to the disassembly of APO and release of DOX. This mechanism is schematically illustrated in Figure 1A. Because of its non-chemical-based encapsulation mechanism, it is possible to use APO for delivery of various drugs, such as DOX,⁹ daunomycin,²⁴ or curcumin.²⁵

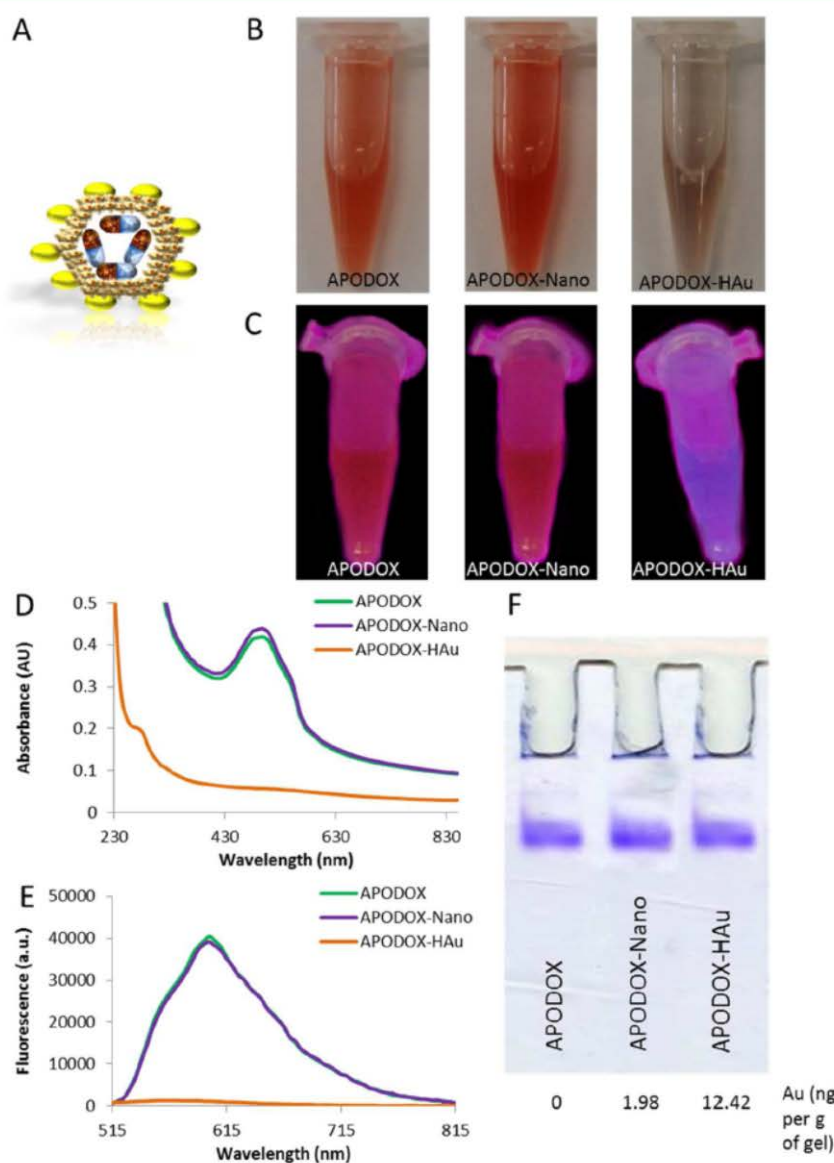


Figure 2. Modification of APODOX with gold. (A) Design of APODOX nanocarrier with surface modification with gold. Visualization of gold-modified and unmodified APODOX in (B) ambient light and (C) UV light (312 nm). (D) Absorbance spectra of gold-modified and unmodified APODOX ($\lambda = 230\text{--}850\text{ nm}$). (E) Fluorescence measurement of gold-modified and unmodified APODOX ($\lambda_{\text{ex}} = 480\text{ nm}$; $\lambda_{\text{em}} = 515\text{--}815\text{ nm}$). (F) Nondenaturing PAGE (6%, 60 mM HEPES with 40 mM imidazole pH 7.4) of gold-modified and unmodified APODOX after 2 h of separation at 10 mA. The Au concentration in cut APO bands measured using ICP-MS equipped with collision–reaction cell.

The surface of APO was modified with targeting antibodies. For the binding of antibodies, HWR peptide linker was used to ensure the correct site-directed orientation of the antibodies. The C-terminus of HWR peptide was made of cysteine and the surface of APO was modified with gold, to which HWR heptapeptide and antibodies were bound. The design of resulting nanocarrier is schematically illustrated in Figure 1B.

3.2. Modification of APO with Gold. Gold nanoparticles and HAu were used to modify the surface of APO. The modified APODOX (Figure 2A) was visualized under ambient (Figure 2B) and UV light (Figure 2C). Optical properties of DOX

changed after modification with HAu (APODOX-HAu) and subsequent reduction with NaBH_4 under both ambient and UV light. There was no significant change after modification with gold nanoparticles (APODOX-Nano).

The changes of optical properties were proven by absorbance (Figure 2D) and fluorescence measurement (Figure 2E). APODOX-HAu showed no apparent absorbance maximum at 280 nm (for DOX), only the absorption maximum at 480 nm (for APO). This was accompanied by a total loss of fluorescence under the appropriate conditions for DOX (excitation wavelength 480 nm). In contrast, the modification with gold

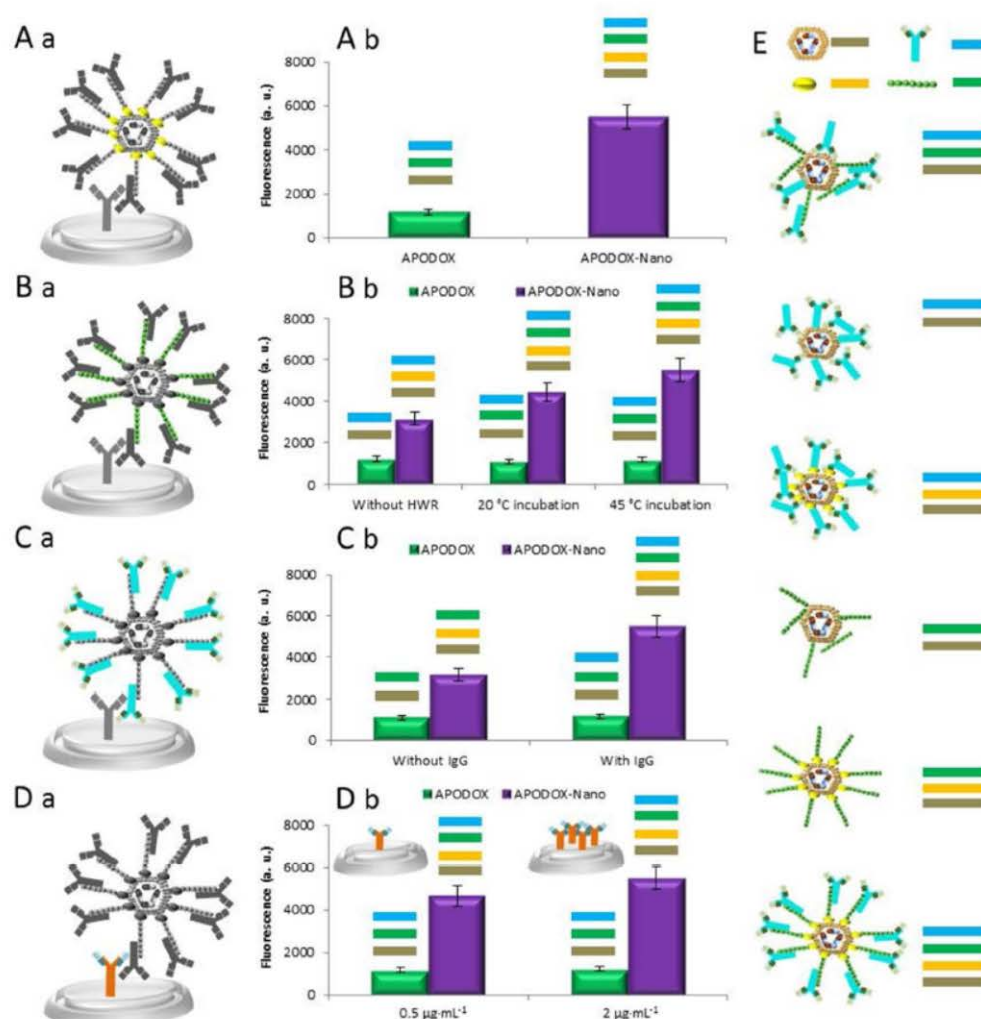


Figure 3. Influence of each component on the nanocarrier geometry using ELISA-like method with 50 μL of nanocarrier, incubated for 1 h in an goat anti-human IgG-coated well revealed by fluorescence ($\lambda_{\text{ex}} = 480 \text{ nm}$, $\lambda_{\text{em}} = 600 \text{ nm}$). (A) Influence of gold nanoparticles. (B) Influence of specific heptapeptide linker. (C) Influence of targeting antibody. (D) Influence of antigen concentration on the amount of bound nanocarrier: a, experimental design with highlighted respective part of nanocarrier; b, influence of the presence of respective part on the amount of bound nanocarrier. (E) Scheme of different compositions of nanocarrier presented in this study.

nanoparticles did not influence DOX fluorescence. It led to only a slight increase in absorbance, but fluorescent properties remained unchanged.

To find whether the gold was bound on the APODOX surface or remained in the solution, we separated APODOX from unbound gold molecules using PAGE (Figure 2F). The APO bands were cut out from the gel and the content of gold was measured by ICP-MS. Higher gold content was measured in APODOX-HAu (12.42 ng per g of gel) than in APODOX-Nano (1.98 ng per g of gel). Nevertheless, APODOX-Nano was used for the following experiments.

3.3. Influence of Individual Components on Nanocarrier Geometry. The influence of each component on nanocarrier ability to bind selectively to the target molecule was studied using an approach similar to the direct ELISA method. The APO surface was modified with human IgG antibodies, and

the surface of a microtiter plate well was coated with goat anti-human IgG. After incubation with the nanocarriers, the well was rinsed to remove unbound molecules and acidified to enhance the fluorescent signal of DOX.

In the first experiment, the influence of gold nanoparticles on the amount of bound nanocarrier was studied (Figure 3A-a). The rest of nanocarrier components remained unchanged; both of the tested nanocarriers were modified with HWR heptapeptide and human IgG antibodies. Figure 3A-b shows the results from fluorescence measurement. The higher fluorescence is associated with a higher amount of nanocarrier bound to the immobilized goat anti-human IgG. A 5-fold higher signal was observed using APODOX-Nano compared to unmodified APODOX.

The second experiment dealt with the influence of HWR peptide and the conditions of incubation of HWR peptide with nanocarrier (Figure 3B-a). Both gold-modified and unmodified

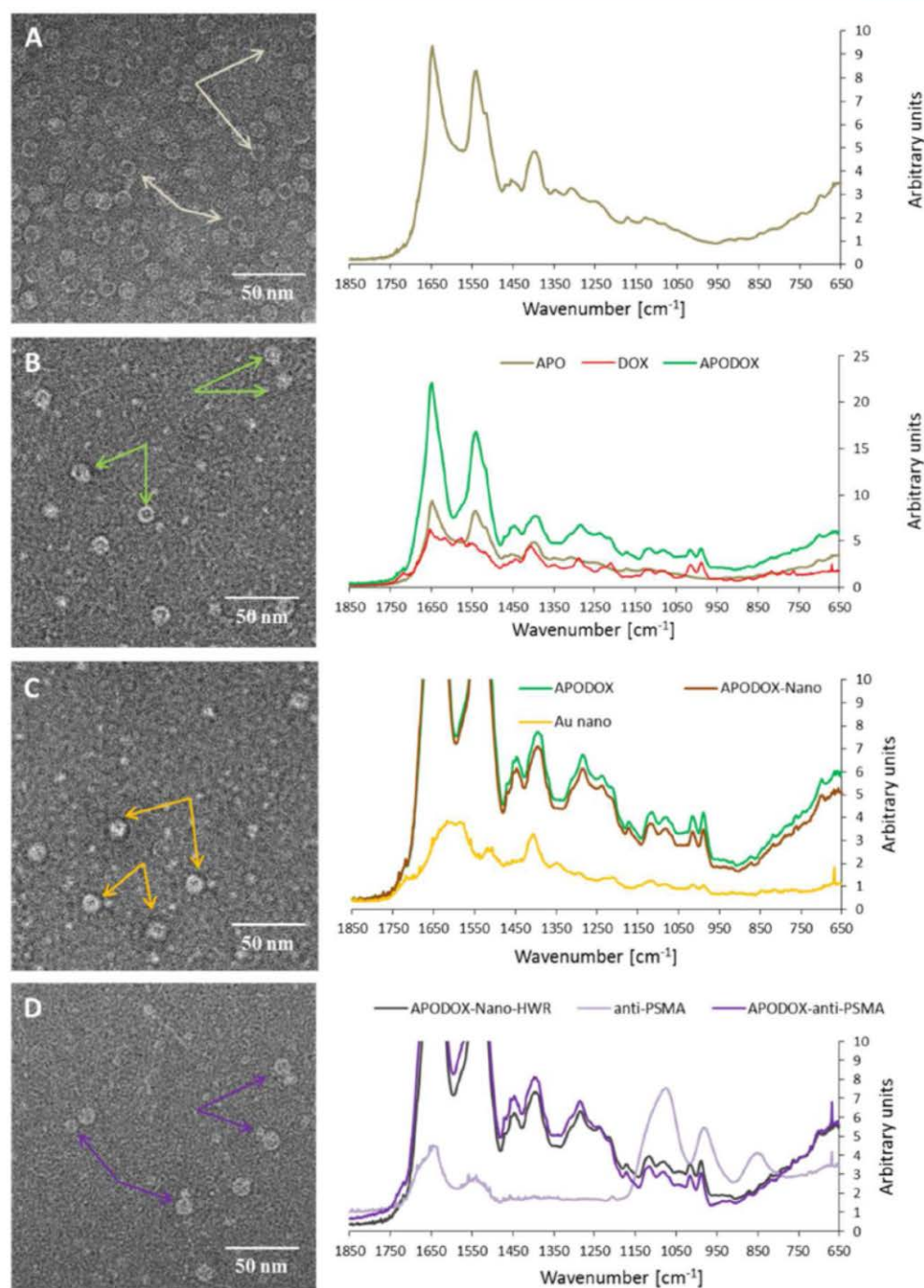


Figure 4. Structural changes of nanocarrier geometry at different stages of its modification with anti-PSMA antibodies revealed by TEM analysis with arrows showing the respective structures and by ATR FT-IR. (A) APO. (B) APODOX. (C) APODOX-Nano. (D) APODOX-Nano-HWR-IgG.

nanocarriers were further conjugated with human IgG antibodies. As can be seen in Figure 3B-b, the presence of HWR heptapeptide had no influence on the targeting ability of the nanocarrier in the case of APODOX. In the case of APODOX-

Nano, a 1.4-fold higher signal was obtained using HWR heptapeptide, and the signal was further increased about 1.7-fold when the interaction between HWR heptapeptide and gold was performed at increased temperature (45 °C).

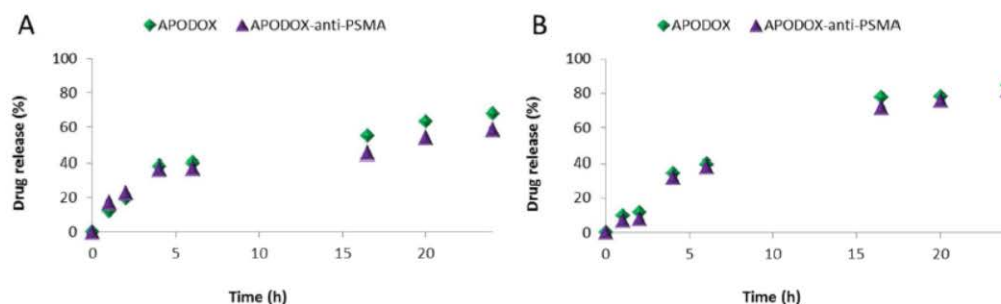


Figure 5. Kinetics of drug release from nontargeted (APODOX) and prostate-cancer-targeted (APODOX-anti-PSMA) nanocarrier in plasma (A) and intracellular environment (B) observed at various time points during 24 h incubation at 37 °C.

In the next experiment, we studied the influence of human IgG antibodies on the amount of bound nanocarrier (Figure 3C-a). The results (Figure 3C-b) showed that the presence or absence of targeting antibodies had no influence on the targeting ability of the nanocarrier in the case of APODOX. In the case of APODOX-Nano, the presence of antibodies significantly (3-fold) increased the targeting ability of nanocarrier.

The last experiment with this experimental design was aimed at investigating the influence of target molecules coating the well surface on the amount of bound nanocarrier (Figure 3D-a). Two different concentrations of goat anti-human IgG antibodies were used for the coating of wells, and the fluorescence of bound nanocarrier was measured (Figure 3D-b). The concentration of target molecules had no influence in the case of APODOX. In the case of APODOX-Nano, the amount of bound nanocarrier was 1.2-fold increased with increasing concentrations of the target molecules. For clarity, all of the different nanocarrier compositions presented in this study are schematically illustrated in Figure 3E.

We also studied the influence of each component on average particle size and zeta potential of the presented nanocarrier (Figure 4). The native APO showed the average particle size of 12 nm with zeta potential of -32.0 mV. Figure 4A shows a TEM image of native APO in which empty cavities in the APO structures can be observed. Figure 4A also shows the ATR FT-IR spectrum of APO.

After encapsulation of DOX (Figure 4B), the cavities observed in the obtained TEM images were filled in all observed APODOX structures, proving successful encapsulation. The average particle size of APODOX remained 12 nm, whereas the zeta potential increased to -19.7 mV. The ATR FT-IR spectroscopy revealed the bands that can be assigned to APO and DOX, proving the presence of both compounds. Only a slight change showing the binding between these two compounds can be observed at 1350 cm^{-1} . Because of the fact that no observable changes in positions of individual bands were present, it can be concluded that only negligible binding interactions are present between these two compounds.

The successful conjugation with gold nanoparticles can be observed as a black layer²⁶ around the surface of APODOX structures (Figure 4C). The average particle size of APODOX-Nano was increased to 14 nm, and the zeta potential was slightly increased to -19.1 mV. The ATR FT-IR spectroscopy revealed residual presence of organic compounds in the gold nanoparticles. Slight changes in the spectrum of APODOX-Nano in comparison with APODOX were observed at 1198, 1370, and

1416 cm^{-1} . These changes showed the binding between gold nanoparticles and APODOX.

After further modification with antibodies, the approximately 8 nm antibodies can be clearly observed on the surface of APO (Figure 4D). The average particle size of APODOX-Nano-HWR-IgG increased to 22 nm, and the created nanocarrier became more stable with a zeta potential of -22 mV. The ATR FT-IR spectroscopy revealed very slight changes in APODOX-Nano spectrum after incubation with HWR peptide at 742, 836, and 1038 cm^{-1} , caused by the binding of HWR to the complex. Only negligible changes at 1222 cm^{-1} were observed after the modification with anti-PSMA antibody.

3.4. Drug Release Kinetics in Plasma and Intracellular Environment. The drug loading efficiency of the presented nanocarrier and the 24 h drug release under the conditions corresponding to conditions in human plasma and intracellular environment were evaluated. The drug loading efficiency of 200 μg of DOX in 1 mg of APO with subsequent surface modifications was calculated as 37%. Ringer's solution as an imitation of human plasma based on the work of Williams et al.²⁰ (Figure 5A) and intracellular fluid based on the work of Corazzari et al.²¹ (Figure 5B) were used for the drug release study. The observed DOX release in plasmatic environment was about 68% for APODOX and 59% for APODOX-anti-PSMA. In the fluid simulating the intracellular environment, the DOX release from APODOX was 85%, and APODOX-anti-PSMA showed 82% release. Therefore, it can be concluded that the surface modification of APODOX-anti-PSMA was able to better protect the cargo from undesired premature release in plasmatic environment (14% lower release) while still retaining the ability to release the drug molecules inside cells (4% lower release).

3.5. Effects of Nanocarrier in Nonmalignant and Prostate Cancer Cells. After the assessment of individual nanocarrier components, an in vitro biological experiment was performed, studying the influence of nontargeted (APODOX) and prostate-cancer-targeted (APODOX-Nano-HWR-anti-PSMA, shortened as APODOX-anti-PSMA) nanocarriers on nonmalignant HUVEC and LNCaP prostate cancer cells.

The proliferation, spreading, and cell attachment kinetics of HUVEC and LNCaP cell lines after treatment with free DOX, APODOX, and APODOX-anti-PSMA during 72 h was studied with the real-time cell analyzer xCELLigence. The LNCaP cell line was treated with 0.25 μM DOX in free form, APO-encapsulated (APODOX), or prostate-cancer-targeted (APODOX-anti-PSMA). The HUVEC cell line was treated accordingly with 0.50 μM DOX, APODOX, or APODOX-anti-PSMA. Figure 6Aa and B-a show representative graphs of the measured

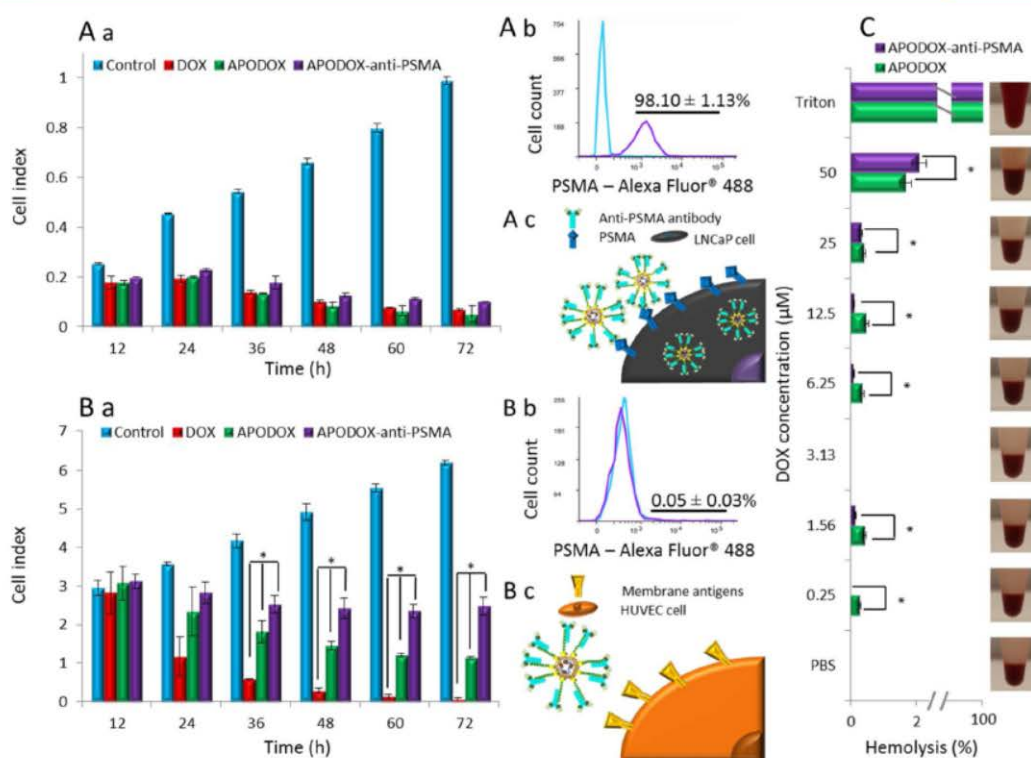


Figure 6. Influence of prostate-cancer-targeted and nontargeted nanocarriers on nonmalignant (HUVEC) and prostate cancer (LNCaP) cell lines. Values are means of three independent replicates ($n = 3$). Vertical bars indicate standard error. Asterisks indicate significant differences at $p < 0.05$ relative to the group treated with DOX (*). (A) Effect of the presented nanocarriers on LNCaP cells revealed by real-time cell analyzer xCELLigence: a, proliferation, spreading, and cell attachment kinetics of 1.5×10^4 of LNCaP cells after 12, 24, 36, 48, 60, and 72 h of treatment with $0.25 \mu\text{M}$ DOX, APODOX, and APODOX-anti-PSMA; b, quantitative expression of PSMA in the membranes of 5×10^5 LNCaP cells investigated by flow cytometry after incubation of cells with anti-PSMA-Alexa Fluor 488 conjugate for 15 min at 20°C in dark. Cyan, unstained cells. Purple, cells with antibody; c, schematic depiction of interactions between nanocarrier and LNCaP expressing PSMA antigen. (B) Effect of the presented nanocarriers on HUVEC cells: a, proliferation, spreading, and cell attachment kinetics of 1.5×10^4 of HUVEC cells after treatment with $0.50 \mu\text{M}$ DOX, APODOX, and APODOX-anti-PSMA; b, quantitative expression of PSMA in the membranes of 5×10^5 HUVEC cells; c, schematic depiction of interactions between nanocarrier and HUVEC cells with limited expression of PSMA antigen. (C) Hemocompatibility assay using RBC in 1:1 ratio with the presented nanocarriers of various concentrations (DOX concentrations of 0.25, 1.56, 3.13, 6.25, 12.5, 25, and $50 \mu\text{M}$) after incubation for 1 h at 37°C , visualization in ambient light, and absorbance measurement (540 nm) with evaluated percentage of hemolytic RBC. Asterisks (*) indicate significant differences at $p < 0.05$ between the group treated with APODOX and APODOX-anti-PSMA.

cell index after 12, 24, 36, 48, 60, and 72 h of treatment for the LNCaP or HUVEC cells, respectively.

The obtained results proved similar sensitivity of LNCaP cancer cell line to all forms of DOX: free DOX, nontargeted APODOX, and prostate-cancer-targeted APODOX-anti-PSMA (Figure 6A-a). After 12 h of treatment, all of the tested forms of DOX showed approximately 30% inhibition of cell growth compared with untreated control, and after 72 h of treatment, all of the tested forms of DOX showed approximately 90% inhibition of cell growth. However, the toxicity of different forms of DOX to nonmalignant HUVEC cells showed significant differences (Figure 6B-a). After 12 h of treatment, all of the tested forms of DOX showed 5% inhibition of cell growth. After 72 h of treatment, free DOX was highly toxic to nonmalignant cells (99% inhibition). However, the cells treated with nontargeted APODOX were spared from DOX toxicity, which resulted in only 82% inhibition of their growth. Nonmalignant cells were further spared using APODOX modified with anti-PSMA antibodies, showing only 57% of cell growth inhibition.

To test the expression of PSMA on the surface of HUVEC and LNCaP cells, flow cytometry with anti-PSMA antibody conjugated with Alexa Fluor 488 was performed. Expression of a high level of PSMA was observed in 98.10% of the LNCaP cells (Figure 6A-b), whereas HUVEC cells lacked PSMA expression (Figure 6B-b). PSMA present on the surface of LNCaP cells enables the targeted APODOX-anti-PSMA nanocarrier to enter these prostate cancer cells and deliver the drug inside (Figure 6A-c). However, the entry of targeted APODOX-anti-PSMA to nonmalignant HUVEC cells expressing no PSMA antigens is hindered (Figure 6B-c).

To evaluate further the toxicity of the presented nanocarriers to nonmalignant cells, a hemocompatibility assay on human RBC was performed using fresh blood from a human donor, via absorbance measurement and visualization in ambient light of lysed RBC (Figure 6C). Both the nontargeted APODOX and prostate-cancer-targeted APODOX-anti-PSMA showed excellent hemocompatibility. Nontargeted APODOX showed approximately 3-fold higher hemolysis than that of prostate-

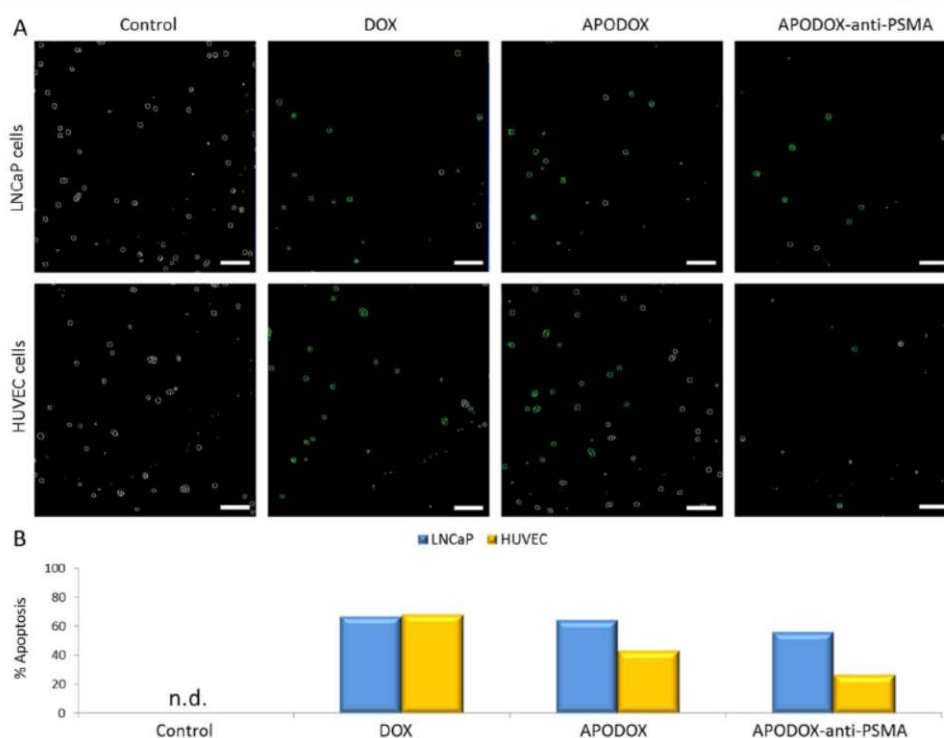


Figure 7. (A) Selected photographs showing fluorescent detection of apoptotic and necrotic cells after 72 h of treatment of 1.5×10^4 LNCaP or HUVEC cell lines with 0.25 (LNCaP) and 0.5 μ M (HUVEC) DOX, APODOX, and APODOX-anti-PSMA performed using CellEvent Caspase-3/7 Green Flow Cytometry Assay Kit and Countess II FL instrument. The length of scale bar is 200 μ m. (B) Calculated percentage of apoptotic cells. No significant necrosis was determined within the tested samples. n.d. indicates no detected apoptosis.

cancer-targeted APODOX-anti-PSMA, but the percentage of hemolysis was $\leq 0.5\%$ for up to 25 μ M DOX in nanocarriers. The highest RBC hemolysis was 1.7 and 2.1%, respectively (observed at 50 μ M of DOX).

The prostate cancer and nonmalignant cells after 72 h of treatment with DOX, APODOX, and APODOX-anti-PSMA were stained using a kit for the fluorescent determination of apoptotic and necrotic cells (Figure 7A,B). In the case of LNCaP prostate cancer cells, the level of apoptosis was comparable for all of the tested forms of DOX, with 67% of apoptotic cells in the case of free DOX, 64% in the case of APODOX, and 56% in the case of APODOX-anti-PSMA. Only a negligible level of necrosis was observed.

In the case of nonmalignant HUVEC cells, the level of apoptosis showed a trend similar to that observed during the proliferation, spreading, and cell attachment kinetics assay with 68% of apoptotic cells in the case of free DOX, 43% apoptosis in the case of APODOX, and 27% apoptosis in the case of APODOX-anti-PSMA. A negligible level of necrosis was observed.

4. DISCUSSION

Various nanocarriers possess many different properties based on their nature, size, encapsulation abilities, surface chemistry, and targeting or releasing mechanisms. These properties influence biodistribution, clearance, toxicity, efficiency, and specificity of the nanocarrier therapeutic application.^{27,28} Releasing mechanisms can be based on pH triggering,²⁹ exposure to ultrasound,³⁰ spontaneous leakage through pores in nanocarrier surface,³¹

temperature,³² light,³³ or contact with some specific substances, such as endolysosomal enzymes,³⁴ vitamins,³⁵ glutathione,³⁶ or matrix metalloprotease 2.³⁷

The drug encapsulation/release in/from APO is based on the apoferritin structure responsiveness to the changes in the surrounding environment. Because of its non-chemical-based encapsulation mechanism, APO can be used for delivery of various drugs such as DOX,⁹ daunomycin,²⁴ or curcumin.²⁵

APO can enter tumor cells via the specific interactions with scavenger receptor class A member 5 (SCARAS) and TfR1 receptors overexpressed in the membranes of tumor cells³⁸ but also is found in the nonmalignant cell membranes.³⁹ To enhance the specificity of APO toward cancer cells, its surface can be modified with a number of targeting molecules such as peptides, aptamers, or antibodies. As a targeting peptide, an RGD derivative is often used, which has high affinity toward integrin $\alpha_v\beta_3$, adhesion molecule expressed by platelets, activated endothelial cells and is up-regulated in different tumor cells.⁴⁰ This approach however requires genetic modification of APO, and the prepared nanocarrier can be prematurely removed from patient's body via the renal clearance as a result of its small size.⁵

To avoid renal clearance and ensure the EPR effect, the size of nanocarrier should be 20–100 nm;⁴¹ thus, it is preferable to modify the surface of APO with larger antibodies. However, simple interaction between nanocarrier surface and antibodies leads to sterically ambiguous complexes with no guarantee of site-directed orientation of antibodies. Therefore, a different approach was used in this work. Proteins A and G are very suitable for immunoglobulin binding because they interact with

their Fc region^{42,43} through histidine on the N-terminus followed by aromatic tryptophan and positively charged arginine,⁴⁴ ensuring site-directed orientation of antibodies.^{45,46} Previously,¹³ we have described HWR heptapeptide based on protein A with cysteine on C-terminus exhibiting high affinity toward gold.⁴⁷ Therefore, the surface of APO was modified with gold, to which HWR heptapeptide and anti-PSMA antibodies were bound. Two different approaches were used to introduce gold nanoparticles on the surface of APODOX. The conjugation of APODOX surface with presynthesized gold nanoparticles did not cause any changes in the DOX properties; however, the reduction of HAu on the surface of APODOX led to significant changes of DOX absorbance and fluorescence, caused likely by the change of DOX structure due to the reduction with NaBH₄ during the modification. Although using the approach of reducing HAu on the surface of APODOX led to higher amount of gold on the APODOX surface as revealed by ICP-MS, as a result of the significant changes in DOX optical properties while reducing HAu on the APODOX surface, APODOX modified with presynthesized gold nanoparticles was used for subsequent experiments.

TEM and ATR FT-IR characterization of the presented nanocarrier conclusively proved the presence of all individual components. Because the encapsulation of DOX in APO is based on physical entrapment,⁴⁸ the spectrum for APODOX showed only one slight change that could be explained by the binding of these two compounds. Nevertheless, ATR FT-IR confirmed the presence of both APO and DOX in APODOX. Compared with APO or DOX, the concentration of gold nanoparticles, HWR, and anti-PSMA antibodies that is applied to this nontargeted nanocarrier during modification is too low for the ATR FT-IR instrument to show significant changes, and only small differences were observed.

The influence of each component on nanocarrier ability to bind selectively to the target molecule was studied using a method similar to direct ELISA. The influence of gold nanoparticles, HWR peptide, targeting antibodies, and the amount of target antibodies on the amount of bound nanocarrier was studied. Without gold modification, the HWR peptide did not always bind to APODOX by cysteine on C-terminus, but it also adsorbed to APODOX by its N-terminus or other parts, thus being unable to bind to the Fc region of targeting antibody and subsequently to the target molecule. Modification with gold favorably influenced the geometry of nanocarrier because other components were able to bind properly. Similar results were observed for HWR and the targeting antibodies. The specificity of nanocarrier binding to the target molecules was also proven. The layout of the nanocarrier was designed with consideration of all its essential parts.

The HWR peptide, derived from protein A, is able to bind to human,⁴⁹ bovine,⁵⁰ mouse,⁵¹ goat,⁵² and rabbit⁵³ immunoglobulins. Because these animals are very often used to produce both monoclonal⁵⁴ and polyclonal⁵⁵ antibodies commercially and because human antibodies can be produced in transgenic animals,⁵⁶ the utilization of HWR peptide offers an opportunity to conveniently immobilize a wide variety of antibodies targeting a number of biologically important antigens.

For the testing of the nanocarrier toxicity for malignant and nonmalignant cells, mouse antibodies with high affinity toward PSMA were chosen. PSMA is a unique membrane-bound glycoprotein, overexpressed manifold in the membranes of many prostate cancer cells including LNCaP⁵⁷ as well as neovasculature of most solid tumors.²¹ The encapsulation of DOX

in APO and its modification with anti-PSMA antibodies does not cause any decrease in DOX toxicity for targeted prostate cancer cells. However, the encapsulation of DOX in APO and its modification with prostate-cancer-targeting antibodies can significantly spare nonmalignant cells from the toxic effects of free DOX. The difference in APODOX toxicity for different cells was likely due to the higher expression of TfR1 in cancer cells compared to that in endothelial cells⁵⁸ because APO can be internalized into the intracellular space of cancer cells after binding to TfR1.¹² The prostate cancer cells showed high expression of PSMA in contrast to the lack of PSMA expression in nonmalignant cells. Antibody-conjugated nanocarriers can enter their target cells via receptor-mediated endocytosis and release the drug in the cells.⁵⁹ Hence, PSMA, which is present on the surface of LNCaP cells, enables the targeted nanocarrier to enter these prostate cancer cells and deliver the drug inside. However, the entry of targeted nanocarrier to nonmalignant cells expressing no PSMA antigens is hindered.

5. CONCLUSIONS

APO can be used for drug delivery with its releasing mechanism suitable for delivery into cancer cells. In this work, we presented an approach offering simple and convenient conjugation of antibodies on a surface of nanocarrier, based on natural interaction between a peptide derivative of immunoglobulin-binding protein A and Fc region of antibodies. We tested the prepared nanocarriers on prostate cancer and nonmalignant endothelial cell lines. The encapsulation of DOX in APO and its modification with targeting antibodies did not cause any decrease in DOX toxicity for target prostate cancer cells. However, the encapsulation of DOX in APO and its further modification with targeting antibodies significantly spared nonmalignant cells from the toxic effects of free DOX. Moreover, the presented nanocarrier showed excellent hemocompatibility.

AUTHOR INFORMATION

Corresponding Author

*E-mail: vojtech.adam@mendelu.cz. Phone: +420-5-4513-3350. Fax: +420-5-4521-2044.

Notes

The authors declare no competing financial interest.

ACKNOWLEDGMENTS

We gratefully acknowledge financial support from the Grant Agency of the Czech Republic (NANOCHEMO GA CR 14-18344S), the Ministry of Health of the Czech Republic for conceptual development of research organization 00064203 (University Hospital Motol, Prague, Czech Republic), and IGA MENDELU IP_28/2016 and CEITEC 2020 LQ1601. We also express our thanks to Dita Munzova, Lucie Dostalova, and Mgr. Michal Horak for perfect technical assistance, Mgr. Jiri Novacek, Ph.D. (CEITEC Core facility, Brno, Czech Republic) for performing the TEM analysis, and Dr. Lukas Richtera for performing the FT-IR analyses.

REFERENCES

- (1) Sumer, B.; Gao, J. M. *Theranostic Nanomedicine for Cancer. Nanomedicine* 2008, 3, 137–140.
- (2) Duncan, R.; Gaspar, R. *Nanomedicine(s) under the Microscope. Mol. Pharmaceutics* 2011, 8, 2101–2141.
- (3) Svenson, S. *Clinical Translation of Nanomedicines. Curr. Opin. Solid State Mater. Sci.* 2012, 16, 287–294.

- (4) Svenson, S. Theranostics: Are We There Yet? *Mol. Pharmaceutics* 2013, 10, 848–856.
- (5) Janib, S. M.; Moses, A. S.; MacKay, J. A. Imaging and Drug Delivery Using Theranostic Nanoparticles. *Adv. Drug Delivery Rev.* 2010, 62, 1052–1063.
- (6) Horcajada, P.; Chalati, T.; Serre, C.; Gillet, B.; Sebrie, C.; Baati, T.; Eubank, J. F.; Heurtaux, D.; Clayette, P.; Kreuz, C.; Chang, J. S.; Hwang, Y. K.; Marsaud, V.; Bories, P. N.; Cynober, L.; Gil, S.; Ferey, G.; Couvreur, P.; Gref, R. Porous Metal-organic-framework Nanoscale Carriers as a Potential Platform for Drug Delivery and Imaging. *Nat. Mater.* 2010, 9, 172–178.
- (7) Chen, Z. Y.; Ma, L. J.; Liu, Y.; Chen, C. Y. Applications of Functionalized Fullerenes in Tumor Theranostics. *Theranostics* 2012, 2, 238–250.
- (8) Yang, X. Q.; Graier, J. J.; Rowland, I. J.; Javadi, A.; Hurley, S. A.; Steeber, D. A.; Gong, S. Q. Multifunctional SPIO/DOX-loaded Wormlike Polymer Vesicles for Cancer Therapy and MR Imaging. *Biomaterials* 2010, 31, 9065–9073.
- (9) Blazkova, L.; Nguyen, H. V.; Dostalova, S.; Kopel, P.; Stanisavljevic, M.; Vaculovicova, M.; Stiborova, M.; Eckschlager, T.; Kizek, R.; Adam, V. Apoferritin Modified Magnetic Particles as Doxorubicin Carriers for Anticancer Drug Delivery. *Int. J. Mol. Sci.* 2013, 14, 13391–13402.
- (10) Tmejova, K.; Hnyek, D.; Kopel, P.; Dostalova, S.; Smerkova, K.; Stanisavljevic, M.; Nguyen, H. V.; Nejd, L.; Vaculovicova, M.; Krizkova, S.; Kizek, R.; Adam, V. Electrochemical Behaviour of Doxorubicin Encapsulated in Apoferritin. *Int. J. Electrochem. Sci.* 2013, 8, 12658–12671.
- (11) Uchida, M.; Klem, M. T.; Allen, M.; Suci, P.; Flenniken, M.; Gillitzer, E.; Varpness, Z.; Liepold, L. O.; Young, M.; Douglas, T. Biological Containers: Protein Cages as Multifunctional Nanoplatfoms. *Adv. Mater.* 2007, 19, 1025–1042.
- (12) Heger, Z.; Skalickova, S.; Zitka, O.; Adam, V.; Kizek, R. Apoferritin Applications in Nanomedicine. *Nanomedicine* 2014, 9, 2233–2245.
- (13) Janu, L.; Stanisavljevic, M.; Krizkova, S.; Sobrova, P.; Vaculovicova, M.; Kizek, R.; Adam, V. Electrophoretic Study of Peptide-mediated Quantum Dot-human Immunoglobulin Bioconjugation. *Electrophoresis* 2013, 34, 2725–2732.
- (14) Sirskyj, D.; Weltzin, R.; Golshani, A.; Anderson, D.; Bozic, J.; Diaz-Mitoma, F.; Azizi, A. Detection of Influenza A and B Neutralizing Antibodies in Vaccinated Ferrets and Macaques Using Specific Biotin-streptavidin Conjugated Antibodies. *J. Virol. Methods* 2010, 163, 459–464.
- (15) Perou, C. M.; Sorlie, T.; Eisen, M. B.; van de Rijn, M.; Jeffrey, S. S.; Rees, C. A.; Pollack, J. R.; Ross, D. T.; Johnsen, H.; Akslen, L. A.; Fluge, O.; Pergamenschikov, A.; Williams, C.; Zhu, S. X.; Lonning, P. E.; Borresen-Dale, A. L.; Brown, P. O.; Botstein, D. Molecular Portraits of Human Breast Tumours. *Nature* 2000, 406, 747–752.
- (16) Huska, D.; Adam, V.; Babula, P.; Hrabeta, J.; Stiborova, M.; Eckschlager, T.; Trnkova, L.; Kizek, R. Square-wave Voltammetry as a Tool for Investigation of Doxorubicin Interactions with DNA Isolated from Neuroblastoma Cells. *Electroanalysis* 2009, 21, 487–494.
- (17) Minotti, G.; Menna, P.; Salvatorelli, E.; Cairo, G.; Gianni, L. Anthracyclines: Molecular Advances and Pharmacologic Developments in Antitumor Activity and Cardiotoxicity. *Pharmacol. Rev.* 2004, 56, 185–229.
- (18) Kilic, M. A.; Ozlu, E.; Calis, S. A Novel Protein-based Anticancer Drug Encapsulating Nanosphere: Apoferritin-doxorubicin Complex. *J. Biomed. Nanotechnol.* 2012, 8, 508–514.
- (19) Krizkova, S.; Adam, V.; Eckschlager, T.; Kizek, R. Using of Chicken Antibodies for Metallothionein Detection in Human Blood Serum and Cadmium-treated Tumour Cell Lines After Dot- and Electroblooming. *Electrophoresis* 2009, 30, 3726–3735.
- (20) Williams, E. L.; Hildebrand, K. L.; McCormick, S. A.; Bedel, M. J. The effect of intravenous lactated Ringer's solution versus 0.9% sodium chloride solution on serum osmolality in human volunteers. *Anesth. Analg.* 1999, 88, 999–1003.
- (21) Corazzari, I.; Gilardino, A.; Dalmazzo, S.; Fubini, B.; Lovisolo, D. Localization of CdSe/ZnS quantum dots in the lysosomal acidic compartment of cultured neurons and its impact on viability: Potential role of ion release. *Toxicol. In Vitro* 2013, 27, 752–759.
- (22) Goswami, S. R.; Sahareen, T.; Singh, M.; Kumar, S. Role of Biogenic Silver Nanoparticles in Disruption of Cell-Cell Adhesion in Staphylococcus Aureus and Escherichia Coli Biofilm. *J. Ind. Eng. Chem.* 2015, 26, 73–80.
- (23) Yau, S. T.; Vekilov, P. G. Direct Observation of Nucleus Structure and Nucleation Pathways in Apoferritin Crystallization. *J. Am. Chem. Soc.* 2001, 123, 1080–1089.
- (24) Luo, Y. A.; Wang, X.; Du, D.; Lin, Y. H. Hyaluronic Acid-conjugated Apoferritin Nanocages for Lung Cancer Targeted Drug Delivery. *Biomater. Sci.* 2015, 3, 1386–1394.
- (25) Geninatti Crich, S.; Cadenazzi, M.; Lanzardo, S.; Conti, L.; Ruiui, R.; Alberti, D.; Cavallo, F.; Cutrin, J. C.; Aime, S. Targeting Ferritin Receptors for the Selective Delivery of Imaging and Therapeutic Agents to Breast Cancer Cells. *Nanoscale* 2015, 7, 6527–6533.
- (26) Natio, P.; Prior, I. A.; Brust, M. Uptake and Intracellular Fate of Surface-modified Gold Nanoparticles. *ACS Nano* 2008, 2, 1639–1644.
- (27) de Jong, W. H.; Borm, P. J. A. Drug Delivery and Nanoparticles: Applications and Hazards. *Int. J. Nanomed.* 2008, 3, 133–149.
- (28) Petros, R. A.; DeSimone, J. M. Strategies in the Design of Nanoparticles for Therapeutic Applications. *Nat. Rev. Drug Discovery* 2010, 9, 615–627.
- (29) Nowag, S.; Haag, R. pH-responsive Micro- and Nanocarrier Systems. *Angew. Chem., Int. Ed.* 2014, 53, 49–51.
- (30) Lin, C. Y.; Javadi, M.; Belnap, D. M.; Barrow, J. R.; Pitt, W. G. Ultrasensitive eLiposomes Containing Doxorubicin for Drug Targeting Therapy. *Nanomedicine* 2014, 10, 67–76.
- (31) Aljuffali, I. A.; Sung, C. T.; Shen, F. M.; Huang, C. T.; Fang, J. Y. Squarticles as a Lipid Nanocarrier for Delivering Diphenylprone and Minoxidil to Hair Follicles and Human Dermal Papilla Cells. *AAPS J.* 2014, 16, 140–150.
- (32) Calejo, M. T.; Sande, S. A.; Nystrom, B. Thermoresponsive Polymers as Gene and Drug Delivery Vectors: Architecture and Mechanism of Action. *Expert Opin. Drug Delivery* 2013, 10, 1669–1686.
- (33) Knezevic, N. Z.; Trewyn, B. G.; Lin, V. S. Y. Light- and pH-responsive Release of Doxorubicin from a Mesoporous Silica-based Nanocarrier. *Chem. - Eur. J.* 2011, 17, 3338–3342.
- (34) Lee, C. S.; Park, W.; Park, S. J.; Na, K. Endolysosomal Environment-responsive Photodynamic Nanocarrier to Enhance Cytosolic Drug Delivery via Photosensitizer-mediated Membrane Disruption. *Biomaterials* 2013, 34, 9227–9236.
- (35) Li, L. L.; Xie, M. Y.; Wang, J.; Li, X. Y.; Wang, C.; Yuan, Q.; Pang, D. W.; Lu, Y.; Tan, W. H. A Vitamin-responsive Mesoporous Nanocarrier with DNA Aptamer-mediated Cell Targeting. *Chem. Commun.* 2013, 49, 5823–5825.
- (36) Zong, S. F.; Wang, Z. Y.; Chen, H.; Yang, J.; Cui, Y. P. Surface Enhanced Raman Scattering Traceable and Glutathione Responsive Nanocarrier for the Intracellular Drug Delivery. *Anal. Chem.* 2013, 85, 2223–2230.
- (37) Zhu, L.; Kate, P.; Torchilin, V. P. Matrix Metalloprotease 2-responsive Multifunctional Liposomal Nanocarrier for Enhanced Tumor Targeting. *ACS Nano* 2012, 6, 3491–3498.
- (38) Xing, R. M.; Wang, X. Y.; Zhang, C. L.; Zhang, Y. M.; Wang, Q.; Yang, Z.; Guo, Z. J. Characterization and Cellular Uptake of Platinum Anticancer Drugs Encapsulated in Apoferritin. *J. Inorg. Biochem.* 2009, 103, 1039–1044.
- (39) Fan, K. L.; Gao, L. Z.; Yan, X. Y. Human Ferritin for Tumor Detection and Therapy. *Wiley Interdiscip. Rev.-Nanomed. Nanobiotechnol.* 2013, 5, 287–298.
- (40) Zhen, Z. P.; Tang, W.; Chen, H. M.; Lin, X.; Todd, T.; Wang, G.; Cowger, T.; Chen, X. Y.; Xie, J. RGD-modified Apoferritin Nanoparticles for Efficient Drug Delivery to Tumors. *ACS Nano* 2013, 7, 4830–4837.
- (41) Choi, H. S.; Liu, W. H.; Liu, F. B.; Nasr, K.; Misra, P.; Bawendi, M. G.; Frangioni, J. V. Design Considerations for Tumor-targeted Nanoparticles. *Nat. Nanotechnol.* 2010, 5, 42–47.

- (42) Sun, X. H.; Yu, D. Q.; Ghosh, R. Study of Hydrophobic Interaction Based Synthetic Membranes Binding of Immunoglobulin G on Synthetic Membranes. *J. Membr. Sci.* **2009**, *344*, 165–171.
- (43) Sun, X. H.; Zhang, G. D.; Keynton, R. S.; O'Toole, M. G.; Patel, D.; Gobin, A. M. Enhanced Drug Delivery via Hyperthermal Membrane Disruption Using Targeted Gold Nanoparticles with PEGylated Protein-G as a Cofactor. *Nanomedicine* **2013**, *9*, 1214–1222.
- (44) Yang, H.; Gurgel, P. V.; Carbonell, R. G. Hexamer Peptide Affinity Resins That Bind the Fc Region of Human Immunoglobulin G. *J. Pept. Res.* **2005**, *66*, 120–137.
- (45) Nagaoka, M.; Akaiki, T. Single Amino Acid Substitution in the Mouse IgG1 Fc Region Induces Drastic Enhancement of the Affinity to Protein A. *Protein Eng., Des. Sel.* **2003**, *16*, 243–245.
- (46) Wines, B. D.; Powell, M. S.; Parren, P.; Barnes, N.; Hogarth, P. M. The IgG Fc Contains Distinct Fc Receptor (FcR) Binding Sites: The Leukocyte Receptors Fc Gamma RI and Fc Gamma RIIa Bind to a Region in the Fc Distinct from That Recognized by Neonatal FcR and Protein A. *J. Immunol.* **2000**, *164*, 5313–5318.
- (47) Hakkinen, H. The Gold-Sulfur Interface at the Nanoscale. *Nat. Chem.* **2012**, *4*, 443–455.
- (48) Zhang, Y. Y.; Tang, Z. W.; Wang, J.; Wu, H.; Lin, C. T.; Lin, Y. H. Apoferritin nanoparticle: a novel and biocompatible carrier for enzyme immobilization with enhanced activity and stability. *J. Mater. Chem.* **2011**, *21*, 17468–17475.
- (49) Murrell, D. S.; Agbaosi, T.; Niedermeyer, S. E.; Penfound, T. A.; Hysmith, N. D.; Dale, J. B. Southern Regional Meeting Abstracts. 212-Bactericidal Activity of Affinity Purified Human Antibodies Against M-related Proteins of Group A Streptococci and Implications for Vaccine Development. *J. Invest. Med.* **2014**, *62*, 471.
- (50) Gunaydin, G.; Zhang, R.; Hammarstrom, L.; Marcotte, H. Engineered Lactobacillus Rhamnosus GG Expressing Igg-Binding Domains of Protein G: Capture of Hyperimmune Bovine Colostrum Antibodies and Protection Against Diarrhea in a Mouse Pup Rotavirus Infection Model. *Vaccine* **2014**, *32*, 470–477.
- (51) Thammavongsa, V.; Rauch, S.; Kim, H. K.; Missiakas, D. M.; Schneewind, O. Protein A-neutralizing Monoclonal Antibody Protects Neonatal Mice Against Staphylococcus Aureus. *Vaccine* **2015**, *33*, 523–526.
- (52) Langone, J. J. I-125-labeled Protein A as a General Tracer in Immunoassay - Suitability of Goat and Sheep Antibodies. *J. Immunol. Methods* **1980**, *34*, 93–106.
- (53) Brady, R. A.; Leid, J. G.; Costerton, W.; Shirliff, M. E. Identification of Proteins Involved in the Antibody-Mediated Immune Response to a Staphylococcus Aureus Osteomyelitis Infection in the Rabbit. In *Abstracts, 105th General Meeting, American Society for Microbiology, Atlanta, Georgia, June 5–9, 2005*; American Society for Microbiology: Washington, DC, 2005; p 335.
- (54) Wang, Z. H.; Mi, T. J.; Beier, R. C.; Zhang, H. Y.; Sheng, Y. J.; Shi, W. M.; Zhang, S. X.; Shen, J. Z. Hapten Synthesis, Monoclonal Antibody Production and Development of a Competitive Indirect Enzyme-linked Immunosorbent Assay for Erythromycin in Milk. *Food Chem.* **2015**, *171*, 98–107.
- (55) Eivazi, S.; Majidi, J.; Aghebati Maleki, L.; Abdolizadeh, J.; Yousefi, M.; Ahmadi, M.; Dadashi, S.; Moradi, Z.; Zolali, E. Production and Purification of a Polyclonal Antibody Against Purified Mouse IgG2b in Rabbits Towards Designing Mouse Monoclonal Isotyping Kits. *Adv. Pharm. Bullet* **2015**, *5*, 109–113.
- (56) Bruggemann, M.; Osborn, M. J.; Ma, B. A.; Hayre, J.; Avis, S.; Lundstrom, B.; Buelow, R. Human Antibody Production in Transgenic Animals. *Arch. Immunol. Ther. Exp.* **2015**, *63*, 101–108.
- (57) Chatalic, K. L. S.; Veldhoven-Zweistra, J.; Bolkestein, M.; Hoeben, S.; Koning, G. A.; Boerman, O. C.; de Jong, M.; van Weerden, W. M. A Novel In-111-Labeled Anti-Prostate-Specific Membrane Antigen Nanobody for Targeted SPECT/CT Imaging of Prostate Cancer. *J. Nucl. Med.* **2015**, *56*, 1094–1099.
- (58) Varshosaz, J.; Farzan, M. Nanoparticles for Targeted Delivery of Therapeutics and Small Interfering RNAs in Hepatocellular Carcinoma. *WJG* **2015**, *21*, 12022–12041.
- (59) Merten, H.; Brandl, F.; Pluckthun, A.; Zangemeister-Wittke, U. Antibody-Drug Conjugates for Tumor Targeting—Novel Conjugation Chemistries and the Promise of non-IgG Binding Proteins. *Bioconjugate Chem.* **2015**, *26*, 2176–2185.

Article 3

Dostalova S, Vasickova K, Hynek D, Krizkova S, Richtera L, Vaculovicova M, Eckschlager T, Stiborova M, Heger Z, Adam V. Apoferritin as an ubiquitous nanocarrier with excellent shelf life. Int J Nanomed 2017;12:2265-2278.

Apo ferritin as an ubiquitous nanocarrier with excellent shelf life

This article was published in the following Dove Press journal:
International Journal of Nanomedicine
24 March 2017
Number of times this article has been viewed

Simona Dostalova^{1,2}
Katerina Vasickova¹
David Hynek^{1,2}
Sona Krizkova^{1,2}
Lukas Richtera^{1,2}
Marketa Vaculovicova^{1,2}
Tomas Eckschlager³
Marie Stiborova⁴
Zbynek Heger^{1,2}
Vojtech Adam^{1,2}

¹Department of Chemistry and Biochemistry, Mendel University in Brno, ²Central European Institute of Technology, Brno University of Technology, Brno, ³Department of Pediatric Hematology and Oncology, Second Faculty of Medicine, University Hospital Motol, Charles University, ⁴Department of Biochemistry, Faculty of Science, Charles University, Prague, Czech Republic

Abstract: Due to many adverse effects of conventional chemotherapy, novel methods of targeting drugs to cancer cells are being investigated. Nanosize carriers are a suitable platform for this specific delivery. Herein, we evaluated the long-term stability of the naturally found protein nanocarrier apoferritin (Apo) with encapsulated doxorubicin (Dox). The encapsulation was performed using Apo's ability to disassemble reversibly into its subunits at low pH (2.7) and reassemble in neutral pH (7.2), physically entrapping drug molecules in its cavity (creating ApoDox). In this study, ApoDox was prepared in water and phosphate-buffered saline and stored for 12 weeks in various conditions (−20°C, 4°C, 20°C, and 37°C in dark, and 4°C and 20°C under ambient light). During storage, a very low amount of prematurely released drug molecules were detected (maximum of 7.5% for ApoDox prepared in PBS and 4.4% for ApoDox prepared in water). Fourier-transform infrared spectra revealed no significant differences in any of the samples after storage. Most of the ApoDox prepared in phosphate-buffered saline and ApoDox prepared in water and stored at −20°C formed very large aggregates (up to 487% of original size). Only ApoDox prepared in water and stored at 4°C showed no significant increase in size or shape. Although this storage caused slower internalization to LNCaP prostate cancer cells, ApoDox (2.5 μM of Dox) still retained its ability to inhibit completely the growth of 1.5×10⁴ LNCaP cells after 72 hours. ApoDox stored at 20°C and 37°C in water was not able to deliver Dox inside the nucleus, and thus did not inhibit the growth of the LNCaP cells. Overall, our study demonstrates that ApoDox has very good stability over the course of 12 weeks when stored properly (at 4°C), and is thus suitable for use as a nanocarrier in the specific delivery of anticancer drugs to patients.

Keywords: anticancer therapy, doxorubicin-loaded apoferritin, encapsulation, long-term stability, protein nanocarriers

Introduction

Doxorubicin (Dox), an anthracycline antibiotic discovered in 1969,¹ is a potent chemotherapeutic drug used in the treatment of various solid and hematological malignancies. These include the most prevalent ones, such as breast,² lung,³ or bladder⁴ cancer, but also less common ones, such as soft-tissue sarcoma⁵ or Hodgkin's lymphoma.⁶ There are several mechanisms through which Dox achieves its high efficacy: intercalation into DNA,⁷ inhibition of topoisomerase II,⁸ and free-radical formation.⁹ These lead to apoptosis, necrosis, autophagy, or senescence. Which of these mechanisms will be the cause of cell death or cell-growth arrest is highly influenced by the individual patient, cell/cancer type, concentration of Dox, and the duration of treatment.¹⁰ Due to its high efficacy, Dox has been included in the biannual World Health Organization's Model List of Essential Medicines since it was first published in 1977.¹¹

The drawback of Dox usage, as well as any other conventional antitumor drugs, is its nonselectivity for cancer cells, resulting in high toxicity for nonmalignant cells. Dox in

Correspondence: Vojtech Adam
Mendel University in Brno, I Zemedelska,
Brno 613 00, Czech Republic
Tel +420 5 4513 3350
Fax +420 5 4521 2044
Email vojtech.adam@mendelu.cz

submit your manuscript | www.dovepress.com
Dovepress
http://dx.doi.org/10.2147/IJN.S139267

International Journal of Nanomedicine 2017:12 2265–2278

2265

© 2017 Dostalova et al. This work is published and licensed by Dove Medical Press Limited. The full terms of this license are available at <http://www.dovepress.com/terms.php> and incorporate the Creative Commons Attribution – Non Commercial (unported, v3.0) License (<http://creativecommons.org/licenses/by-nc/3.0/>). By accessing the work you hereby accept the Terms. Non-commercial uses of the work are permitted without any further permission from Dove Medical Press Limited, provided the work is properly attributed. For permission for commercial use of this work, please see <http://www.dovepress.com/terms.php>.

clinical practice severely affects the heart (causing cumulative dose-limiting cardiotoxicity), liver, and hematopoiesis.¹² The consequences of this toxicity can be apparent immediately after administration of the drug, but they can also take many years to manifest.¹³ Dox causes the formation of reactive oxygen species, and iron oxidation induces a release of cytochrome C from mitochondria, leading to apoptosis.¹⁴ This is most prominent in the heart, where these mechanisms lead to cardiac hypertrophy, but they are also prominent in cells of brain and liver. Dox interference with mitochondrial complexes I and IV, which leads to superoxide increase and vitamin E and antioxidant decrease, has been shown to cause damage to glomeruli in rabbits and mice.¹⁵

Various approaches to mitigate these side effects have been taken. One approach is the coadministration of Dox with a cardioprotective agent.¹⁶ The most studied and clinically used cardioprotective agent is dexrazoxane. This reduces the reactive oxygen species formed by Dox activity, and serves as a chelator of iron. By combining these effects, it reduces the risk of heart failure by almost 80%.¹⁷ However, previous research has shown that dexrazoxane administration may increase the incidence of secondary malignancies.¹⁸

Another approach in mitigating the adverse effects is the encapsulation of Dox inside a suitable nanocarrier,¹⁹ allowing for targeted delivery to diseased tissue while avoiding healthy cells. These nanosized carriers can target diseased tissue and cells via passive targeting (due to their size)²⁰ or active targeting (due to specific moieties on their surface).²¹ Various materials have been tested for targeted Dox delivery, including inorganic,²² polymeric,²³ lipid-based,²⁴ or proteins.²⁵ The first US Food and Drug Administration-approved nanoformulation was liposome-encapsulated Dox (Doxil®/Caelyx® or Myocet®). This nanoformulation was proven to increase the therapeutic index of Dox by significant lowering its toxicity for normal cells.²⁶

The major drawback of liposomal Dox is its short shelf life. While separated, Dox and liposomes can be stored for up to 18 months. The shelf life of liposome-encapsulated Dox, however, is only 5 days when stored at 2°C–8°C.²⁷ Moreover, bare liposomes are often recognized by the mononuclear phagocyte system and removed from the organism, lowering their efficacy. Therefore, stealth coating with polyethylene glycol (PEGylation) is often used.²⁸ However, PEGylated nanocarriers cause other adverse effects, such as swelling of palms and feet (palmar–plantar erythrodysesthesia).²⁶

Due to these reasons, the potential use of alternative nanocarriers naturally present in the human body is being investigated. Nanocarriers prepared using ubiquitous proteins or protein cages appear to be a suitable alternative.²⁵

We have previously employed an ubiquitous protein, apoferritin (Apo), to be a potential carrier for Dox, with a simple-to-use encapsulation protocol (creating ApoDox).²⁹ Also, heavy-chain ferritin,³⁰ as well as other ferritins, have been used for delivery of anticancer drugs,³¹ small nutrients,³² and imaging molecules.³³ Subsequently, we modified the Apo surface with small molecules,³⁴ as well as antibodies for active targeting to cells of a chosen cancer type. We proved that surface-modified ApoDox retained the high toxicity of Dox for targeted cancer cells while sparing 50% of nonmalignant cells.²¹

In this work, we evaluated the long-term stability of ApoDox. For 12 weeks, we continuously monitored changes in undesirable premature Dox release during storage, its optical properties, and the size and ζ -potential of the Apo nanocarrier, as well as its toxicity for prostate cell lines.

Materials and methods

Chemicals

All chemicals of American Chemical Society purity were obtained from Sigma-Aldrich (St Louis, MO, USA), unless otherwise stated. The pH was measured using an InoLab (Xylem, Rye Brook, NY, USA).

Encapsulation of Dox into Apo and its storage

9,600 μL of 1 $\text{mg}\cdot\text{mL}^{-1}$ DOX was added to 960 μL of 50 $\text{mg}\cdot\text{mL}^{-1}$ horse-spleen Apo and 4,800 μL of water, and 120 μL of 1 M hydrochloric acid was added to decrease the pH of the solution and disintegrate the Apo. The solution was mixed for 15 minutes, then 120 μL of 1 M sodium hydroxide was added to increase the pH and encapsulate the Dox inside Apo (creating ApoDox). The solution was mixed for 15 minutes and divided into two equal parts. The parts were diafiltered three times with water or phosphate-buffered saline (PBS; 137 mM NaCl, 2.7 mM KCl, 1.8 mM KH_2PO_4 , and 4.3 mM Na_2HPO_4 , pH 7.4), respectively, using an Amicon® Ultra (0.5 mL 3K; Merck Millipore, Billerica, MA, USA) at 6,000 g for 15 minutes and filled to 24,000 μL with the same solvent used for diafiltration. The samples were divided into 300 μL aliquots to avoid repeated freeze–thaw cycles and stored for 12 weeks at -20°C , 4°C , 20°C , and 37°C , and two of the samples stored at 4°C and 20°C were also stored under ambient light for evaluation of light influence on the stability of the sample.

Characterization of nanocarrier changes during storage

Every week of storage, aliquots from all storage conditions were collected, and prematurely released drug molecules

were removed by diafiltration with the respective solvent using the Amicon Ultra at 6,000 g for 15 minutes. The amount of released drug was determined by measurement of free Dox fluorescence compared with fluorescence of the whole sample. Fluorescence measurement was performed using an Infinite 200 Pro (Tecan, Männedorf, Switzerland) with excitation wavelength of 480 nm and emission wavelengths of 515–815 nm. The encapsulated drug was evaluated by absorbance-scan measurement using the Infinite 200 Pro with wavelengths in the range of 230–850 nm.

Visualization of nanocarriers prior to removal of released drug molecules was performed using transmission electron microscopy (TEM) with negative staining technique. For this purpose, an organotungsten compound, Nano-W (Nanoprobes, Yaphank, NY, USA) was utilized. Then, 4 μL of samples was deposited onto 400-mesh copper grids coated with a continuous carbon layer. Dried grids were imaged by TEM (Tecnai F20; FEI, Hillsboro, OR, USA) at 80,000 \times magnification.

The average size of nanocarriers was determined by quasielastic dynamic light scattering with a Zetasizer Nano ZS (Malvern Instruments, Malvern, UK). Prior to removal of released drug, nanocarriers were diluted 100 \times with distilled water, placed into polystyrene latex cells, and measured at a detector angle of 173 $^\circ$, wavelength of 633 nm, and temperature of 25 $^\circ\text{C}$, with refractive index of dispersive phase 1.45 and 1.333 for dispersive environment. For each measurement, Zen0040 disposable cuvettes (Brand GmbH, Wertheim, Germany) were used, containing 50 μL of sample. Equilibration time was 120 seconds. Measurements were performed in hexaplicate.

The surface ζ -potential of the nanocarrier diluted 20 \times was measured using the Zetasizer Nano ZS. For each measurement, disposable cells (DTS1070) were employed. The number of runs varied between 20 and 40, and calculations considered the diminution of particle concentration based on the Smoluchowski model, with an $F(ka)$ of 1.5 and an equilibration time of 120 seconds. Measurements were performed in triplicate.

Fourier-transform infrared (FT-IR) spectra were collected using a Nicolet iS10 with diamond attenuated total reflection (ATR) attachment (Thermo Fisher Scientific, Waltham, MA, USA). The sample solution was supplied dropwise (5 μL) on the diamond crystal of the ATR cell, and thin film was measured after spontaneous evaporation of the solvent. IR spectra were recorded from 650 to 4,000 cm^{-1} at a resolution of 2 cm^{-1} . Each spectrum was acquired by adding together 64 interferograms. Spectra were acquired at 22 $^\circ\text{C}$ for each sample. Omnic software was used for IR-spectra

recording, and JDXView version 0.2 software was used for further spectra evaluation.

Influence of nanocarrier on prostate cancer cell line

The human prostate adenocarcinoma-derived cell line LNCaP, purchased from Public Health England (London, UK), was maintained in Roswell Park Memorial Institute 1640 medium supplemented with 10% fetal bovine serum. Cells were incubated in 5% CO_2 in air at 37 $^\circ\text{C}$. Cells (10^5) in 1 mL medium were seeded in each of six wells in 12-well culture plates and cultivated for 21 hours. After cultivation, the medium was discarded and replaced with 90 μL of fresh medium containing 34 μM Dox/ApoDox, followed by incubation for 2 hours. Live cells were washed with 200 μL of phosphate buffered saline (PBS) and stained with Hoechst 33342 and CellRox Green stains (Thermo Fisher Scientific) in dilutions of 1:2,000 and 1:500, respectively, and the cells were incubated for 30 minutes. Then cells were washed with 200 μL PBS and studied under inverted fluorescence microscopy (IX 71S8F-3; Olympus, Tokyo, Japan). Cell morphology was recorded under ambient light, the 4',6-diamidin-2-fenylindol (DAPI) filter was used (excitation 360–370 nm, emission 420–460 nm, dichroic mirror 400 nm) for visualization of nuclei, redox stress was monitored using the fluorescein isothiocyanate filter (excitation 460–495 nm, emission 510–550 nm, dichroic mirror 505 nm), and Dox fluorescence was monitored using the Texas Red filter (excitation 545–580 nm, emission 610 nm, dichroic mirror 600 nm) at 200 \times magnification. Photographs were recorded, merged, and processed using Stream Basic software.

An xCelligence real-time cell analysis dual purpose instrument (Hoffman-La Roche Ltd, Basel, Switzerland) was used to evaluate the in vitro cytotoxicity of ApoDox after 12 weeks of storage at various conditions through real-time label-free monitoring of cell impedance. The background impedance signal was measured using 100 μL cell-culture media with ApoDox. Then, 1.5×10^4 LNCaP cells were seeded in each well of 16-well plates (E-plates; Hoffman-La Roche), followed by incubation at 37 $^\circ\text{C}$ in atmosphere with 5% CO_2 . Final concentrations of ApoDox were 2.5 μM in 200 μL total volume in each well. Proliferation, spreading, and cell-attachment kinetics were monitored every 15 minutes for the first 26 hours, then every hour for 72 hours. Experiments were performed in two independent repetitions.

Descriptive statistics

Results are expressed as mean \pm standard deviation, unless noted otherwise. Differences between groups were analyzed using Student's paired *t*-test and analysis of variance. Unless

noted otherwise, the threshold for significance was $P < 0.05$. Statistica 12 software (Statistica, Tulsa, OK, USA) was employed for analyses.

Results and discussion

Experimental design

Ferritins are proteins that serve as one of the detoxifying factors, preventing the formation of reactive oxygen species by transforming ferrous ions into their insoluble ferric form.³⁵ Subsequently, they reversibly store these ferric ions and can transfer them to the site of action.³⁶ Ferritins are found in most organisms and bacteria, including humans,³⁷ and there is very high (85%–90%) interspecies homology of ferritin sequences from the same tissue with low (40%–50%) intraspecies homology of ferritins from different tissues.³⁸

Without the iron content, ferritins self-assemble into hollow rhombic dodecahedral cage Apo, with outer diameter of 12–13 nm and inner diameter of 7–8 nm. The 450–475 kDa shell³⁹ is composed of 24 heavy and light subunits. Horse-spleen Apo (450 kDa), the best-studied Apo,³⁸ can reversibly dissociate and associate based on the surrounding pH.⁴⁰ It has been shown that while disassembled, Apo can be mixed with

drug molecules, and these are encapsulated within the Apo cavity once reassembled.^{29,34,41}

This easy-to-use encapsulation protocol was employed in this work. Figure 1 shows the design of the whole experiment. Horse-spleen Apo was mixed with Dox at a 1:155 molar ratio. The pH was lowered from 6.7 to 2.7 to disassemble the Apo structure, and the mixture was shaken for 15 minutes to create a homogeneous solution. After mixing, the pH was returned back to neutral (7.2), and the mixture was incubated for a further 15 minutes to enable the reassembly of the Apo structure and encapsulation of Dox molecules within (creating ApoDox).

The aim of this study was to evaluate the long-term stability of ApoDox in various conditions. For this purpose, free Dox molecules were removed from ApoDox by diafiltration and filled to 1 mg·mL⁻¹ of Apo with water (final pH 5.6) or PBS (final pH 7.0), which was used as a model of the physiological environment. Prepared samples were aliquoted to avoid repeated freeze–thaw cycles and excess protein loss caused by repeated diafiltration. These aliquots were stored for 12 weeks in the dark and at various temperatures: –20°C, 4°C, 20°C, and 37°C. Since free Dox

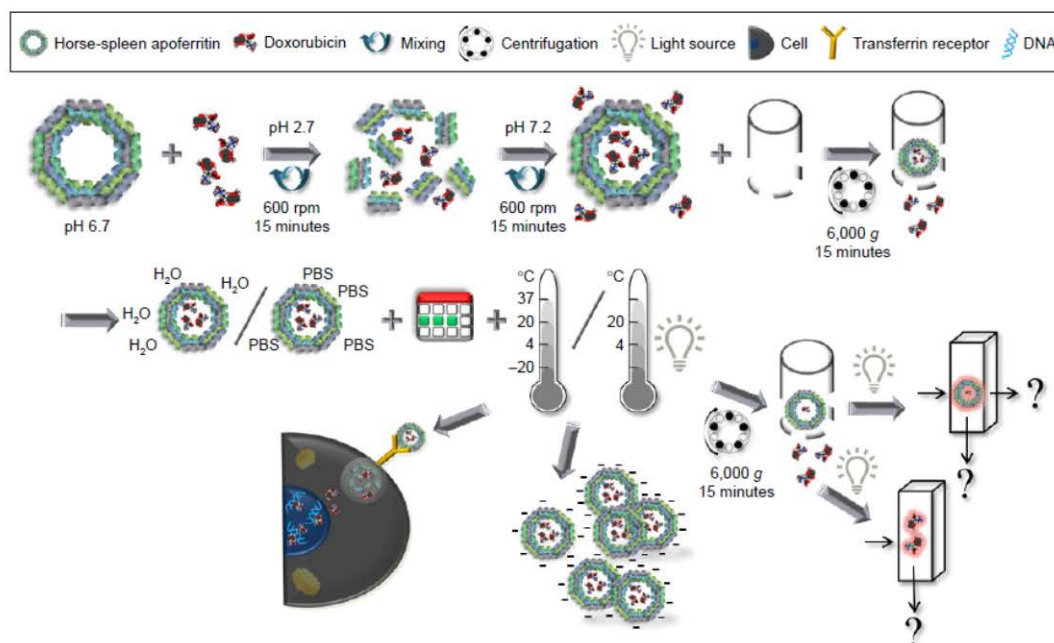


Figure 1 Design of the experiment.

Note: Dox-encapsulation protocol into Apo cavity by employing the responsiveness of the Apo structure to surrounding pH, as well as depiction of various measurements performed to evaluate the long-term (12-week) stability of ApoDox.

Abbreviations: Dox, doxorubicin; Apo, apoferritin; PBS, phosphate-buffered saline.

molecules are degradable by light,⁴² in addition to storage in dark, aliquots stored at 4°C and 20°C were also under direct ambient light to evaluate the influence of illumination during storage on the stability of ApoDox.

Each week of storage, aliquots were collected from the various storage conditions and subjected to multiple analyses. Prematurely released Dox was removed by diafiltration, and the amount of both encapsulated and released Dox was measured using its unique optical properties. Changes in size and surface ζ -potential of nanocarriers were also evaluated each week, as well as their ability to enter cells and release the Dox cargo within them for therapeutic activity.

Optical properties of encapsulated and prematurely released Dox

Dox structure is mainly formed by anisole, quinone, and hydroquinone, along with several residues, such as the amine group, ketone groups, and hydroxyl groups.⁴³ The resulting conjugated system of bonds in Dox tetracene structure

with partially disrupted aromaticity causes typical Dox absorbance, with a maximum at approximately 480 nm, as well as its fluorescence, with emission maximum at approximately 600 nm.⁴⁴

Changes in optical properties of an encapsulated drug, both absorbance and fluorescence, can be caused by different amounts of prematurely released drug, changes in the molecular structure of the drug, or even the structure of the nanocarrier. Absorbance (Figure 2A and C) and fluorescence (Figure 2B and D) of the encapsulated drug in nanocarriers prepared in water (Figure 2A and B) and PBS (Figure 2C and D) were collected every week. The observed changes were rapid, and did not significantly change on a week-to-week basis. The results are thus presented as average change throughout the 12-week period.

Significant ($P < 0.05$) increases in encapsulated drug absorbance were observed in samples stored at most storage temperatures and solutions. No significant changes were observed between samples stored in dark and under ambient

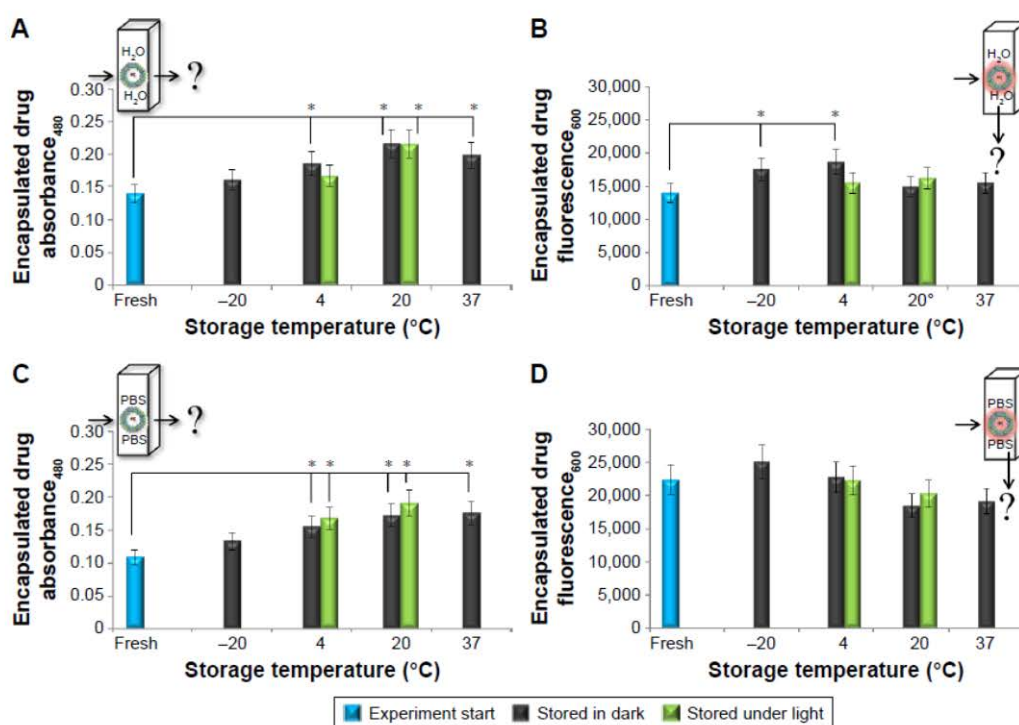


Figure 2 Observed changes in optical properties of Dox encapsulated in Apo prepared in water (A, B) and PBS (C, D).

Notes: (A, C) Absorbance of encapsulated Dox (480 nm). (B, D) Fluorescence of encapsulated Dox (excitation at 480 nm, emission at 600 nm). Values expressed as means of 12 measurements over 12 weeks ($n=12$). * $P < 0.05$ compared with start of experiment or between storage in dark and under direct ambient light.

Abbreviations: Dox, doxorubicin; Apo, apoferritin; PBS, phosphate-buffered saline.

light. At the start of the experiment, absorbance of the encapsulated drug was 0.14 AU for ApoDox prepared in water and 0.11 AU for ApoDox prepared in PBS. The highest absorbance change for nanocarriers prepared in water compared with the state at the start of the experiment was observed for ApoDox stored at 20°C (55% increase, both in dark and under ambient light) and 37°C (42% increase). ApoDox stored at 4°C showed a 33% increase in encapsulated drug absorbance when stored in dark and a nonsignificant 19% increase when stored under ambient light. ApoDox stored at -20°C showed 15% (insignificant) increase in encapsulated drug absorbance.

Absorbance changes for ApoDox prepared in PBS followed the same trend as those prepared in water when compared with freshly prepared ApoDox. The highest absorbance change was again observed for ApoDox stored at 20°C (58% increase for storage in dark and 75% increase for storage under light) and 37°C (62% increase). ApoDox stored at 4°C also showed high change with 42% increase when stored in dark and 54% increase when stored under direct ambient light. ApoDox stored at -20°C showed an insignificant 22% increase in encapsulated drug absorbance. These changes in drug absorbance could account for decreased amounts of prematurely released drug or some structural changes.

Almost no significant ($P < 0.05$) changes were observed in encapsulated drug fluorescence. At the start of the experiment, the fluorescence of the encapsulated drug was 13,936 AU for ApoDox prepared in water and 22,333 AU for ApoDox prepared in PBS. The only significant increases (compared with freshly prepared samples) for ApoDox prepared in water were observed for ApoDox stored at 4°C (34% for storage in dark and nonsignificant 11% for storage under light) and -20°C (25%). ApoDox stored at 37°C

showed a nonsignificant 11% increase in encapsulated drug fluorescence, and ApoDox stored at 20°C showed nonsignificant changes, with 9% increase for storage in dark and 16% increase for storage under ambient light. The increased fluorescence could also account for decreased amounts of prematurely released drug or could indicate some structural changes in the nanocarrier.

Encapsulated drug fluorescence for nanocarriers prepared in PBS did not significantly increase in any of the tested temperatures, contrary to the results from ApoDox prepared in water. The highest fluorescence increase for nanocarriers prepared in PBS was observed for ApoDox stored at -20°C (12%). ApoDox stored at 20°C and 37°C showed a slight decrease in fluorescence (18% for storage in dark and at 20°C and 15% for storage at 37°C). These results did not correspond to the results from encapsulated drug absorbance.

To help explain observed changes, the amount of prematurely released drug from nanocarriers stored under different conditions was evaluated each week. For this evaluation, only Dox fluorescence was employed, since the concentration of the released drug was too low for absorbance detection. The observed changes did not significantly change on a week-to-week basis. The results are thus presented as an average percentage of released drug molecules throughout the 12 week period. Figure 3 shows the percentage of released drug from nanocarriers prepared in water (Figure 3A) and PBS (Figure 3B). Premature release of cargo molecules, whether in patient organism or during storage, is one of the most undesirable properties of a nanocarrier, since it can lead to increased toxicity for healthy cells. Lower premature drug release decreases the nonspecific interactions of the drug molecules with these healthy cells.⁴⁵

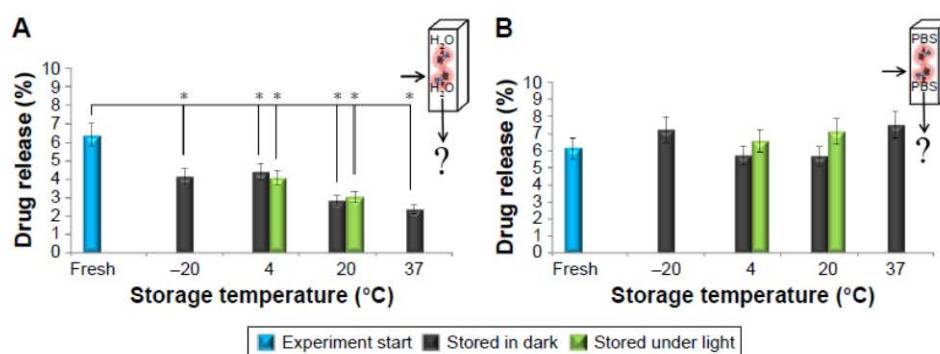


Figure 3 Changes in premature release of encapsulated Dox from Apo cavity as revealed by Dox fluorescence (excitation at 480 nm, emission at 600 nm).

Notes: Release was calculated as percentage of total drug molecules in sample. (A) ApoDox prepared in water. (B) ApoDox prepared in PBS. Values expressed as means of 12 measurements over the course of 12 weeks ($n=12$). * $P < 0.05$ compared with start of experiment or between storage in dark and under direct ambient light.

Abbreviations: Dox, doxorubicin; Apo, apoferritin; PBS, phosphate-buffered saline.

All samples prepared in water and stored at all storage temperatures showed significant ($P < 0.05$) decreases in the amount of prematurely released drug compared to the freshly prepared sample, which is highly favorable. No significant influence of light was detected at the start of the experiment, the percentage of unencapsulated drug was 6.4% for ApoDox prepared in water. The lowest undesired drug release after storage was observed for ApoDox stored at 37°C (2.4%) and 20°C (2.8% for samples stored in dark and 3% for samples stored under ambient light). ApoDox stored at -20°C showed 4.2% release, and ApoDox stored at 4°C showed 4.4% release. The decrease in the prematurely released drug correlated with the observed higher absorbance and fluorescence values of encapsulated drug for samples stored in water (Figure 2).

On the contrary, none of the samples prepared in PBS showed any significant ($P < 0.05$) changes in the amount of prematurely released drug, which is in contrast to the results from encapsulated drug absorbance and correlates with encapsulated drug fluorescence for samples stored in PBS (Figure 2B and D). At the start of the experiment, the percentage of unencapsulated drug was 6.1% for ApoDox prepared in water. The only samples that showed slight decrease in the amount of prematurely released drug were ApoDox stored at 4°C and 20°C, both in dark (5.7%). The highest increase in the amount of prematurely released drug was observed for ApoDox stored at 37°C (7.5%). ApoDox stored at -20°C showed 7.2% release, ApoDox stored under ambient light at 20°C showed 7.1% release, and ApoDox stored under ambient light at 4°C showed 6.6% release. Overall, our premature-release results indicate that the encapsulation of Dox in Apo is stable, with very low premature release over the course of 12 weeks.

Structural changes in ApoDox

Size, shape, and surface charge are among the most important parameters influencing the *in vivo* biodistribution of nanoparticles.⁴⁶ With nanocarriers of suitable size (20–100 nm), it is possible to utilize fully the enhanced permeability and retention (EPR) effect⁴⁷ while avoiding extravasation from normal blood vessels (for particles below 10 nm)⁴⁸ and removal from body through renal clearance (for particles below 5 nm) or elimination by the reticuloendothelial system (RES, for particles larger than 100 nm).⁴⁹ The EPR effect is caused by 1) tumor angiogenesis, where the newly formed blood vessels are underdeveloped and contain large pores, making them leaky, thus increasing accumulation of nanoparticles in tumor tissue; and 2) lack of lymphatic vessels

in tumors, thus increasing retention of nanoparticles in the tissue.⁵⁰ Moreover, there are various modes of entry to cells with which nanoparticles can engage, ie, clathrin- or caveolae-mediated endocytosis, phagocytosis, or macropinocytosis. The size of these nanoparticles has a great impact on the mode of utilized cellular internalization, and thus which microenvironment the nanoparticles will face upon internalization.⁴⁶

Nanoparticle shape can also greatly influence both internalization in cells and removal by the RES. Macrophages rapidly internalize exogenous spherical nanoparticles, shortening their circulation time, and preventing their accumulation in the site of action. In the case of elliptical nanoparticles, the same internalization is observed only if the contact with nanoparticles was along their major axis, whereas contact along the minor axis meant prolonged circulation time and thus higher chance of accumulation in tumors.⁴⁶ Cubic shape favorably influences internalization to target cells, where HeLa cells have been shown to be able to internalize 3 μm cubic nanoparticles, even though they are technically unable to perform phagocytosis.⁵¹

Surface charge influences the internalization of nanoparticles in cells, but its neutralization (as well as increased hydrophilicity) can also slow the opsonization process and removal by the RES.⁴⁶ The higher the charge of nanocarriers is (both cationic and anionic), the easier they are opsonized and removed from the circulation.⁵² Also, positively charged nanocarriers induce opsonization more than negatively charged nanocarriers. In contrast, negatively charged nanocarriers are unable to enter cells via micropinocytosis, and have to be internalized using other forms of endocytosis.⁵³

One of the reasons Apo was chosen in this experiment was its ubiquitous presence in nature and natural property to self-assemble into uniform icosahedral nanocages that are highly stable and do not form aggregates in the physiological environment.³⁸ However, Dox was found to form aggregates containing up to 40 molecules at 0.5 mg·mL⁻¹. This aggregation is highly dependent on Dox concentration (aggregates of more Dox molecules with higher concentration) and its charge (protonated Dox creates fewer aggregates than neutral Dox).⁵⁴ The isoelectric point of Dox has been found to be 8.8.⁵⁵

Changes in shape and size of ApoDox nanocarriers were observed using TEM, and weekly changes in surface ζ-potential were investigated using dynamic light scattering. Figure 4 shows the average changes in shape and ζ-potential for nanocarriers stored in water (Figure 4A) and PBS (Figure 4B).

At the start of the experiment, ApoDox stored in water (Figure 4A, pH 5.6) showed individual Apo nanocarriers with

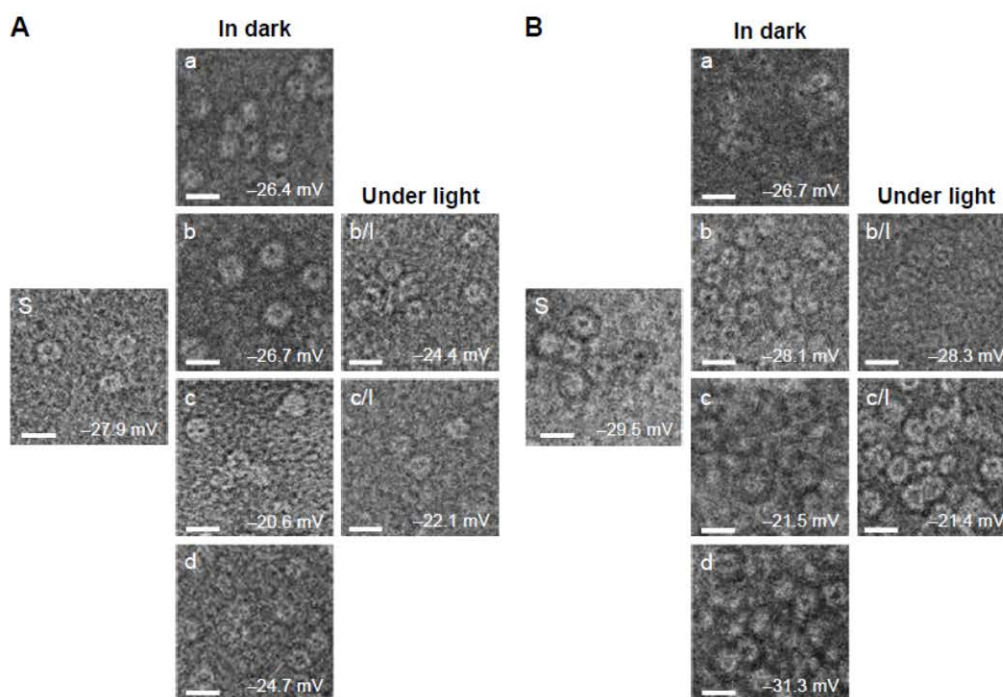


Figure 4 TEM revealing the average changes in the shape for ApoDox prepared in water (**A**) and PBS (**B**).

Notes: Subparts present state at start of experiment (S) and average changes in ζ -potential during storage at -20°C (a), 4°C (storage in dark [b] and storage under direct ambient light [b/l]), 20°C (storage in dark [c] and storage under direct ambient light [c/l]), and 37°C (d). Values expressed as means of 12 measurements over the course of 12 weeks ($n=12$). The length of scale bars is 20 nm.

Abbreviations: TEM, transmission electron microscopy; ApoDox, apoferritin–doxorubicin.

the cavity filled with Dox. Samples stored for 12 weeks at 4°C and in dark (pH 5.7) still showed individual nanocarriers with no change in shape or size, while samples stored at 4°C under light (pH 5.4) showed aggregation of multiple nanocarriers, changing both the size and shape of the nanocarrier, while other nanocarriers remained individual. Most of the ApoDox nanocarriers stored at -20°C (pH 6) formed large multinanocarrier aggregates, changing shape from regular, icosahedral particles to irregular particles. This was probably caused by the higher amount of neutral Dox molecules. ApoDox stored at 20°C (both in dark [pH 5.5] and under light [pH 5.4]), as well as ApoDox stored at 37°C (pH 5.6), also showed formation of aggregates, while some nanocarriers remained individual. These aggregates were probably caused by Dox instability at increased temperatures.⁵⁶ The ζ -potential of samples stored at most storage conditions remained similar to that measured in freshly prepared samples, with the exception of samples stored at 20°C , where negative ζ -potential was lowered from -27.9 mV to -20.6 mV (for storage in dark) and -22.1 mV (for storage under light), showing lower stability.

ApoDox stored in PBS (Figure 4B, pH 7.0) formed aggregates even at the start of the experiment, which could again have been caused by a presence of neutral Dox on the surface of nanocarriers, connecting multiple nanocarriers together. These aggregates remained similar to those found at the start of the experiment in the case of storage at -20°C (pH 6.9). It can be seen that storage at other temperatures (pH 7) caused formation of even larger aggregates of many nanocarriers with a very low number of individual nanocarriers. Such formation of large aggregates explains the increased absorbance of encapsulated drug observed in the previous part of the experiment. The ζ -potential of samples stored under most storage conditions remained similar to that measured in freshly prepared samples, with the exception of samples stored at 20°C , where the negative ζ -potential was lowered from -29.5 mV to -21.5 mV (for storage in dark) and -21.4 mV (for storage under light), showing lower stability of the nanocarrier.

We further investigated changes in nanocarrier size. The observed changes were again rapid, and did not significantly change on a week-to-week basis. The results are thus

presented as average change throughout the 12-week period (Figure 5A and C). Also, ATR FT-IR spectra of the nanocarriers were collected (Figure 5B and D).

There was a significant ($P < 0.05$) increase in size of ApoDox nanocarriers in samples stored at most storage temperatures and solutions, as well as between most samples stored in dark and under ambient light. The highest change in average size for ApoDox prepared in water (Figure 5A) was observed in ApoDox stored at -20°C (304% increase in size), corresponding to the changes observed using TEM. ApoDox stored at 4°C and in dark showed no significant increase in size, while samples stored under ambient light showed 152% increase in size. ApoDox stored at 20°C showed 67% increase in size while stored in dark and 123% increase in size while stored under ambient light. ApoDox stored at 37°C showed 68% increase in size. ATR FT-IR spectra showed no changes in any of the ApoDox samples stored at various conditions (Figure 5B).

Significant ($P < 0.05$) increase in size was observed in all samples prepared in PBS (Figure 5C). The highest increase was observed for ApoDox stored at 4°C (362% for storage in dark and 487% for storage under ambient light). ApoDox stored at -20°C showed 126% increase in size, while ApoDox stored at 20°C showed 318% (stored in dark) and 244% (stored under light) increase in size. ApoDox stored at 37°C showed 405% increase in size. ATR FT-IR spectra showed no changes in any of the ApoDox samples stored in various conditions (Figure 5D). The large differences observed between samples stored in dark and under ambient light could have been caused by photodegradation of Dox molecules.⁴² These molecules were shown to be encapsulated not only within the Apo cavity (up to 28 Dox molecules per Apo molecule)⁴¹ but also attached by Dox–Apo π – π interactions on the external surface of Apo.⁴³ The degraded Dox products could have been one of the reasons for the formation of the observed aggregates.

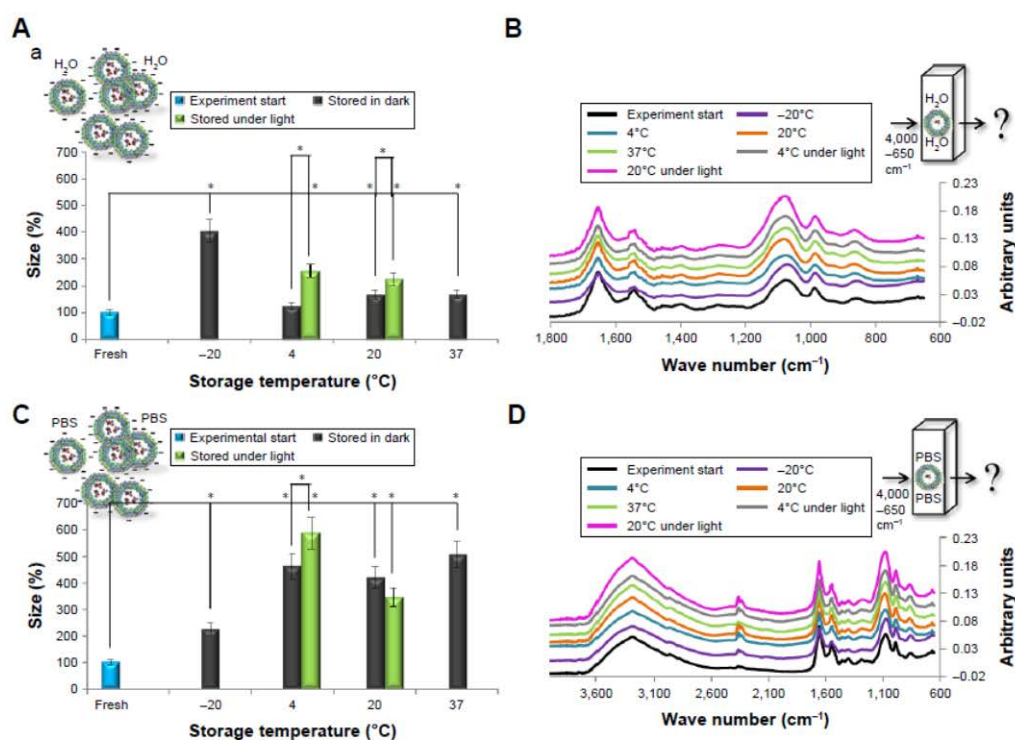


Figure 5 Changes in size and FT-IR spectra of nanocarrier.

Notes: Changes in average size for ApoDox prepared in water (A) and PBS (C) revealed by quasielastic dynamic light scattering. Size was calculated as percentage increase compared with size at start of experiment. Values expressed as means of 12 measurements over the course of 12 weeks ($n=12$). $*P < 0.05$ compared with start of experiment or between storage in dark and under direct ambient light. (B, D) Overlaid ATR Fourier-transform infrared spectra of freshly prepared ApoDox and ApoDox stored in various conditions.

Abbreviations: FT-IR, Fourier-transform infrared; ApoDox, apoferritin–doxorubicin; PBS, phosphate-buffered saline; ATR, attenuated total reflection.

In vitro assessment of differently stored ApoDox influence on cancer cells

Probably the most important property of a nanocarrier is its ability to internalize into target cells and the ability of its cargo to reach the organelle where it can effectively inhibit cell growth.⁵³ In our previous work, we proved that the encapsulation of Dox inside Apo has similar influence on cancer cells as free Dox, whereas normal, noncancer cells are significantly protected from Dox influence.²¹ Therefore, in the present experiment we tested the internalization of ApoDox stored at various conditions using only the androgen-dependent metastatic prostate cancer cell line LNCaP.

LNCaP cells were treated with Dox, either free or encapsulated in freshly prepared ApoDox, or ApoDox stored at various conditions. After 2 hours of treatment, nuclei were stained with Hoechst 33342 to help distinguish whether the encapsulated Dox was able to get to its site of action properly. Moreover, since one of the main mechanisms of Dox inhibition is the formation of free oxygen radicals,¹⁴ cell redox stress was investigated by staining with CellRox Green stains. Figure 6 shows the morphology, stained nuclei, and redox stress of these cells for ApoDox prepared in water.

Ambient-light microscopy revealed that the treated cells were more round as they started to detach from the surface

of the well and also at formation of first apoptotic bodies, both of which are the first sign of onset of apoptosis. The untreated cells (Figure 6 [Control]) showed blue nucleus fluorescence with no red (Dox) fluorescence and very low redox stress, almost always in the cytoplasm. Cells treated with free Dox (Figure 6 [Dox]) showed red Dox fluorescence and higher oxidative stress, both colocalized in nuclei. Cells treated with freshly prepared ApoDox (Figure 6 [S]) showed much higher intensity of Dox fluorescence than cells treated with free Dox, which indicated that ApoDox internalized in the cells more quickly than free Dox, probably through the overexpressed transferrin receptors on the surface of LNCaP cells.⁵⁷ These cells also showed medium redox stress, mainly in the cytoplasm. ApoDox stored at -20°C (Figure 6 [a]) showed very similar results as those obtained with freshly prepared ApoDox: high Dox fluorescence in nuclei and medium redox stress in cytoplasm. ApoDox stored at 4°C and in dark (Figure 6 [b]) showed some fluorescence in both nuclei and cytoplasm, indicating slower internalization, as well as medium redox stress in both nuclei and cytoplasm. ApoDox stored at 4°C under ambient light (Figure 6 [b/l]) showed higher Dox fluorescence and redox stress, but mostly in cytoplasm, although there was also observable Dox fluorescence in nuclei. ApoDox stored at 20°C and in dark (Figure 6 [c])

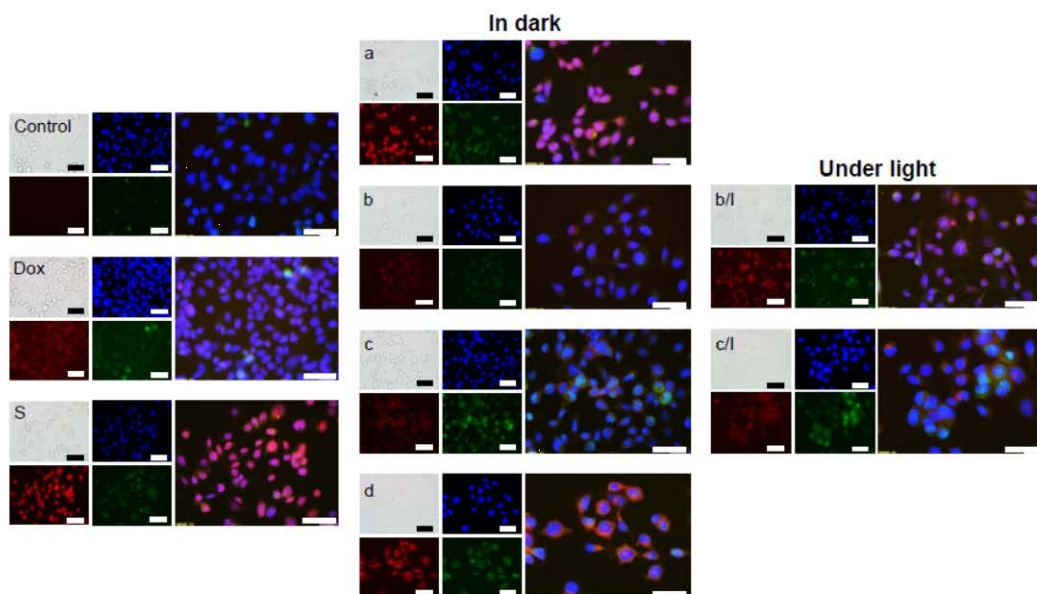


Figure 6 Living cell fluorescence imaging.

Notes: Nuclei (blue) localization (Hoechst 33258), Dox fluorescence (red) and formation of redox stress (green) in LNCaP cells exposed to $34\ \mu\text{M}$ of free Dox, freshly prepared ApoDox in water (S), and ApoDox prepared in water and stored at 20°C (a), 4°C (storage in dark [b] and storage under direct ambient light [b/l]), 20°C (storage in dark [c] and storage under direct ambient light [c/l]), and 37°C (d). Merged figures show the colocalization of blue, red, and green fluorescence. The length of scale bars is $100\ \mu\text{m}$.

Abbreviations: Dox, doxorubicin; Apo, apoferritin.

showed higher Dox fluorescence than ApoDox stored at 4°C; however, this was localized exclusively in cytoplasm, proving that no or negligible Dox was able to get inside the nucleus. This could have been caused by different internalization mechanisms of large aggregates or slower release of drug molecules from these aggregates in endosomes; however, the precise mechanism needs to be further elucidated. These cells also showed high levels of cytoplasmic redox stress. ApoDox stored at 20°C under ambient light (Figure 6 [c/l]) showed similar results, with slightly higher Dox fluorescence and redox stress localized only in cytoplasm. ApoDox stored at 37°C (Figure 6 [d]) showed very high Dox fluorescence, but again almost always localized in the cytoplasm (only a very small percentage was observed in nuclei).

Figure 7 shows the morphology, stained nuclei, and redox stress of these cells for ApoDox prepared in PBS. Ambient-light microscopy again revealed the starting apoptosis in treated cells, which became more rounded as they started to detach from the surface of the well and apoptotic bodies became visible. Untreated cells (Figure 7 [Control]) showed only blue nucleus fluorescence with negligible red (Dox) fluorescence and very low redox stress, almost always in the cytoplasm. Cells treated with free Dox (Figure 7 [Dox]) showed red Dox fluorescence only in nuclei. Also, higher oxidative stress was observed in the nucleus. Cells treated with freshly prepared ApoDox (Figure 7 [S]) showed much

higher intensity of Dox fluorescence than cells treated with free Dox, which was probably again caused by faster internalization of ApoDox due to overexpressed transferrin receptors. However, this Dox fluorescence was mostly localized in the cytoplasm with smaller percentages in nuclei. Also, redox stress was observed mainly in the cytoplasm. ApoDox stored at -20°C (Figure 7 [a]) showed Dox fluorescence in both cytoplasm and nuclei, where we also observed redox stress. ApoDox stored at 4°C and in dark (Figure 7 [b]) showed only very low Dox fluorescence, as well as redox stress in cytoplasm. ApoDox stored at 4°C under ambient light (Figure 7 [b/l]) showed very high Dox fluorescence in cytoplasm, as well as redox stress, with only low percentage of Dox and redox-stress fluorescence in nuclei. ApoDox stored at 20°C and in dark (Figure 7 [c]) showed medium Dox fluorescence, localized only in the cytoplasm. However, redox stress was observed in both nuclei and cytoplasm. ApoDox stored at 20°C under ambient light (Figure 7 [c/l]) again showed very high Dox fluorescence and redox stress in cytoplasm, with a small percentage in nuclei. ApoDox stored at 37°C (Figure 7 [d]) showed Dox fluorescence and redox stress mainly in cytoplasm (only a very small percentage was observed in nuclei).

Next, real-time label-free monitoring of cell impedance was used to evaluate the 72-hour *in vitro* toxicity of ApoDox stored at various conditions for LNCaP cells. Since the

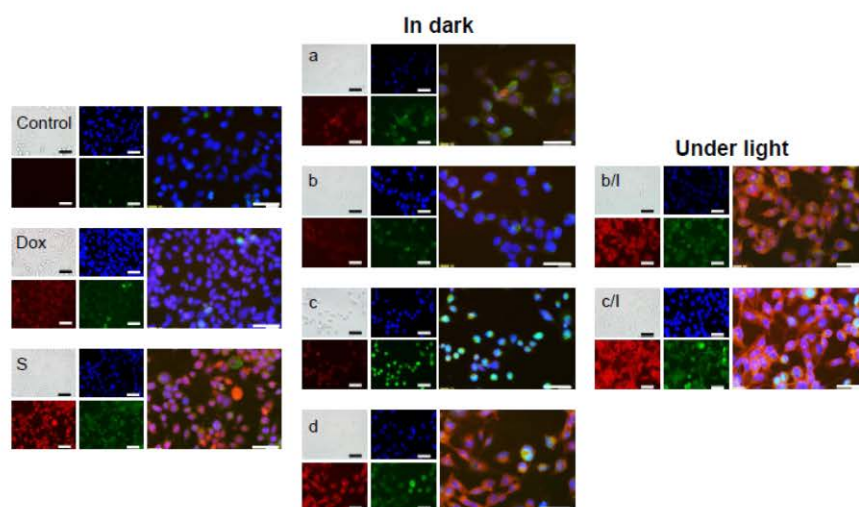


Figure 7 Living cell fluorescence imaging.

Notes: Nuclei (blue) localization (Hoechst 33258), Dox fluorescence (red) and formation of redox stress (green) in LNCaP cells exposed to 34 μ M of free Dox, freshly prepared ApoDox in PBS (S), and ApoDox prepared in PBS and stored at 20°C (a), 4°C (storage in dark [b] and storage under direct ambient light [b/l]), 20°C (storage in dark [c] and storage under direct ambient light [c/l]), and 37°C (d). Merged figures show the colocalization of blue, red, and green fluorescence. The length of scale bars is 100 μ m.

Abbreviations: Dox, doxorubicin; Apo, apoferritin; PBS, phosphate-buffered saline.

experiment revealed that ApoDox prepared in PBS formed very large aggregates and was mostly unable to deliver the Dox cargo into nuclei, only ApoDox prepared in water was used for the cytotoxicity assay.

Control cells still proliferating can be seen in Figure 8 as a dark blue line. All cells treated with free Dox (Figure 8 [red]) were dead after 55 hours of treatment. After 72 hours of treatment, freshly prepared ApoDox in water (Figure 8 [black]) showed inhibition of 95% of cells. ApoDox stored at 20°C (Figure 8 [orange]) and 37°C (Figure 8 [light green]) were mostly unable to retain their ability to kill cancer cells, showing only 23% and 9% of dead cells, respectively. Storage under light showed similar results between temperatures, with 76% of dead cells for storage at 4°C (Figure 8 [gray]) and 58% of dead cells for storage at 20°C (Figure 8 [pink]), respectively.

The highest cytotoxicity was obtained using ApoDox stored at -20°C (Figure 8 [purple]). It was able to kill all cells within 46 hours of treatment, even faster than in the case of free Dox, corresponding to its fast internalization and induction of redox stress. However, this storage temperature is not suitable for use in patients, since ApoDox stored at -20°C creates very large aggregates that would be removed rapidly from the body by the RES.⁴⁹ All cells had died after 68 hours of treatment with ApoDox stored at 4°C and in dark (Figure 8 [cyan]), which was slightly better than in the case of freshly prepared ApoDox. Moreover, storage at this temperature showed the highest stability with regard to size, shape, and surface charge. Storage at 4°C in water was thus evaluated as the most stable condition.

Conclusion

In conclusion, Apo is a natural nanocarrier that has a suitable cargo-release mechanism for delivery to cancer cells. In this study, we performed a comprehensive investigation of the long-term stability of the ApoDox nanocarrier stored at various conditions. We prepared the ApoDox nanocarrier in two different solvents (water and PBS), and stored it for 12 weeks in various conditions (-20°C, 4°C, 20°C, and 37°C in dark and 4°C and 20°C under ambient light). We tested the optical properties of the encapsulated cargo; the amount of prematurely released drug molecules; size, shape, ζ -potential, and the FT-IR spectra of the whole nanocarrier; and the ability to internalize into cancer cells and deliver the drug to nuclei. Many of the tested storage conditions caused formation of large aggregates of multiple nanocarriers, which would be unsuitable for use in patients. The optimal storage conditions seem to be 4°C in dark and in water, where the ApoDox showed very good stability over the course of 12 weeks. The obtained data are very helpful for future use of Apo as a nanocarrier for anticancer therapy. Long-term stability of a suitable nanocarrier can help overcome the higher cost of nanocarrier-based treatment compared with conventional anticancer drugs. The ApoDox nanocarrier will be tested further in *in vivo* experiments.

Acknowledgments

The authors gratefully acknowledge financial support from the Grant Agency of the Czech Republic (GA CR

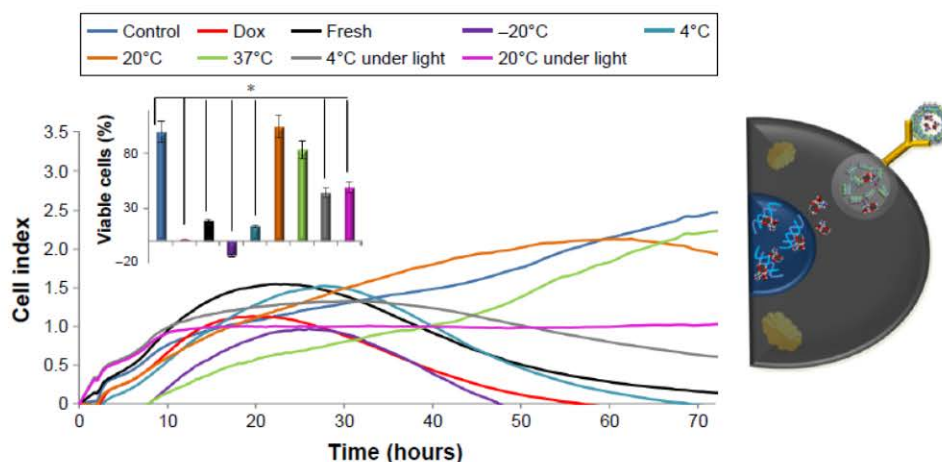


Figure 8 Real-time cell-impedance analyses showing growth profiles over the course of 72 hours.

Notes: LNCaP cells untreated and treated with 2.5 μ M Dox, freshly prepared in ApoDox in water, and ApoDox prepared in water after storage at various conditions. Inset shows percentage of viable cells after 55 hours' treatment. * $P < 0.05$ compared with start of experiment or between storage in dark and under direct ambient light.

Abbreviations: Dox, doxorubicin; Apo, apoferritin.

17-12816S), IGA MENDELU IP_28/2016, and CEITEC 2020 (LQ1601). They also express thanks to Michal Horak for perfect technical assistance. The authors acknowledge the CF CEITEC – Core Facility Cryo-Electron Microscopy and Tomography, supported by the CIISB research infrastructure (LM2015043 funded by MEYS CR), for their support with obtaining the TEM micrographs.

Disclosure

The authors report no conflicts of interest in this work.

References

1. Dimarco A, Gaetani M, Scarpinato B. Adriamycin (NSC-123, 127): a new antibiotic with antitumor activity. *Cancer Chemother Rep*. 1969;53(1):33–37.
2. Pilco-Ferreto N, Calaf GM. Influence of doxorubicin on apoptosis and oxidative stress in breast cancer cell lines. *Int J Oncol*. 2016;49(2):753–762.
3. Lv LX, An XM, Li HY, Ma LX. Effect of miR-155 knockdown on the reversal of doxorubicin resistance in human lung cancer A549/dox cells. *Oncol Lett*. 2016;11(2):1161–1166.
4. Shang C, Guo Y, Zhang H, Xue YX. Long noncoding RNA HOTAIR is a prognostic biomarker and inhibits chemosensitivity to doxorubicin in bladder transitional cell carcinoma. *Cancer Chemother Pharmacol*. 2016;77(3):507–513.
5. Tap WD, Jones RL, Van Tine BA, et al. Olaratumab and doxorubicin versus doxorubicin alone for treatment of soft-tissue sarcoma: an open-label phase 1B and randomised phase 2 trial. *Lancet*. 2016;388(10043):488–497.
6. Bürkle C, Borchmann P. Diagnostik und Therapie des Hodgkin-Lymphoms [Diagnosis and treatment of Hodgkin lymphoma]. *Onkologie*. 2016;22(8):603–616. German.
7. Agudelo D, Bourassa P, Bérubé G, Tajmir-Riahi HA. Review on the binding of anticancer drug doxorubicin with DNA and tRNA: structural models and antitumor activity. *J Photochem Photobiol B Biol*. 2016;158:274–279.
8. Kumar A, Ehrenshaft M, Tokar EJ, Mason RP, Sinha BK. Nitric oxide inhibits topoisomerase II activity and induces resistance to topoisomerase II-poisons in human tumor cells. *Biochim Biophys Acta*. 2016;1860(7):1519–1527.
9. Agustini FD, Arozal W, Louisa M, et al. Cardioprotection mechanism of mangiferin on doxorubicin-induced rats: focus on intracellular calcium regulation. *Pharm Biol*. 2016;54(7):1289–1297.
10. Meredith AM, Dass CR. Increasing role of the cancer chemotherapeutic doxorubicin in cellular metabolism. *J Pharm Pharmacol*. 2016;68(6):729–741.
11. World Health Organization. WHO model list of essential medicines. 2015. Available from: <http://www.who.int/medicines/publications/essentialmedicines/en>. Accessed September 20, 2016.
12. Li XY, Wu MY, Pan LM, Shi JL. Tumor vascular-targeted co-delivery of anti-angiogenesis and chemotherapeutic agents by mesoporous silica nanoparticle-based drug delivery system for synergetic therapy of tumor. *Int J Nanomedicine*. 2016;11:93–105.
13. Mercurio V, Pirozzi F, Lazzarini E, et al. Models of heart failure based on the cardiotoxicity of anticancer drugs. *J Card Fail*. 2016;22(6):449–458.
14. Tacar O, Sriamornsak P, Dass CR. Doxorubicin: an update on anticancer molecular action, toxicity and novel drug delivery systems. *J Pharm Pharmacol*. 2013;65(2):157–170.
15. Xia CC, Yadav AK, Zhang K, et al. Synchrotron radiation (SR) diffraction enhanced imaging (DEI) of chronic glomerulonephritis (CGN) mode. *J Xray Sci Technol*. 2016;24(1):145–159.
16. Fanous I, Dillon P. Cancer treatment-related cardiac toxicity: prevention, assessment and management. *Med Oncol*. 2016;33(8):84.
17. Schuler MK, Gerdes S, West A, et al. Efficacy and safety of dexrazoxane (DRZ) in sarcoma patients receiving high cumulative doses of anthracycline therapy: a retrospective study including 32 patients. *BMC Cancer*. 2016;16:619.
18. Shaikh F, Dupuis LL, Alexander S, Gupta A, Mertens L, Nathan PC. Cardioprotection and second malignant neoplasms associated with dexrazoxane in children receiving anthracycline chemotherapy: a systematic review and meta-analysis. *J Natl Cancer Inst*. 2016;108(4):d3v357.
19. Luhmann T, Meinel L. Nanotransporters for drug delivery. *Curr Opin Biotechnol*. 2016;39:35–40.
20. Maeda H, Tsukigawa K, Fang J. A retrospective 30 years after discovery of the enhanced permeability and retention effect of solid tumors: next-generation chemotherapeutics and photodynamic therapy problems, solutions, and prospects. *Microcirculation*. 2016;23(3):173–182.
21. Dostalova S, Cerna T, Hynek D, et al. Site-directed conjugation of antibodies to apoferritin nanocarrier for targeted drug delivery to prostate cancer cells. *ACS Appl Mater Interfaces*. 2016;8(23):14430–14441.
22. Tian DY, Wang WY, Li SP, Li XD, Sha ZL. A novel platform designed by Au core/inorganic shell structure conjugated onto MTX/LDH for chemo-photothermal therapy. *Int J Pharm*. 2016;505(1–2):96–106.
23. Jena SK, Sangamwar AT. Polymeric micelles of amphiphilic graft copolymer of α -tocopherol succinate-g-carboxymethyl chitosan for tamoxifen delivery: synthesis, characterization and in vivo pharmacokinetic study. *Carbohydr Polym*. 2016;151:1162–1174.
24. Lindqvist A, Friden M, Hammarlund-Udenaes M. Pharmacokinetic considerations of nanodelivery to the brain: using modeling and simulations to predict the outcome of liposomal formulations. *Eur J Pharm Sci*. 2016;92:173–182.
25. Agudelo D, Berube G, Tajmir-Riahi HA. An overview on the delivery of antitumor drug doxorubicin by carrier proteins. *Int J Biol Macromol*. 2016;88:354–360.
26. Alphanery E, Grand-Dewyse P, Lefevre R, Mandawala C, Durand-Dubief M. Cancer therapy using nanoformulated substances: scientific, regulatory and financial aspects. *Expert Rev Anticancer Ther*. 2015;15(10):1233–1255.
27. Kim HS, Wainer IW. Simultaneous analysis of liposomal doxorubicin and doxorubicin using capillary electrophoresis and laser induced fluorescence. *J Pharm Biomed Anal*. 2010;52(3):372–376.
28. Suk JS, Xu QG, Kim N, Hanes J, Ensign LM. PEGylation as a strategy for improving nanoparticle-based drug and gene delivery. *Adv Drug Deliv Rev*. 2016;99(Pt A):28–51.
29. Tmejova K, Hynek D, Kopel P, et al. Electrochemical behaviour of doxorubicin encapsulated in apoferritin. *Int J Electrochem Sci*. 2013;8(12):12658–12671.
30. Liang MM, Fan KL, Zhou M, et al. H-ferritin-nanocaged doxorubicin nanoparticles specifically target and kill tumors with a single-dose injection. *Proc Natl Acad Sci U S A*. 2014;111(41):14900–14905.
31. Cutrin JC, Crich SG, Burghelca D, Dastru W, Aime S. Curcumin/Gd loaded apoferritin: a novel “theranostic” agent to prevent hepatocellular damage in toxic induced acute hepatitis. *Mol Pharm*. 2013;10(5):2079–2085.
32. Zang J, Chen H, Guanghua Z, Wang F, Ren F. Ferritin cage for encapsulation and delivery of bioactive nutrients: from structure, property to applications. *Crit Rev Food Sci Nutr*. Epub 2016 Mar 16.
33. Crich SG, Cadenazzi M, Lanzardo S, et al. Targeting ferritin receptors for the selective delivery of imaging and therapeutic agents to breast cancer cells. *Nanoscale*. 2015;7(15):6527–6533.
34. Blazkova I, Nguyen HV, Dostalova S, et al. Apoferritin modified magnetic particles as doxorubicin carriers for anticancer drug delivery. *Int J Mol Sci*. 2013;14(7):13391–13402.
35. Bulvik BE, Berenshtein E, Meyron-Holtz EG, Konijn AM, Chevion M. Cardiac protection by preconditioning is generated via an iron-signal created by proteasomal degradation of iron proteins. *PLoS One*. 2012;7(11):e48947.
36. Asano T, Komatsu M, Yamaguchi-Iwai Y, Ishikawa F, Mizushima N, Iwai K. Distinct mechanisms of ferritin delivery to lysosomes in iron-depleted and iron-replete cells. *Mol Cell Biol*. 2011;31(10):2040–2052.

37. Smith JL. The physiological role of ferritin-like compounds in bacteria. *Crit Rev Microbiol*. 2004;30(3):173–185.
38. Gallois B, d'Estaintot BL, Michaux MA, et al. X-ray structure of recombinant horse L-chain apoferritin at 2.0 angstrom resolution: implications for stability and function. *J Biol Inorg Chem*. 1997;2(3):360–367.
39. Haussler W. Structure and dynamics in apoferritin solutions with paracrystalline order. *Chem Phys*. 2003;292(2–3):425–434.
40. Kim M, Rho Y, Jin KS, et al. pH-dependent structures of ferritin and apoferritin in solution: disassembly and reassembly. *Biomacromolecules*. 2011;12(5):1629–1640.
41. Kilic MA, Ozlu E, Calis S. A novel protein-based anticancer drug encapsulating nanosphere: apoferritin-doxorubicin complex. *J Biomed Nanotechnol*. 2012;8(3):508–514.
42. Wood MJ, Irwin WJ, Scott DK. Photodegradation of doxorubicin, daunorubicin and epirubicin measured by high-performance liquid-chromatography. *J Clin Pharm Ther*. 1990;15(4):291–300.
43. Konecna R, Nguyen HV, Stanisavljevic M, et al. Doxorubicin encapsulation investigated by capillary electrophoresis with laser-induced fluorescence detection. *Chromatographia*. 2014;77(21–22):1469–1476.
44. Dai XW, Yue ZL, Eccleston ME, Swartling J, Slater NK, Kaminski CF. Fluorescence intensity and lifetime imaging of free and micellar-encapsulated doxorubicin in living cells. *Nanomed Nanotechnol Biol Med*. 2008;4(1):49–56.
45. Yang K, Luo HQ, Zeng M, Jiang YY, Li JM, Fu XL. Intracellular pH-triggered, targeted drug delivery to cancer cells by multifunctional envelope-type mesoporous silica nanocontainers. *ACS Appl Mater Interfaces*. 2015;7(31):17399–17407.
46. Petros RA, DeSimone JM. Strategies in the design of nanoparticles for therapeutic applications. *Nat Rev Drug Discov*. 2010;9(8):615–627.
47. Svenson S. Theranostics: are we there yet? *Mol Pharm*. 2013;10(3):848–856.
48. Appelbe OK, Zhang Q, Pelizzari CA, Weichselbaum RR, Kron SJ. Image-guided radiotherapy targets macromolecules through altering the tumor microenvironment. *Mol Pharm*. 2016;13(10):3457–3467.
49. Liu T, Chao Y, Gao M, et al. Ultra-small MoS₂ nanodots with rapid body clearance for photothermal cancer therapy. *Nano Res*. 2016;9(10):3003–3017.
50. Svenson S. Clinical translation of nanomedicines. *Curr Opin Solid State Mater Sci*. 2012;16(6):287–294.
51. Gratton SE, Ropp PA, Pohlhaus PD, et al. The effect of particle design on cellular internalization pathways. *Proc Natl Acad Sci U S A*. 2008;105(33):11613–11618.
52. Zamboni WC, Torchilin V, Patri AK, et al. Best practices in cancer nanotechnology: perspective from NCI nanotechnology alliance. *Clin Cancer Res*. 2012;18(12):3229–3241.
53. Stylianopoulos T, Jain RK. Design considerations for nanotherapeutics in oncology. *Nanomed Nanotechnol Biol Med*. 2015;11(8):1893–1907.
54. Fülöp Z, Gref R, Loftsson T. A permeation method for detection of self-aggregation of doxorubicin in aqueous environment. *Int J Pharm*. 2013;454(1):559–561.
55. Righetti PG, Menozzi M, Gianazza E, Valentini L. Protolytic equilibria of doxorubicin as determined by isoelectric-focusing and electrophoretic titration curves. *FEBS Lett*. 1979;101(1):51–55.
56. Beijnen JH, Wiese G, Underberg WJ. Aspects of the chemical-stability of doxorubicin and seven other anthracyclines in acidic solution. *Pharm Weekbl Sci*. 1985;7(3):109–116.
57. Liu AY. Differential expression of cell surface molecules in prostate cancer cells. *Cancer Res*. 2000;60(13):3429–3434.

International Journal of Nanomedicine

Publish your work in this journal

The International Journal of Nanomedicine is an international, peer-reviewed journal focusing on the application of nanotechnology in diagnostics, therapeutics, and drug delivery systems throughout the biomedical field. This journal is indexed on PubMed Central, MedLine, CAS, SciSearch®, Current Contents®/Clinical Medicine,

Submit your manuscript here: <http://www.dovepress.com/international-journal-of-nanomedicine-journal>

Dovepress

Journal Citation Reports/Science Edition, EMBase, Scopus and the Elsevier Bibliographic databases. The manuscript management system is completely online and includes a very quick and fair peer-review system, which is all easy to use. Visit <http://www.dovepress.com/testimonials.php> to read real quotes from published authors.

Article 4

Konecna R, Nguyen HV, Stanisavljevic M, Blazkova I, Krizkova S, **Vaculovicova M**, Stiborova M, Eckschlager T, Zitka O, Adam V, Kizek R. Doxorubicin Encapsulation Investigated by Capillary Electrophoresis with Laser-Induced Fluorescence Detection. *Chromatographia* 2014 Nov;77(21-22):1469-1476.

Doxorubicin Encapsulation Investigated by Capillary Electrophoresis with Laser-Induced Fluorescence Detection

Romana Konecna · Hoai Viet Nguyen · Maja Stanisavljevic · Iva Blazkova ·
Sona Krizkova · Marketa Vaculovicova · Marie Stiborova · Tomas Eckschlager ·
Ondrej Zitka · Vojtech Adam · Rene Kizek

Received: 18 February 2014 / Revised: 16 May 2014 / Accepted: 24 June 2014 / Published online: 17 August 2014
© Springer-Verlag Berlin Heidelberg 2014

Abstract Doxorubicin (DOX) belongs to the group of anthracycline antibiotics with very effective anticancer properties. On the other hand, the cardiotoxic effects limit its application over the maximum cumulative dose. To overcome this obstacle, encapsulation of this drug into the protective nanotransporter such as apoferritin is beneficial. In this study, fluorescent behavior of DOX in various solvents was determined by fluorescence spectrometry, demonstrating the fluorescence quenching effect of water, which is often used as a solvent. It was found that by increasing the amount of the organic phase in the DOX solvent the dynamic

quenching is significantly suppressed. Ethanol, acetonitrile and dimethyl sulfoxide were tested and the best linearity of the calibration curve was obtained when above 50 % of the solvent was present in the binary mixture with water. Moreover, pH influence on the DOX fluorescence was also observed within the range of 4–10. Two times higher fluorescence intensity was observed at pH 4 compared to pH 10. Further, the DOX behavior in capillary electrophoresis (CE) was investigated. Electrophoretic mobilities (CE) in various pH of the background electrolyte were determined within the range from 16.3 to $-13.3 \times 10^{-9} \text{ m}^{-2} \text{ V}^{-1} \text{ s}^{-1}$. Finally, CE was also used to monitor the encapsulation of DOX into the cavity of apoferritin as well as the pH-triggered release.

Published in the topical collection *Advances in Chromatography and Electrophoresis & Chiral 2014* with guest editor Jan Petr.

R. Konecna · H. V. Nguyen · M. Stanisavljevic · I. Blazkova ·
O. Zitka · V. Adam · R. Kizek
Department of Chemistry and Biochemistry,
Faculty of Agronomy, Mendel University in Brno,
Zemedelska 1, 61300 Brno, Czech Republic

S. Krizkova · M. Vaculovicova · O. Zitka · V. Adam · R. Kizek
Central European Institute of Technology, Brno University
of Technology, Technicka 3058/10, 61600 Brno, Czech Republic

M. Stiborova
Department of Biochemistry, Faculty of Science, Charles
University, Albertov 2030, 12840 Prague 2, Czech Republic

T. Eckschlager
Department of Paediatric Haematology and Oncology,
2nd Faculty of Medicine, Charles University, and University
Hospital Motol, V Uvalu 84, 15006 Prague 5, Czech Republic

R. Kizek (✉)
Central European Institute of Technology and Department
of Chemistry and Biochemistry, Mendel University in Brno,
Zemedelska 1, 61300 Brno, Czech Republic
e-mail: kizek@sci.muni.cz

Keywords Capillary electrophoresis · Fluorescence ·
Drug delivery · Doxorubicin · Apoferritin

Introduction

Anthracyclines belong to the most effective anticancer drugs, whereas doxorubicin (DOX) as one of their main representatives is highly efficient and widely used. This compound was firstly isolated from *Streptomyces peuce-tius* in 1960s [1]. In spite of the high efficiency and decades of the using, the administration of the drug over the cumulative dose 550 mg/m^2 of body surface area lead to severe side effects including high risk of cardiomyopathy [2, 3], which usually arises the first year after therapy. Nevertheless, cardiac failures can be identified at smaller doses too. This cardiotoxicity is the main force driving the progress towards less toxic formulations enabling also targeted delivery of the drug [4–10].

Due to the optical properties of DOX as well as its biological activity, this molecule is still a target of numerous

investigations [11–13]. The DOX fluorescence in relation to the surrounding conditions such as its concentration, nature of solvent and/or presence of quenchers has been exploited [14]. It is thanks to these fluorescent properties that it is possible to track DOX and its formulations including apoferritin- or liposome-encapsulated forms designed to diminish its toxicity by numerous bioanalytical methods [15]. Besides capillary electrophoresis (CE) also HPLC with fluorescence [16], electrochemical detection [17] and/or mass spectrometric detection [18] has been used. Capillary electrophoresis, in particular, has been utilized for analysis of liposome-encapsulated DOX [19], daunorubicin [20] and/or oxaliplatin [21]. Encapsulation of DOX to nanoparticles preserves the antitumor activity while reducing to risk of cardiotoxicity and increasing distribution of drug to the tumor site. Nowadays, only one commercially available encapsulated DOX is liposome-DOX, called Myocet. The cumulative dose of DOX was increased to 750 mg/m² to not reach above-mentioned side effects [22].

In our study, the fluorescent behavior of DOX in the presence of various fluorescence quenchers was investigated followed by capillary electrophoretic study of encapsulation of DOX into the cavity of protein based nanotransporter called apoferritin. The behavior of DOX in CE using various electrolytes differing in pH values was investigated due to the requirement of exploration of DOX release from the apoferritin cage by the pH change.

Experimental Section

Fluorescence Spectrometry

Doxorubicin (5, 10, 20, 30, 40 and 50 µg/mL) was dissolved in water to investigate the behavior depending on concentration. Besides, to explore the influence of organic solvent, DOX (5, 10, 20, 30, 40 and 50 µg/mL) was dissolved in 12.5, 25, 50, 75 and 100 % mixtures of organic solvents (*v/v*, ethanol, acetonitrile, and dimethyl sulfoxide) and water. Finally, DOX (5, 10, 20, 30, 40 and 50 µg/mL) was dissolved in buffers of pH ranges 4–10 (acetate pH 4 and 5, phosphate pH 6, 7, 8, borate pH 9, 10). All chemicals were purchased from Sigma Aldrich (USA). Fluorescence intensity was measured at 600 nm after excitation by the light with emission wavelength of 480 nm using the TECAN Infinite 200 PRO microtitration plate reader (Switzerland).

Spectrophotometry

Apoferritin was dissolved in water in concentrations of 0.4, 0.8, 1.6 and 3.2 mg/mL. Absorbance spectra were measured using the TECAN microtitration plate reader

Infinite 200 PRO (Switzerland) in the wavelength range 230–600 nm using 50 µL of the sample in the UV transparent 96-well plate. Each absorbance value is an average of 5 measurements.

Preparation of Apoferritin Encapsulated DOX (APODOX)

Various volumes of DOX (2 mg/mL) 25, 50, 75, 100 and 200 µL were filled with water up to 300 µL and mixed with 20 µL of apoferritin (50 mg/mL). The pH 2 was adjusted by HCl to disassemble the apoferritin structure. Subsequently, the pH was adjusted to 7 using NaOH to reassemble the cage. To remove the excess of the DOX, the samples were filtered using Amicon 3K centrifuge filter at 6,000g for 15 min.

Capillary Electrophoresis

Apoferritin characterization was performed using CE with UV detection (CE 7100, Agilent Technologies, Germany) and DOX and APODOX were analyzed by CE-LIF (PACE MDQ, Beckman Coulter, USA). In both cases, fused silica capillary with internal diameter of 75 µm and with the total length 64.5 cm (54 cm to detector window) was used. The separation voltage of 20 kV and hydrodynamic injection by 3 psi for 10 s was employed.

Results and Discussion

Study of DOX by Fluorescence Spectrometry

Because of the fact that the fluorescence behavior of DOX (chemical structure shown in inset in Fig. 1a) is one of the main advantages of application of this drug as a model cytostatic drug, this behavior has to be well known and characterized. In our study, solutions of DOX within the concentration range of 5–50 µg/mL were used. It was found that above 50 µg/mL, a significant quenching effect was determined. This quenching is caused by several synergic effects including (a) concentration quenching when the concentration of 50 µg/mL is exceeded and (b) solvent quenching caused by water molecules present in the solution.

Taking into account the fact that solvent influences DOX fluorescence, we studied also the effect of pH. The same concentration range of DOX was prepared with three buffers (acetate, phosphate, and/or borate) covering the pH range 4–10. The fluorescence intensities of DOX in above-mentioned buffers are shown in Fig. 1a. It was found that the fluorescence of DOX was enhanced in acidic pH. The fluorescence of DOX solution with concentration of 50 µg/mL at pH 4 was 2.7-fold higher than at pH 10; however, the

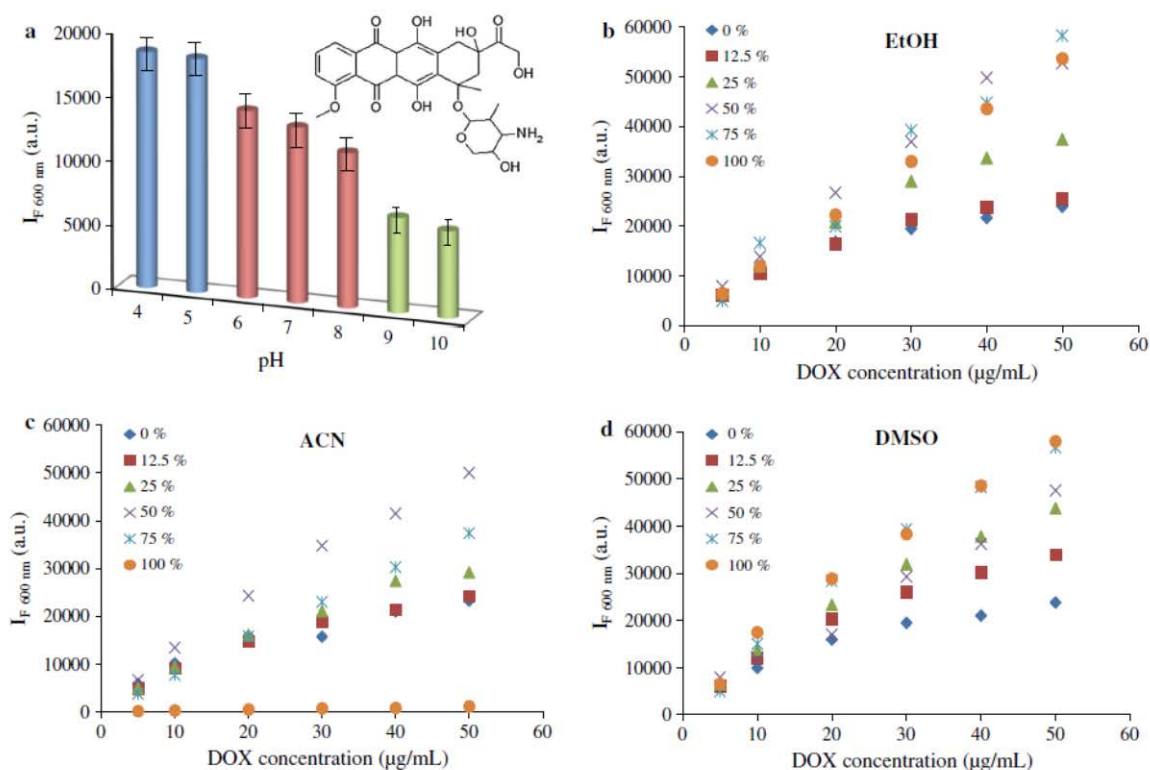


Fig. 1 Characterization of DOX fluorescence measured in various solvents. **a** Dependence of DOX (50 µg/mL) fluorescence intensity on pH of the solvent (*blue* acetate buffer pH 4 and 5, *red* phosphate buffer pH 6, 7 and 8, *green* borate buffer pH 9 and 10). **b–d** Dependence

of the fluorescence intensity of DOX dissolved in solution containing different percentage of organic solvent 0, 12.5, 25, 50, 75 and 100 % **b** EtOH **c** ACN **d** DMSO. Excitation 480 nm, emission 600 nm

increase in the fluorescence was not linearly dependent on pH. It follows from the results that the nature of the buffer played a role and some proton-exchanging reaction should be taken into the account.

Due to the polar character of water, significant dynamic quenching occurs when water is used as a solvent. To characterize the behavior of DOX in less polar environment, three organic solvents with different physico-chemical properties were used as ethanol, acetonitrile and dimethyl sulphoxide. Binary water mixtures of each solvent were prepared containing 12.5, 25, 50, 75 and 100 % of the organic phase (v/v). In these mixtures, DOX solutions within concentration range of 5–50 µg/mL were prepared. It follows from the obtained data that the increasing portion of the organic solvent in the mixture leads to the enhancement of the DOX fluorescence. In the other words, the decreasing water portion caused lowering of the quenching effect. If we take a look at the single non-water solvents, the results of EtOH–water mixture used for DOX dissolution are shown in Fig. 1b. The DOX solutions prepared in water exhibit a significant nonlinearity over the selected

concentration range (logarithmic trend); however, with the increasing of the organic phase the linearity was significantly improved. Therefore, linear trend line was used for all the curves and the linearity of the calibration curve (coefficient of determination, R^2) was used as a parameter characterizing the solvent effect (Table 1). The increasing linearity of the calibration curve expresses the elimination of water quenching effect. Similarly, it was observed that the slope of each curve increased depending on the increasing organic part. This result highlights the fact that the sensitivity of fluorimetric determination of DOX increases according to the organic phase. Same investigation was carried out using ACN as a solvent (Fig. 1c). The linearity increase depending on ACN percentage was similar to the results obtained in EtOH (Table 1), however, the employment of 75 and 100 % ACN led to the significant decrease in the slope. This fact is caused by diminishing of the sensitivity caused by restricted solubility of DOX under these conditions. Finally, the behavior of DOX in DMSO: water mixtures exhibited the same trend as previous two solvents (Fig. 1d). The linearity as well as the slope of the

Table 1 Summary of regression equations and coefficients of determination for measuring of dependence of peak height on doxorubicin concentration in water mixtures containing various percentages of tested organic solvent

| Percentage of organic solvent (v/v) | EtOH | ACN | DMSO |
|-------------------------------------|---------------------------------------|--------------------------------------|---------------------------------------|
| 0 | $y = 362.03x + 7,338.5 R^2 = 0.9208$ | $y = 361.71x + 5,956.3 R^2 = 0.9372$ | $y = 374.94x + 6,382.3 R^2 = 0.9424$ |
| 12.5 | $y = 427.93x + 6,226.3 R^2 = 0.9390$ | $y = 417.48x + 4,676.2 R^2 = 0.9621$ | $y = 603.83x + 5,784.1 R^2 = 0.9625$ |
| 25 | $y = 694.42x + 5,310.5 R^2 = 0.9692$ | $y = 548.99x + 3,836.8 R^2 = 0.9747$ | $y = 813.22x + 5,162.9 R^2 = 0.9798$ |
| 50 | $y = 1,049.2x + 4,240.3 R^2 = 0.9792$ | $y = 952.64x + 3,822.2 R^2 = 0.9903$ | $y = 876.06x + 2,312.7 R^2 = 0.988$ |
| 75 | $y = 1,133.8x + 1,353.2 R^2 = 0.9726$ | $y = 746.4x + 369.64 R^2 = 0.9993$ | $y = 1,032.4x + 6,539.2 R^2 = 0.9902$ |
| 100 | $y = 1,051.2x + 1,322.4 R^2 = 0.9999$ | $y = 20.959x + 51.562 R^2 = 0.9886$ | $y = 1,005.6x + 8,029.4 R^2 = 0.9989$ |

calibration curve increased with the portion of the organic phase. The results are summarized in Table 1. From the obtained data it can be concluded that all three organic solvents are able to diminish the dynamic quenching of DOX fluorescence caused by the presence of water molecules. In the case of ACN the determination is affected only by the limited solubility of DOX. From the results it also follows that DMSO supports the DOX fluorescence the most because the signal of 50 $\mu\text{g/mL}$ DOX increased 2.2-fold in EtOH and 2.4-fold in DMSO.

Capillary Electrophoretic Study of DOX

The behavior of the analyte in various environments is one of the key aspects that have to be considered prior to analysis by capillary electrophoresis. Compared with the stationary fluorimetric measurements, analysis by separation methods such as capillary electrophoresis with laser-induced fluorescence detection, may provide valuable information on the presence of various components, contaminations or even analyte species in the studied solution. Due to the complex structure of DOX and due to the presence of several functional groups, DOX may occur as a cation, anion, zwitterion and/or neutral molecule depending on the environment. Structure of anionic and cationic form is shown in Fig. 2a. To determine the form of DOX, simple method using CE can be utilized. As expected, the fluorescence signal of the obtained peaks is linearly proportional to the concentration of DOX. The peak height plotted over the concentration of DOX exhibits the linear tendency with regression equation $y = 6.9652x - 0.31$ and determination coefficient $R^2 = 0.9981$.

To determine the ionic form of DOX and its pI, phosphate buffer with pH 3, 4, 6, 8, 10, or 11 was used as a separation electrolyte and coumarin 334 was employed as an EOF marker. The obtained electropherograms are shown in Fig. 2b. pH as low as 3 caused very slow EOF and therefore only DOX peak was obtained, however, the increasing pH above this value, peaks of both DOX and coumarin 334 were detected. DOX migrated as a cation

(before the EOF marker) in the pH up to 10. When the pH was increased to 11, the peak of DOX occurred after the EOF marker, which confirmed the anionic form of DOX. As expected, based on previous fluorimetric experiments, the peak height of DOX decreased with the increasing pH (Fig. 2c left). From the migration times, the electrophoretic mobilities were calculated (Fig. 2c right). It clearly follows from the results obtained that the electrophoretic mobilities change over the range from 16.3×10^{-9} to $-13.2 \times 10^{-9} \text{ m}^2 \text{ V}^{-1} \text{ s}^{-1}$.

For the following experiments, it was also necessary to evaluate the behavior of DOX when the pH of the BGE and sample (DOX) zone does not match. As it was expected, the sample stacking occurred due to the dynamic pH junction phenomenon. To demonstrate this fact, the pH of BGE was kept constant (6) and the pH of sample zone was 4, 6, and/or 8. In the case of sample zone pH 4, 2-fold increase in DOX peak height was observed. The signal of DOX measured in the presence of solution of pH 8 was negligible (when matching the BGE and sample zone pH); however, using the described non-matching conditions, the detection of DOX was possible (Fig. 2d left). Because the optimization of sample stacking was not the primary aim of this study, no further improvement in this direction was carried out. Calculating the electrophoretic mobility confirmed that the behavior of the analyte under used condition is independent on the pH of the sample zone and it migrated with the mobility given by the BGE ($13.3 \times 10^{-9} \text{ m}^2 \text{ V}^{-1} \text{ s}^{-1}$) (Fig. 2d right).

CE Characterization of Apoferritin

Apoferritin is a naturally occurring protein serving as a reservoir of iron ions in the living organisms. This protein has a ball-like structure with 12 nm in diameter containing a hollow cavity of 8 nm in size. This protein is capable of pH-dependent disassembling and reassembling allowing encapsulation of desired molecules in the cavity. This process is utilized for application of apoferritin as a nano-carrier of targeted molecule [8, 10, 23]. In this study the

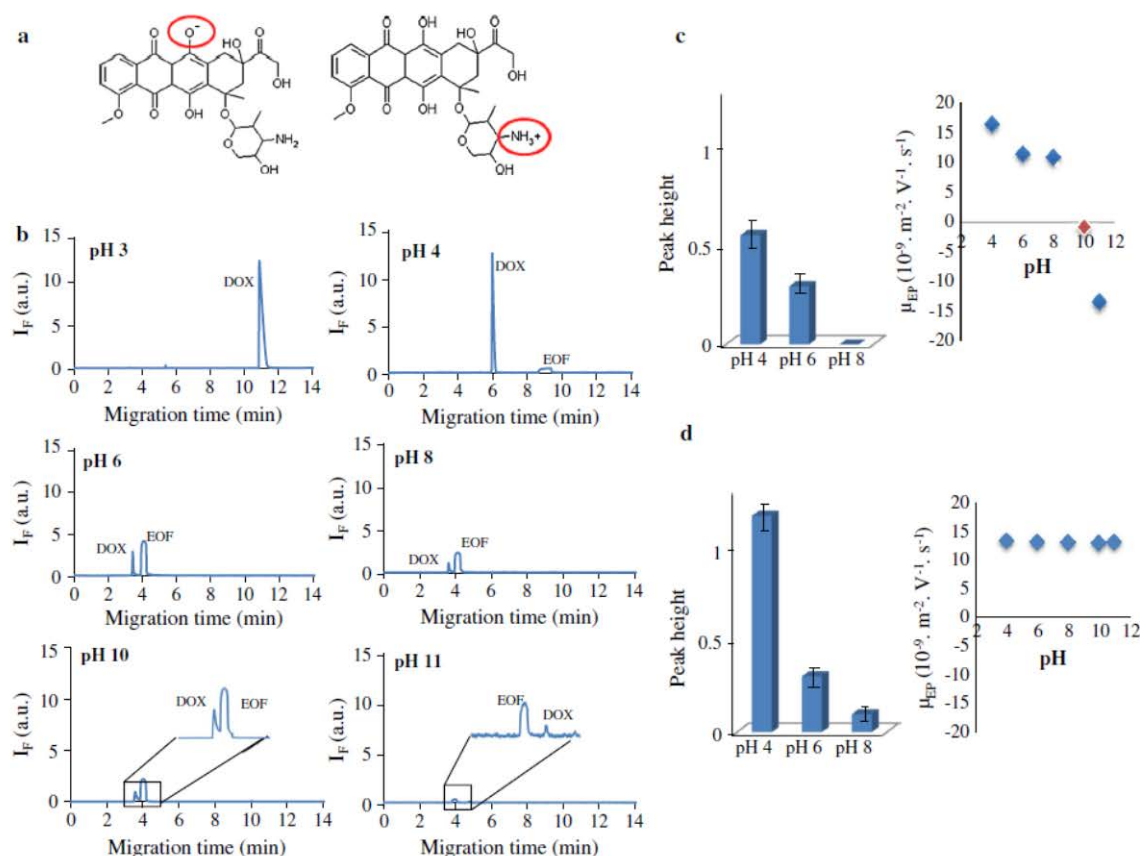


Fig. 2 a Structure of DOX in anionic and cationic form. b CE-LIF of DOX with pH matching to BGE pH. DOX concentration 0.5 μg/mL, CE conditions: capillary 75 μm, 64.5/54 cm; voltage +20 kV; injection 3 psi, 10 s; BGE 10 mM sodium phosphate pH 3, 4, 6, 8, 10 or 11. c *Left* DOX peak heights obtained when BGE pH matched sample zone pH (BGE 10 mM phosphate buffer pH 4, 6 and 8), *right*

electrophoretic mobilities of DOX under conditions matching the pH of BGE and DOX zone. d *Left* DOX peak heights obtained for BGE pH mismatching the sample zone pH (BGE 10 mM phosphate buffer pH 6, sample zone pH 4, 6 and 8), *right* electrophoretic mobilities of DOX for pH of BGE mismatching the DOX zone

apoferritin was utilized to encapsulate DOX and the process was monitored by CE.

At first, CE-UV analysis of apoferritin was carried out determining the possibility of CE analysis using the phosphate buffer as it is shown in Fig. 3. The pI of apoferritin is 4.4 and therefore under used CE conditions, the protein was in an anionic form and migrated after the EOF (Fig. 3a). It was observed that the dependence of peak height on concentration was linear with coefficient of determination $R^2 = 0.9956$ and the equation $y = 1.405x + 1.7503$. The spectrophotometric analysis of apoferritin of different concentration is shown in the inset in Fig. 3a Due to the beneficial apoferritin properties enabling the pH-triggered disassembling of its structure this protein has perfect qualities for encapsulation of drug such as DOX. To exploit these properties, it was necessary to observe the behavior

of apoferritin under various pH conditions by CE. As it is shown in Fig. 3b the peak height of the protein decreased with its pH. On the other hand, the influence of the pH on the migration time was not so significant. The summary of the peak heights as well as migration times depending on the pH is shown in the inset in Fig. 3b.

APODOX

In this study, apoferritin was used as a transporter of doxorubicin and CE-LIF was tested as a method of the monitoring of the encapsulation. The pH-directed apoferritin disassembling and reassembling as well as DOX encapsulation is schematically shown in Fig. 4a. To determine the encapsulation of DOX into the apoferritin cavity, a set of APODOX samples was prepared using a different amount of

Fig. 3 a CE-UV of apoferritin (detection 214 nm, capillary ID 75 μ m, length 54/62.5, buffer 10 mM sodium phosphate pH 6, injection 3 psi 10 s, voltage +20 kV); *inset* absorption spectra of apoferritin; b CE-UV of apoferritin in different pH, conditions same as in Fig. 3a *inset* concentration dependence of the apoferritin peak height and migration time

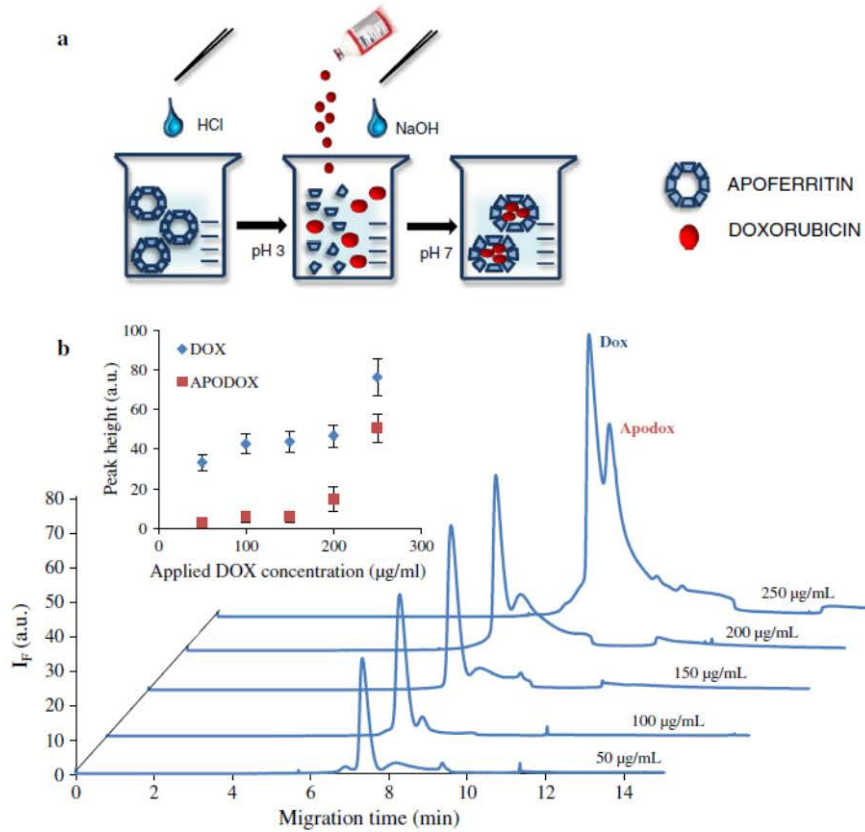
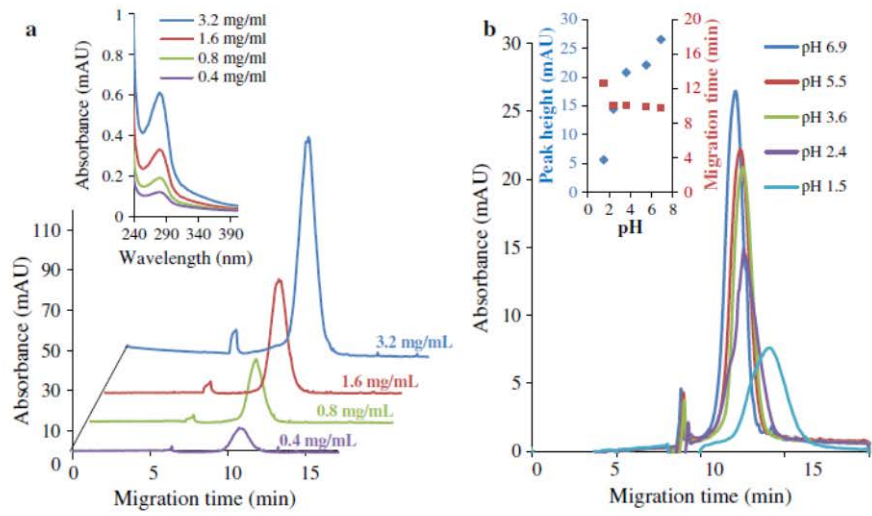


Fig. 4 a Scheme of encapsulation of DOX into the apoferritin and its pH-regulated release. b CE-LIF of Apodox formed by the increasing applied concentration of DOX (BGE: 10 mM phosphate, pH 6, cap-

illary ID 75 μ m, 64.5/54 cm, voltage +20 kV, injection 3 psi, 10 s, detection ex 488 nm/em 600 nm); *inset* dependence of peak height on DOX concentration

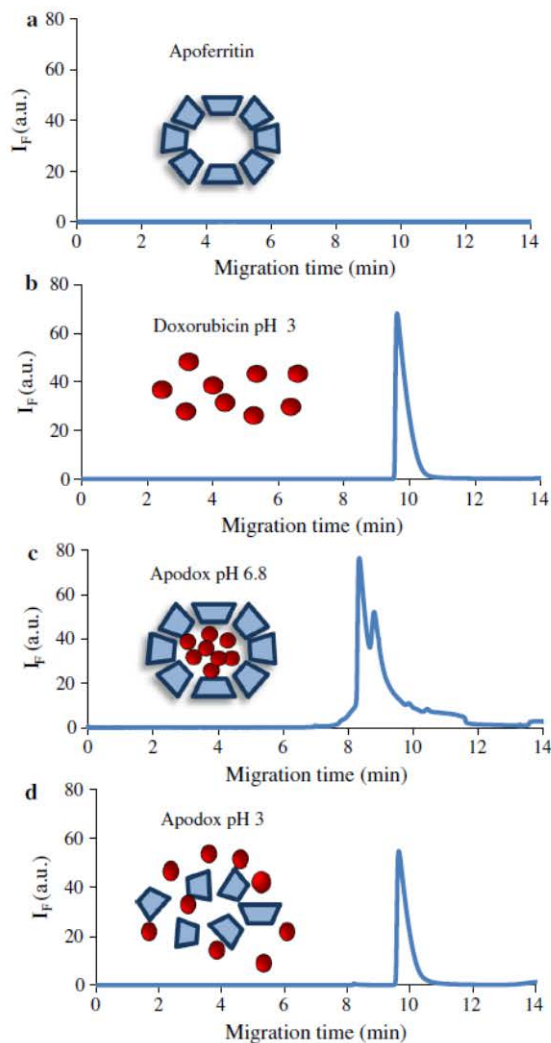


Fig. 5 a CE-LIF of apoferritin (1.6 mg/mL), inset schematics of apoferritin structure. b CE-LIF of DOX (3 $\mu\text{g/mL}$) at pH 3, inset schematics of DOX molecules. c CE-LIF of APODOX at pH 6.8, inset scheme of DOX encapsulated in apoferritin. d CE-LIF of APODOX at pH 2, inset schematic APODOX disassembling by low pH; (BGE: 10 mM phosphate, pH 6, capillary ID 75 μm , 64.5/54 cm, voltage +20 kV, injection 3 psi, 10 s, detection ex 488 nm/em 600 nm)

applied DOX (50–250 $\mu\text{g/mL}$). Subsequently, the samples were analyzed by CE-LIF and typical electropherograms are shown in Fig. 4b. The two major signals were identified. The first peak represents DOX molecule adsorbed on the apoferritin surface and released by electric field. The second peak labeled “APODOX” is attributed to DOX encapsulated into the cavity of apoferritin. As shown in the inset in Fig. 4b, the increase in the applied DOX concentration led to the increase in both signals. Similarly to gel

electrophoresis the highest intensities of two main peaks were detected in the sample with applied 250 $\mu\text{g/mL}$ of DOX.

The pH-triggered release was demonstrated by electrophoretic analysis (Fig. 5). Due to the fact that apoferritin does not exhibit any fluorescence, there is no signal present in the CE-LIF analysis of apoferritin (Fig. 5a). Subsequently, DOX solution with pH adjusted to 3 was analyzed providing a peak with migration time of 10 min. (Fig. 5b). This was compared to the electropherogram of APODOX (Fig. 5c) with pH of 6.8 as well as APODOX with pH decreased to 3 (Fig. 5d). Comparing these three electropherograms, it can be concluded that lowering the pH of APODOX to 3 led to the occurring of a single peak matching the migration time to the DOX at the same conditions. Based on these results, the release of the DOX was proven.

Conclusion

The fluorescent properties of DOX are strongly dependent on the environment and the increasing pH as well as the presence of water causes the fluorescence quenching. Using CE, the electrophoretic mobility of DOX as well as the pI was calculated. Finally, CE-LIF has been proven to be an effective tool for monitoring of the encapsulation into the apoferritin cavity as well as controlled pH-triggered release.

Acknowledgments The financial support from GA CR CYTORES P301/10/0356 is highly acknowledged.

Conflict of interest Authors declare no conflict of interest.

References

- Weiss RB (1992) *Semin Oncol* 19:670–686
- Zagotto G, Gatto B, Moro S, Sissi C, Palumbo M (2001) *J Chromatogr B* 764:161–171
- Singal PK, Iliskovic N (1998) *N Engl J Med* 339:900–905
- Zhen ZP, Tang W, Guo CL, Chen HM, Lin X, Liu G, Fei BW, Chen XY, Xu BQ, Xie J (2013) *ACS Nano* 7:6988–6996
- Meng LJ, Zhang XK, Lu QH, Fei ZF, Dyson PJ (2012) *Biomaterials* 33:1689–1698
- Tacar O, Srimornsak P, Dass CR (2013) *J Pharm Pharmacol* 65:157–170
- Wang YG, Wei XL, Zhang CL, Zhang FY, Liang W (2010) *Ther Del* 1:273–287
- Blazkova I, Nguyen HV, Dostalova S, Kopel P, Stanisavljevic M, Vaculovicova M, Stiborova M, Eckschlager T, Kizek R, Adam V (2013) *Int J Mol Sci* 14:13391–13402
- Drbohlavova J, Chomoucka J, Adam V, Ryvolova M, Eckschlager T, Hubalek J, Kizek R (2013) *Curr Drug Metab* 14:547–564
- Tmejova K, Hynek D, Kopel P, Dostalova S, Smerkova K, Stanisavljevic M, Nguyen HV, Nejd L, Vaculovicova M, Krizkova S, Kizek R, Adam V (2013) *Int J Electrochem Sci* 8:12658–12671
- Baran TM, Foster TH (2013) *Laser Surg Med* 45:542–550

12. Li DA, Zhang YT, Yu M, Guo J, Chaudhary D, Wang CC (2013) *Biomaterials* 34:7913–7922
13. Schenone AV, Culzoni MJ, Campiglia AD, Goicoechea HC (2013) *Anal Bioanal Chem* 405:8515–8523
14. Karukstis KK, Thompson EH, Whiles JA, Rosenfeld RJ (1998) *Biophys Chem* 73:249–263
15. Perez-Ruiz T, Martinez-Lozano C, Sanz A, Bravo E (2001) *Electrophoresis* 22:134–138
16. Ali RMM, Reimold I, Fricker G, Haefeli WE, Burhenne J (2009) *Br J Clin Pharmacol* 68:34
17. Riley CM, Runyan AK, Grahampole J (1987) *Anal Lett* 20:97–116
18. Mazuel C, Grove J, Gerin G, Keenan KP (2003) *J Pharm Biomed Anal* 33:1093–1102
19. Kim HS, Wainer IW (2010) *J Pharm Biomed Anal* 52:372–376
20. Griese N, Blaschke G, Boos J, Hempel G (2002) *J Chromatogr A* 979:379–388
21. Franzen U, Nguyen T, Vermehren C, Gammelgaard B, Ostergaard J (2011) *J Pharm Biomed Anal* 55:16–22
22. Mross K, Niemann B, Massing U, Dreves J, Unger C, Bhamra R, Swenson C (2004) *Cancer Chemother Pharmacol* 54:514–524
23. Dospivova D, Hynek D, Kopel P, Bezdekova A, Sochor J, Krizkova S, Adam V, Trnkova L, Hubalek J, Babula P, Provaznik I, Vrba R, Kizek R (2012) *Int J Electrochem Sci* 7:6378–6395

Article 5

Janu L, Stanisavljevic M, Krizkova S, Sobrova P, Vaculovicova M, Kizek R, Adam V. Electrophoretic study of peptide-mediated quantum dot-human immunoglobulin bioconjugation. Electrophoresis 2013;34(18):2725-2732.

Libor Janu¹
Maja Stanisavljevic¹
Sona Krizkova^{1,2}
Pavlina Sobrova^{1,2}
Marketa Vaculovicova^{1,2}
Rene Kizek^{1,2}
Vojtech Adam^{1,2}

¹Department of Chemistry and Biochemistry, Faculty of Agronomy, Mendel University in Brno, Brno, Czech Republic
²Central European Institute of Technology, Brno University of Technology, Brno, Czech Republic

Received February 14, 2013

Revised March 26, 2013

Accepted March 27, 2013

Research Article

Electrophoretic study of peptide-mediated quantum dot-human immunoglobulin bioconjugation

The bioconjugation of quantum dots (QDs) is a key process in their application for bioanalysis as well as imaging. The coupling of QDs with biologically active molecules such as peptides, nucleic acids, and/or antibodies enables their fluorescent labeling, and therefore, selective and sensitive tracking during the bioanalytical process, however, the efficiency of the labeling and preservation of the biological activity of the bioconjugate have to be considered. In this study, a new approach of the bioconjugation of CdTe-QDs and human immunoglobulin employing a small peptide is described. The heptapeptide (HWRGWVC) was synthesized and characterized by mass spectrometry, liquid chromatography, and capillary electrophoresis. Moreover, the peptide was used as a capping agent for QDs synthesis. The CdTe-QDs were synthesized by microwave synthesis (600 W, 20 min) using 3.2 mM CdCl₂ and 0.8 mM Na₂TeO₃. The bioconjugation of QDs capped by this peptide with immunoglobulin was investigated by capillary electrophoresis and magnetic immunoextraction coupled with electrochemical detection by differential pulse voltammetry. Furthermore, the applicability of prepared bioconjugates for fluorescent immunodetection was verified using immobilized goat antihuman IgG antibody.

Keywords:

Antibody / Bioconjugation / Gel electrophoresis / Immunoglobulin / Quantum dot
DOI 10.1002/elps.201300088

1 Introduction

The development of biocompatible, highly fluorescent nanoparticles including quantum dots (QDs) for chemical and biochemical labeling, immunoanalysis, molecular imaging, and/or targeted therapy is a field attracting an extensive attention [1–15]. The main reason is that nanometer-sized particles have functional and structural properties that are not available from either discrete molecules or bulk materials [16–19]. When conjugated with biomolecular affinity ligands, such as antibodies, peptides, or small molecules, these nanoparticles can be used to target specific molecules such as DNA, proteins, and/or even cells [20–23]. Conjugation of QDs and other biomolecules can be done by covalent coupling, physical adsorption, and hydrophobic adsorption. One of the most frequently used methods is the cross-linking through an *N*-(3-dimethylaminopropyl)-*N*-ethylcarbodiimide hydrochloride (EDC)/*N*-hydroxysuccinimide reaction [24–28]. In the EDC coupling, there is a possibility that the antigen bind-

ing sites of antibodies are blocked by the nonselective formation of amide bonds at the vicinity of Fab (fragment antigen-binding) region of the antibody.

Another conjugation method is based on avidin and/or streptavidin-biotin linkage [29], which provides high specificity and stability. However, due to the sizes of all components (QD, streptavidin, antibody) the result of this method is relatively large nanoparticle (more than 40 nm). Moreover, the biotinylated antibody usually contains multiple biotinylated sites, which leads to the multiple labeling and also the orientation of antibody relative to the QD surface cannot be controlled and may lead to the production of nanoprobe without required functionality. To address these issues, numerous other methods have been developed including high-resolution hybrid gel system specially designed for fractionation of nanoparticle bioconjugates [30]. The conjugation strategy employing an engineered molecular adaptor protein, attached to the QDs via electrostatic/hydrophobic self-assembly [31, 32] and/or protein A as an adaptor protein for binding of antibody to QDs [33]. Protein A is a surface protein found in the cell wall of the bacteria *Staphylococcus aureus*. This protein has an ability to bind immunoglobulins through interaction with their Fc region [34]. Protein-A-mediated antibody conjugation has an advantage that the orientation of antibody can be controlled to face the antigen

Correspondence: Dr. Vojtech Adam, Department of Chemistry and Biochemistry, Mendel University, Brno, Zemedelska 1, CZ-613 00 Brno, Czech Republic
E-mail: vojtech.adam@mendelu.cz
Fax: +420-5-4521-2044

Abbreviations: HlgG, human Ig; HWR, synthetic heptapeptide HWRGWVC; QD, quantum dot

Colour Online: See the article online to view Figs. 1–5 in colour.

binding site outward. Moreover, it was found that a family of linear hexapeptides composed of histidine on the N-terminus followed by aromatic amino acids and positively charged amino acids are able to recognize human Ig (HIgG) through its Fc region, and their selectivity to Fc is comparable to protein A [35]. One of such peptides, HWRGWV, binds all HIgG subclasses and IgGs from bovine, mouse, goat, and rabbit. Capillary electrophoresis provides a high separation power, and therefore, it has a high application potential for analysis and characterization of peptides, QDs, and their bioconjugates [36–39].

In this study, a novel self-assembling bioconjugation method of QDs and antibodies was developed employing the synthetic heptapeptide (HWRGWVC, abbreviated as HWR) and its selective affinity to Fc fragment of IgG.

2 Materials and methods

2.1 Chemicals, pH measurements, and MilliQ water preparation

Cadmium chloride, water, and other chemicals were purchased from Sigma-Aldrich (USA) in ACS purity (chemicals meet the specifications of the American Chemical Society) unless noted otherwise. The pH value and conductivity was measured using inoLab Level 3 (Wissenschaftlich-Technische Werkstätten, Weilheim, Germany). Deionized water underwent demineralization by reverse osmosis using the instruments Aqua Osmotic 02 (Aqua Osmotic, Tisnov, Czech Republic) and then it was subsequently purified using Millipore RG (Millipore, USA, 18 M Ω)—MilliQ water.

2.2 Synthesis of HWR peptide

Peptide with the amino acid sequence HWR was prepared on Prelude peptide synthesizer (Protein Technologies, USA) by standard Fmoc solid-phase peptide synthesis. We used fourfold excess of amino Fmoc-acid with respect to the resin. Deblock of Fmoc protecting group was performed with 20% piperidine v/v in DMF. Coupling was achieved using 1:1:0.5:2 amino acids/*O*-benzotriazole-*N,N,N',N'*-tetramethyl-uronium-hexafluoro-phosphate/*N*-hydroxybenzotriazole/*N,N*-diisopropylethylamine. Cleavage of side chain protecting groups was performed by treating the peptidyl resin with 91.5% TFA v/v, 1.5% phenol v/v, 5% H₂O v/v, and 2% triisopropylsilane v/v for 2 h.

Purity of the crude peptide was analyzed using HPLC (Shimadzu, Japan) with standard mobile phases 0.1% TFA (in water, v/v, A); 80% ACN (in water, v/v), and 0.08% TFA (in water, v/v) (B). MALDI-TOF-MS (Ultraflex III instrument, Bruker Daltonik, Germany) was used to verify the identity of the final product.

2.3 Synthesis of QD-HWR

Cadmium chloride solution (0.04 M, 2 mL) was diluted to 21 mL with ACS water. Then, 50 mg trisodium citrate dihydrate and 2 mL Na₂TeO₃ (0.01 mol/L) were added successively under magnetic stirring. After complete dissolution of the precursors, 0.5 mL of the reaction mixture was transferred to the glass reaction vessel. Two milligrams of peptide HWR was dissolved in 50 μ L DMF and then added to the 0.5 mL of reaction mixture. After that excess of NaBH₄ was added immediately. Reaction vessels were loaded into Microwave digestion system (Anton Paar, Germany) and irradiated with 600 W for 20 min. Temperature limit was 160°C. After microwave irradiation, the mixture was cooled down to 50°C and removed from digestion system.

2.4 Conjugation of QDs with IgG

One hundred microliters of QDs was mixed with 13 μ L IgG from human serum (concentration of IgG was 10 mg/mL) in a sealed vial and 100 μ L of QDs was mixed with 5 μ L IgY (chicken immunoglobulins) from chicken yolk (concentration was 26.2 mg/mL) in a sealed vial. The mixture was vortex-mixed for 2 h at 20°C.

2.5 CE

Electrophoretic measurements were carried out using CE system Beckman P/ACE MDQ with absorbance detection at 214 nm (CE-UV) and Beckman PACE/5500 with LIF detection with excitation at 488 nm (CE-LIF). Uncoated fused silica capillary was used with total length of 60 cm and effective length of 50 cm for CE-UV and 47 cm of total length and effective length of 40 cm for CE-LIF. In both cases, the internal diameter of the capillary was 75 μ m and the outer diameter was 375 μ m. A total of 20 mM sodium borate buffer prepared from sodium tetraborate (the pH 9 was adjusted by 1 M NaOH solution) was used as a background electrolyte and the separation was carried out using 20 kV with hydrodynamic injection for 20 s at 3.4 kPa.

2.6 Fluorimetric measurement

Fluorescence spectra were acquired by multifunctional microplate reader Tecan Infinite 200 PRO (TECAN, Switzerland). An excitation wavelength of 480 nm was used and the fluorescence scan was measured within the range from 510 to 850 nm per 5 nm steps. Each intensity value is an average of five measurements. The detector gain was set to 100. The sample (50 μ L) was placed in transparent 96 well microplate with flat bottom by Nunc.

2.7 SDS-PAGE

Electrophoresis was performed using a Mini Protean Tetra apparatus with gel dimensions of $8.3 \times 7.3 \times 0.1$ cm (Bio-Rad, USA). First 7% w/v running, then 5% w/v stacking gel was poured. The gels were prepared from 30% w/v acrylamide stock solution with 1% w/v bisacrylamide. The polymerization of the running or stacking gels was carried out at room temperature for 45 min. Prior to analysis, the samples were mixed with reducing (3.3% β -mercaptoethanol, v/v) or non-reducing sample buffer in a 1:1 ratio. "Precision plus protein standards" protein ladder from Bio-Rad was used to determine molecular mass. The electrophoresis was run at 150 V for 45 min at laboratory temperature (Power Basic, Bio-Rad) in Tris-glycine buffer (0.025 M Trizma-base, 0.19 M glycine and 3.5 mM SDS, pH 8.3). In order to confirm the conjugation of QDs and IgG, the pH of the running buffer was adjusted to 9.0 with NaOH. After separation the gels were stained with Coomassie-blue according to Wong et al. [40].

2.8 Agarose gel electrophoresis

One-centimeter-thick gels were prepared from 1.5% agarose v/v in $0.5 \times$ TAE buffer (20 mM Tris, 10 mM acetic acid, 0.5 mM EDTA, pH 8). The samples were loaded 5:1 in tris-tricine sample buffer (Bio-Rad). The electrophoresis was run at 100 V for 30 min at laboratory temperature (Biometra, Germany) in $0.5 \times$ TAE buffer.

2.9 Paramagnetic beads modification

IgG from human serum (#I4506) were purchased from Sigma-Aldrich. Chicken antibodies were prepared by HENA, (Prague, Czech Republic) according to the following protocol. Two hens were immunized with Zn-KLH (keyhole limpet hemocyanin) complex. IgY fraction reactive to Zn-KLH was obtained from egg yolk. The antibodies were stabilized with 0.1% NaN_3 v/v in PBS and protein concentration was 39.6 mg/mL in immunoglobulin fraction.

For covalent antibody immobilization, *p*-toluenesulphonyl chloride – activated superparamagnetic polystyrene beads coated with polyurethane layer were used (Dynabeads®MyOne™Tosylactivated, #655.01). Antibody preparation and immobilization protocol was adapted from the supplier's manual (Invitrogen, Norway). For immobilization, 1000 μg of the antibodies per 25 mg of beads was used. Prior to immobilization, NaN_3 was removed and antibodies were acidified to pH 2.5 by addition of HCl. After 15 min, the antibodies were brought into physiological pH 7.4. For all buffer exchanges, Amicon Ultra 0.5 columns with membrane cutoff 50 K (Millipore) were used. Covalent immobilization was carried out in total volume of 625 μL in the presence of 0.1 M borate buffer of pH 9.5 with 0.1 M $(\text{NH}_4)_2\text{SO}_4$ for 24 h under mild rotation. Particle-free surfaces were then blocked with 0.5% BSA in PBS w/v and

0.05% Tween-20 v/v for 10 h. After blocking, the beads were washed three times with 1 mL of 0.1% BSA in PBS w/v with 0.05% Tween-20 v/v and resuspended in 625 μL of storage buffer (washing buffer with 0.02% NaN_3 w/v).

2.10 Immunomagnetic isolation of CdTe-QDs

A 15 μL of Dynabeads®MyOne™ Tosylactivated with human antibodies (Invitrogen) was washed three times with 15 μL of 0.1% BSA in PBS w/v with 0.05% Tween-20 v/v in 1.5 mL tube (Eppendorf, Germany). The washed beads were dispensing to 15 μL of borate buffer (0.1 M NaOH + $\text{Na}_2\text{B}_4\text{O}_7 \cdot 10 \text{H}_2\text{O}$; adjusted by HCl on pH 9.24). Finally, 15 μL CdTe-QDs were added. Immunoextraction was performed for 2 h at room temperature on a rotating programmable rotator-mixer (Biosan, Latvia). The beads were then separated from the solution and washed with 15 μL of borate buffer. Beads were used for the mineralization. The same procedure was carried out for bioconjugation with chicken antibodies.

2.11 Method for detection of cadmium in QDs

Prior to Cd determination, the samples were digested using microwave heating. The mineralization of samples was carried out using a microwave system Multiwave3000 (Anton-Paar). The beads conjugated with QDs (15 μL) was placed into MG5 glass vials and 150 μL of hydrogen peroxide (30%, w/w) and 350 μL of nitric acid (65%, w/w) were added. Prepared samples were sealed and placed into a 64MG5 rotor (Anton-Paar). The rotor with the samples was inserted into the microwave system and the microwave digestion was carried out under the following conditions: power 50 W for 10 min, power 100 W for 30 min, cooling (power 0 W) for 10 min, maximum temperature 80°C. After mineralization, 10 μL mineralized sample was pipetted into Eppendorf tubes with 990 μL of 0.2 M sodium acetate buffer (pH 5.00 adjusted by mixing 0.2 M sodium acetate and 0.2 M acetic acid) and electrochemically analyzed.

Electrochemical measurements were performed at 663 VA Stand, 800 Dosing and 846 Dosing Interface (Metrohm, Switzerland) using a standard cell with three electrodes. A hanging mercury drop electrode with a drop area of 0.4 mm² was employed as the working electrode. An Ag/AgCl/3 M KCl electrode served as the reference electrode and auxiliary electrode was a glassy carbon electrode. All measurements were performed in the presence of 0.2 M sodium acetate buffer (0.2 M CH_3COOH + 0.2 M CH_3COONa , pH 5.0) at 25°C. Samples were deoxygenated with argon (99.99%, 60 s). For smoothing and baseline correction, the software GPES 4.9 supplied by EcoChemie was employed. For electrochemical detection of cadmium, differential pulse voltammetry was used. The parameters of electrochemical determination were as follows: initial potential –0.9 V; end potential –0.1 V; deposition potential –0.9 V; duration 600 s; equilibration time 5 s; modulation time 0.057; time

interval 0.2 s; potential step 0.00195 V; modulation amplitude 0.02505.

2.12 ELISA

Microtitration plate was coated either with of 1 $\mu\text{g}/\text{mL}$ of goat antihuman IgG antibody (Greiner Diagnostics, Germany) or chicken IgY (HENA) diluted in 0.05 M carbonate buffer (0.032 M Na_2CO_3 and 0.068 M NaHCO_3 , pH 9.6) in amount of 50 μL per well overnight at 4°C. Then, the wells were washed five times with 350 μL of 0.005% PBS-T v/v (Hydroflex, TECAN) and blocked for 30 min at 37°C with 50 μL of 1% BSA w/v diluted in PBS. After washing with PBS-T, 50 μL of QDs was pipetted in and the plate was incubated in 37°C for 60 min. After the removing of the solution and washing with PBS-T, the fluorescence scan (510–850 nm) was measured by multifunctional microplate reader Tecan Infinite 200 PRO (TECAN) at excitation wavelength of 480 nm. The fluorescence measuring step was 5 nm. Each intensity value is an average of five measurements and the detector gain was set to 100.

2.13 Statistics

Data were processed using MICROSOFT EXCEL® (USA) and STATISTICA.CZ Version 8.0 (Czech Republic). Results are expressed as mean \pm SD unless noted otherwise (EXCEL®).

3 Results and discussion

3.1 Characterization of the peptide

A short amino acid sequence composed of aromatic and positively charged amino acids is mostly responsible for the specific interaction of HIgG and protein A. Based on this knowledge, an artificial hexapeptide HWRGWV was synthesized with additional cysteine at the C end (HWR) ensuring the ability to work as a capping agent for stabilization of colloidal CdTe quantum dot solution. The synthetically prepared heptapeptide was characterized by mass spectrometry (Fig. 1A), HPLC (Fig. 1B) and capillary electrophoresis (Fig. 1C). According to the mass spectrometry, the molecular mass of the heptapeptide is 942.452 Da. The other found in the spectrum is caused by the presence of adduct of the heptapeptide with tert-butyl, which serves as a protective agent during the peptide synthesis. The characterization by liquid chromatography confirmed the presence of the majority of product by the peak with retention time of 22.5 min (and the contamination with retention time of 23.7 min). The purity of the product was 70%. Finally, one major peak with migration time of 3.8 min and number of un-resolved peaks of possible contaminants were obtained by capillary electrophoresis with photometric detection. Based on the characterization by above-mentioned methods, the quality of the synthesized peptide was found sufficient for further experiments.

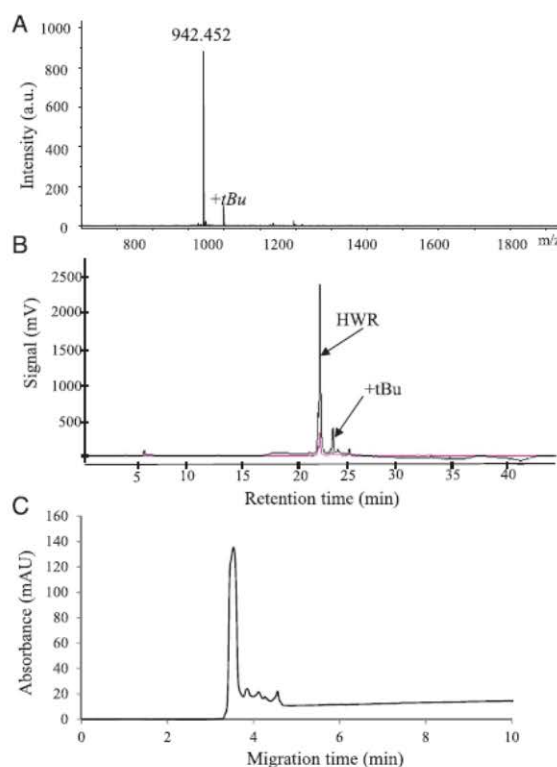


Figure 1. Characterization of synthetic HWR peptide. (A) Mass spectrum of the peptide. (B) HPLC characterization of the peptide. (C) CE characterization of the peptide. CE-UV, conditions—detection: 214 nm; capillary: 75 μm id, 60 cm/50 cm; BGE: 20 mM sodium borate, pH 9.2; voltage: +20 kV; injection: 3.4 kPa, 20 s. MS and HPLC conditions are described in Section 2.

3.2 CdTe-QDs covered with the synthesized peptide

This peptide was subsequently employed as a capping agent for CdTe-QDs. These QDs were characterized by fluorescence spectrometry (Fig. 2A) and capillary electrophoresis (Fig. 2B). Scheme of ideal HWR-QDs structure is shown in the inset of Fig. 2A. The excitation maximum of the HWR-QDs was found to be 480 nm and the emission maximum was 525 nm. These properties are suitable for CE-LIF with excitation wavelength of 488 nm. Prepared QDs were conjugated with HIgGs and because the heptapeptide HWR binds all HIgG subclasses and IgGs from bovine, mouse, goat, and rabbit [35], IgY were used as a nonreactive control, as IgY lack Fc region in their structure [41].

The conjugates were separated by capillary electrophoresis with both laser-induced fluorescence (Fig. 3A) and UV absorbance detection (Fig. 3B). The signals obtained were well developed and separated. QDs incubated with IgY exhibited the same electromigration properties as nonconjugated QDs (migration time of 4.1 min, Fig. 3A and B); however, the migration time of IgG-conjugated QDs (scheme in the

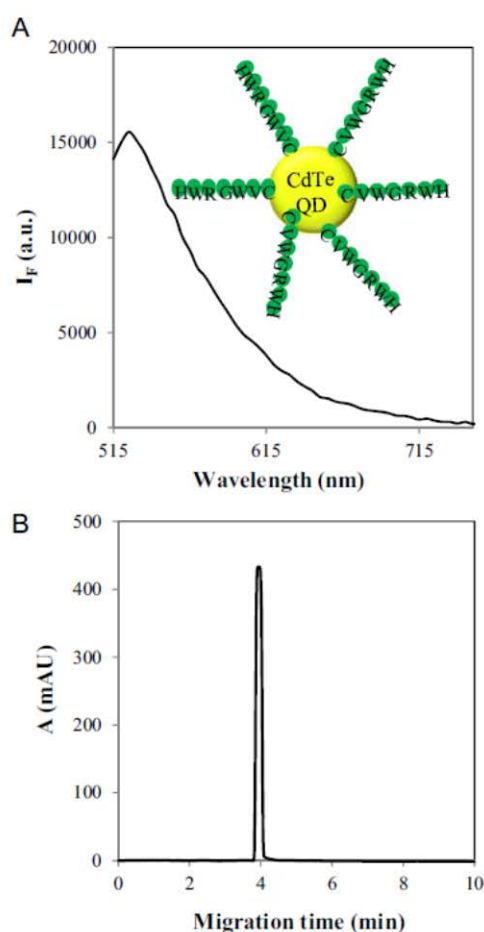


Figure 2. Characterization of HWR-QDs. (A) Emission spectrum of HWR-QDs (excitation 480 nm); inset: scheme of ideal structure of HWR-QDs. (B) CE-UV of HWR-QDs. Experimental conditions—detection wavelength: 214 nm; capillary: 75 μm id, 60 cm/50 cm; BGE: 20 mM sodium borate, pH 9.2; voltage: +20 kV; injection: 3.4 kPa, 20 s.

inset of Fig. 3B) was increased due to the conjugation. After binding of IgG, migration time enhanced to 5 min.

It is known that pI of HIgG is within the range from 6.4 to 9.0 and therefore under the CE conditions used. The IgG molecule is negatively charged so as HWR-QDs. The electrophoretic mobility of HWR-QDs of $-8.13 \pm 0.41 \times 10^{-9} \text{ m}^2 \text{ V}^{-1} \text{ s}^{-1}$ and $-7.81 \pm 0.38 \times 10^{-9} \text{ m}^2 \text{ V}^{-1} \text{ s}^{-1}$ was determined by CE-UV and CE-LIF, respectively. After the conjugation with IgG, the electrophoretic mobility changed to $-14.91 \pm 0.73 \times 10^{-9} \text{ m}^2 \text{ V}^{-1} \text{ s}^{-1}$ and $-14.4 \pm 1.1 \times 10^{-9} \text{ m}^2 \text{ V}^{-1} \text{ s}^{-1}$ determined by CE-UV and CE-LIF. Moreover, we analyzed the conjugate using differential pulse voltammetry after purification, because the dots contain cadmium, which is highly electroactive. Using this, we verified the presence of the HWR-QDs because of detection of Cd(II) peak (inset of Fig. 3B).

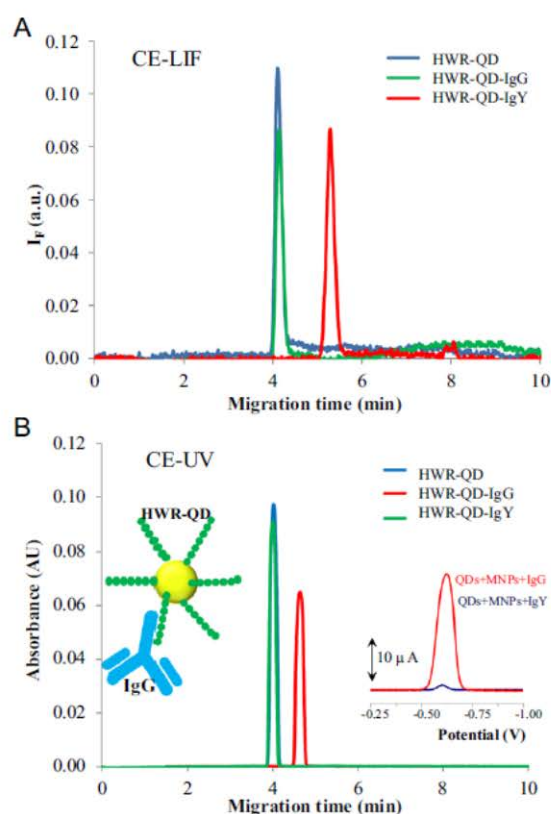


Figure 3. CE of HWR-QD and their bioconjugates with immunoglobulins. (A) CE-LIF conditions—excitation: 488 nm; emission: 520 nm; capillary: 75 μm id, 47.5 cm/40 cm; BGE: 20 mM sodium borate, pH 9.2; voltage: +20kV; injection: 3.4 kPa, 20 s. (B) CE-UV, conditions—detection: 214 nm; capillary: 75 μm id, 60 cm/50 cm; BGE: 20 mM sodium borate, pH 9.2; voltage: +20 kV; injection: 3.4 kPa, 20 s; left inset: scheme of HWR-QD-IgG; right inset: differential pulse voltammograms of Cd determination extracted by magnetic particles coated with IgG and IgY. Experimental conditions—dilution: 1:1000; electrolyte: 0.2 M acetate buffer (0.2 M CH_3COOH + 0.2 M CH_3COONa , pH 5.0) at 25°C; initial potential: -0.9 V ; end potential: -0.1 V ; deposition potential: -0.9 V ; duration: 600 s; equilibration time: 5 s; modulation time: 0.057; time interval: 0.2 s; potential step: 0.00195 V; modulation amplitude: 0.02505.

3.3 Gel electrophoretic analysis

To verify the conjugation of HWR-QD and IgG the gel electrophoresis was employed. At first, the SDS-PAGE analysis of HWR-QDs, IgG and IgY standards as well as HWR-QD-IgG or HWR-QD-IgY conjugates under reducing and nonreducing conditions was carried out (Fig. 4A). After fluorescence imaging it was not possible to detect any fluorescence (not shown). IgG and IgY standards were resolved as expected. Under nonreducing conditions at IgG, three bands in size of approximately 150–170, 140, and 100 kDa corresponding to whole and partially fragmented IgG molecules were present and three bands in size of approximately 180, 170,

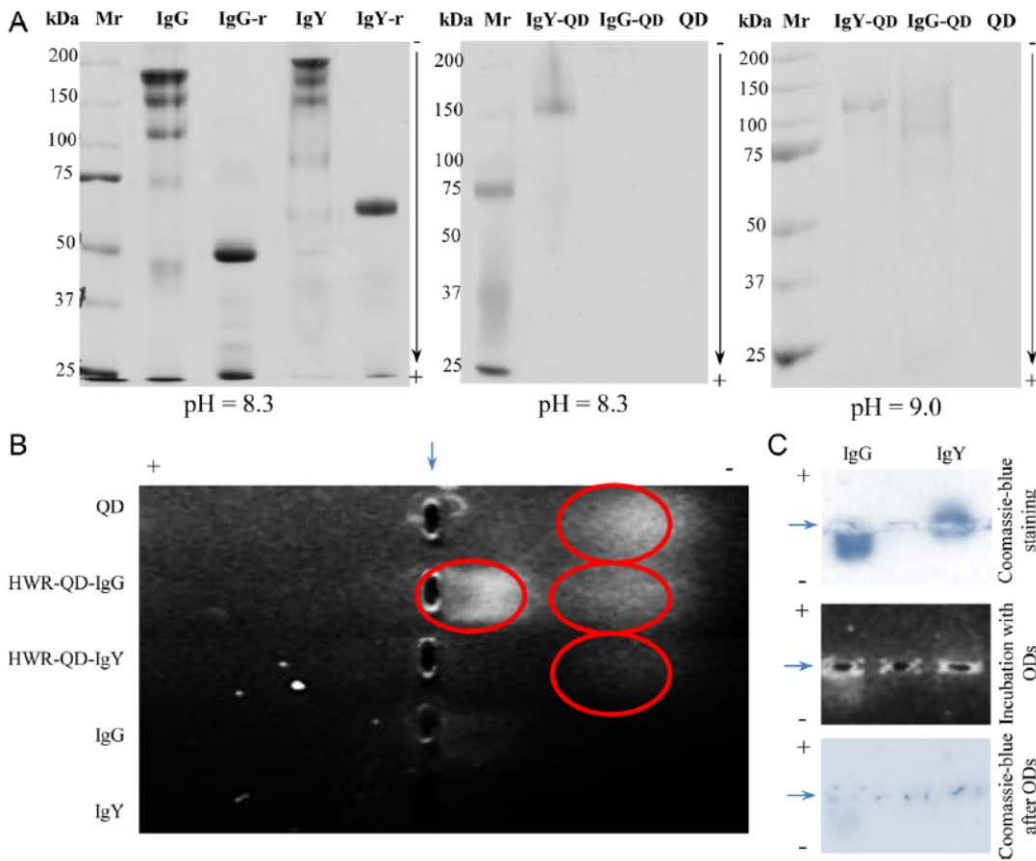


Figure 4. (A) SDS-PAGE electropherogram of 1000 ng of IgG and IgY standards under reducing (3.3% β -mercaptoethanol v/v, labeled as -r) and nonreducing conditions in running electrolyte pH 8.3 (left), SDS-PAGE electropherogram of QD-IgG and IgY conjugates in running electrolyte pH 8.3 (in the middle), SDS-PAGE electropherogram of QD-IgG and IgY conjugates in running electrolyte pH 9.0 (right). (B) Agarose gel electropherogram of QD-IgG and IgY conjugates, and pH of the running buffer is 8.0. Arrow indicates wells position, and (+) and (-) indicate poles orientation. (C) Agarose gel electropherogram of IgG and IgY stained either with Coomassie-blue (above) or incubated with QDs (in the middle) and consequently with Coomassie-blue (below), and pH of the running buffer is 8.0. Arrows indicate wells positions, and (+) and (-) indicate poles orientation.

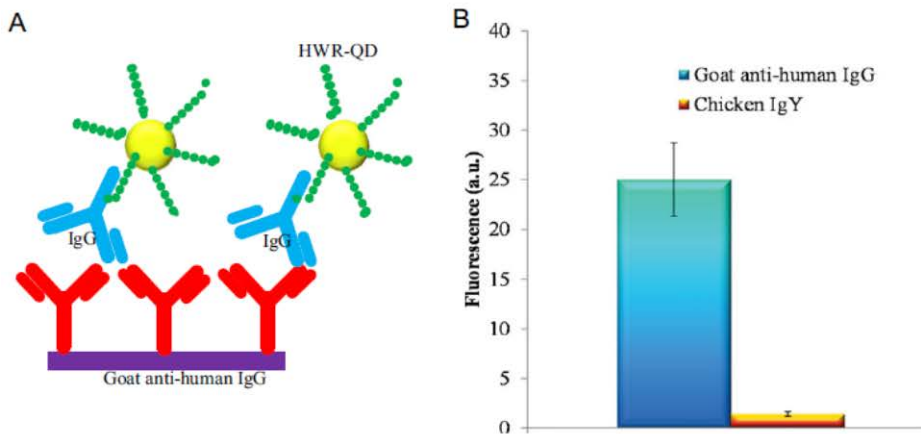


Figure 5. Fluorescent immunodetection. (A) Scheme of the possible interaction between HWR-QD-IgG and goat antihuman IgG. (B) Fluorescence intensity determined in the wells coated with goat antihuman IgG and chicken IgY (excitation: 480 nm and emission: 525 nm).

and 130 kDa corresponding whole and partially fragmented IgY molecules were present at IgY. Under reducing conditions at IgG two bands in size of approximately 50 and 25 kDa corresponding to large and small IgG subunits were present and two bands in size of approximately 65 and 20 kDa corresponding to large and small IgY subunits were present at IgY. For HWR-QD-IgG conjugate or HWR-QDs alone, no bands were detected, only a weak band of molecular size corresponding to partially reduced IgY molecule was observed for HWR-QD-IgY.

Binding of QDs modified with HWR peptide to IgG might affect migration of IgG conjugate, even though SDS binding to the proteins surface unifies their charge. Reduced SDS binding to HWR-QD-IgG conjugate is also possible. Therefore, the samples were run under the same conditions, but with switched poles. However, still no bands were observed (not shown). After changing of running buffer pH to 9.0, bands of sizes corresponding to partially reduced whole immunoglobulin molecules were observed after Coomassie-blue staining for both HWR-QD-IgG and HWR-QD-IgY conjugates, but no fluorescence was detected even for HWR-QDs alone. Different behavior of IgG and IgY mixtures dependent on running buffer pH indicates that HWR-QDs bound to IgG molecules, and did not bind to IgY molecules, but the fluorescence of HWR-QDs might be quenched during the electrophoresis. Fluorescence of both HWR-QDs and HWR-QDs-IgG conjugates was observed after agarose gel electrophoresis (Fig. 4B). In running electrolyte of pH 8.0, both HWR-QDs and HWR-QD-IgG conjugates migrated to negative pole and at HWR-QD-IgY mixture only the band corresponding to unconjugated HWR-QDs was recorded. Only very weak fluorescence was detected for IgG and IgY standards. As it is shown in Fig. 4C, after staining the agarose gel of immunoglobulin standards with Coomassie-blue, the weak fluorescence signals might be caused by IgG themselves. To confirm it, we incubated IgG and IgY resolved in agarose gel with HWR-QDs in running electrolyte for 16 h. After incubation, the fluorescence was observed in IgG only. The same gel was stained with Coomassie-blue and very weak band disproportional to original signal was observed in IgG only. This indicates that IgG was stabilized in the gel by HWR-QDs binding, while IgY was completely washed out.

The results of SDS-PAGE and agarose electrophoresis are consistent and confirm binding of QDs modified with HWR to IgG, but not to IgY. In addition, after HWR-QDs binding to IgG, their charge is modified. Moreover, HWR-QDs are applicable for IgG detection in agarose gels.

3.4 ELISA detection of HWR-QDs

To demonstrate the applicability of developed conjugates for immunodetection, ELISA experiment was carried out. The microtitration plate was coated with goat anti-human IgG (or chicken IgY—as a nonbinding control) in concentration of 1 µg/mL and subsequently incubated with HWR-QD-IgG according to scheme shown in Fig. 5A. It was found out that

the intensity of fluorescence in the wells coated with goat antihuman IgG exhibited significantly higher fluorescence at 525 nm than the wells coated with chicken IgY (Fig. 5B). The suggested procedure could be used for sensitive immuno-based techniques [42], for imaging approaches [6] and for microarrays technologies to determine Alzheimer's disease biomarkers [43], tumor markers [44], and C-reactive peptides [45].

4 Concluding remarks

The surface modification and functionalization of QDs is extensively studied due to the possibility of fine-tuning of the properties according to the requirements. Their functionalization by antibodies enables the fluorescent visualization of interactions between the antigen and antibody as well as biodistribution. However, the bond between the antibody and QD has to exhibit correct sterical orientation to preserve the biological activity of the antibody and to provide required efficiency. It was demonstrated that small synthetic heptapeptide (HWR) can serve as a QD capping agent providing suitable surface properties for interaction with Fc fragment of human IgG.

Financial support from the following projects PGS07_2012, NanoBioTECell GA CR P102/11/1068, CEITEC CZ.1.05/1.1.00/02.0068 and CZ.1.07/2.3.00/30.039 is highly acknowledged. The authors wish to express their thanks to Eva Jilkova for perfect technical assistance.

The authors have declared no conflict of interest.

5 References

- [1] Medintz, I. L., Uyeda, H. T., Goldman, E. R., Mattoussi, H., *Nat. Mater.* 2005, 4, 435–446.
- [2] Michalet, X., Pinaud, F. F., Bentolila, L. A., Tsay, J. M., Doose, S., Li, J. J., Sundaresan, G., Wu, A. M., Gambhir, S. S., Weiss, S., *Science* 2005, 307, 538–544.
- [3] Drbohlavova, J., Chomoucka, J., Hrdy, R., Prasek, J., Janu, L., Ryvolova, M., Adam, V., Kizek, R., Halasova, T., Hubalek, J., *Int. J. Electrochem. Sci.* 2012, 7, 1424–1432.
- [4] Drbohlavova, J., Vorozhtsova, M., Hrdy, R., Kizek, R., Salyk, O., Hubalek, J., *Nanoscale Res. Lett.* 2012, 7, 1–4.
- [5] Krejcová, L., Huska, D., Hýnek, D., Kopel, P., Adam, V., Hubalek, J., Trnkova, L., Kizek, R., *Int. J. Electrochem. Sci.* 2013, 8, 689–702.
- [6] Ryvolova, M., Chomoucka, J., Drbohlavova, J., Kopel, P., Babula, P., Hýnek, D., Adam, V., Eckschlager, T., Hubalek, J., Stiborova, M., Kaiser, J., Kizek, R., *Sensors* 2012, 12, 14792–14820.
- [7] Krejcová, L., Dospivová, D., Ryvolova, M., Kopel, P., Hýnek, D., Krizkova, S., Hubalek, J., Adam, V., Kizek, R., *Electrophoresis* 2012, 33, 3195–3204.
- [8] Chen, G. H., Sun, J., Dai, Y. J., Dong, M., *Electrophoresis* 2012, 33, 2192–2196.

- [9] Hlavacek, A., Skladal, P., *Electrophoresis* 2012, 33, 1427–1430.
- [10] Chen, Q. D., Fung, Y. S., *Electrophoresis* 2010, 31, 3107–3114.
- [11] Kleparnik, K., Voracova, I., Liskova, M., Prikryl, J., Hezínova, V., Foret, F., *Electrophoresis* 2011, 32, 1217–1223.
- [12] Ryvolova, M., Chomoucka, J., Janu, L., Drbohlavova, J., Adam, V., Hubalek, J., Kizek, R., *Electrophoresis* 2011, 32, 1619–1622.
- [13] Wang, J. J., Huang, X. Y., Zan, F., Guo, C. G., Cao, C. X., Ren, J. C., *Electrophoresis* 2012, 33, 1987–1995.
- [14] Frigerio, C., Ribeiro, D. S. M., Rodrigues, S. S. M., Abreu, V., Barbosa, J. A. C., Prior, J. A. V., Marques, K. L., Santos, J. L. M., *Anal. Chim. Acta* 2012, 735, 9–22.
- [15] Kuang, H., Zhao, Y., Ma, W., Xu, L. G., Wang, L. B., Xu, C. L., *Trac-Trends Anal. Chem.* 2011, 30, 1620–1636.
- [16] Biju, V., Itoh, T., Anas, A., Sujith, A., Ishikawa, M., *Anal. Bioanal. Chem.* 2008, 391, 2469–2495.
- [17] Ledentsov, N. N., Ustinov, V. M., Shchukin, V. A., Kop'ev, P. S., Alferov, Z. I., Bimberg, D., *Semiconductors* 1998, 32, 343–365.
- [18] Yoffe, A. D., *Adv. Phys.* 2001, 50, 1–208.
- [19] Chomoucka, J., Drbohlavova, J., Masarik, M., Ryvolova, M., Huska, D., Prasek, J., Horna, A., Trnkova, L., Provaznik, I., Adam, V., Hubalek, J., Kizek, R., *Int. J. Nanotechnol.* 2012, 9, 746–783.
- [20] Auyeung, E., Cutler, J. I., Macfarlane, R. J., Jones, M. R., Wu, J. S., Liu, G., Zhang, K., Osberg, K. D., Mirkin, C. A., *Nat. Nanotechnol.* 2012, 7, 24–28.
- [21] Boukany, P. E., Morss, A., Liao, W. C., Henslee, B., Jung, H. C., Zhang, X. L., Yu, B., Wang, X. M., Wu, Y., Li, L., Gao, K. L., Hu, X., Zhao, X., Hemminger, O., Lu, W., Lafyatis, G. P., Lee, L. J., *Nat. Nanotechnol.* 2011, 6, 747–754.
- [22] Chivers, C. E., Crozat, E., Chu, C., Moy, V. T., Sherratt, D. J., Howarth, M., *Nat. Methods* 2010, 7, 391–U376.
- [23] Tikhomirov, G., Hoogland, S., Lee, P. E., Fischer, A., Sargent, E. H., Kelley, S. O., *Nat. Nanotechnol.* 2011, 6, 485–490.
- [24] Wang, Y., Bai, Y., Wei, X., *IET Nanobiotechnol.* 2011, 5, 14–19.
- [25] Li, J., Zhou, X. P., Ni, S. Y., Wang, X. Q., *Colloid J.* 2010, 72, 710–715.
- [26] Hua, X. F., Liu, T. C., Cao, Y. C., Liu, B., Wang, H. Q., Wang, J. H., Huang, Z. L., Zhao, Y. D., *Anal. Bioanal. Chem.* 2006, 386, 1665–1671.
- [27] Kuo, Y. C., Wang, Q., Ruengruglikit, C., Yu, H. L., Huang, Q. R., *J. Phys. Chem. C* 2008, 112, 4818–4824.
- [28] Llopis, X., Pumera, M., Alegret, S., Merkoci, A., *Lab. Chip.* 2009, 9, 213–218.
- [29] Goldman, E. R., Balighian, E. D., Mattoussi, H., Kuno, M. K., Mauro, J. M., Tran, P. T., Anderson, G. P., *J. Am. Chem. Soc.* 2002, 124, 6378–6382.
- [30] Liu, H. Y., Gao, X. H., *Bioconjugate Chem.* 2011, 22, 510–517.
- [31] Goldman, E. R., Anderson, G. P., Tran, P. T., Mattoussi, H., Charles, P. T., Mauro, J. M., *Anal. Chem.* 2002, 74, 841–847.
- [32] Goldman, E. R., Balighian, E. D., Kuno, M. K., Labrenz, S., Tran, P. T., Anderson, G. P., Mauro, J. M., Mattoussi, H., *Phys. Status Solidi B-Basic Res.* 2002, 229, 407–414.
- [33] Jin, T., Tiwari, D. K., Tanaka, S., Inouye, Y., Yoshizawa, K., Watanabe, T. M., *Mol. Biosyst.* 2010, 6, 2325–2331.
- [34] Krizkova, S., Ryvolova, M., Hynek, D., Eckschlager, T., Hodek, P., Masarik, M., Adam, V., Kizek, R., *Electrophoresis* 2012, 33, 1824–1832.
- [35] Yang, H., Gurgel, P. V., Carbonell, R. G., *J. Pept. Res.* 2005, 66, 120–137.
- [36] Carrillo-Carrion, C., Moliner-Martinez, Y., Simonet, B. M., Valcarcel, M., *Anal. Chem.* 2011, 83, 2807–2813.
- [37] Huang, X. Y., Weng, J. F., Sang, F. M., Song, X. T., Cao, C. X., Ren, J. C., *J. Chromatogr. A* 2006, 1113, 251–254.
- [38] Kasicka, V., *Electrophoresis* 2012, 33, 48–73.
- [39] Song, X. T., Li, L., Chan, H. F., Fang, N. H., Ren, J. C., *Electrophoresis* 2006, 27, 1341–1346.
- [40] Wong, P., Barbeau, A., Roses, A. D., *Anal. Biochem.* 1985, 150, 288–293.
- [41] Mizutani, N., Sugita-Konishi, Y., Omoe, K., Shinagawa, K., Kawakami, H., Kanno, S., Sugiyama, K., Kamata, Y., *Int. J. Food Sci. Technol.* 2012, 47, 155–159.
- [42] Liu, J. M., Lin, L. P., Liu, Z. B., Yang, M. L., Wang, X. X., Zhang, L. H., Cui, M. L., Jiao, L., *J. Fluoresc.* 2012, 22, 419–429.
- [43] Morales-Narvaez, E., Monton, H., Fomicheva, A., Merkoci, A., *Anal. Chem.* 2012, 84, 6821–6827.
- [44] Tian, J. N., Zhou, L. J., Zhao, Y. C., Wang, Y., Peng, Y., Zhao, S. L., *Talanta* 2012, 92, 72–77.
- [45] Luo, Y., Zhang, B., Chen, M., Jiang, T. L., Zhou, D. Y., Huang, J. F., Fu, W. L., *J. Transl. Med.* 2012, 10, 24.

Article 6

Ryvolova M, Chomoucka J, Janu L, Drbohlavova J, Adam V, Hubalek J, Kizek R. Biotin-modified glutathione as a functionalized coating for bioconjugation of CdTe-based quantum dots. *Electrophoresis* 2011 Jun;32(13):1619-1622.

Marketa Ryvolova¹
 Jana Chomoucka²
 Libor Janu¹
 Jana Drbohlavova²
 Vojtech Adam¹
 Jaromir Hubalek²
 Rene Kizek¹

¹Department of Chemistry and Biochemistry, Faculty of Agronomy, Mendel University in Brno, Brno, Czech Republic
²Department of Microelectronics, Faculty of Electrical Engineering and Communication, Brno University of Technology, Brno, Czech Republic

Received November 29, 2010
 Revised February 4, 2011
 Accepted February 7, 2011

Short Communication

Biotin-modified glutathione as a functionalized coating for bioconjugation of CdTe-based quantum dots

In this study, biotin-conjugated glutathione was synthesized using peptide bonding of the biotin carboxy group and amino group of the γ -glutamic acid to prepare an alternative coating for CdTe quantum dots (QDs). This type of coating combines the functionality of the biotin with the fluorescent properties of the QDs to create a specific, high-affinity fluorescent probe able to react with avidin, streptavidin and/or neutravidin. Biotin-functionalized glutathione-coated CdTe QDs were prepared by a simple one-step method using Na_2TeO_3 and CdCl_2 . Obtained QDs were separated from the excess of the biotin-conjugated glutathione by CE employing 300 mM borate buffer with pH 7.8 as a background electrolyte. The detection of sample components was performed by the photometric detection at 214 nm and LIF employing Ar^+ ion laser (488 nm).

Keywords:

Biotin-conjugated glutathione / CE / Glutathione / Quantum dot / Streptavidin-biotin
 DOI 10.1002/elps.201000634

Quantum dots (QDs) with the dimensions in the range of 2–10 nm belong to the family of nanomaterials having a significant impact on chemical as well as on biological research. QDs are semiconductor nanocrystals with unique spectral properties featured mainly by the size-tunable emissions due to quantum size effects and high resistance toward photobleaching. The emission spectra of homogeneously sized QDs are narrower than typical fluorophores and a variety of QDs types can be produced covering almost the whole spectral range [1, 2]. Since their first appearance in the late 1980s [3–5], the interest in QDs has increased extremely; however, the application of QDs as fluorescent probes has been triggered by their bioconjugation to the target compounds enabling the specific fluorescent labeling of biological samples. Currently, QDs play an important role mainly in the imaging and as fluorescent probes for biological sensing [2]. The most popular types of QDs include CdTe, CdSe, ZnSe and ZnS; however, other semiconductor metals such as In, Ga and many others also can be used [6, 7]. Majority of sensing techniques employing QDs in biological systems are applied in solution (colloidal form) [8–10]. To date, two original approaches have been reported for the synthesis of colloidal QDs. The organome-

talic way produces QDs, which are generally capped with hydrophobic ligands (e.g. trioctylphosphine oxide (TOPO)) and hence cannot be directly employed in bioapplications. The second way is the aqueous synthesis route, producing QDs with excellent water solubility, biological compatibility and stability. Thiol-capped QDs could be prepared directly in aqueous solution with thiols as efficient stabilizers. Cysteine [11, 12], mercaptopropionic acid [9, 13] and reduced glutathione (GSH) [14–16] are the most popular coatings among thiols; however, quantum yields only up to 10% were typically obtained without any following treatment [17]. On the other hand, GSH due to its key function in detoxification of heavy metals in organisms [18] provides an additional functionality to the QDs. The fluorescence is considerably quenched at the presence of heavy metals and therefore glutathione-coated QDs (GSH-QDs) were successfully employed for determination of heavy metals [19, 20]. In addition, GSH-QDs exhibit high sensitivity to H_2O_2 produced from the glucose oxidase catalyzing oxidation of glucose and therefore glucose can be sensitively detected by the quenching of the GSH-QDs fluorescence [21]. Beside the application as simple sensors, QDs have much higher impact as unique fluorescent labels. Various specific labeling strategies are known and most of these approaches are based on bioconjugation with other biomolecules exhibiting some specific affinity to the target compound. Summary of these approaches was recently presented in a review article published by Algar et al. [2]. One of these strategies utilizes the biotin-avidin (respectively, streptavidin and neutravidin) interaction, exhibiting very high specificity. Modification of QDs by the streptavidin proved

Correspondence: Dr. Rene Kizek, Department of Chemistry and Biochemistry, Mendel University, Czech Republic
 E-mail: kizek@sci.muni.cz
 Fax: +420-5-4521-2044

Abbreviations: B-GSH, biotinylated glutathione; B-GSH-QDs, QDs coated with B-GSH; GSH, reduced glutathione; GSH-QDs, quantum dots coated with reduced glutathione; QDs, quantum dots

Colour Online: See the article online to view Figs. 2 and 3 in colour

to be a very successful method evaluated in various publications [22–24] and due to this success streptavidin-QDs are nowadays also commercially available. Also, biotin-functionalized QDs have been developed to exploit the same interaction [25–28]. However, so-called multicolor QDs, which means that particles modified by several different molecules, are now of great interest.

Therefore, the aim of this study was to prepare QDs applicable in organisms based on the biocompatible properties due to the presence of GSH and also with the possibility to be employed in modern biotechnological biotin–avidin (or its homologues) applications. The first aim was to prepare biotinylated GSH, which would be subsequently used concurrently as a stabilizer of QDs and bio-reactive layer.

Biotin and GSH were conjugated via standard peptide bond using carboxy group of the biotin and amino group of the γ -glutamic acid. The biotinylation at the N-end of the tripeptide was the last step of the peptide synthesis. The purification of the product was carried out using high-performance liquid chromatography and the purity of 99% was reached. Final product (for structure, see Fig. 1) was analyzed by mass spectrometry (MS). Matrix-assisted laser desorption/ionization-time of flight-mass spectrometry (MALDI-TOF-MS) was carried out using an Ultraflex III instrument (Bruker Daltonik, Germany). Samples (0.6 μ L) were pre-mixed with 2.4 μ L of the matrix solution (saturated solution of α -cyano-4-hydroxycinnamic acid in a water/acetonitrile mixture 1:1, v/v) and 0.6 μ L of this mixture was deposited on a stainless steel MALDI target. Measurements were carried out in a reflectron positive ion detection arrangement. The obtained MS spectrum is shown in Fig. 1. The major peak in the spectrum has the molecular mass of 532.185, which is in good agreement with the theoretical molecular mass of 532.2 Da calculated for the biotinylated glutathione (B-GSH). Then, B-GSH was used as an alter-

native coating for CdTe-based QDs (emission maximum at 504 nm). The procedure for synthesis of these dots was adapted from the work of Duan et al. [29]. Sodium tellurite was used as the Te source. Owing to the fact that sodium tellurite is air stable, all of the operations were performed in the air without requiring any inert atmosphere. The synthesis pathway is thus very simple using harmless aqueous solutions. The synthesis of CdTe QDs and their subsequent coating were as follows: 330 μ L of the CdCl₂ solution ($c = 0.04$ mol/L) was diluted with 2.5 mL of water. During constant stirring, 8 mg of sodium citrate, 330 μ L of Na₂TeO₃ solution ($c = 0.01$ mol/L), 15 mg of B-GSH and 3.3 mg of NaBH₄ were added into water–cadmium(II) solution. The mixture was kept at 95 °C under the reflux cooling for 2.5 h. As a result, yellow solution of the QDs coated with B-GSH (B-GSH-QDs) was obtained. An inset in Fig. 2 shows the solution of the B-GSH-QDs under the ambient light (left) and the fluorescence under the illumination by the UV lamp is shown in the right.

Synthesized B-GSH-QDs were analyzed by CE (Beckman Coulter, PACE 5500) with absorbance detection at 214 nm and with the LIF detection (Ar⁺, $\lambda_{\text{ex}}=488$ nm/ $\lambda_{\text{em}}=530$ nm). Separation of the excess of B-GSH and GSH was carried out using uncoated fused-silica capillary with 50 m internal diameter and 375 m *b* outer diameter. Total length was 47 cm and the effective length was 40 cm. Borate buffer (300 mmol/L, pH 7.8) was used as a background electrolyte (BGE). The typical electropherogram of the B-GSH-QD solution is shown in Fig 2A. Signals of GSH, B-GSH as well as B-GSH-QDs were baseline separated with the resolutions of 1.9 (GSH–B-GSH) and 4.2 (B-GSH–B-GSH-QDs). The identification of GSH and B-GSH signals was done by the standard addition method and identification of the B-GSH-QDs signal was done by CE-LIF (Fig. 2B).

CE-LIF was also used for monitoring of the stability of B-GSH-QDs during storage in the dark at 4 °C. QDs were

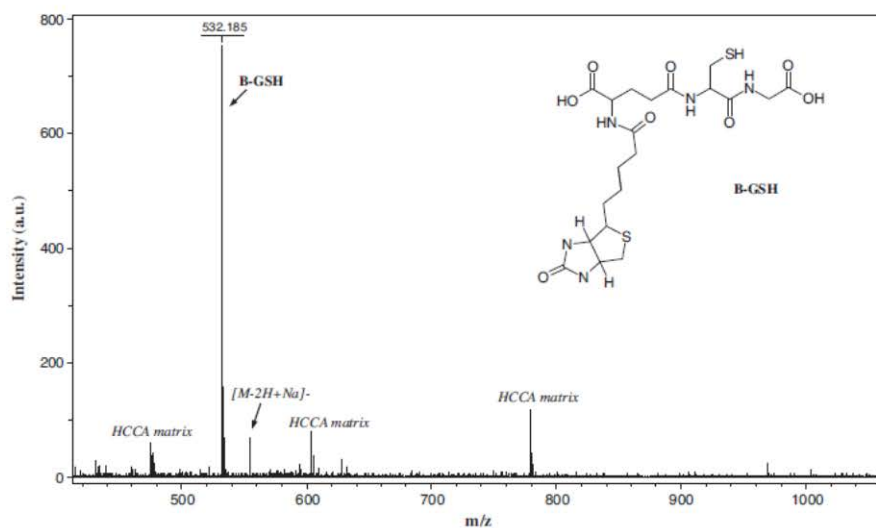


Figure 1. MALDI-TOF MS spectrum obtained for B-GSH (matrix: α -cyano-4-hydroxycinnamic acid; for more details, see text) and structure of the B-GSH.

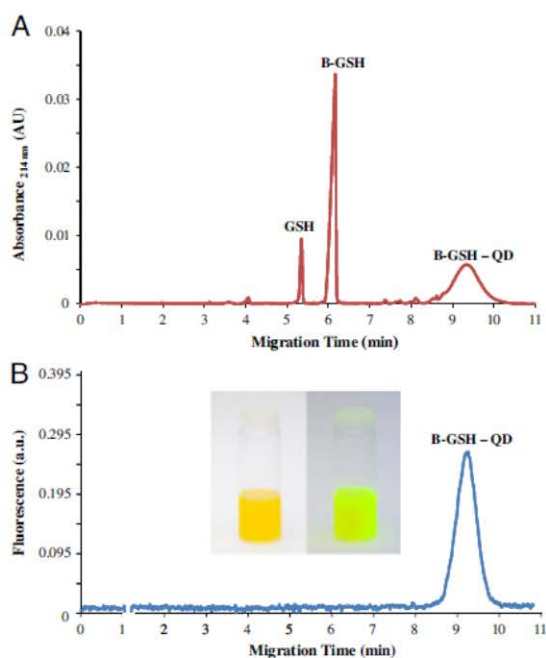


Figure 2. Electropherogram of the mixture of the B-GSH-QDs and excess B-GSH and GSH; BGE: 300 mmol/L sodium borate buffer, pH 7.8; U: +20 kV; injection: 0.5 psi for 20 s; (A) UV detection at 214 nm; (B) LIF detection (488 nm/530 nm); inset: B-GSH-QDs under ambient light (left), B-GSH-QDs under UV light illumination (right).

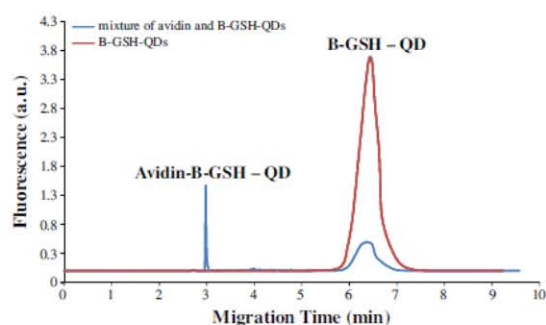


Figure 3. Electropherogram of the mixture of the B-GSH-QDs and avidin solution; BGE: 20 mmol/L sodium borate buffer, pH 9.5; U: +20 kV; injection: 0.5 psi for 20 s; LIF detection (488 nm/530 nm).

sampled per 6 h and the signal height of B-GSH-QDs was observed. The height of the signal steadily decreased with increasing time of the storage. After 3 days, the height decreased for more than 80%. Based on the results obtained, it can be concluded that the B-GSH-QDs are less stable in comparison with the QDs coated with unmodified GSH (GSH-QDs) created according to the same procedure [29].

The functionality of B-GSH-QDs was tested by addition of the avidin solution. The resulted mixture was analyzed by

CE-LIF and typical electropherogram is shown in Fig. 3. The separation procedure was adapted from Huang et al. [30] and sodium borate buffer (20 mmol/L, pH 9.5) was used as a BGE. It was observed that the protein-QD complex was well separated from the QDs and the signal intensity of the avidin-B-GSH-QD complex was directly proportionate to the concentration of the avidin added and the signal of B-GSH-QDs decreased accordingly.

It follows from the results obtained that B-GSH is a suitable alternative coating for the elegant single-step synthesis of thiol-stabilized CdTe QDs. Obtained QDs are of good properties for the fluorimetric detection with the excitation by Ar⁺ laser at the wavelength of 488 nm and emission of 530 nm. Moreover, we show that CE is an efficient method for the separation of the GSH and B-GSH excess from the B-GSH-QDs and for stability control.

This work was supported by NANOSEMED GA AV KAN208130801 and GA CR 102/10/P618.

The authors have declared no conflict of interest.

References

- [1] Drbohlavova, J., Adam, V., Kizek, R., Hubalek, J., *Int. J. Mol. Sci.* 2009, 10, 656–673.
- [2] Algar, W. R., Tavares, A. J., Krull, U. J., *Anal. Chim. Acta* 2010, 673, 1–25.
- [3] Reed, M. A., Bate, R. T., Bradshaw, K., Duncan, W. M., Frensley, W. R., Lee, J. W., Shid, H. D., *J. Vac. Sci. Technol. B* 1986, 4, 358–360.
- [4] Takagahara, T., *Phys. Rev. B* 1987, 36, 9293–9296.
- [5] Miller, D. A. B., Chemla, D. S., Schmittrink, S., *Appl. Phys. Lett.* 1988, 52, 2154–2156.
- [6] Green, M., O'Brien, P., *Chem. Commun.* 1998, 2459–2460.
- [7] Goodwin, T. J., Leppert, V. J., Risbud, S. H., Kennedy, I. M., Lee, H. W. H., *Appl. Phys. Lett.* 1997, 70, 3122–3124.
- [8] Quan, C., Li, A. M., Gao, N. B., *J. Hazard. Mater.* 2010, 179, 911–917.
- [9] Ndangili, P. M., Arotiba, O. A., Baker, P. G. L., Iwuoha, E. I., *J. Electroanal. Chem.* 2010, 643, 77–81.
- [10] Veilleux, V., Lachance-Quirion, D., Dore, K., Landry, D. B. et al., *Nanotechnology* 2010, 21, 6.
- [11] Zhao, W. F., Fung, Y. S., O, W. S., Cheung, M. P. L., *Anal. Sci.* 2010, 26, 879–884.
- [12] Li, M. Y., Zhou, H. M., Zhang, H. Y., Sun, P., Yi, K. Y., Wang, M., Dong, Z. Z., Xu, S. K., *J. Lumin.* 2010, 130, 1935–1940.
- [13] Wang, C., Gao, X., Ma, Q., Su, X. G., *J. Mater. Chem.* 2009, 19, 7016–7022.
- [14] Ali, E. M., Zheng, Y. G., Yu, H. H., Ying, J. Y., *Anal. Chem.* 2007, 79, 9452–9458.
- [15] Zheng, Y. G., Gao, S. J., Ying, J. Y., *Adv. Mater.* 2007, 19, 376–380.

- [16] Zheng, Y. G., Yang, Z. C., Ying, J. Y., *Adv. Mater.* 2007, **19**, 1475–1479.
- [17] Gaponik, N., Talapin, D. V., Rogach, A. L., Hoppe, K., Shevchenko, E. V., Kornowski, A., Eychmuller, A., Weller, H., *J. Phys. Chem. B* 2002, **106**, 7177–7185.
- [18] Ambrosi, A., Pumera, M., *Chem. Eur. J.*, 2010, **16**, 1786–1792.
- [19] Ali, E. M., Zheng, Y. G., Yu, H. H., Ying, J. Y., *Anal. Chem.* 2007, **79**, 9452–9458.
- [20] Zhang, L. J., Xu, C. L., Li, B. X., *Microchim. Acta* 2009, **166**, 61–68.
- [21] Yuan, J. P., Guo, W. W., Yin, J. Y., Wang, E. K., *Talanta* 2009, **77**, 1858–1863.
- [22] Bottini, M., Cerignoli, F., Dawson, M. I., Magrini, A., Rosato, N., Mustelin, T., *Biomacromolecules* 2006, **7**, 2259–2263.
- [23] Shao, J., You, X. G., Gao, F., He, R., Cui, D. X., *Chin. J. Anal. Chem.* 2006, **34**, 1625–1628.
- [24] Wu, Y., Lopez, G. P., Sklar, L. A., Buranda, T., *Anal. Biochem.* 2007, **364**, 193–203.
- [25] Susumu, K., Uyeda, H. T., Medintz, I. L., Mattoussi, H., *J. Biomed. Biotechnol.* 2007, 1–7.
- [26] Al Terary, S., Mangeney, C., Brayner, R., Antoun, T., Fievet, F., Yassar, A., *Sensor Lett.* 2008, **6**, 511–517.
- [27] Jiang, X. Z., Ahmed, M., Deng, Z. C., Narain, R., *Bioconjug. Chem.* 2009, **20**, 994–1001.
- [28] Dif, A., Touchet, S., Nagarajan, S., Baudy-Floc'h, M., Dahan, M., Plehler, J., Marchi-Artzner, V., in: Osinski, M., Jovin, T. M., Yamamoto, K. (Eds.), *Colloidal Quantum Dots for Biomedical Applications* Iii, Spie-Int Soc Optical Engineering, Bellingham 2008, p. L8660.
- [29] Duan, J. L., Song, L. X., Zhan, J. H., *Nano Res.* 2009, **2**, 61–68.
- [30] Huang, X. Y., Weng, J. F., Sang, F. M., Song, X. T., Cao, C. X., Ren, J. C., *J. Chromatogr. A* 2006, **1113**, 251–254.

Article 7

Stanisavljevic M, Chomoucka J, Dostalova S, Krizkova S, Vaculovicova M, Adam V, Kizek R. Interactions between CdTe quantum dots and DNA revealed by capillary electrophoresis with laser-induced fluorescence detection. *Electrophoresis* 2014;35(18):2587-2592.

Maja Stanisavljevic¹
 Jana Chomoucka²
 Simona Dostalova¹
 Sona Krizkova^{1,2}
 Marketa Vaculovicova^{1,2}
 Vojtech Adam^{1,2}
 Rene Kizek^{1,2}

¹Department of Chemistry and Biochemistry, Faculty of Agronomy, Mendel University in Brno, Zemedelska, Czech Republic

²Central European Institute of Technology, Brno University of Technology, Technicka, Czech Republic

Received April 16, 2014

Revised June 12, 2014

Accepted June 18, 2014

Research Article

Interactions between CdTe quantum dots and DNA revealed by capillary electrophoresis with laser-induced fluorescence detection

Quantum dots (QDs) are one of the most promising nanomaterials, due to their size-dependent characteristics as well as easily controllable size during the synthesis process. They are promising label material and their interaction with biomolecules is of great interest for science. In this study, CdTe QDs were synthesized under optimal conditions for 2 nm size. Characterization and verification of QDs synthesis procedure were done by fluorimetric method and with CE. Afterwards, QDs interaction with chicken genomic DNA and 500 bpDNA fragment was observed employing CE-LIF and gel electrophoresis. Performed interaction relies on possible matching between size of QDs and major groove of the DNA, which is approximately 2.1 nm.

Keywords:

Bacteriophage / DNA / Interaction / Quantum dots

DOI 10.1002/elps.201400204

1 Introduction

Nanoscale materials with very good electronic, optical, magnetic, and catalytic properties have made nanotechnology one of the most perspective scientific fields today. Quantum dots (QDs) belong to a large family of nanoparticles attracting enormous attention especially due to the small size and size-dependent characteristics. With their size (1–20 nm) they do not obey rules of classical physics and they belong to unpredictable laws of quantum mechanics. Precisely, their optical and electronic properties are caused by phenomena called quantum confinement [1]. Wide absorbance band, narrow emission spectrum, and/or photostability are well-known properties of QDs, which made them the most promising substitute for organic dyes. Another advantage of these materials is their ability to be easily modified, which is primarily done to decrease potential danger of inorganic core toxicity, but these surface modification can be also done to target some biomolecules and, thus, to image biochemical pathways *in vivo*. Beside their successful application in *in vivo* imaging [2–5] and/or biology [6] in general, their applications into proteomics gain more and more attention [7–10]. Moreover, currently a great attention is paid to the targeted drug/gene delivery and the combination of therapeutic and diagnostic

properties of various bioconjugates is explored, QDs are an excellent option for fluorescent labeling of numerous delivery systems. Not only a range of modern artificial nanomaterials but also traditionally utilized viral-based nanocarriers such as bacteriophages belong among such nanocarriers employed for targeted delivery [11]. In the case of nucleic acids delivery, revolutionary discovery of DNA structure done by Watson and Crick in 1953 [12] opened numerous challenges in this field of research. Rapid growth of nanomaterials such as QDs induced their inevitable encounter with DNA. Possible interaction between DNA and other molecules or species is provided by electrostatic binding in major groove of dsDNA and intercalation between base pairs [13]. Investigation of QDs and DNA have not been only directed to their interaction [14], but QDs have been successfully functionalized by DNA and used for fluorescence monitoring *in vivo* or *in vitro* [15, 16].

CE-LIF is a very powerful method for analysis of different nanoparticles in size, shape, or due to their charge [17–19]. QDs have been successfully characterized by CE-LIF [17, 20, 21], which have been also applied for separation and characterization of biomolecules labeled with QDs as a fluorescent marker [5, 22–25]. For biological application of QDs, their conjugation to biomolecules is an ongoing problematic and research challenge. The overview of advances can be found in various review articles [26–28].

Based on aforementioned knowledge, CE-LIF was chosen as a suitable method for monitoring of interaction between QDs and DNA depending on the concentration, time of interaction, length of the DNA strand, and/or its form (ssDNA

Correspondence: Dr. Rene Kizek, Department of Chemistry and Biochemistry, Mendel University in Brno, Zemedelska 1, CZ-613 00 Brno, Czech Republic
 E-mail: kizek@sci.muni.cz
 Fax: +420-5-4521-2044

Abbreviations: GSH, glutathione; QD, quantum dot

Colour Online: See the article online to view Figs. 1–5 in colour.

vs. dsDNA). This method can be used for a very simple DNA labeling with QDs and/or observing possible toxic impact of QDs to DNA and its biological function.

2 Materials and methods

2.1 Chemicals

All chemicals were purchased from Sigma Aldrich (St. Louis, MA, USA) in ACS purity unless noted otherwise. Lyophilized highly polymerized DNA (Reanal, Hungary) was isolated from chicken erythrocytes ($M_w = 400\,000$ g/mol). The stock solution of DNA (1 mg/mL) was prepared by dissolving in ACS water.

2.2 DNA amplification and isolation

Taq PCR kit and DNA isolated from bacteriophage λ (48 502 bp) were purchased from New England BioLabs (USA). Primers for PCR were synthesized by Sigma-Aldrich. The sequence of a forward primer was 5'-CCTGCTGCGCCTTCACGC-3' and the sequence of a reverse primer was 5'-TCCGGATAAAAACGTCGATGACATTTC-3'. Fifty microliters reaction mixture was composed of 5 μ L 10 \times standard *Taq* reaction buffer, 1 μ L of 10 μ M dNTP solution mix, 1 μ L of each primer (10 μ M), 0.25 μ L of 5 U/ μ L *Taq* DNA polymerase, 1 μ L of 0.5 μ g/ μ L λ DNA, and 40.75 μ L H₂O (sterile). The PCR tubes with mixture were placed into the cycler (Eppendorf, Germany) and cycling conditions were as follows: initial denaturation at 95°C for 120 s; 25 cycles of denaturation at 95°C for 15 s, annealing at 64°C for 15 s, extension at 72°C for 45 s and a final extension at 72°C for 5 min. Hundred microliters of PCR product (500 bp) was purified by MinElute PCR Purification Kit (Qiagen, Germany) according to manufacturer's instruction and DNA was concentrated to 10 μ L of water solution. DNA concentration was determined by spectrophotometric analysis at 260 nm using spectrophotometer Specord 210 (AnalytikJena, Germany).

2.3 CdTe quantum dots synthesis

The procedure for synthesis of these dots was adapted from the work of Duan et al. [29]. Briefly, the synthesis of CdTe QDs and their subsequent coating were as follows: 4 mL of the CdCl₂ solution (0.04 M) was diluted with 42 mL of water. During constant stirring, 100 mg of sodium citrate, 4 mL of Na₂TeO₃ solution (0.01 M), 300 mg of reduced glutathione (GSH), and 50 mg of NaBH₄ were added into water-cadmium(II) solution. The mixture was kept at 95°C under the reflux cooling for 4 h. As a result, yellow solution of the GSH-QDs was obtained.

2.4 Spectroscopic and size analysis

Fluorescence and absorbance spectra were measured by multifunctional microplate reader Tecan Infinite 200 PRO 132 (TECAN, Männedorf, Switzerland). Excitation wavelength was 230 nm and emission range was measured from 300 to 850 nm per 5 nm steps. The absorbance was acquired within the range from 230 to 800 nm with 5 nm steps as an average of five measurements per well. The detector gain was set to 80. The sample volume of 50 μ L was placed in UV-transparent 96-well microplate with flat bottom by Costar (Corning, New York, USA). Zetasizer 3000 HSa (Malvern Instruments, Worcestershire, UK) was used for determination of size nanoparticles based on dynamic light scattering technique.

2.5 Capillary electrophoresis

Backman P/ACE™ MDQ electrophoresis system (Brea, CA, USA) with laser-induced detector was used for CE measurements. Excitation wavelength was 488 nm (argon ion laser) and emission wavelength was 520 nm. An uncoated fused silica capillary was used with total length of 60.5 cm, effective length of 50 cm, and internal diameter 75 μ m. A 20 mM borate (pH 9.2) was used as BGE. Separation was carried out at 20 kV in positive polarity and sample was injected hydrodynamically for 20 s using 3.4 kPa.

2.6 Agarose gel electrophoresis

Agarose gel (2% v/v, high melt, medium fragments, Chemos CZ, Prague, Czech Republic) was prepared with 1 \times TAE buffer (40 mM Tris, 20 mM acetic acid, and 1 mM ethylenediaminetetraacetic acid). Five microliters of samples were prepared with 5% v/v bromophenol blue and 3% v/v glycerol and loaded into the gel. A 100 bp DNA ladder (New England Biolabs, Ipswich, MA, USA) was used to monitor the size of analyzed DNA. The electrophoresis was run at 60 V and 6°C for 160 min. The gel was stained in 100 mL of TAE buffer with 50 μ L of ethidium bromide for 20 min and visualized by UV transilluminator (312 nm). The intensity of fluorescence was quantified using Carestream molecular imaging software (Carestream, USA)

3 Results and discussion

3.1 Quantum dots characterization

QDs are known as size-dependent nanomaterials. The size is controllable during the synthesis process, which can give us a desired absorbance and emission spectra important for their further application. In this study of DNA interaction with QDs, desired 2 nm sized QDs were synthesized according to the method described elsewhere [29]. The size of the QDs and

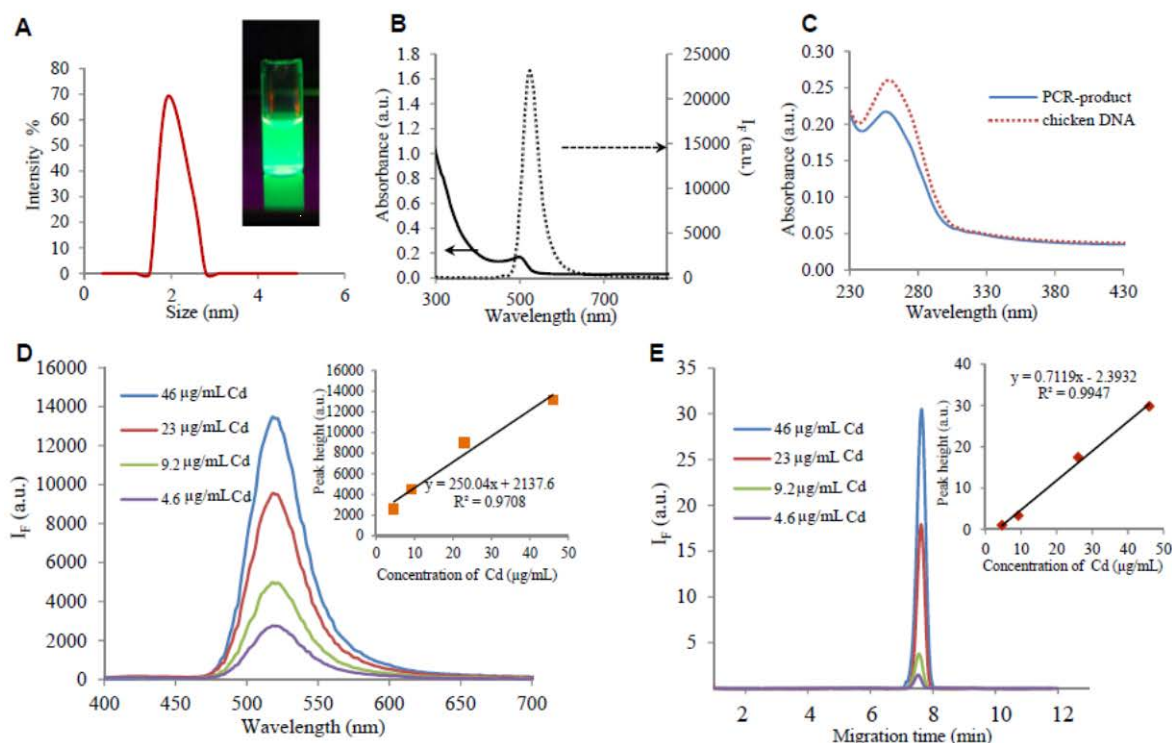


Figure 1. (A) Size determination of QDs by zeta-sizer, inset: photograph of QDs solution under UV light illumination. (B) Fluorescence and absorbance characterization of QDs. (C) Absorbance characterization of DNA and 500 bp fragment (200 $\mu\text{g}/\text{mL}$). (D) Fluorescence characterization of QDs diluted in water. All characterization was done by Tecan Infinite 200 PRO 132 under the following conditions: excitation wavelength was 230 nm and emission range was measured from 300 to 850 nm per 5 nm steps. The absorbance was acquired within the range from 230 to 1000 nm with 5 nm steps as an average of five measurements per well. Each intensity value is an average of five measurements. The detector gain was set to 80. The sample volume of 50 μL was placed in UV-transparent 96-well microplate with flat bottom by Costar. (E) CE characterization of QDs diluted in water. CE measurement is done by Beckman P/ACETM MDQ electrophoresis system with LIF detector. Excitation wavelength was 488 nm and emission wavelength was 520 nm. An uncoated fused silica capillary was used with total length of 60.5 cm, effective length of 50 cm and internal diameter 75 μm . The 20 mM borate (pH 9.2) was used as BGE. Separation was carried out at 20 kV in positive polarity and sample was injected hydrodynamically for 20 s using 3.4 kPa. Concentration of QDs was recalculated to Cd concentration of 460 $\mu\text{g}/\text{mL}$ according to [30].

their size-distribution is shown in Fig. 1A. The majority of the nanoparticles were 2 nm in diameter. The photograph of the solution of synthesized QDs under UV light illumination is shown in the inset in Fig. 1A exhibiting significant green light emission. Afterwards, their fluorescent properties were examined and their absorption maximum in visible range of spectra is 490 nm as indicated in Fig. 1B. The emission maximum after excitation by 490 nm light is at 525 nm. The absorption spectra of chicken genomic DNA and 498 bp fragment of bacteriophage λ used in the following experiments are shown in Fig. 1C.

To verify the linearity of the fluorescence signal depending on the concentration, the emission spectra of QDs were acquired (Fig. 1D). The concentration of QDs was expressed as the concentration of cadmium (inset in Fig. 1D). The Cd concentration in QDs was determined as described by Sobrova et al. [30]. The same characterization was performed by CE-LIF as shown in Fig. 1E. The peak of QDs with migration time of 7.5 min was observed and its height is lin-

early dependent on Cd concentration as shown in the inset in Fig. 1E.

3.2 CE-LIF analysis of interaction between DNA and quantum dots

After size and fluorescent characteristics of the QDs were verified, the interaction of these nanomaterials with DNA was studied. In the first experiment, the interaction between QDs and chicken genomic DNA was observed and results are shown in Fig. 2. The time dependence of complex formation can be seen in Fig. 2A. The peak 1 represents the DNA-QD complex and peak 2 represents the excess of the QDs. The increasing of the interaction time led to the increase of the peak 1 height. The dependence of the peak 1 height on time is shown in the inset in Fig. 2A. The same experiment measured by fluorescence spectroscopy exhibited only a very slight increase of the fluorescence intensity with the increasing time

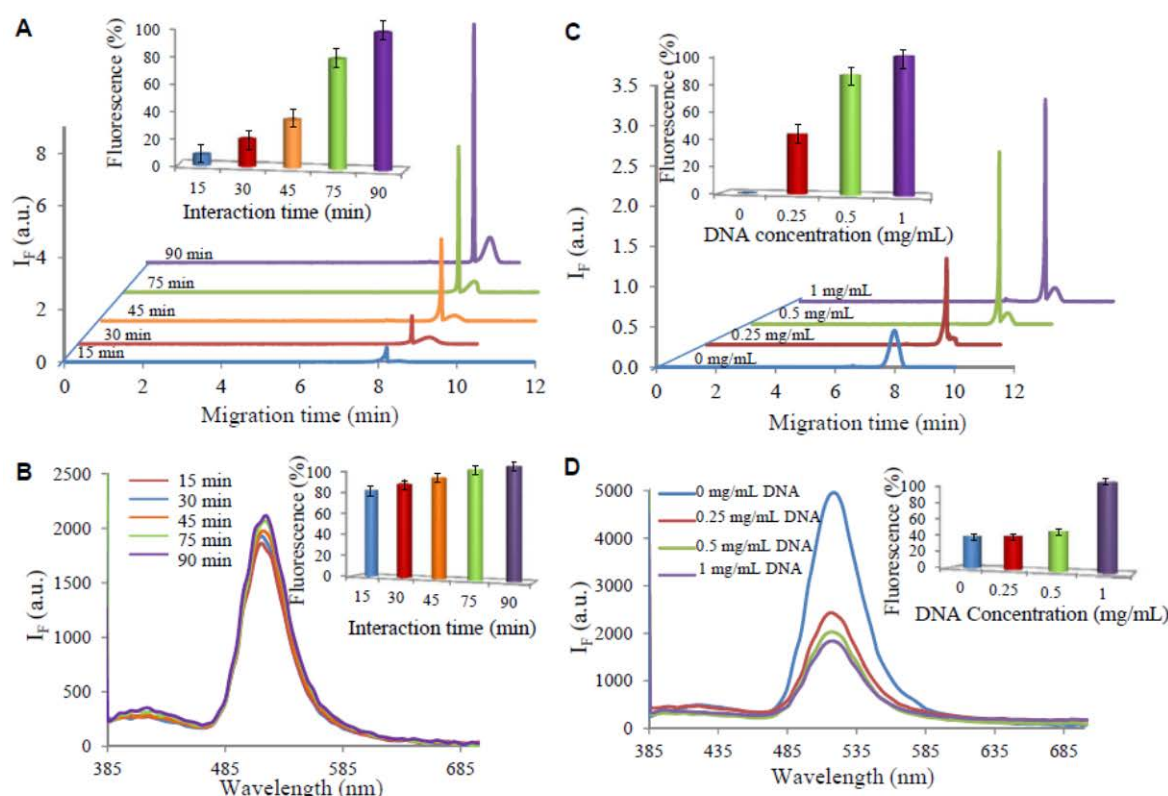


Figure 2. CE-LIF and fluorimetric characterization of QDs-DNA interaction. (A) QDs and DNA (500 $\mu\text{g}/\text{mL}$) time interaction (15, 30, 45, 75, and 90 min) monitored by CE-LIF, inset: the peak height dependence on time of interaction (peak 1 – QD-DNA complex, peak 2 – QDs). (B) QDs and DNA time interaction (15, 30, 45, 75, and 90 min) monitored by fluorescence spectrometry, inset: fluorescence intensity dependence on the interaction time. (C) QDs and DNA interaction with different concentrations of DNA (0, 0.25, 0.5, and 1 mg/mL) measured by CE-LIF, inset: dependence of created complex peak height on DNA concentration (peak 1 – QD-DNA complex, peak 2 – QDs). (D) QDs and DNA interaction with different concentrations of DNA (0, 0.25, 0.5, and 1 mg/mL) measured by fluorescence spectrometry, inset: fluorescence intensity dependence on the DNA concentration. CE and measurement with fluorimetric conditions are the same as in Fig. 1.

of interaction (Fig. 2B). The dependence of fluorescence intensities at 520 nm on the interaction time is shown in the inset in Fig. 2B. These results suggest that CE-LIF exhibits higher sensitivity for investigation of complex formation.

Subsequently, the dependence on DNA concentration was investigated. As it is shown in Fig. 2C, the increase in DNA concentration (from 0.25 to 1 mg/mL) led to the increase in peak height of the DNA-QD complex. Concentration dependence is shown in the inset in Fig. 2C. Using the fluorescence spectroscopy to verify the interaction, significant quenching effect of DNA on the QDs fluorescence was observed, however only a very small change of fluorescence was observed according to DNA concentration (Fig. 2D). In addition, the dependence of fluorescence intensities at 520 nm on the DNA concentration is shown in the inset in Fig. 2D.

The basic mechanism of interaction suggested in this study is based on the QDs incorporation into the major groove of DNA. The double-helical DNA structure creates major and

minor grooves with dimensions of 2.1 nm and 0.6 nm, respectively. Due to the matching size of QD (2 nm) to the size of major groove (2.1 nm) it can be suggested that the QD is incorporated into the major groove of DNA. This conclusion corresponds to previous work done by [31]. The scheme is shown in the inset in Fig. 3. To confirm this hypothesis, the interaction between QDs and ssDNA or dsDNA was monitored (Fig. 3). Results showed that dsDNA is needed for the complex (peak 1) to be created, while the complex is not observed with ssDNA.

Further, the interaction of QDs with 500 bp-long DNA fragment and as well as the influence of the DNA length was investigated. The 500 bp-long fragment induced formation of the QD-DNA complex in the same way as long DNA (Fig. 4). The complex formation (peak 1) with the increasing tendency depending on the interaction time was observed. The dependence of the peak height on the interaction time is shown in the inset in Fig. 4A. However, compared to the genomic DNA, the interaction of the fragment with QDs monitored by

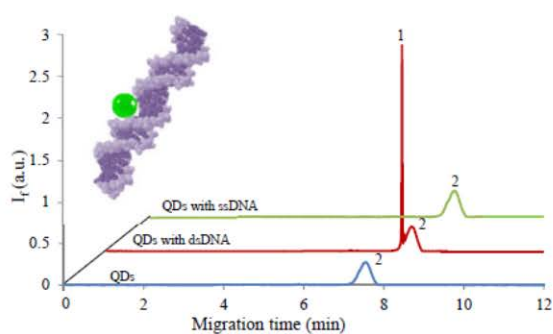


Figure 3. CE-LIF study of interaction between QDs (blue trace) and dsDNA (red trace, 500 $\mu\text{g}/\text{mL}$) or ssDNA (green trace, 500 $\mu\text{g}/\text{mL}$), (peak 1- QD-DNA complex, peak 2 – QDs), inset: the suggested scheme of the interaction between QD and major groove of dsDNA. Conditions of CE measurement are the same as in Fig. 1D.

fluorescence spectrometry did not exhibit the same increasing trend as observed by CE-LIF. Based on the comparison of the genomic DNA interaction to the DNA fragment interaction it can be assumed that the length of the DNA plays a key role especially due to the probability of the formation of numerous secondary structures. This has to be investigated in more details to reveal the impact of the DNA length on the interaction.

3.3 Gel electrophoresis

Gel electrophoresis was employed for DNA-QDs interaction verification. The gel after ethidium bromide staining is shown in Fig. 5A. The lines 1 and 13 were injected by the DNA ladder. The lines 2, 5, and 8 were injected with the QDs solution at concentration of 23, 46, and 460 $\mu\text{g}/\text{mL}$ mixed 1:1 with

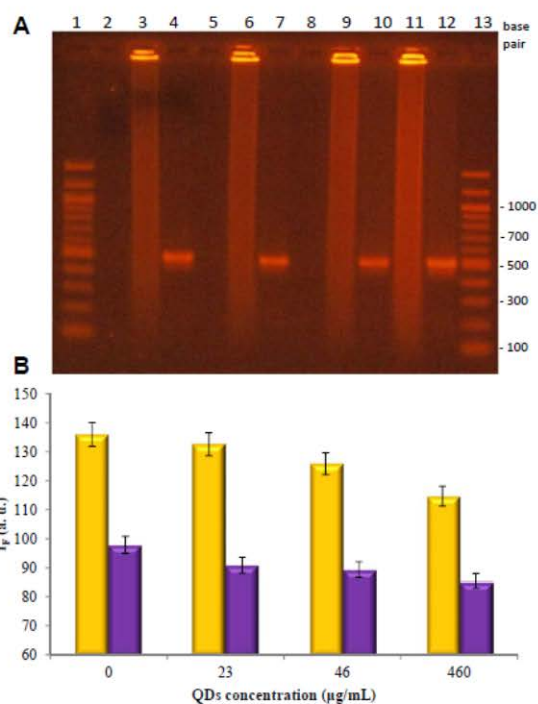


Figure 5. (A) Gel electrophoresis of the QD-DNA complex. (1) DNA Ladder, (2) QDs (230 $\mu\text{g}/\text{mL}$), (3) QDs 460 $\mu\text{g}/\text{mL}$ + chicken DNA (400 $\mu\text{g}/\text{mL}$) (1:1 v/v), (4) QDs (460 $\mu\text{g}/\text{mL}$) + 500 bp (50 $\mu\text{g}/\text{mL}$) (1:1 v/v); (5) QDs (23 $\mu\text{g}/\text{mL}$), (6) QDs 46 $\mu\text{g}/\text{mL}$ + DNA (400 $\mu\text{g}/\text{mL}$) (1:1 v/v), (7) QDs diluted 46 $\mu\text{g}/\text{mL}$ + 500 bp (50 $\mu\text{g}/\text{mL}$) (1:1 v/v), (8) QDs 11.5 $\mu\text{g}/\text{mL}$, (9) QDs 23 $\mu\text{g}/\text{mL}$ + DNA (400 $\mu\text{g}/\text{mL}$) (1:1 v/v), (10) QDs 23 $\mu\text{g}/\text{mL}$ + 500 bp (50 $\mu\text{g}/\text{mL}$) (1:1 v/v), (11) DNA (200 $\mu\text{g}/\text{mL}$), (12) 500 bp (25 $\mu\text{g}/\text{mL}$), (13) DNA ladder. For measurements 2% agarose gel in TAE buffer was used and run for 160 min at 60 V. Total amount of the samples was 10 μL . (B) Quenching of the signal dependent on the amount of QDs (chicken DNA–yellow columns, 500 bp DNA fragment–purple columns).

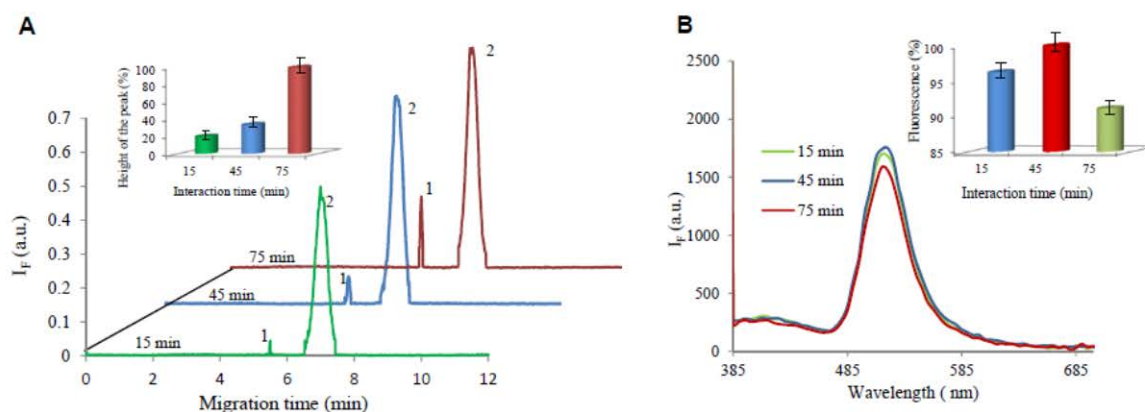


Figure 4. (A) CE-LIF and (B) fluorimetric characterization of the interaction between QDs (peak 2) and 500 bp long DNA fragment of bacteriophage λ (500 $\mu\text{g}/\text{mL}$). CE-LIF and fluorimetric measurement conditions are set as in the Fig. 1, inset: peak height dependence of QDs-DNA fragment complex on the reaction time.

water. In the lines 3, 6, and 9 there are the mixture samples of chicken DNA and 23, 46, and 460 $\mu\text{g}/\text{mL}$ of QDs in ratio 1:1, respectively. The same samples prepared using 500 bp DNA fragment and QDs are shown in the lines 4, 7, and 10. In lines 11 and 12, DNA and 500 bp fragment signal is observed. After software analysis of the gel image, the quenching of the signal dependent on the amount of QDs was observed for both chicken DNA as well as 500 bp fragment (Fig. 5B). This is probably due to the fact that QDs are preventing the DNA to be stained by the ethidium bromide.

4 Concluding remarks

It clearly follows from the results obtained that the interaction between DNA and QDs occurs. Monitoring and verification was successfully done by combination of CE-LIF and gel electrophoresis, whereas CE is analytical method with excellent separation characteristics and in the combination with LIF detector it provides very high selectivity needed for monitoring of DNA-QDs interaction. The obtained data confirm the hypothesis that the interaction mechanism is based on the size of QDs, which matches the size of DNA major groove.

The author M.V. wishes to express her thanks to project CZ.1.07/2.3.00/30.0039 for financial support. The author J.C. thanks to project GP 13-20303P.

The authors have declared no conflict of interest.

5 References

- [1] Adams, F. C., Barbante, C., *Spectrosc. Acta Pt. B-Atom. Spectr.* 2013, *86*, 3–13.
- [2] Mattoussi, H., Palui, G., Na, H. B., *Adv. Drug Deliv. Rev.* 2012, *64*, 138–166.
- [3] Lacroix, L. M., Delpech, F., Nayral, C., Lachaize, S., Chaudret, B., *Interface Focus* 2013, *3*, 1–19.
- [4] Acharya, A., *J. Nanosci. Nanotechnol.* 2013, *13*, 3753–3768.
- [5] Wang, Y. C., Hu, R., Lin, G. M., Roy, I., Yong, K. T., *ACS Appl. Mater. Interfaces* 2013, *5*, 2786–2799.
- [6] Byers, R. J., Hitchman, E. R., *Prog. Histochem. Cytochem.* 2011, *45*, 201–237.
- [7] Wu, H. F., Gopal, J., Abdelhamid, H. N., Hasan, N., *Proteomics* 2012, *12*, 2949–2961.
- [8] Fowler, B. A., Conner, E. A., Yamauchi, H., *Toxicol. Appl. Pharmacol.* 2008, *233*, 110–115.
- [9] Marko, N. F., Weil, R. J., Toms, S. A., *Expert Rev. Proteomics* 2007, *4*, 617–626.
- [10] Soman, C., Giorgio, T., *Nanomed.-Nanotechnol. Biol. Med.* 2009, *5*, 402–409.
- [11] Henry, M., Debarbieux, L., *Virology* 2012, *434*, 151–161.
- [12] Watson, J. D., Crick, F. H. C., *Cold Spring Harbor Symp. Quant. Biol.* 1953, *18*, 123–131.
- [13] Pang, D. W., Zhao, Y. D., Fang, P. F., Cheng, J. K., Chen, Y. Y., Qi, Y. P., Abruna, W. D., *J. Electroanal. Chem.* 2004, *567*, 339–349.
- [14] Mahtab, R., Sealey, S. M., Hunyadi, S. E., Kinard, B., Ray, T., Murphy, C. J., *J. Inorg. Biochem.* 2007, *101*, 559–564.
- [15] Sun, D. Z., Gang, O., *Langmuir* 2013, *29*, 7038–7046.
- [16] Zhang, C. L., Ji, X. H., Zhang, Y., Zhou, G. H., Ke, X. L., Wang, H. Z., Tinnefeld, P., He, Z. K., *Anal. Chem.* 2013, *85*, 5843–5849.
- [17] Pereira, M., Lai, E. P. C., Hollebhone, B., *Electrophoresis* 2007, *28*, 2874–2881.
- [18] Clarot, I., Wolpert, C., Morosini, V., Schneider, R., Balan, L., Diez, L., Leroy, P., *Curr. Nanosci.* 2009, *5*, 154–159.
- [19] Li, Y. Q., Wang, H. Q., Wang, J. H., Guan, L. Y., Liu, B. F., Zhao, Y. D., Chen, H., *Anal. Chim. Acta* 2009, *647*, 219–225.
- [20] Song, X. T., Li, L., Chan, H. F., Fang, N. H., Ren, J. C., *Electrophoresis* 2006, *27*, 1341–1346.
- [21] Stewart, D. T. R., Celiz, M. D., Vicente, G., Colon, L. A., Aga, D. S., *Trac-Trends Anal. Chem.* 2011, *30*, 113–122.
- [22] Wang, J. H., Li, Y. Q., Zhang, H. L., Wang, H. Q., Lin, S., Chen, J., Zhao, Y. D., Luo, Q. M., *Colloid Surf. A-Physicochem. Eng. Asp.* 2010, *364*, 82–86.
- [23] Akinfiyeva, O., Nabiev, I., Sukhanova, A., *Crit. Rev. Oncol./Hematol.* 2013, *86*, 1–14.
- [24] Wang, F. B., Rong, Y., Fang, M., Yuan, J. P., Peng, C. W., Liu, S. P., Li, Y., *Biomaterials* 2013, *34*, 3816–3827.
- [25] Stanisavljevic, M., Janu, L., Smerkova, K., Krizkova, S., Pizurova, N., Ryvolova, M., Adam, V., Hubalek, J., Kizek, R., *Chromatographia* 2013, *76*, 335–343.
- [26] Frigerio, C., Ribeiro, D. S. M., Rodrigues, S. S. M., Abreu, V. L. R. G., Barbosa, J. A. C., Prior, J. A. V., Marques, K. L., Santos, J. L. M., *Analytica Chimica Acta* 2012, *735*, 9–22.
- [27] Sang, F. M., Huang, X. Y., Ren, J. C., *Electrophoresis* 2014, *35*, 793–803.
- [28] Kuang, H., Zhao, Y., Ma, W., Xu, L. G., Wang, L. B., Xu, C. L., *Trac-Trends Anal. Chem.* 2011, *30*, 1620–1636.
- [29] Duan, J. L., Song, L. X., Zhan, J. H., *Nano Res.* 2009, *2*, 61–68.
- [30] Sobrova, P., Ryvolova, M., Hubalek, J., Adam, V., Kizek, R., *Int. J. Mol. Sci.* 2013, *14*, 13497–13510.
- [31] Xu, Q., Wang, J. H., Wang, Z., Yin, Z. H., Yang, Q., Zhao, Y. D., *Electrochem. Commun.* 2008, *10*, 1337–1339.

Article 8

Adam V, Vaculovicova M. Nanomaterials for sample pretreatment prior to capillary electrophoretic analysis. Analyst 2017;142(6):849-857.

Cite this: *Analyst*, 2017, **142**, 849

Nanomaterials for sample pretreatment prior to capillary electrophoretic analysis

Vojtech Adam^{a,b} and Marketa Vaculovicova^{*a,b}

Nanomaterials are, in analytical science, used for a broad range of purposes, covering the area of sample pretreatment as well as separation, detection and identification of target molecules. This review covers the application of nanomaterials for sample pretreatment in capillary electrophoresis. It targets the utilization of nanomaterials for sample purification, preconcentration and/or extraction coupled both off-line and on-line with capillary electrophoretic analysis. Especially due to their large surface area, nanoparticles and nanomaterials are exceptionally helpful in making up for the limited concentration detection limits provided by capillary electrophoresis. This method possesses excellent separation power; however, its sensitivity may be problematic in some cases. Therefore, this review is focused on utilization of nanomaterials as a powerful tool for sample preconcentration, which is so often required prior to capillary electrophoretic analysis.

Received 7th December 2016,
Accepted 2nd February 2017

DOI: 10.1039/c6an02608g

rsc.li/analyst

1. Introduction

Nanotechnology has been defined as a technology in which dimensions and tolerances within the range of 0.1–100 nm play a critical role. At the nanoscale, gravity becomes less of an

issue, the strength of materials becomes a more significant influence, and the quantum size effect is also an important factor. Due to their unique and size-dependent spectroscopic, electronic, and thermal features as well as their chemical properties and ability to be functionalized, which result from their small sizes and high surface-to-volume ratios, nanomaterials (NMs) have found applications not only in physics, electronics, and engineering but also in the life sciences, including chemistry,^{1–3} biology,⁴ and medicine.^{5,6} NMs have greatly influenced numerous scientific fields, and these influences can be observed in different ways. In chemistry, the

^aDepartment of Chemistry and Biochemistry, Mendel University in Brno, Zemelska 1, CZ-613 00 Brno, Czech Republic

^bCentral European Institute of Technology, Brno University of Technology, Parkynova 123, CZ-612 00 Brno, Czech Republic. E-mail: marketa.vaculovicova@mendelu.cz; Fax: +420-5-4521-2044; Tel: +420-5-4513-3350



Vojtech Adam

Vojtech Adam, Ph.D. is currently Professor and Head of the Department of Chemistry and Biochemistry, Mendel University in Brno and a Senior Researcher at the Central European Institute of Technology, Brno University of Technology. He received his Ph.D. in cellular and molecular biology at Masaryk University for work on the use of electrochemical techniques in cancer diagnosis. He is the author of more than 400 ISI indexed

papers with over 7500 citations and an H-index of 43. His research is primarily focused on cell metallomics.



Marketa Vaculovicova

Marketa Vaculovicova, Ph.D. is currently a post-doctoral fellow at the Central European Institute of Technology, Brno University of Technology. She received her Ph.D. in analytical chemistry at Masaryk University for work on method and instrumentation development for capillary electrophoresis. She is the author of 90 ISI indexed papers with 900 citations and an H-index of 18. Her research is currently focused primarily on development of bioanalytical and (bio)sensing methods.

range of sizes has historically been associated with colloids, micelles, polymer molecules, and similar structures (*i.e.*, typically, notably large molecules or aggregates of many molecules). More recently, structures such as carbon nanotubes, silicon nanorods, and semiconductor quantum dots have emerged as particularly interesting classes of nanostructures. In physics and electrical engineering, nanoscience is most often associated with quantum behavior and the behavior of electrons and photons in nanoscale structures. Biology and biochemistry are also fields in which this interest in nanostructures runs deep. Nanostructures can act as cell components, and indeed, the most interesting structures in biology can be thought of as nanostructures, including DNA, viruses and subcellular organelles.⁷

2. Nanomaterials as sample pretreatment tools coupled with capillary electrophoresis

The nano-phenomenon has clearly influenced the entire scientific world, including instrumental analytical chemistry; therefore, scientists are not only developing new approaches and assays using nanotechnologies, they are also upgrading standard techniques. One of the methods most influenced by this phenomenon is capillary electrophoresis (CE). CE offers its advantages as a method for characterization used during nanomaterial synthesis and modification as well as the monitoring of properties and interactions with other molecules,⁸ however on the other hand, nanomaterials have been used for enhancement of capillary electrophoresis performance either in terms of increasing the separation resolution or for improvement of the detection.⁹

Low sensitivity is one of the main drawbacks of CE connected with the most common detection method – spectrophotometric detection. It is associated with both the short optical path-length of the capillary used as a detection cell and the small sample volumes that are injected. A preconcentration step is thus favored for analysis of rather dilute analyte solutions. Additionally, one or more pretreatment steps are needed to achieve the required selectivity and/or sensitivity because complex biological matrices significantly interfere with in the CE analysis. The resulting sample solution must often be devoid of salts because a high ionic strength imparts a low electrical resistance that can interfere with the sample stacking process. Furthermore, the electro-osmotic flow can be altered, and the detector baseline can also be perturbed by differences in sample and background electrolyte pH values.¹⁰ Two approaches are mainly used in sample pretreatment and preconcentration: (I) an electrophoretic approach and (II) a chromatographic approach. Electrophoretic techniques are based on differences in the electrophoretic mobilities of the analytes or on differences in the interactions with the pseudo-stationary phase (or electrolyte additives) in different zones. Four main types of these techniques exist: transient iso-

tachophoresis,^{11,12} stacking,^{13–15} sweeping,^{16–18} and dynamic pH junction.^{19,20} In contrast, chromatographic techniques are based on analyte sorption in a solid-phase material. These preconcentration techniques enable loading of multiple capillary volumes because analytes from a large volume of sample are concentrated on a sorbent and subsequently eluted in a small amount of solvent, thus leading to lower detection limits.²¹ In cases of small sample volumes, the losses are significant. Solid-phase extraction (SPE) and solid-phase microextraction (SPME) have been the most popular chromatography-based techniques. SPE can be combined with CE in several ways, including off-line, at-line, on-line, and in-line. This approach is especially beneficial if a large volume of sample that contains an analyte at low concentration is available. The coupling of SPE to CE, particularly in in-line and on-line modes, was reviewed by Ramautar *et al.*²² The simplest combination is the off-line mode in which there is no integration between the two techniques and the sample is transferred manually from the SPE sorbent to the CE system. Because this approach is rather laborious and time-consuming, the trend in recent years has been towards automation. The hyphenation of sample pretreatment to numerous analytical techniques has been overviewed by Ali *et al.*²³ Due to properties such as large surface-to-volume ratios and easy modification, NMs have been studied as effective sorbents in the field of separation science, and it has proven more effective and efficient to use nanoparticles (NPs) as the stationary phase in SPE separation due to their enormous surface areas and adsorption properties.²⁴ The most commonly used NMs are most likely carbon nanotubes (CNTs),^{25–28} although other structures have been used for SPE purposes, including NPs,^{29–31} nanofibers,³² and nanorods.^{33,34} Therefore, the new term “solid-phase nanoextraction” has been introduced.³⁵

Further, liquid phase microextraction should be noticed,^{36,37} however its application is not very frequent compared with previously mentioned techniques.

2.1. Off-line sample pretreatment and/or preconcentration

In this section, we focus on applications that use NMs as extraction tools coupled to CE in off-line mode. This arrangement is instrumentally simpler than on-line (or in-line) coupling, which is discussed later (Fig. 1). Off-line mode enables the use of such separation techniques as centrifugation, precipitation, solvent extraction, and liquid–liquid extraction. Compared with bulk materials, the advantages of NMs in this arrangement can be observed mainly in their significantly higher surface-to-volume ratios, which provide for greater sorption abilities and therefore higher extraction efficiencies. The difference in surface area between micro- and nanoparticles can be demonstrated using the example of a carbon micro-particle with a diameter of 60 μm , which has a surface area of 0.01 mm^2 . The same amount of carbon in nanoparticle form with a diameter of 60 nm has a surface area of 11.3 mm^2 . Similar to the increase in the surface area, the reactivity is also increased by approximately three orders of magnitude.

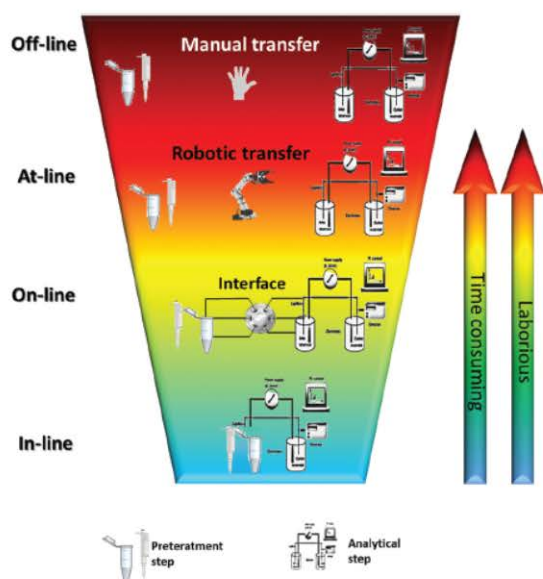


Fig. 1 Schematic representation of connections between sample pre-treatment step and analytical step.

In addition, smaller particles result in lower binding energy per atom in cases of atoms on the surface.

2.1.1 Gold particles. Gold nanoparticles (AuNPs) provide excellent extraction power due to their high affinity for thiol-containing compounds. Applications of AuNPs in SPE extraction have been covered in a review article by Sykora *et al.*³⁸ This paper presents promising uses of AuNPs for sample preparation, preconcentration, and pre-separation of selected analytes from complex matrices as well as their applications in separation methods such as CE, chip CE, micellar electrokinetic chromatography (MEKC), capillary electrochromatography (CEC), high-performance liquid chromatography (HPLC), and gas chromatography. Wu *et al.*³⁹ provided an overview of certain important applications of AuNPs as stationary phases in open-tubular capillary electrochromatography, gas chromatography, and HPLC as well as their use as running buffer additives to enhance separation and for preconcentration in chromatographic, electrophoretic, and chip-based systems. This topic was also partially covered by Liu in an earlier, exhaustive review article.⁴⁰ Because this topic has been deeply studied and reviewed several times, we only highlight several much-discussed applications. The combination of AuNPs and CE has been successfully used to extract thiol-containing compounds *via* AuNPs capped with Tween 20,^{41–43} melamine *via* AuNPs capped with 11-mercaptoundecanoic acid,⁴⁴ and amino thiols *via* AuNPs capped with nonionic surfactants.⁴⁵ Additionally, neutral steroids,⁴⁶ indoleamines,⁴⁷ aromatic hydrocarbon metabolites⁴⁸ and C8-conjugated nucleosides and oligonucleotides⁴⁹ have been extracted using AuNPs prior to CE. The work of Yeh and Tseng⁵⁰ described the application

of human serum albumin-coated AuNPs for the selective extraction of lysozyme. Under optimal extraction conditions, the detection limit for lysozyme reached as low as 8 nM. The suggested methods are compatible with matrix-assisted laser desorption/ionization time-of-flight mass spectrometry.

2.1.2 Magnetic particles. Magnetic separation is a technology that uses magnetism for the efficient separation of paramagnetic and superparamagnetic particles from chemical or biological suspensions. The concept of using magnetic separation techniques to purify biologically active compounds (such as nucleic acids^{51–53} and proteins^{54–56}), cells, and cell organelles has received renewed interest over the past decade. This approach takes advantage of the possibility of surface modification of magnetic NPs to enable so-called immunoextraction. Particles can be chemically modified using either antibodies for specific capture of proteins and peptides or oligonucleotide fragments with sequences complementary to the extracted nucleic acid. Paramagnetic particles can be immobilized using an external magnetic field if necessary and subsequently resuspended back into the solution when the magnetic field is removed. The possible surface modifications used in connection with the magnetic particles are shown schematically in Fig. 2A, and the two main principles of their utilization (off-line and in-line) for sample pretreatment and preconcentration are shown in Fig. 2B and C.

Magnetic particles are produced from various synthetic polymers⁵⁷ and biopolymers⁵⁸ and also might be based on such inorganic magnetic materials as surface-modified iron oxides.⁵⁹ Coupling of magnetic particles and CE primarily involves the enrichment of biomolecules followed by CE separation. Dong *et al.*⁶⁰ reported magnetic NPs functionalized with a guanidine group as a useful sorbent for isolating proteins with pI values lower than 7. Those authors tested their approach on highly abundant bovine serum albumin. Testing such protein structure modifiers as sodium dodecyl sulfate could enhance the applicability of this approach, and a tool might be obtained for easy and rapid isolation of all proteins from a sample. Due to the affinity of the magnetic particles for proteins, such particles can also be used for removing these substances from a sample. For example, Wu *et al.*⁶¹ successfully determined the immunoglobulin G (IgG) and analyzed it by MEKC-UV after extraction of excessive human serum albumin by magnetic particles. This method achieved a detection limit for IgG of 0.1 $\mu\text{g mL}^{-1}$.

Functionalization of magnetic particles appears to be promising for the isolation of more specific groups of biomolecules. Dou *et al.*⁶² used boronate-functionalized magnetic NPs for isolating *cis*-diols represented by riboflavin. The particles were found to be useful not only from the viewpoint of their isolation potential but also from that of establishing a pH junction as a bridge for coupling of the isolation assay with CE. The specific functionalization of magnetic particles with alumina created a tool for isolating glyphosate and its major metabolite aminomethylphosphonic acid.⁶³ Such isolated molecules were detected using CE with electrochemiluminescence detection with good enrichment factors (460 and 64 for

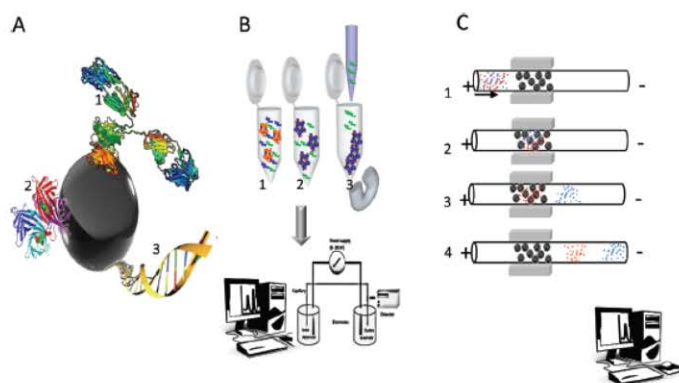


Fig. 2 Schematic expression of magnetic particle utilization in sample pretreatment: (A) magnetic particle surface modifications by (1) antibodies, (2) streptavidin, and (3) DNA used for selective extraction prior to CE analysis. (B) Schematic representation of off-line sample extraction: (1) mixing of the sample with appropriate NPs, (2) immobilization of interferents on the surfaces of NPs, and (3) immobilization of NPs via magnet and injection of analyte into CE. (C) Schematic representation of in-line sample extraction: (1) injection of the sample into the capillary while magnetic particles are immobilized by permanent magnets around the capillary, (2) interaction of sample components with magnetic NPs, (3) elution of first analyte directly during CE separation, and (4) elution of second analyte directly during CE separation. Adapted from ref. 104.

glyphosate and aminomethylphosphonic acid, respectively). In addition to assays for medical purposes, CE can also be coupled with magnetic particles for use in addressing environmental issues. Magnetic NPs coated with polydopamine or polypyrrole and polymethacrylic acid-co-ethylene glycol dimethacrylate submicron particles have been investigated for their rapid binding kinetics with bisphenol A, proflavine, naphthalene acetic acid, and *Escherichia coli*.⁶⁴ Researchers developed a method for the rapid determination of the percentage binding by sequential injection of particles followed by injection of compounds (or *E. coli*) into a fused-silica capillary. The binding during electrophoretic migration was influenced by the applied voltage but not by the current flow. In addition, Hong and Chen⁶⁵ successfully tested magnetic particles bound to serum albumin as a low-cost alternative for the isolation of ochratoxin A with subsequent CE mass spectrometric determination of this mycotoxin. Magnetic NPs functionalized with carboxylic groups can also be used for preconcentration of metals in juice samples prior to determination by CE,⁶⁶ and Fe₃O₄@Al₂O₃ magnetic particles are applicable for extraction of bisphosphonate drugs.^{67,68} Although chemical functionalization of NPs by organic or inorganic⁶⁹ functionalities is the technique most commonly used to ensure selectivity towards the target analyte, the molecular imprinting strategy is also gaining attention. Molecularly imprinted magnetic NPs represent an interesting approach to isolation in a preconcentration process.⁷⁰

The isolation of nucleic acids using magnetic particles is one of the areas in which magnetic NPs are most broadly utilized as a pretreatment prior to any analytical method of choice, not only CE. Various mechanisms are employed: (1) the interaction between nucleic acids and the silica surfaces of magnetic NPs is the main principle used for the extraction of the total nucleic acid content or (2) immobilization of a

specific sequence to isolate a targeted nucleic acid sequence.^{71–75}

2.1.3 Carbon nanomaterials. The use of carbon nanotubes for SPE (or SPME) is based on their ability to establish π - π interactions as well as excellent van der Waals interactions with other molecules and particularly with hydrophobic molecules. These materials also possess large surface areas, especially on the outsides and in the interstitial spaces within the nanotube bundles; their chemical, mechanical, and thermal stabilities are also considerations.⁷⁶

The distortion of planar graphene into a cylinder greatly complicates the orbital overlap and results in carbon atoms becoming wound in a helical fashion. As a consequence, nanotubes readily undergo fluctuating and induced dipole moments, and this property results in excellent van der Waals adhesion to other molecules.⁷⁷ As a rule, multi-wall carbon nanotubes (MWCNTs) possess higher sorption capacities than single-wall carbon nanotubes (SWCNTs).⁷⁸ Therefore, MWCNTs have been used as sorbents in packed mini-columns for the extraction of a wide range of aromatic compounds.^{79–82} CNTs also have shown strong adsorption affinity toward organic and inorganic molecules. Carbon nanohorns, which are structurally similar to nanotubes, have been used for extracting 4-nitrophenol from water samples.⁸³ The wide range of applications that use CNTs as analytical tools was reviewed by Valcarcel *et al.*,^{78,84} and special attention has been devoted to SPE using carbon nanotubes in a paper published by Ravelo-Perez²⁵ and Socas-Rodriguez.⁸⁵

The mentioned reviews indicate various types of carbon materials that are of great interest to analytical chemists, and their previously mentioned properties could be used for isolating such simple organic molecules as pesticides,⁸⁶ herbicides,⁸⁷ antibiotics^{88–90} and other drugs.⁹¹ The detection limits of the developed methods have been on the order of

tens of ng L^{-1} . CNT-modified filters for microextraction by packed sorbent followed by nonaqueous CE have been used for the extraction of ionic liquids from river water.⁹² The absorption properties of fullerenes were summarized by Valcarcel *et al.*⁹³ Moreover, a section of a paper by Scida *et al.*⁹⁴ covered fullerenes as an extraction tool, and even graphene has been used for SPE.^{95,96}

2.1.4 Others. Despite the great development of micro- and nanomaterials, materials other than the previously mentioned types are rare. Zhou *et al.*⁹⁷ preconcentrated paraquat and diquat *via* SPE prior to CE determination using nitrogen-doped TiO_2 nanotube cartridges. Considering the high recoveries of both compounds from environmental samples, one might suggest using these materials in selected lab-on-chip devices for on-line environmental monitoring. Another environmentally directed study in environmental water samples demonstrated the use of nanometer-sized alumina packed microcolumn SPE in combination with field-amplified sample stacking-capillary electrophoresis for speciation analysis of inorganic selenium.⁹⁸ Recently, diamino functionalized silica NPs were used for preconcentration of food colorants in beverage samples.⁹⁹

2.2 In-line pretreatment and/or preconcentration

Biomolecules such as peptides and proteins are commonly extracted from biological matrices using various sample-preparation techniques, including homogenization, centrifugation, precipitation, solvent extraction, liquid-liquid extraction, solid-phase extraction, (micro)dialysis, and ultrafiltration.¹⁰⁰ Compared with the off-line connection of extraction methods, the in-line approach is more specific. Nevertheless, certain obstacles exist that must be overcome, particularly with CE and microchip CE.¹⁰¹

In-line preconcentration and/or pretreatment techniques use either a surface-binding strategy or a porous material approach. Surface-binding methods use the interaction of an analyte with the surfaces of such fixed nanostructures as monoliths, nanopillars, immobilized NPs, and other NMs. All of these types have been used previously in combination with either capillary-based CE or microfluidic CE. Immobilized NMs deposited either on the capillary wall as a thin coating layer or packed within the capillary are commonly used as stationary phases for CEC. Several review articles devoted to SPE-CE have been published,^{22,102,103} but nanomaterial applications are not their main focus. Because this article focuses particularly on NMs, monolithic and porous membrane-based devices for pretreatment and/or preconcentration have been excluded from this paper.

2.2.1 Magnetic particles. Because they can be simply manipulated using external magnets, magnetic particles are well suited for immobilization inside a capillary to provide the preconcentration step. Moreover, the possibility of surface modification enables design of the interaction between nanoparticle and analyte. Magnetic particles immobilized by a magnetic field in a short region of a capillary and subsequently in a microfluidic device have been demonstrated.^{104–110}

A method for capturing specific molecules separated by CE has been explored in the work of Kaneta *et al.*¹⁰⁹ To demonstrate on-column capture of migrating analytes, two detection windows were fabricated on the capillary. Magnetic beads containing immobilized molecules with an affinity to the target molecules were placed between the detection windows in the capillary using magnets. Molecules in a sample solution injected into the capillary were separated and detected at the first detection window. After passing through the first detection window, the separated molecules encountered the magnetic beads, where the specific analyte was captured. The disadvantage of this system consists of the necessity of correcting for migration time between the first and second detection windows because they are located 30 cm apart in the proposed arrangement (Fig. 3). Chen *et al.*¹⁰⁷ later described a CE immunoassay using magnetic beads. To subsequently capture anti- β -lactoglobulin (β -LG) from a sample, magnetic beads

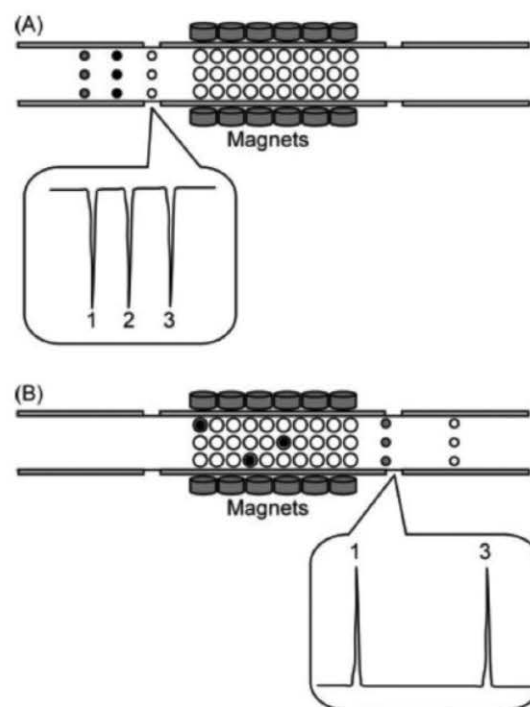


Fig. 3 Principle of capturing specific molecules during CE separation: (A) all solutes are detected in the first detection window, resulting in negative peaks. (B) Solutes other than the target analyte are detected in the second detection window. The target analyte has been captured on magnetic beads. Reprinted with permission from ref. 109. Two detection windows were fabricated on the capillary. Magnetic beads containing immobilized molecules with an affinity to the target molecules were placed between the detection windows in the capillary using magnets. Molecules in a sample solution injected into the capillary were separated and detected at the first detection window. After passing through the first detection window, the separated molecules encountered the magnetic beads, where the specific analyte was captured.

coated with protein A were immobilized in a capillary, and β -LG antibodies were subsequently captured on the beads *via* their strong affinity for protein A. Once the immunocomplexes formed, a discontinuous buffer system was used to release the partners and preconcentrate them by transient isotachopheresis. The antigens and antibodies were finally separated using CE. A limit of quantification at 55 nM was thereby achieved. In contrast to the previous method, the work by Chen *et al.* required intensive immobilization and washing steps for analyte binding. The isolation step does not occur during the CE run.

A magnetic bead-based immunoaffinity assay with laser-induced fluorescence detection has been used for total serum immunoglobulin E determination.¹⁰⁸ The presented method exhibited notably high sensitivity (low picomolar range) and required only 1 μ l of serum, and the analysis was completed in less than 50 min. Yu *et al.*¹¹¹ employed enzyme-immobilized magnetic NPs for in-line CE and drug biotransformation studies. As suggested by those authors, the proposed method might be of interest for enzyme kinetics. In that study, horseradish peroxidase (HRP)-immobilized magnetic NPs were injected and magnetically trapped in the capillary. The enzymatic reaction of the HRP with paracetamol (*N*-acetyl-*p*-aminophenol) was monitored, and the apparent Michaelis-Menten constant between HRP and the drug was determined.

Affinity assays based on magnetic beads are applicable not only for proteins but also for nucleic acids. In a work by Adachi *et al.*,¹⁰⁶ bacterial rRNAs from *E. coli* and *Pseudomonas putida* were analyzed. In their method, RNA extracted from a microbial community was modified with biotin and mixed with streptavidin-modified paramagnetic beads. This mixture was injected into a capillary and held using a magnet on the capillary wall. Subsequently, a fluorescent-labeled probe for detecting the target gene *16S* rRNA was injected. The probe conjugated to the RNA was subsequently dissociated by formamide and detected *via* fluorescence detection. The main advantage of on-line isolation of nucleic acids compared with immunoaffinity isolation using antibodies is the simplicity of tailoring the conditions responsible for coupling of the probe with a targeted nucleic acid. Such an interaction is determined primarily by temperature, which is easily adjusted in CE.

A completely different approach to magnetic bead-based assays was used by Okamoto *et al.*¹⁰⁵ In this work, the magnetic beads served as carriers of target analytes, and their mobility in the capillary was selectively influenced by an external magnetic field. The advantage of this method lies in the fact that the analytes are detected indirectly using a fluorescent label present on the surfaces of the beads, and no release step is needed. A notably low limit of detection (4.3×10^{-13} M) for low-density lipoproteins was thereby achieved.

The suitability of a magnetic particle-based assay for miniaturization and microfluidic application was demonstrated by Tennico and Remcho.¹⁰⁴ Magnets were used to immobilize the beads inside a capillary or microchip. Analyte extraction, elution, and detection were performed sequentially without further intervention by the operator. The in-line extraction was

performed using a disposable poly(methyl methacrylate) microfluidic device with laser-induced fluorescence detection. Electrophoretic separation of the fluorescent dyes rhodamine 110 and sulforhodamine B was completed in 60 s.

2.2.2 Carbon nanomaterials. Among the materials that are able to serve as sorbents, CNTs play a prominent role. One of the most important issues is the ability of CNTs to adsorb analytes onto their surfaces due to the highly conjugated system of double bonds, and for this reason, their applicability as extraction agents is increasing. Manipulation with CNTs is not as easy as with magnetic particles, and the arrangement often uses a short column packed with CNTs prior to the CE separation capillary. In-line coupling of the flow system to the CE equipment using CNTs¹¹² has been used to preconcentrate trace tetracyclines from environmental water samples. The MWCNTs were packed in a mini-column (<1 mm long \times 9 mm internal diameter) connected to the CE *via* a six-port valve. The MWCNTs showed higher capacity than two other SWCNTs. Preconcentration of tetracyclines on MWCNTs followed by CE-mass spectrometry enabled detection of 0.30–0.69 μ g L⁻¹ of tetracyclines using 10 mL of sample. A similarly simple and rapid method was developed using MWCNTs for chlorsulfuron and metsulfuron-methyl determination in water samples.⁸⁷

Determination of non-steroidal anti-inflammatory drugs in urine by combining an immobilized carboxylated carbon nanotube mini-column for solid-phase extraction with CE-mass spectrometry was presented by Suarez *et al.*¹¹³ This work demonstrated that immobilized carboxylated single-walled carbon nanotubes (c-SWCNTs) offer clear advantages over CNTs, and their higher adsorption capacity has been attributed to the special orientation of c-SWCNT molecules on the glass surface.

3. Conclusions

The NM boom and their application in a broad range of areas did not leave the field of separation analytical techniques untouched. NMs have been employed not only for improvement of separation resolution or detection sensitivity. They have also been utilized in a variety of modifications for sample pretreatment and preconcentration. The key properties responsible for such a huge upswing are their immense surface area as well as the flexibility they provide of tailoring the surface functionalities according to the target analyte.

As mentioned several times in this article, the extremely high surface-volume ratio of NMs makes them an excellent and powerful tool for sample pretreatment. Moreover, the diversity of the family of NMs represents a great selection of properties, functionalities and chemistries for almost any analyte of interest.

Acknowledgements

Financial support was provided by the Grant agency of Czech Republic (GACR 16-23647Y) and project CEITEC 2020 (LQ1601)

with financial support from the Ministry of Education, Youth and Sports of the Czech Republic under the National Sustainability Programme II.

References

- 1 A. C. Grimsdale and K. Mullen, *Angew. Chem., Int. Ed.*, 2005, **44**, 5592–5629.
- 2 X. Chen and S. S. Mao, *Chem. Rev.*, 2007, **107**, 2891–2959.
- 3 C. N. R. Rao, A. K. Sood, K. S. Subrahmanyam and A. Govindaraj, *Angew. Chem., Int. Ed.*, 2009, **48**, 7752–7777.
- 4 N. C. Seeman, *Annu. Rev. Biochem.*, 2010, **79**, 65–87.
- 5 R. J. Egli and R. Luginbuehl, *Swiss Med. Wkly.*, 2012, **142**, w13647.
- 6 X. J. Liang, C. Y. Chen, Y. L. Zhao, L. Jia and P. C. Wang, *Curr. Drug Metab.*, 2008, **9**, 697–709.
- 7 G. M. Whitesides, *Small*, 2005, **1**, 172–179.
- 8 C. K. Chua and M. Pumera, *Electrophoresis*, 2013, **34**, 2007–2010.
- 9 M. Pumera and A. Escarpa, *Electrophoresis*, 2009, **30**, 3315–3323.
- 10 P. R. Haddad, P. Doble and M. Macka, *J. Chromatogr. A*, 1999, **856**, 145–177.
- 11 Z. K. Shihabi, *Electrophoresis*, 2002, **23**, 1612–1617.
- 12 A. R. Timerbaev and T. Hirokawa, *Electrophoresis*, 2006, **27**, 323–340.
- 13 J. L. Beckers and P. Bocek, *Electrophoresis*, 2000, **21**, 2747–2767.
- 14 J. P. Quirino and S. Terabe, *J. Chromatogr. A*, 2000, **902**, 119–135.
- 15 Z. K. Shihabi, *J. Chromatogr. A*, 2000, **902**, 107–117.
- 16 A. T. Aranas, A. M. Guidote and J. P. Quirino, *Anal. Bioanal. Chem.*, 2009, **394**, 175–185.
- 17 J. P. Quirino, J. B. Kim and S. Terabe, *J. Chromatogr. A*, 2002, **965**, 357–373.
- 18 J. P. Quirino and S. Terabe, *Anal. Chem.*, 2000, **72**, 1023–1030.
- 19 P. Britz-McKibbin and D. D. Y. Chen, *Anal. Chem.*, 2000, **72**, 1242–1252.
- 20 A. A. Kazarian, E. F. Hilder and M. C. Breadmore, *J. Sep. Sci.*, 2011, **34**, 2800–2821.
- 21 P. Puig, F. Borrell, M. Calull and C. Aguilar, *Anal. Chim. Acta*, 2008, **616**, 1–18.
- 22 R. Ramautar, G. J. de Jong and G. W. Somsen, *Electrophoresis*, 2012, **33**, 243–250.
- 23 I. Ali, V. K. Gupta, H. Y. Aboul-Enein and A. Hussain, *J. Sep. Sci.*, 2008, **31**, 2040–2053.
- 24 N. N. Liang and B. Zhang, *Comb. Chem. High Throughput Screening*, 2011, **14**, 182–190.
- 25 L. M. Ravelo-Perez, A. V. Herrera-Herrera, J. Hernandez-Borges and M. A. Rodriguez-Delgado, *J. Chromatogr. A*, 2010, **1217**, 2618–2641.
- 26 C. Basheer, A. A. Ainedhary, B. S. M. Rao, S. Valliyaveetil and H. K. Lee, *Anal. Chem.*, 2006, **78**, 2853–2858.
- 27 C. S. Pan, S. Y. Xu, H. F. Zou, Z. Guo, Y. Zhang and B. C. Guo, *J. Am. Soc. Mass Spectrom.*, 2005, **16**, 263–270.
- 28 M. Tuzen, K. O. Saygi and M. Soylak, *J. Hazard. Mater.*, 2008, **152**, 632–639.
- 29 Y. R. Song, S. L. Zhao, P. Tchounwou and Y. M. Liu, *J. Chromatogr. A*, 2007, **1166**, 79–84.
- 30 S. X. Zhang, H. Y. Niu, Z. J. Hu, Y. Q. Cai and Y. L. Shi, *J. Chromatogr. A*, 2010, **1217**, 4757–4764.
- 31 Y. Peng, Y. Xie, J. Luo, L. Nie, Y. Chen, L. N. Chen, S. H. Du and Z. P. Zhang, *Anal. Chim. Acta*, 2010, **674**, 190–200.
- 32 S. Chigome, G. Darko and N. Torto, *Analyst*, 2011, **136**, 2879–2889.
- 33 D. Wang, Q. T. Wang, Z. M. Zhang and G. N. Chen, *Analyst*, 2012, **137**, 476–480.
- 34 D. Wang, Z. M. Zhang, L. Luo, T. M. Li, L. Zhang and G. N. Chen, *Nanotechnology*, 2009, **20**, 465702.
- 35 H. Y. Wang and A. D. Campiglia, *Anal. Chem.*, 2008, **80**, 8202–8209.
- 36 T. T. Ho, Z. G. Li, H. Y. Lin and M. R. Lee, *J. Chin. Chem. Soc.*, 2013, **60**, 1033–1042.
- 37 E. Caballero-Diaz, B. Simonet and M. Valcarcel, *Analyst*, 2013, **138**, 5913–5919.
- 38 D. Sykora, V. Kasicka, I. Miksik, P. Rezanka, K. Zaruba, P. Matejka and V. Kral, *J. Sep. Sci.*, 2010, **33**, 372–387.
- 39 C. S. Wu, F. K. Liu and F. H. Ko, *Anal. Bioanal. Chem.*, 2011, **399**, 103–118.
- 40 F. K. Liu, *J. Chromatogr. A*, 2009, **1216**, 9034–9047.
- 41 C. C. Shen, W. L. Tseng and M. M. Hsieh, *J. Chromatogr. A*, 2009, **1216**, 288–293.
- 42 C. W. Chang and W. L. Tseng, *Anal. Chem.*, 2010, **82**, 2696–2702.
- 43 C. C. Shen, W. L. Tseng and M. M. Hsieh, *J. Chromatogr. A*, 2012, **1220**, 162–168.
- 44 C. W. Chang, S. P. Chu and W. L. Tseng, *J. Chromatogr. A*, 2010, **1217**, 7800–7806.
- 45 M. D. Li, T. L. Cheng and W. L. Tseng, *Electrophoresis*, 2009, **30**, 388–395.
- 46 F. K. Liu, *J. Chromatogr. A*, 2008, **1215**, 194–202.
- 47 M. D. Li, W. L. Tseng and T. L. Cheng, *J. Chromatogr. A*, 2009, **1216**, 6451–6458.
- 48 G. Knobel, K. Calimag-Williams and A. D. Campiglia, *Analyst*, 2012, **137**, 5639–5647.
- 49 V. Bosi, E. Sarti, M. L. Navacchia, D. Perrone, L. Pasti, A. Cavazzini and M. L. Capobianco, *Anal. Bioanal. Chem.*, 2015, **407**, 5405–5415.
- 50 P. R. Yeh and W. L. Tseng, *J. Chromatogr. A*, 2012, **1268**, 166–172.
- 51 S. Berensmeier, *Appl. Microbiol. Biotechnol.*, 2006, **73**, 495–504.
- 52 B. I. Haukanes and C. Kvam, *Biotechnology*, 1993, **11**, 60–63.
- 53 I. M. Hsing, Y. Xu and W. T. Zhao, *Electroanalysis*, 2007, **19**, 755–768.
- 54 M. Franzreb, M. Siemann-Herzberg, T. J. Hobley and O. R. T. Thomas, *Appl. Microbiol. Biotechnol.*, 2006, **70**, 505–516.
- 55 A. Ito, M. Shinkai, H. Honda and T. Kobayashi, *J. Biosci. Bioeng.*, 2005, **100**, 1–11.

- 56 S. M. Nie, Y. Xing, G. J. Kim and J. W. Simons, *Annu. Rev. Biomed. Eng.*, 2007, 9, 257–288.
- 57 L. Balaita and M. Popa, *Rev. Roum. Chim.*, 2009, 54, 185–199.
- 58 C. L. Dong, W. Chen, C. Liu, Y. Liu and H. C. Liu, *Colloids Surf., A*, 2014, 446, 179–189.
- 59 X. N. Wang, C. S. Wang, S. Anderson and X. Zhang, *Mater. Lett.*, 2013, 110, 122–126.
- 60 Y. L. Dong, H. J. Zhang, N. Yan, L. Zhou, Z. Y. Zhang, Z. U. Rahman and X. G. Chen, *J. Nanosci. Nanotechnol.*, 2011, 11, 10387–10395.
- 61 Y. W. Wu, J. F. Liu, Z. L. Deng, J. Zhang, F. Jiang, K. Xiong and H. L. Zhang, *J. Sep. Sci.*, 2010, 33, 3068–3074.
- 62 P. Dou, L. Liang, J. G. He, Z. Liu and H. Y. Chen, *J. Chromatogr. A*, 2009, 1216, 7558–7563.
- 63 C. C. Hsu and C. W. Whang, *J. Chromatogr. A*, 2009, 1216, 8575–8580.
- 64 Z. Iqbal, S. Alsudir, M. Miah and E. P. C. Lai, *Electrophoresis*, 2011, 32, 2181–2187.
- 65 C. Y. Hong and Y. C. Chen, *J. Chromatogr. A*, 2007, 1159, 250–255.
- 66 A. Carpio, F. Mercader-Trejo, L. Arce and M. Valcarcel, *Electrophoresis*, 2012, 33, 2446–2453.
- 67 S. W. Su, Y. C. Liao and C. W. Whang, *J. Sep. Sci.*, 2012, 35, 681–687.
- 68 Y. S. Huang, S. N. Chen and C. W. Whang, *Electrophoresis*, 2011, 32, 2155–2160.
- 69 Y.-l. Dong, D.-q. Guo, H. Cui, X.-j. Li and Y.-j. He, *Anal. Methods*, 2015, 7, 5862–5868.
- 70 S. Qi, H. Zhang, Q. Zhu, H. Chen, Y. Dong, L. Zhou, C. Ren and X. Chen, *Anal. Methods*, 2014, 6, 1219–1226.
- 71 M. G. Milia, T. Alice, G. Gregori, S. Mussino, G. Orofino, S. Bonora and V. Ghisetti, *J. Clin. Virol.*, 2010, 47, 8–12.
- 72 L. Krejcova, D. Huska, D. Hynek, P. Kopel, V. Adam, J. Hubalek, L. Trnkova and R. Kizek, *Int. J. Electrochem. Sci.*, 2013, 8, 689–702.
- 73 L. Krejcova, D. Hynek, P. Kopel, V. Adam, J. Hubalek, L. Trnkova and R. Kizek, *Chromatographia*, 2013, 76, 355–362.
- 74 K. Smerkova, S. Dostalova, H. Skutkova, M. Ryvolova, V. Adam, I. Provaznik and R. Kizek, *Chromatographia*, 2013, 76, 329–334.
- 75 C. Jiang, S. Xu, S. Zhang and L. Jia, *Anal. Biochem.*, 2012, 420, 20–25.
- 76 A. V. Herrera-Herrera, M. A. Gonzalez-Curbelo, J. Hernandez-Borges and M. A. Rodriguez-Delgado, *Anal. Chim. Acta*, 2012, 734, 1–30.
- 77 G. Alberti, V. Amendola, M. Pesavento and R. Biesuz, *Coord. Chem. Rev.*, 2012, 256, 28–45.
- 78 M. Valcarcel, S. Cardenas and B. M. Simonet, *Anal. Chem.*, 2007, 79, 4788–4797.
- 79 Y. Q. Cai, G. B. Jiang, J. F. Liu and Q. X. Zhou, *Anal. Chem.*, 2003, 75, 2517–2521.
- 80 G. H. Liu, J. L. Wang, Y. F. Zhu and X. R. Zhang, *Anal. Lett.*, 2004, 37, 3085–3104.
- 81 Q. X. Zhou, W. D. Wang, J. P. Xiao, J. H. Wang, G. G. Liu, Q. Z. Shi and G. L. Guo, *Microchim. Acta*, 2006, 152, 215–224.
- 82 L. P. Wang, H. X. Zhao, Y. M. Qiu and Z. Q. Zhou, *J. Chromatogr. A*, 2006, 1136, 99–105.
- 83 S. Y. Zhu, W. X. Niu, H. J. Li, S. Han and G. B. Xu, *Talanta*, 2009, 79, 1441–1445.
- 84 M. Valcarcel, B. M. Simonet, S. Cardenas and B. Suarez, *Anal. Bioanal. Chem.*, 2005, 382, 1783–1790.
- 85 B. Socas-Rodriguez, A. V. Herrera-Herrera, M. Asensio-Ramos and J. Hernandez-Borges, *J. Chromatogr. A*, 2014, 1357, 110–146.
- 86 M. Asensio-Ramos, J. Hernandez-Borges, L. M. Ravelo-Perez and M. A. Rodriguez-Delgado, *Electrophoresis*, 2008, 29, 4412–4421.
- 87 V. H. Springer and A. G. Lista, *Talanta*, 2010, 83, 126–129.
- 88 A. V. Herrera-Herrera, L. M. Ravelo-Perez, J. Hernandez-Borges, M. M. Afonso, J. A. Palenzuela and M. A. Rodriguez-Delgado, *J. Chromatogr. A*, 2011, 1218, 5352–5361.
- 89 N. S. Ye, P. Z. Shi, Q. Wang and J. Li, *Chromatographia*, 2013, 76, 553–557.
- 90 V. Springer, J. Jacksen, P. Ek, A. G. Lista and A. Emmer, *J. Sep. Sci.*, 2014, 37, 158–164.
- 91 E. Caballero-Diaz and M. Valcarcel, *J. Sep. Sci.*, 2014, 37, 434–439.
- 92 M. L. Polo-Luque, B. M. Simonet and M. Valcarcel, *Talanta*, 2012, 89, 124–128.
- 93 M. Valcarcel, S. Cardenas, B. M. Simonet, Y. Moliner-Martinez and R. Lucena, *TrAC, Trends Anal. Chem.*, 2008, 27, 34–43.
- 94 K. Scida, P. W. Stege, G. Haby, G. A. Messina and C. D. Garcia, *Anal. Chim. Acta*, 2011, 691, 6–17.
- 95 Q. H. Wu, C. Feng, G. Y. Zhao, C. Wang and Z. Wang, *J. Sep. Sci.*, 2012, 35, 193–199.
- 96 L. L. Xu, J. J. Feng, J. B. Li, X. Liu and S. X. Jiang, *J. Sep. Sci.*, 2012, 35, 93–100.
- 97 Q. X. Zhou, J. L. Mao, J. P. Xiao and G. H. Xie, *Anal. Methods*, 2010, 2, 1063–1068.
- 98 J. K. Duan, B. Hu and M. He, *Electrophoresis*, 2012, 33, 2953–2960.
- 99 F. J. Liu, C. T. Liu, W. Li and A. N. Tang, *Talanta*, 2015, 132, 366–372.
- 100 N. Visser, H. Lingeman and H. Irth, *Anal. Bioanal. Chem.*, 2005, 382, 535–558.
- 101 M. Pumera, *Chem. Commun.*, 2011, 47, 5671–5680.
- 102 R. Ramautar, G. W. Somsen and G. J. de Jong, *Electrophoresis*, 2010, 31, 44–54.
- 103 F. W. A. Tempels, W. J. M. Underberg, G. W. Somsen and G. J. de Jong, *Electrophoresis*, 2008, 29, 108–128.
- 104 Y. H. Tennico and V. T. Remcho, *Electrophoresis*, 2010, 31, 2548–2557.
- 105 Y. Okamoto, F. Kitagawa and K. Otsuka, *Anal. Chem.*, 2007, 79, 3041–3047.

- 106 K. Adachi, M. Yamaguchi, M. Nakashige, T. Kanagawa, M. Torimura, S. Tsuneda, Y. Sekiguchi and N. Noda, *J. Biosci. Bioeng.*, 2009, 107, 662–667.
- 107 H. X. Chen, J. M. Busnel, A. L. Gassner, G. Peltre, X. X. Zhang and H. H. Girault, *Electrophoresis*, 2008, 29, 3414–3421.
- 108 H. X. Chen, J. M. Busnel, G. Peltre, X. X. Zhang and H. H. Girault, *Anal. Chem.*, 2008, 80, 9583–9588.
- 109 T. Kaneta, J. Inoue, M. Koizumi and T. Imasaka, *Electrophoresis*, 2006, 27, 3218–3223.
- 110 T. Baciú, F. Borrull, C. Neuss, C. Aguilar and M. Calull, *Electrophoresis*, 2016, 37, 1232–1244.
- 111 D. H. Yu, P. Van Antwerpen, S. Patris, B. Blankert and J. M. Kauffmann, *Comb. Chem. High Throughput Screening*, 2010, 13, 455–460.
- 112 B. Suadrez, B. Santos, B. M. Simonet, S. Cardenas and M. Valcarcel, *J. Chromatogr. A*, 2007, 1175, 127–132.
- 113 B. Suarez, B. M. Simonet, S. Cardenas and M. Valcarcel, *J. Chromatogr. A*, 2007, 1159, 203–207.

Article 9

Adam V, Vaculovicova M. Capillary electrophoresis and nanomaterials - Part I: Capillary electrophoresis of nanomaterials. *Electrophoresis* 2017 Oct;38(19):2389-2404.

Vojtech Adam^{1,2}
Marketa Vaculovicova^{1,2}

¹Department of Chemistry and
Biochemistry, Mendel
University in Brno, Brno, Czech
Republic

²Central European Institute of
Technology, Brno University of
Technology, Brno, Czech
Republic

Received March 6, 2017

Revised June 2, 2017

Accepted June 22, 2017

Review

Capillary electrophoresis and nanomaterials – Part I: Capillary electrophoresis of nanomaterials

Nanomaterials are in analytical science used for a broad range of purposes, covering the area of sample pretreatment as well as separation, detection, and identification of target molecules. This part of the review covers capillary electrophoresis (CE) of nanomaterials and focuses on the application of CE as a method for characterization used during nanomaterial synthesis and modification as well as the monitoring of their properties and interactions with other molecules. The heterogeneity of the nanomaterial family is extremely large. Depending on different definitions of the term Nanomaterial/Nanoparticle, the group may cover metal and polymeric nanoparticles, carbon nanomaterials, liposomes and even dendrimers. Moreover, these nanomaterials are usually subjected to some kind of surface modification or functionalization, which broadens the diversity even more. Not only for purposes of verification of nanomaterial synthesis and batch-to-batch quality check, but also for determination the polydispersity and for functionality characterization on the nanoparticle surface, has CE offered very beneficial capabilities. Finally, the monitoring of interactions between nanomaterials and other (bio)molecules is easily performed by some kind of capillary electromigration technique.

Keywords:

Capillary electrophoresis / Carbon nanotubes / Liposomes / Nanoparticles / Quantum dots
DOI 10.1002/elps.201700097

1 Introduction

The nano phenomenon has clearly influenced the entire scientific world, including instrumental analytical chemistry; therefore, scientists are not only developing new approaches and assays using nanotechnologies, they are also upgrading standard techniques. One of the methods most influenced by this phenomenon is capillary electrophoresis (CE). In 1937, moving boundary electrophoresis was developed by Tiselius [1], and after approximately 30 years of development, a CE method using 3-mm rotating capillaries was presented by Hjertén [2]. Since 1981, when Jorgenson and Lukacs first presented high-voltage CE separations in 75- μm capillaries [3], this powerful analytical technique has advanced significantly not only in terms of instrumentation but also with respect to methodology and data processing. The number of CE applications has also increased markedly. Over the decades, applications of CE have grown to encompass an enormous range of analytes, from simple inorganic ions [4–8] and small organic molecules [9–11] to such large biomolecules as proteins [12–14] and DNA [15–17]. Out of numerous fundamental contributions of many scientists, the contributions of Karger [18] and Dovichi [19] in the field of DNA analysis and sequencing should be particularly highlighted.

Correspondence: Dr. Marketa Vaculovicova, Department of Chemistry and Biochemistry, Mendel University in Brno, Czech Republic
Fax: +420-5-4521-2044
E-mail: marketa.vaculovicova@mendelu.cz

The golden age of CE occurred during the 1990s, when the Human Genome Project promoted the widespread application of automated 96-capillary array sequencers to achieve rapid and reliable results [20]. The sequencing of the human genome in its entirety was successfully completed in 2006 with the identification of approximately 20 000–25 000 genes in human DNA and the determination of the sequences of three billion chemical base pairs that make up human DNA.

Another boom period for CE began when the concept of the micro total analysis system (μTAS) was suggested [21]. Even earlier, a miniaturized analysis system was developed by Terry et al. in the form of a gas chromatograph fabricated on a silicon wafer [22]. The relatively simple instrumentation and ease of miniaturization of CE led to rapidly growing interest in microfluidics and particularly in chip-based CE [23–26]. CE delivers rapid results with high efficiency and resolution and low sample consumption; however, the benefits provided by the large number of theoretical plates can be overshadowed by the low sensitivity of commonly employed UV detection systems [27]. New methods are therefore needed to overcome this weakness, and applications for nanomaterials are under extensive study.

2 Nanomaterials

The name “nanomaterials” (NMs) is a general term that covers an extremely large group of materials. A generally

Colour Online: See the article online to view Figs. 1, 3, 5 and 6 in colour.

accepted definition is that a nanomaterial is “any material that has an average particle size of between 1 and 100 nanometres at least in one dimension.” The European Commission defines a nanomaterial as “a natural, incidental or manufactured material containing particles, in an unbound state or as an aggregate or as an agglomerate and where, for 50% or more of the particles in the number size distribution, one or more external dimensions is in the size range 1 nm–100 nm” [28].

Strict adherence to these definitions permits application of the term “nanomaterials” to a wide range of biomolecules including proteins or nucleic acids. For example, the size of an albumin molecule is approximately 7 nm in diameter [29], and this biomolecule fits the definition of a nanomaterial perfectly; however, it is not usually included in this group. Therefore, we have decided to also discuss dendrimers in our paper even though these polymeric molecules with sizes on the order of nanometers are not typical nanomaterials.

At the same time, several types of materials with dimensions that exceed 100 nm also might be included in the nanomaterial group because they exhibit properties that differ significantly from those of bulk materials. Due to the fine line defining the nanomaterial family, we prefer the definition given in the work by Buzea et al. [30]. These authors stated that, despite certain exceptional examples, most of the exciting properties of nanomaterials become apparent in systems smaller than 1 μm . In both parts of our review, we are also generous in terms of definitions, and in this paper, we include materials that might not be strictly defined as nanomaterials but are nevertheless interesting in the context of the primary definition through the terms nanomaterial and CE.

Nanomaterials include materials with a wide variety of natures and highly diverse properties. According to their specific properties, we can classify materials as metal or metal oxide nanoparticles (NPs), semiconductor nanocrystals (quantum dots [31]), carbon NMs (nanodiamonds, fullerenes, graphene, carbon nanotubes, nanohorns, and carbon dots) [32, 33], or polymer NMs (e.g., chitosan, polystyrene, and dendrimers) [34, 35]. According to their shapes, we identify dots, rods, spindles, wires, tubes, ribbons, nanobelts, nanoscales, nanosheets, and nanobuds. Moreover, we can classify NMs according to various key characteristics, such as their optical/fluorescent (e.g., quantum dots), electronic (e.g., fullerenes), magnetic (e.g., metallic NPs), and biological (e.g., liposomes) properties. An overview of the NMs that are the main subjects of this paper is given in Fig. 1.

3 CE separations of nanomaterials

As mentioned previously, numerous types of nanoparticles have been prepared and used in different applications recently. Therefore, analytical methods for the efficient characterization of nanoparticles are of current interest. Planar gel electrophoresis can readily be used for separation of nanoma-

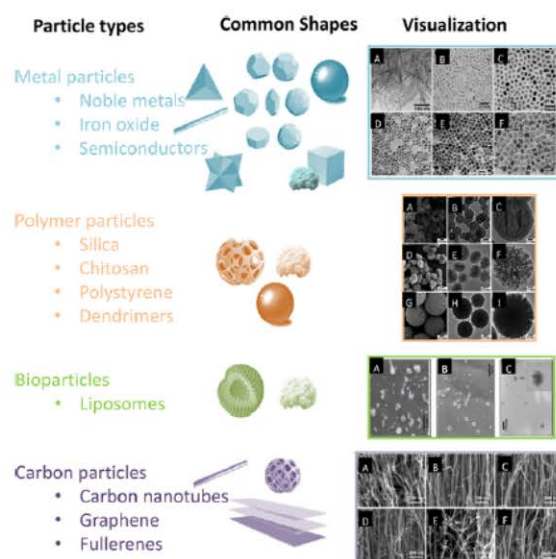


Figure 1. Overview of the main nanomaterial types discussed in this review, including the principal members of each group and main possible shapes as well as examples of their visualizations via electron microscopy (scanning electron microscopy – SEM, transmission electron microscopy – TEM).

Metal particles. TEM images of face-centered cubic FePt nanoparticles with various shapes: (A) nanowires ($150 \pm 20 \text{ nm} \times 3 \pm 0.5 \text{ nm}$), (B) nanorods ($20 \pm 5 \text{ nm} \times 3 \pm 0.5 \text{ nm}$), (C) oval-shaped nanoparticles ($8 \pm 1.5 \text{ nm}$), (D) spherical nanoparticles ($8 \pm 0.8 \text{ nm}$), (E) nanocubes ($9 \pm 0.9 \text{ nm}$), and (F) nanosized multipods ($18 \pm 1.5 \text{ nm}$). Reprinted with permission from [255]

Polymer particles. SEM (A, D, G) and TEM (B, C, E, F, H, I) images of fabricated hollow mesoporous silica nanoparticles (A–C) and nanoparticles with hierarchical pores under an ethanol/ethyl ether volume ratio of 0.5 (D–F) and 1 (G–I), respectively. Reprinted with permission from [256]

Bioparticles. Electron microscopy micrographs for Dex-5CA/liposome mixtures at $C_{\text{DMPC}} = 16.0 \text{ mM}$ (DMPC: 1,2-dimyristoyl-sn-glycero-3-phosphocholine). Cryo-SEM micrographs: (A) pure DMPC vesicles in water, and (B) for Dex-4CA-liposomes, a mixture with $R(\text{inside group}/\text{nDMPC}) = 0.0075$ ($C_{\text{sg}} = 0.12 \text{ mM}$). (C) TEM micrograph from the solution above the sediment (supernatant) in the Dex-5CA-liposome mixture system with $R(\text{inside group}/\text{nDMPC}) = 0.075$ ($C_{\text{sg}} = 1.2 \text{ mM}$). Reprinted with permission from [257]

Carbon particles. Selected SEM micrographs of vertically aligned carbon nanotube turfs for (A)-CNT 7, (B)-CNT 10, (C)-CNT 17, (D)-CNT 18, (E)-CNT 19, and (F)-CNT 20 (specimens from six different growth conditions). Densities were measured directly from these and other similar images. Reprinted with permission from [258].

terials according to their size or shape [36]. However, CE is suitable for separating nanoparticles according to their size, surface properties, and conjugation with biomolecules [37]. Electrophoresis is applicable because colloidal particles possess surface charges, and fundamental electrophoretic laws can be applied to separation of nanoparticles.

Determination of electrophoretic mobility yields information on the electric potential at the shear plane (ζ -potential) and/or the particle size. At the same time, these two parameters present two main factors responsible for unsuc-

cessful CE analysis of NMs. Due to the relatively small internal diameters of capillary or microfluidic chip channels, the particle size, the polydispersity of the solution and the stability of the colloidal NM solution are crucial. It is generally accepted that colloidal solutions are unstable, and particles tend to aggregate when ζ -potential values are in the range of -30 to $+30$ mV. Such aggregation might not only cause poor repeatability of the separation but might also cause complete clogging of the capillary or channel. If a rigid charged sphere is placed in an electrolyte solution, it is surrounded by a “cloud” composed of ions compensating for the charge of the particle. The distribution of the space charge can be calculated from the Poisson–Boltzmann equation. Use of a Debye–Hückel approximation of this equation results in the well-known equation for the inverse thickness of the double-layer κ , which corresponds to the inverse thickness of the ion cloud (1):

$$\kappa = \sqrt{\frac{e^2 N_A \sum z_i^2 c_i}{\epsilon_r \epsilon_0 k T}} \quad (1)$$

where e is the elementary electric charge, N_A is Avogadro's number, z_i is the charge number (valence) of the i^{th} component, c_i is the molar concentration of the i^{th} component, ϵ_r is the relative electric permittivity of the electrolyte, ϵ_0 is the electric permittivity of vacuum, k is the Boltzmann constant, and T is the absolute temperature [38].

3.1 Size and surface characterization

Due to powerful, high-resolution separation, CE enables understanding of the complexity and diversity of nanomaterial solutions that vary according to the NM size and surface characteristics. Due to the high separation power and wide variety of modalities, CE can be used to characterize the properties of NMs.

The most important parameter in the nanoscale world is size, although the surface chemistry and general characterization of a nanomaterial also might be important for particular purposes [39]. In this section, we focus on papers that describe methods and protocols that use CE in various modes for the separation and characterization of nanomaterials from numerous points of view, including size and shape characterization, surface characterization, and even for the investigation of the interactions between NMs and other (bio)molecules.

Reviews devoted to CE analysis of nanoparticles were published in 2004 by Rodriguez and Armstrong [40], in 2009 by Surugau and Urban [37], in 2010 by Pyell [38], in 2011 by Lopez-Lorente et al. [41], in 2015 by Ban [42], and in 2016 by Mebert et al. [43]. A more narrowly focused review of CE analysis of poly(amidoamine) dendrimeric structures was prepared by Shi et al. [44]. Other reviews devoted to the application of CE and other separation techniques for AuNPs [45, 46] and QDs [47, 48] analysis are also available.

The common methods for determining size distribution are transmission electron microscopy (TEM) and/or size

exclusion chromatography. However, these methods have several disadvantages, including high costs for instrumentation, time-consuming and laborious sample preparation, and high demands on operators for interpreting results. Therefore, CE is a good alternative for characterizing colloids and nanomaterials.

Two methods are available to calculate NM size from electrophoretic mobility [49]. These methods use (1) a calibration curve constructed by measuring the electrophoretic mobilities of NMs with known sizes [50] (Fig. 2), and (2) an approximate mathematical expression based on the ζ -potential and characteristics of the electrolyte solution [51–54].

To calculate the ζ -potential of a spherical colloidal particle from the measured electrophoretic mobility μ , the relationship between μ and ζ is required. This relationship is most widely defined as Smoluchowski's mobility (2):

$$\mu = \frac{\epsilon_r \epsilon_0 \zeta}{\eta} \quad (2)$$

where ϵ_r and η are the relative permittivity and the viscosity of the electrolyte solution, respectively, and ϵ_0 is the permittivity of a vacuum.

This formula is applicable in the case of sufficiently large κa (where κ is the Debye–Hückel parameter and a is the particle radius). For notably small κa , Hückel's formula is used to express the mobility (3):

$$\mu = \frac{2\epsilon_r \epsilon_0 \zeta}{3\eta} \quad (3)$$

In the case of low ζ ($\zeta < 25$ – 50 mV), the mobility is given by Henry's formula (4):

$$\mu = \frac{2\epsilon_r \epsilon_0 \zeta}{3\eta f(\kappa a)} \quad (4)$$

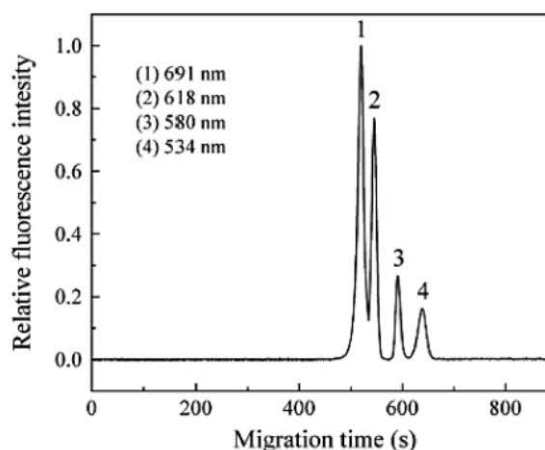


Figure 2. Electropherograms of a mixture of four QDs. Samples are water-soluble CdSe/ZnS core-shell QDs with emission wavelengths at 534, 580, 618, and 691 nm. Concentrations of QDs in the mixture were all 2.038×10^{-6} M. Polyethylene glycol (4%) was used as a sieving medium, and the applied voltage was 14 kV. Reprinted with permission from [50].

In the case of nanoparticle dispersions that are stabilized against coagulation by electrostatic repulsion, in general, higher ζ potentials are reached, such that the Henry equation does not model the electrophoretic behavior of nanoparticles with adequate accuracy [38]. This equation can be further extended and improved, as shown by Ohshima [51], but it is already obvious that the calculation of NM size from electrophoretic data is a complex process involving a number of theoretical considerations [38]. From an experimental point of view, it should be emphasized that a single sample might frequently contain a distribution of properties and therefore of electrophoretic mobilities, which contribute to the total variance of the peak width, peak broadening, and irregularity of the peak shape. Recently, a method for size distribution functions calculated from electropherograms was presented using silica nanoparticle separation [55]. The factors that complicate CE analysis of colloids are discussed in a review by Rodriguez and Armstrong [40], although numerous studies still use the simplified approach that neglects the size and charge distributions within the sample and correlates the electrophoretic mobility directly with the size of the nanomaterial. Systematic investigation in this area was also discussed in a work by Pyell et al. [56, 57]. Also Qu et al. realized that under certain experimental conditions, neither Smoluchowski nor Hückel approximation was suitable for describing the nanoparticle behavior [58]. Authors realized that even with the same core size, the migration behaviors varied significantly among the different coatings and relaxation effect of the potential gradient was factor that can affect the electrophoretic mobility (Fig. 3).

Most likely, due to the complexity and inaccuracy of size determination based on CE data, the vast majority of studies use CE mainly to demonstrate the ability to separate a mixture of nanoparticles of different sizes. In these works, size is determined mostly via TEM and size exclusion chromatography.

The first efforts into the application of CE for the separation of nanoparticles according to size were reported by Vanorman and McIntire in 1990 [59, 60]. Later, in 1991, McCormick presented work on the successful separation of a series of silica particle populations ranging in size from 5 to 500 nm [61]. Since that time, CE has been used for the separation of numerous types of colloids, such as gold nanoparticles [62–65], silica sols [61, 66, 67], modified latex [68, 69], metal oxide particles [70, 71], and polystyrene nanoparticles [72–74]. An example of size-dependent separation is shown in Fig. 4. In 1997, Schnabel et al. [75] separated gold nanoparticles (core diameters of 5.2–14.6 nm) without any sieving additive. The mobility of the particles with a given core diameter were found to decrease with decreasing ionic strength as the thickness of the electric double layer increased. A size-based characterization of the nanoparticles was obtained due to the good linear dependence of the mobility on the reciprocal of the core radius.

Precise control of the surface chemistry and particle size is crucial in nanomaterial applications. The large ratio of surface area to volume in the case of nanomaterials versus bulk materials is responsible for the increase in their overall surface energy and thus their enhanced reactivity. Surface chemistry is an important tool in preventing uncontrolled nanoparticle aggregation in commonly used CE buffers in the presence of target molecules, on the capillary wall, and/or with other nanomaterials during separation. First, the degree of nanoparticle–nanoparticle interactions is quantified using the critical nanoparticle concentration (CNC), which is defined as the lowest concentration of nanoparticles that induces predominant nanoparticle aggregation under specific buffer conditions. Exceeding the CNC value leads to irreproducible separation. Second, nanoparticle–analyte interactions are determined by electrostatic interactions that depend on the analyte pK(a) and on the surface charge of the nanoparticle. Finally, nanoparticle–capillary interactions occur in a

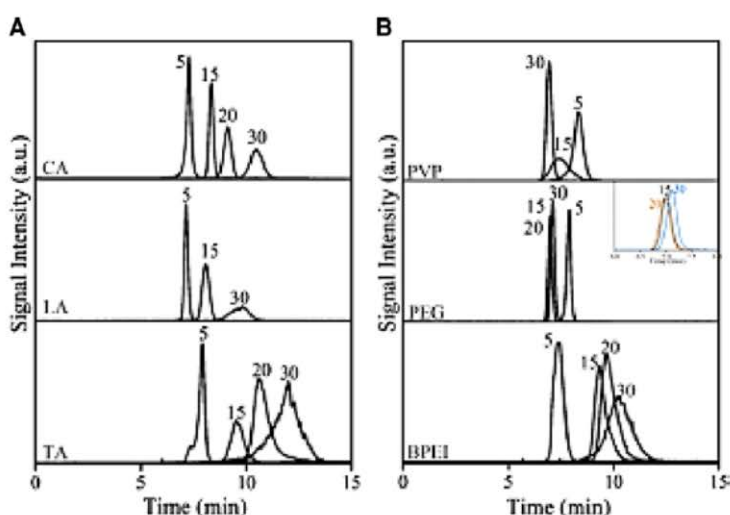


Figure 3. (A), (B) Electropherogram of gold NPs with different surface coatings. (Separation conditions: SDBS, 70 mM; CHES, 10 mM; pH 10.0; and voltage, 30 kV). Nanoparticles with different surface coatings were individually injected and analyzed by the CE-ICPMS method, and the electropherograms of nanoparticles of different sizes with the same coating material were plotted together in a graph. Reprinted with permission from [58].

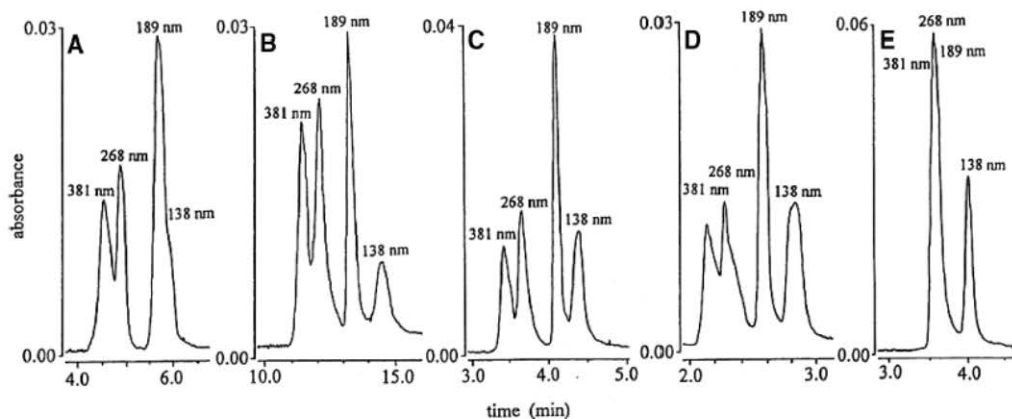


Figure 4. Representative electropherograms for mixtures of polystyrene latex microspheres with radii of 138, 189, 268, and 381 nm subjected to CE. Conditions: Coated capillary with 150 μm inside diameter and 40 cm effective length, 25°C, detection at 340 nm. (A) TBE/64 buffer (Tris/Borate/EDTA), 300 V/cm; (B) TBE/16 buffer, 100 V/cm; (C) TBE/16 buffer, 300 V/cm; (D) TBE/16 buffer, 500 V/cm; and (E) TBE/4 buffer, 300 V/cm. Reprinted with permission from [69].

surface chemistry-dependent manner. The viscosity of the separation buffer is influenced by the formation of a nanoparticle steady-state pseudostationary phase along the capillary wall [76].

3.1.1 CE of metal and metal oxide nanoparticles

The first and most likely the largest and most diverse group discussed in this part of the review consists of metal and metal oxide nanoparticles. They are attractive for a wide variety of applications, i.e., in catalysis, as sensors, as (opto)electronic materials, and for environmental remediation.

Gold and silver are the two metals that are used most often to synthesize nanoparticles. The generation of spherical gold nanoparticles (AuNPs) is commonly performed via the citrate reduction method reported by Turkevitch in 1951 [77]. The size distribution of the gold nanospheres obtained in this way is controlled by the temperature, the ratio of gold to citrate, and the order in which the reagents are added. Other methods of synthesis have been developed, such as the seeding technique [78], the two-phase reaction method [79], and approaches using inverse micelles [80] and dendrimers [81].

Colloidal silver is of particular interest because of its distinctive properties, such as good conductivity, chemical stability, and catalytic activity. Chemical reduction is the most frequently applied method for the preparation of silver nanoparticles (AgNPs) as stable colloidal dispersions in water or organic solvents. Commonly used reductants include borohydride, citrate, ascorbate, and elemental hydrogen [82].

The noble metals platinum [83, 84], palladium [85–87], rhodium [88, 89], ruthenium and osmium [90–92] have also been described and exploited for use in nanoparticles, primarily because of their catalytic properties.

3.1.1.1 Gold and silver nanoparticles

To achieve separation of nanoparticles with very small size differences, the addition of surfactant to the background electrolyte has proven to be beneficial. Separation of AuNPs with diameter differences at the level of 1 nm with resolution $R = 1$ was achieved via the addition of the cationic surfactant tetradecyltrimethylammonium bromide [72]. However, the anionic surfactant sodium dodecyl sulfate (SDS) is a popular buffer modifier that is also widely used for nanoparticle separation.

Separation of AuNPs was achieved by Liu et al. under optimized separation conditions involving SDS (70 mM) [93]. The charged surfactants associated onto the surfaces of the AuNPs and caused a change in the charge-to-size ratio of the nanoparticles; this ratio is determined by the nanoparticle surface area and the concentration of surfactant in the separation electrolyte. When the surfaces of gold nanoparticles are fully occupied with SDS, a linear relationship exists between the electrophoretic mobility and nanoparticle diameters in the range from 5.3 to 38 nm.

In the cases of silver nanoparticles and nanorods, methods for separation according to size and shape have been developed, and the morphological properties of these nanomaterials have been investigated. The addition of SDS to the running electrolyte prevented coalescence of the silver particles during the CE process, and limited their agglomeration by electrostatic repulsion between the nanoparticles [94]. Silver nanocubes have also been analyzed by CE [95] using a diode-array detector, thus demonstrating the ability to distinguish between different shapes of nanoparticles due to their spectroscopic properties.

A CE method for separating Au/Ag core/shell nanoparticles that enables the chemical characterization of NP species was developed using 3-(cyclohexylamino)propanesulfonic acid and SDS as a background electrolyte (BGE) [96, 97]. Modification of this protocol by implementation of reversed

electrode polarity stacking mode led to dramatic 130-fold [98] and 260-fold [99] improvements in the observed signal. Even greater AuNP signal enhancement (500-fold) with the same stacking method (reversed electrode polarity stacking mode) was observed by Liu [100]. Based on the reported results, SDS can be considered a good additive for size characterization of gold and silver nanoparticles. However, SDS is not the only one of many molecules with the same or even better properties. In the case of metal nanoparticles, the use of certain organic acids with high affinities for metal ions, such as sodium dodecyl benzenesulfonate, chitosan, cetyltrimethylammonium bromide, sodium dodecylbenzenesulfonate and hyaluronic acid, was suggested [58, 101, 102].

From a detection point of view, recent work by Matczuk [103] compared UV detection, conductometric detection, and inductively coupled plasma mass spectrometric (ICP-MS) detection for AuNPs analysis, and under optimized conditions, CE-ICP-MS achieved a limit of detection as low as 2×10^{-15} M. The ICP-MS has been proven to be effective detection technique also for speciation analysis of gold and silver NPs [104, 105].

3.1.1.2 Iron oxide nanoparticles

Ferrofluids, such as maghemite ($\gamma\text{-Fe}_2\text{O}_3$), which consists of particles suspended in their stabilizing acidic or basic aqueous media, have been investigated using CE [106]. Particular attention has been devoted to the study of positively charged ferrofluids, although in such cases, the capillary wall must be modified to prevent particle adsorption. Despite the narrow particle size distribution, partial separation was obtained with a selectivity that was dependent on the electrolyte ionic strength [107, 108]. Additionally, the diffusion coefficients of maghemite nanoparticles were determined via Taylor dispersion analysis using CE [109]. The obtained values were compared with the z-average diffusion coefficients derived from dynamic light scattering experiments, and the measured diffusion coefficients were found to depend on the particle volume fraction and electrolyte ionic strength. These results show that iron nanoparticles behave differently than gold and silver nanoparticles. As mentioned previously, an acidic separation environment and selected modification of the capillary wall (capillary inner walls semi-permanent or positive coating with didodecyltrimethylammonium bromide or permanent and neutral modification with hydroxypropylcellulose) [110, 111] appear to be highly beneficial for CE characterization of these materials. This observation can be associated with the acido-basic properties of iron and the inertness of the mentioned noble metals.

3.1.1.3 Others

Characterization of nanoparticles by size and other physico-chemical properties is particularly important for polymer particles because their properties are mutable depending on the surrounding environment. In the case of chitosan particles, for example, highly labile behavior has been observed

in which both aggregation and disintegration processes occurred [112]. Although these results are discouraging, testing metal ions such as silver could stabilize the complex [113, 114] and offer advantages for further CE characterization of this polymeric material.

CE was also chosen for characterization of nanoparticles of pentosan polysulfate (PPS). The protocol suggested by Abdel-Haq et al. [115] was able to determine both the profile of the NPs and the species of PPS entrapped within them in addition to quantifying free and bound PPS with high reproducibility, acceptable accuracy, and a good degree of precision. Moreover, this approach allowed evaluation of the sizes and charges of the NPs.

Extensive attention in terms of characterization also has been focused on latex [116–121], silica [122] as well as other polymeric nanoparticles [123], particularly due to the diversity of this material. This type of nanoparticles was used for detailed modeling of electrophoretic behavior and for the prediction of the signs and magnitudes of the surface potentials of the particles, which strongly correlate with their aggregation processes.

3.1.2 CE of semiconductor nanocrystals (quantum dots)

The properties of semiconductor nanoparticles are also strongly associated with the size and shape of the nanoparticle, and these characteristics differ significantly from those of macroscopic semiconductor materials. The shapes vary from nanorods, nanowires, and nanotubes to the currently popular quantum dots (QDs).

QDs are a special group of metal/metalloid particles (more specifically, semiconductor nanocrystals) that have gained enormous popularity in the past three decades [124, 125]. Originating from the quantum confinement of electrons and holes within the nanocrystal core material, the fluorescence from QDs is unique compared with that from traditional organic fluorophores. Compared with organic dyes and fluorescent proteins, QDs have unique optical and chemical properties. QDs have molar extinction coefficients that are 10–50 times greater than those of organic dyes, which make them much brighter in photon-limited *in vivo* conditions. Their long lifetimes (on the order of 10–40 ns) increase the probability of absorption at shorter wavelengths and produce a broad absorption spectrum. Furthermore, QD emission wavelengths are size-tunable [49], and researchers have shown enormous interest in and focus on the synthesis [126, 127], photophysical property characterization [128–131], and bioconjugation of QDs [126, 132, 133].

Because the properties of QDs are defined primarily by their composition and size (more so than in the case of other NMs), it is necessary to determine the size accurately and quickly [54]. Commonly used methods for measuring the size of QDs are relatively time consuming, require large amounts of sample, and might not be suitable for environmental or biological samples. In this case, CE provides the

required separation efficiency, speed, and simplicity. Certain applications, including environmental analyses, cannot rely on such standard methods as photometry and/or fluorimetry because the complex biological matrices affect or interfere with the analyses. In such cases, a separation technique such as CE is beneficial. A review summarizing the potential of CE for size characterization of QDs was published in 2011 [49]. The reported methods used polymer solutions such as polyvinylpyrrolidone (PVP), polyacrylamide (PAA), and hydroxypropyl methylcellulose (HPMC) as sieving media [50, 134]. Although CE is used to evaluate the quality of QDs produced in the lab in most cases [53, 135], commercial QDs also have been characterized to lay the foundations for CE-based immunoassays [136]. A simple and rapid methodology for the separation and characterization of free CdSe QDs in aqueous medium was presented by Carrillo-Carrion et al. [137]. The procedure required derivatization based on the formation of a complex between the QDs and surfactants such as trioctylphosphine oxide/trioctylphosphine (TOPO/TOP) and SDS to enhance the hydrophilicity and stability of the QDs. These free QDs were separated via CE based on differences in the charge-to-mass ratios of the QDs–TOPO/TOP–SDS complexes. Under optimal conditions, the method was able to separate QDs that differed by only 0.5 nm in diameter and 19 nm in fluorescence emission maximum. The application of a micellar plug as a tool for the preconcentration of QD samples has also been reported [138]. In the presented work, the distribution of CdSe nanoparticles between two zones depended on the affinity of nanocrystals for the micellar zone. This approach relies on the type of surface ligands attached to the CdSe nanoparticles and on the electrophoretic conditions applied.

Investigation of the surface properties of quantum dots is highly important, particularly for the determination of the influence of capping agents or other modifiers. Fine-tuning of the surface properties influences not only the spectral properties of these QDs but also their bioconjugation abilities and might assure their use in numerous applications, including fluorescent labeling of non-fluorescent molecules and optical sensor signaling of the presence of a molecule of interest via changes in fluorescence intensity. The variety of CE modes (zone, micellar, microemulsion) is highly beneficial in this particular case because it allows the analysis of QDs with various surface properties and even QDs with uncharged surface coatings composed of bidentate ligands [139]. Verification of the synthesis process and the functionality of the biotin or streptavidin surface coating can also easily be performed by CE [140, 141].

3.1.3 CE of carbon nanomaterials

Due to its covalent in-plane carbon bonds, the inherent structural strength of graphene is considered to be among the sturdiest in nature. This attraction of this material lies in the fact that it consists of a flat monolayer of carbon atoms organized into a two-dimensional (2D) honeycomb structure

that can be wrapped up into 0D fullerenes, rolled into 1D nanotubes, or stacked into 3D graphite [142]. From the point of view of this review article, it should be noted that CE analysis/characterization of graphene is not as common as in case of other NMs. Graphene and its modifications (graphene oxide or reduced graphene oxide) are more commonly employed either as stationary phases in capillary electrochromatography or solid phase extraction media for sample pretreatment. However, several publications may be mentioned [143, 144].

Fullerenes are closed-cage carbon molecules with three-coordinate carbon atoms tiling their spherical or nearly spherical surfaces. The smallest stable and most abundant fullerene is the *Ih*-symmetrical buckminsterfullerene C₆₀. The next stable homologue is C₇₀, followed by higher fullerenes such as C₇₆, C₇₈, C₈₀, C₈₂, and C₈₄ [145]. Fullerenes exhibit antiviral and antioxidant activity, and due to the hollow cavity in their structure, they are used for gene and drug delivery [146].

Carbon nanotubes (CNTs) are well-ordered, hollow graphitic nanomaterials consisting of cylinders of sp²-hybridized carbon atoms [147]. Single-walled carbon nanotubes (SWCNTs) are formed from a single graphene sheet that is seamlessly wrapped into a cylindrical tube. Multi-walled carbon nanotubes (MWCNTs) include arrays of nanotubes that are concentrically arranged. CNTs can range in length from several hundred nanometers to several millimeters. Their diameters vary in the range of 0.4–2 nm in the case of SWCNTs and 2–100 nm for MWCNTs. Moreover, a number of morphologies can occur in MWCNTs. These morphologies are known as “hollow tube,” “bamboo” and “herringbone” [148].

The youngest member of carbon nanomaterial family is the group of carbon dots (often called also carbon quantum dots). They possess size-tunable luminescent properties similarly as semiconductor quantum dots however; they are low toxic, environmentally friendly and the preparation methods are inexpensive and simple [149].

Size characterization of carbon nanotubes using CE in combination with Raman spectroscopy has enabled differentiation between various bundles of single-walled carbon nanotubes and individual nanotubes [150–152]. SDS has proven to be beneficial as a buffer additive [150, 153], as in the cases of silver and gold nanoparticles. Improved separation of CNTs has been achieved using ionic liquids in combination with SDS [154]. In that case, the separation of solubilized CNTs was accomplished using a 50 mM formic acid solution at pH 2.0 as a BGE, and two types of bundles subsequently exhibited characteristic electrophoretic profiles that could be used to control the purity of CNTs [154]. Adding SDS and also a small amount (0.025%) of hydroxypropyl methyl cellulose has been shown to improve the performance of the analytical system [153]. Moreover, the methodology thereby developed facilitated study of the interactions of different types of carbon nanotubes with molecular probes such as pentachlorophenol.

Derivatization of nanotubes with fluorescein-based labels has enabled the formation of fluorescently labeled carbon nanotube probes (CNTPs), the distribution of which

was quantitatively determined in yeast using CE with laser-induced fluorescence detection (CE-LIF) [155]. The detection sensitivity for CNTP was greatly improved compared with that of UV absorbance and Raman detection. Calculation of the apparent permeability coefficient suggested that endocytosis is the mechanism used to permeate into the yeast. This study implies that CNTP could act as a fine drug transporter and might find broad use in multidrug resistance research and microorganism detection. A similar approach was used later by a subset of the same authors to analyze CNTP in multidrug-resistant cells (K562A) and parent cells (K562S) [156]. Analysis of CNTP in the two cell lines using both CE-LIF and flow cytometry showed that CNTP could traverse the cellular membrane without being pumped out by P-glycoprotein.

Although it is well known that the field of nanomedicine might be greatly advanced by drugs carried on nanotransporters [157–159], another approach might involve the transport of therapeutic nucleic acids (gene therapy) [160, 161]. To achieve this goal, DNA sequences can be wrapped around carbon nanotubes. Prior to the application of such an arrangement, several questions must be answered: How much DNA is wrapped around the nanotube? What is the charge of such a hybrid? Is it just a single DNA strand or are several strands wound around the nanotube? In the work of Khripin et al. [162], the electrical charge on a DNA–CNT hybrid was estimated based on electrophoretic mobilities, and a molecular model was developed for an ordered arrangement of DNA around CNTs that was consistent with the measured charge density.

Although fullerenes are not as widely characterized by CE as CNTs, several papers focused on the electrophoretic separation of fullerenes have nevertheless been published. A relatively complex electrolyte systems have been used, such as 200 mM TFA/20 mM NaOAc in MeOH/acetonitrile (10:90, v/v) [163], tetra-*n*-decylammonium bromide (200 mM), and tetraethylammonium bromide (40 mM) in 6% MeOH and 10% CH₃COOH in acetonitrile/chlorobenzene (50:50 v/v) [164]. Thus, nonaqueous capillary electrophoresis has become a rapid and useful alternative to high performance liquid chromatography for the separation of fullerenes.

Recently discovered carbon quantum dots can be seen not only as a less toxic alternative to semiconductor quantum dots but also as a natural link between quantum dots and carbon nanomaterials. Even though carbon dots are attracting great attention, the number of publications focused on CE of carbon dots is not very high, yet [165].

3.1.4 CE of dendrimers

Dendrimers are macromolecular compounds that make up a series of branches surrounding an inner core. When the core of a dendrimer is removed, a number of identical fragments known as dendrons remain. The number of dendrons depends on the multiplicity of the central core. Ideally, these structures are perfectly monodisperse macromolecules with a regular and highly branched three-dimensional architecture.

Due to their structure, dendrimers are often used for drug [166, 167] and gene [168, 169] delivery, but their range of applications also encompasses catalysis [170, 171], imaging [172, 173], and tissue engineering [174].

Due to the polydispersity of dendrimers, the benefits of CE are especially valuable for characterizing the overall quality of synthesis and the presence of side products. The first use of CE for the analysis of dendrimers was presented in 1996, when on-line coupling of CE with a sector mass spectrometer via an electrospray ionization (ESI) source was used to separate and identify polydisperse dendrimeric diaminobutane-based polynitriles [175]. A sample of the corresponding second generation consisted of a complex mixture of the product accompanied by several by-products.

Polyamidoamine (PAMAM) dendrimers can be separated reasonably well at acidic pH but not at neutral pH. This point was considered in a number of papers directed towards the isolation and characterization of dendrimers [176–180]. To improve run-to-run reproducibility, a silanized capillary was used [44], and monitoring of the removal of excess succinic anhydride/succinic acid enabled more detailed characterization of PAMAM samples [181].

In addition to the analysis and characterization of complex mixtures, CE can also be used to isolate one specific dendrimer. The method is capable of separating the targeted dendrimer from impurities with lower molecular weights. The optimized BGE consisted of 15 mM sodium phosphate at pH 6.3 containing 0.5 mM hexadecyltrimethylammonium bromide [182].

The combination of polyacrylamide gel electrophoresis (PAGE) and CE analysis provides an alternative and effective method for characterizing this group of PAMAM-succinamic acid dendrimers [183]. PAGE results showed that the relative mobilities of dendrimers decrease with increasing number of generations. The electrophoretic mobilities of individual generations of PAMAM polyanions as determined by CE were similar, leading to the conclusion that their separation primarily depends on their approximately identical charge/mass ratio [183].

In addition to analytical characterization of dendrimers, PAMAM dendrimer-based nanodevices provide novel nanoplatforms for targeting, imaging, and treatment of cancers *in vitro* and *in vivo*. The advances in the analysis and characterization of a variety of PAMAM dendrimer-based nanoparticles (polycationic and polyanionic PAMAM derivatives, PAMAMs of different generations and defined substitutions, complex multifunctional PAMAM nanodevices containing targeting ligands, dyes, and drugs) have been reviewed [184].

3.1.5 CE of liposomes

Liposomes, or (phospho)lipid vesicles, are self-assembled colloidal particles that occur naturally and can be prepared artificially. These materials display spherical and self-closed structures formed by one or more concentric lipid bilayers with

an aqueous phase inside and between the lipid bilayers. Several practical applications emerged in the 1970s, most notably in drug delivery. Today, these materials serve as very useful models, reagents, and tools in various scientific disciplines, including mathematics, theoretical physics, biophysics (properties of cell membranes and channels) [185], chemistry (catalysis, energy conversion, photosynthesis) [186], colloid science (stability, thermodynamics of finite systems), biochemistry (function of membrane proteins) [187], and biology (excretion, cell function, trafficking and signaling, gene delivery function) [188, 189].

Although liposomes are not typical members of the nanomaterials group, we decided to include this group of vesicles in this paper despite their size (10–1000 nm) [190].

As early as 1996, a CE method was developed for characterizing liposome behavior [191]. Automated delivery of lysis agents by multiple electrokinetic injections was demonstrated, and on-capillary reactions between liposomes and other reagents were induced. In addition, on-line chemiluminescence detection using a peroxyoxalate system was used for the analysis of eosin Y- or rhodamine B-containing liposome solutions to provide information on size distribution, stability, permeability, and surface charge [192, 193]. Individual liposome measurement has been performed by CE with post-column laser-induced fluorescence detection [194]. Furthermore, liposomes showed entrapped volumes of fluorescein solution that varied between 0.3 and 13 fL with an apparent radius in the range of 370 nm to 1.8 μm .

In addition, CE has been demonstrated as a powerful tool for investigating the compositional homogeneity of liposomal membranes composed of phospholipids and guest molecules [195]. The ions distributed randomly within the liposomal membrane were observed to be responsible for formation of liposomal particles that differed in charge and therefore in electrophoretic mobility. This observation led to the presence of a number of peaks even though the solution was monodisperse from the particle point of view. When liposomes of identical surface charge density were subjected to CE and size-dependent electrophoretic separation was observed [196, 197], it was shown that size-dependent migration is primarily a function of KR , where K^{-1} is the thickness of the electric double layer and R is the liposome radius.

Due to the biological properties of liposomes, these structures are currently under extensive study as nanocarriers for targeted drug delivery [198, 199]. It should come as no surprise that CE is used in this research to verify the encapsulation and selective release of the cargo carried in these nanovehicles [200–211]. An important aspect of many preparations in biological processes is the presence of a pH gradient across the membrane. This gradient has a significant effect on electrophoretic migration, which is induced principally by a change in effective charge [212]. To further improve the pharmacological application of liposomes, hybrids of these NMs with protein via hexa-histidine-tag have been synthesized, and the success of that synthesis was evaluated using CE [213].

3.2 CE monitoring of interactions of NMs with (bio)molecules

CE is an analytical method with the ability to investigate interactions between molecules, and therefore, an entire field has become known as “affinity capillary electrophoresis” (ACE) [214, 215]. Although many interactions are being investigated and employed, the term ACE appears to be more or less reserved for stronger interactions with specific stoichiometries. Therefore, micellar electrokinetic chromatography or chiral separations are not commonly labeled ACE methods [216].

The main aim of the ACE analysis is to determine the binding and dissociation constants of two interacting molecules, i.e., receptor (R) and ligand (L). The basic assumption is that when two molecules R and L that differ in electrophoretic mobilities form a complex, the complex could have a mobility that is different from either of the components due to a change in either charge or molecular mass [215, 216].

ACE can be operated in three different modes: off-capillary, on-capillary, or immobilized selection [216]. In off-capillary analysis, binding partners are incubated, and the mixture is injected into the CE system, which separates and quantifies the formed complex. On-capillary analysis includes one of the binding partners in the running buffer, and the other binding agent is injected and electrophoresed. When complex formation involves a change in the charge-to-size ratio, the migration of the injected analyte is a function of binding to the affinity agent in the running buffer. The migration shift in response to running buffer composition therefore reflects the degree of binding. In immobilized selection, affinity selectors are immobilized to capture or rapidly screen for affinity [217]. The high and reproducible separation efficiencies typical for CE ensure that interactions leading to even small changes in mobilities are sensitively detected [218].

The surfaces of NMs can be easily functionalized and modified with numerous molecules that might subsequently enter into interactions with other molecules of interest. In this case, CE can function in several ways: (i) monitoring the direct interaction between the NM and analyte (the signal is provided by both the analyte and NM), (ii) monitoring the interaction between two analytes mediated by the NM (the signal is provided by the analytes themselves, not by the NM), and (iii) monitoring the interaction between two analytes reported by a change in the signal of the NM.

For instance, a CE-LIF method for monitoring conjugation of proteins to magnetic nanoparticles was presented by Wang et al. in 2003 [219]. This method evaluated the interactions among bovine serum albumin, streptavidin, or goat anti-rabbit immunoglobulin G and magnetic nanoparticles with carboxylic or aminopropyltrimethoxysilane groups at their surface. Due to the fluorescent labeling of the conjugate, detection limits at the level of pg/nL were determined. Subsequently, CE methods that investigate the interactions of proteins with gold NPs [220], iron NPs [221], and silver NPs [222] have been published as well. These reports include measurements of binding constants and saturated binding

capacities as well as calculations of dissociation constants and cooperativity coefficients. The group of applications focused on protein–protein interactions in the presence of nanomaterials also can include analyses via nanoparticle-immobilized enzymes [223–225]. Interactions between nucleic acids and NMs have been used for various techniques, such as genotyping of human c-K-ras using a DNA-modified polystyrene nanoparticle suggested by Adachi et al. [226]. A microchip CE method for DNA separation using a gold nanoparticle as a tag also has been suggested [227]. Another example is determination of the encapsulation of an analyte (e.g., a drug) into a nanoparticle [203–205, 228–230]. In such cases, CE is able to quantify interactions, drug entrapment, and dissolution of pharmaceutical nanoparticles. The results suggest that the quantification of a drug located inside the nanoparticles is possible. Furthermore, interactions of NMs with biomarkers of serious diseases, including Alzheimer's disease [231], have been investigated using CE, as shown in a recent review by Sobrova et al. [232]. In the area of medicine, potential uses of CE for interactions between tumor-targeting nanoparticles and proteins have been explored [233] as well as the influence of heparin-functionalized poly(lactide-co-glycolide) nanoparticles on bone marrow stromal cells [234] and interaction of iron-regulating hormone hepcidin with molecularly imprinted nanoparticles [235].

An interesting group of studies that investigate interactions and conformational arrangements of molecules reports on a collection of methods based on fluorescence resonance energy transfer (FRET).

FRET is a non-radiative process in which an excited-state donor transfers energy to a proximal ground-state acceptor. The acceptor must absorb energy emitted by the donor [236]. FRET usually occurs when the distance between donor and acceptor is approximately 10–100 Å. Because this distance corresponds to the dimensions of most biological macromolecules, FRET could be used to measure such distances at the molecular level. The energy transfer rate $k_T(r)$ between a single donor–acceptor pair is dependent on the distance r between the donor and acceptor and can be expressed in terms of the Förster distance R_0 . Along this distance, 50% of the excited donor molecules decay by energy transfer, whereas the other half decay through other radiative or non-radiative means [236].

Due to their exceptional optical properties, selected nanoparticles constitute an excellent set of tools for FRET applications. QDs, in particular, can be used as tools for FRET-based steric conformation studies of biomolecules [237–239]. The binding interactions among multivalent ligands, polyhistidine peptide dendrimers (PHPD), and CdSe-ZnS QDs have been probed using CE. Cy5-labeled PHPD assembled on glutathione-capped QDs showed a higher FRET signal than that of the assembly between Cy5-labeled hexahistidine peptide and QDs. CE also revealed that PHPD outcompetes other QD-binding small molecules, peptides, and proteins in cell lysate [238]. The benefits of CE experiments lie in highly efficient separation of donor–acceptor immunocomplexes and detailed monitoring of the FRET process.

However, the direct effect of the analyte on the fluorescent properties of QDs in combination with changes in the electrophoretic mobility can also provide valuable information on their mutual interactions [240, 241] as well as the efficiency of the bioconjugation [242–244] or self-assembly characterization of QDs [245–249].

The interactions between QDs as fluorescent tags and their target molecules require detailed investigation to evaluate the labeling efficiency and suitability of a particular QD surface modification for a given bioconjugation reaction [47]. Traditionally, 1-ethyl-3-(3-dimethylaminopropyl) carbodiimide hydrochloride (EDC) and N-hydroxysulfosuccinimide (sulfo-NHS) are agents used to link QDs with proteins, antibodies, and enzymes [250]. The linkers are clearly important for bioconjugation. Liskova et al. [251] tested zero-length cross-linkers and long-chain linkers for the coupling of quantum dots with proteins using anti-ovalbumin, anti-proliferating cell nuclear antigen, anti-hemagglutinin, and anti-CD3 membrane protein as model antibodies and annexin V as high-specificity selectors. The conjugation method via carbonyldiimidazole cross-linkers was found to be a good alternative to the commonly used EDC/sulfo-NHS method. Further, the presented analysis of the protein conjugates with luminescent CdTe QDs demonstrated that homogeneity of the proteins and an unambiguous stoichiometry of the conjugates are essential prerequisites for highly efficient CE-LIF immunoassays, although no-linkers could allow QDs interact with proteins [252, 253]. In this case, it is necessary to determine the effect of such factors as the isoelectric points (pI) of bio-macromolecules and buffer pH on the bioconjugation of QDs. Bioconjugation of QDs can also be performed by simple electrostatic interaction, as reported in the work of Stanisavljevic et al. [140], demonstrated the conjugation of QDs to streptavidin and verified the functionality of such a complex by CE-LIF and CE-UV. An example of bioconjugation of biotin-modified QDs with avidin presented in the work of Ryvolova et al. [141] is illustrated in Fig. 5. Bioconjugation using protein G as a link between QD and immunoglobulins has also been suggested [254].

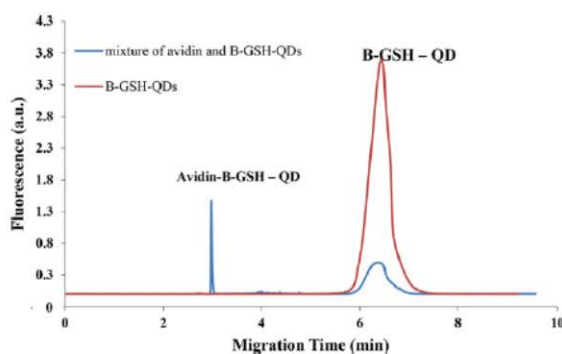


Figure 5. Electropherogram for a mixture of B-GSH-QDs and avidin solution. BGE: 20 mmol/L sodium borate buffer, pH 9.5; U: +20 kV; Injection: 0.5 psi for 20 s; LIF detection (488 nm/530 nm). Reprinted with permission from [141].

From a certain viewpoint, a large number of works focused on immune analysis using NMs should also be included in this section due to the specific interactions between antigens and antibodies that are monitored by CE. However, most studies of this type use NMs as tools for enhancing detection or for introducing such detectable properties as fluorescence or electroactivity into the system. For this reason, special attention is devoted to immunoanalyses in the second part of this review focused on the enhancement of electrophoretic performance.

4 Conclusion

The area of nanomaterials (e.g. nanoparticles, carbon nanomaterials, liposomes, and dendrimers) belongs to one of the most attractive and rapidly developing, whereas these materials possess often advantageous properties for numerous applications.

Their synthesis, however, presents problem especially in terms of batch-to-batch repeatability and in some cases, tools for characterization of nanomaterial composition and properties are missing. Even within a single batch, the polydispersity of the particles and the variability of their properties may present insurmountable problem for reliable application. We believe that once these obstacles are overcome, nanomaterials will reach completely new dimensions in terms of number of their applications.

It is not surprising that many methods and procedures how to synthesize and characterize the nanoparticles have been developed. From the wide of group of methods, capillary electrophoresis has its unreplaceable position due to many advantages discussed above enabling us to use this easy to use and low cost technique in various modes for studying nanoparticles parameters, such as their size, surface chemistry, and interaction abilities. Based on the published results it can be concluded that electromigration techniques, in general, represent a group of effective techniques for nanomaterial characterization, evaluation, and observation (Fig. 6). The future directions could be seen in manufacturing of hand-held CE based analyzers for in situ and immediate characterizing of the nanomaterial as well as incorporating of CE into some industrial machines for high throughput producing of nanomaterials as quality control.

On the other hand, the nanoparticles and nanomaterials of various kinds can also be used to improve significantly the performance of CE in terms of both detection sensitivity as well as separation efficiency. This field is covered in the second part of this article

Financial support was provided by Grant agency of Czech Republic (GACR 16–23647Y) and project CEITEC 2020 (LQ1601) with financial support from the Ministry of Education, Youth and Sports of the Czech Republic under the National Sustainability Programme II.

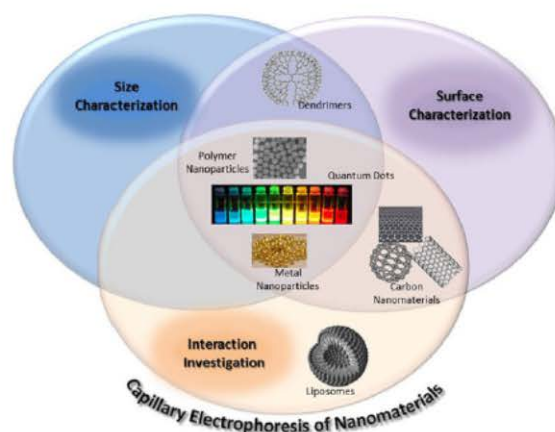


Figure 6. Schematic classification of nanomaterials according to properties characterized by CE.

The authors have declared no conflict of interest.

5 References

- [1] Tiselius, A., *Trans. Faraday Soc.* 1937, 33, 524–531.
- [2] Hjerten, S., *Chromatogr. Rev.* 1967, 9, 122–219.
- [3] Jorgenson, J. W., Lukacs, K. D., *Anal. Chem.* 1981, 53, 1298–1302.
- [4] Haddad, P. R., Doble, P., Macka, M., *J. Chromatogr. A* 1999, 856, 145–177.
- [5] Macka, M., Haddad, P. R., *Electrophoresis* 1997, 18, 2482–2501.
- [6] Timerbaev, A. R., *Electrophoresis* 2002, 23, 3884–3906.
- [7] Timerbaev, A. R., *Electrophoresis* 2004, 25, 4008–4031.
- [8] Timerbaev, A. R., Shpigun, O. A., *Electrophoresis* 2000, 21, 4179–4191.
- [9] Soga, T., Ross, G. A., *J. Chromatogr. A* 1999, 837, 231–239.
- [10] Soga, T., Imaizumi, M., *Electrophoresis* 2001, 22, 3418–3425.
- [11] DeBacker, B. L., Nagels, L. J., *Anal. Chem.* 1996, 68, 4441–4445.
- [12] Dolnik, V., *Electrophoresis* 2008, 29, 143–156.
- [13] Haselberg, R., de Jong, G. J., Somsen, G. W., *J. Chromatogr. A* 2007, 1159, 81–109.
- [14] Huang, Y. F., Huang, C. C., Hu, C. C., Chang, H. T., *Electrophoresis* 2006, 27, 3503–3522.
- [15] Kleparnik, K., Bocek, P., *Chem. Rev.* 2007, 107, 5279–5317.
- [16] Heller, C., *Electrophoresis* 2001, 22, 629–643.
- [17] Righetti, P. G., Gelfi, C., D'Acunto, M. R., *Electrophoresis* 2002, 23, 1361–1374.
- [18] Ruizmartinez, M. C., Berka, J., Belenkii, A., Foret, F., Miller, A. W., Karger, B. L., *Anal. Chem.* 1993, 65, 2851–2858.
- [19] Swerdlow, H., Wu, S., Harke, H., Dovichi, N. J., *J. Chromatogr.* 1990, 516, 61–67.

- [20] Venter, J. C., Adams, M. D., Myers, E. W., Li, P. W., Mural, R. J., Sutton, G. G., Smith, H. O., Yandell, M., Evans, C. A., Holt, R. A., Gocayne, J. D., Amanatides, P., Ballew, R. M., Huson, D. H., Wortman, J. R., Zhang, Q., Kodira, C. D., Zheng, X. Q. H., Chen, L., Skupski, M., Subramanian, G., Thomas, P. D., Zhang, J. H., Miklos, G. L. G., Nelson, C., Broder, S., Clark, A. G., Nadeau, C., McKusick, V. A., Zinder, N., Levine, A. J., Roberts, R. J., Simon, M., Slayman, C., Hunkapiller, M., Bolanos, R., Delcher, A., Dew, I., Fasulo, D., Flanigan, M., Florea, L., Halpern, A., Hannenhalli, S., Kravitz, S., Levy, S., Mobarry, C., Reinert, K., Remington, K., Abu-Threideh, J., Beasley, E., Biddick, K., Bonazzi, V., Brandon, R., Cargill, M., Chandramouliswaran, I., Charlab, R., Chaturvedi, K., Deng, Z. M., Di Francesco, V., Dunn, P., Eilbeck, K., Evangelista, C., Gabrielian, A. E., Gan, W., Ge, W. M., Gong, F. C., Gu, Z. P., Guan, P., Heiman, T. J., Higgins, M. E., Ji, R. R., Ke, Z. X., Ketchum, K. A., Lai, Z. W., Lei, Y. D., Li, Z. Y., Li, J. Y., Liang, Y., Lin, X. Y., Lu, F., Merkulov, G. V., Milshina, N., Moore, H. M., Naik, A. K., Narayan, V. A., Neelam, B., Nusskern, D., Rusch, D. B., Salzberg, S., Shao, W., Shue, B. X., Sun, J. T., Wang, Z. Y., Wang, A. H., Wang, X., Wang, J., Wei, M. H., Wides, R., Xiao, C. L., Yan, C. H., Yao, A., Ye, J., Zhan, M., Zhang, W. Q., Zhang, H. Y., Zhao, Q., Zheng, L. S., Zhong, F., Zhong, W. Y., Zhu, S. P. C., Zhao, S. Y., Gilbert, D., Baumhueter, S., Spier, G., Carter, C., Cravchik, A., Woodage, T., Ali, F., An, H. J., Awe, A., Baldwin, D., Baden, H., Barnstead, M., Barrow, I., Beeson, K., Busam, D., Carver, A., Center, A., Cheng, M. L., Curry, L., Danaher, S., Davenport, L., Desilets, R., Dietz, S., Dodson, K., Doup, L., Ferrera, S., Garg, N., Gluecksmann, A., Hart, B., Haynes, J., Haynes, C., Heiner, C., Hladun, S., Hostin, D., Houck, J., Howland, T., Ibegwam, C., Johnson, J., Kalush, F., Kline, L., Koduru, S., Love, A., Mann, F., May, D., McCawley, S., McIntosh, T., McMullen, I., Moy, M., Moy, L., Murphy, B., Nelson, K., Pfannkoch, C., Pratts, E., Puri, V., Qureshi, H., Reardon, M., Rodriguez, R., Rogers, Y. H., Romblad, D., Ruhfel, B., Scott, R., Sitter, C., Smallwood, M., Stewart, E., Strong, R., Suh, E., Thomas, R., Tint, N. N., Tse, S., Vech, C., Wang, G., Wetter, J., Williams, S., Williams, M., Windsor, S., Winn-Deen, E., Wolfe, K., Zaveri, J., Zaveri, K., Abril, J. F., Guigo, R., Campbell, M. J., Sjolander, K. V., Karlak, B., Kejariwal, A., Mi, H. Y., Lazareva, B., Hatton, T., Narechania, A., Diemer, K., Muruganujan, A., Guo, N., Sato, S., Bafna, V., Istrail, S., Lipert, R., Schwartz, R., Walenz, B., Yooshep, S., Allen, D., Basu, A., Baxendale, J., Blick, L., Caminha, M., Carnes-Stine, J., Caulk, P., Chiang, Y. H., Coyne, M., Dahlke, C., Mays, A. D., Dombroski, M., Donnelly, M., Ely, D., Esparham, S., Fosler, C., Gire, H., Glanowski, S., Glasser, K., Glodek, A., Gorokhov, M., Graham, K., Gropman, B., Harris, M., Heil, J., Henderson, S., Hoover, J., Jennings, D., Jordan, C., Jordan, J., Kasha, J., Kagan, L., Kraft, C., Levitsky, A., Lewis, M., Liu, X. J., Lopez, J., Ma, D., Majoros, W., McDaniel, J., Murphy, S., Newman, M., Nguyen, T., Nguyen, N., Nodell, M., Pan, S., Peck, J., Peterson, M., Rowe, W., Sanders, R., Scott, J., Simpson, M., Smith, T., Sprague, A., Stockwell, T., Turner, R., Venter, E., Wang, M., Wen, M. Y., Wu, D., Wu, M., Xia, A., Zandieh, A., Zhu, X. H., *Science* 2001, 291, 1304–1351.
- [21] Manz, A., Graber, N., Widmer, H. M., *Sens. Actuator B-Chem.* 1990, 1, 244–248.
- [22] Terry, S. C., Jerman, J. H., Angell, J. B., *IEEE Trans. Electron Devices* 1979, 26, 1880–1886.
- [23] Dolnik, V., Liu, S. R., Jovanovich, S., *Electrophoresis* 2000, 21, 41–54.
- [24] Breadmore, M. C., *J. Chromatogr. A* 2012, 1221, 42–55.
- [25] Dolnik, V., Liu, S. R., *J. Sep. Sci.* 2005, 28, 1994–2009.
- [26] Li, S. F. Y., Kricka, L. J., *Clin. Chem.* 2006, 52, 37–45.
- [27] Osbourn, D. M., Weiss, D. J., Lunte, C. E., *Electrophoresis* 2000, 21, 2768–2779.
- [28] European Commission, 2015 http://ec.europa.eu/environment/chemicals/nanotech/faq/definition_en.htm.
- [29] Armstrong, J. K., Wenby, R. B., Meiselman, H. J., Fisher, T. C., *Biophys. J.* 2004, 87, 4259–4270.
- [30] Buzea, C., Pacheco, I., Robbie, K., *Biointerphases* 2007, 2, MR17–MR71.
- [31] Alivisatos, A. P., *Science* 1996, 271, 933–937.
- [32] Shenderova, O. A., Zhimov, V. V., Brenner, D. W., *Crit. Rev. Solid State Mat. Sci.* 2002, 27, 227–356.
- [33] Guldi, D. M., Rahman, A., Sgobba, V., Ehli, C., *Chem. Soc. Rev.* 2006, 35, 471–487.
- [34] Paul, D. R., Robeson, L. M., *Polymer* 2008, 49, 3187–3204.
- [35] Balazs, A. C., Emrick, T., Russell, T. P., *Science* 2006, 314, 1107–1110.
- [36] Hanauer, M., Pierrat, S., Zins, I., Lotz, A., Sonnichsen, C., *Nano Lett.* 2007, 7, 2881–2885.
- [37] Surugau, N., Urban, P. L., *J. Sep. Sci.* 2009, 32, 1889–1906.
- [38] Pyell, U., *Electrophoresis* 2010, 31, 814–831.
- [39] Ivanov, M. R., Haes, A. J., *Analyst* 2011, 136, 54–63.
- [40] Rodriguez, M. A., Armstrong, D. W., *J. Chromatogr. B* 2004, 800, 7–25.
- [41] Lopez-Lorente, A. I., Simonet, B. M., Valcarcel, M., *Trac-Trends Anal. Chem.* 2011, 30, 58–71.
- [42] Ban, E., Yoo, Y. S., Song, E. J., *Talanta* 2015, 141, 15–20.
- [43] Mebert, A. M., Tuttolomondo, M. V., Echazu, M. I. A., Foglia, M. L., Alvarez, G. S., Vescina, M. C., Santo-Orihuela, P. L., Desimone, M. F., *Electrophoresis* 2016, 37, 2196–2207.
- [44] Shi, X. Y., Banyai, I., Lesniak, W. G., Islam, M. T., Orszagh, I., Balogh, P., Baker, J. R., Balogh, L. P., *Electrophoresis* 2005, 26, 2949–2959.
- [45] Liu, F. K., *J. Chromatogr. A* 2009, 1216, 9034–9047.
- [46] Wu, C. S., Liu, F. K., Ko, F. H., *Anal. Bioanal. Chem.* 2011, 399, 103–118.
- [47] Sang, F. M., Huang, X. Y., Ren, J. C., *Electrophoresis* 2014, 35, 793–803.
- [48] Stanisavljevic, M., Vaculovicova, M., Kizek, R., Adam, V., *Electrophoresis* 2014, 35, 1929–1937.
- [49] Stewart, D. T. R., Celiz, M. D., Vicente, G., Colon, L. A., Aga, D. S., *Trac-Trends Anal. Chem.* 2011, 30, 113–122.
- [50] Li, Y. Q., Wang, H. Q., Wang, J. H., Guan, L. Y., Liu, B. F., Zhao, Y. D., Chen, H., *Anal. Chim. Acta* 2009, 647, 219–225.
- [51] Ohshima, H., *J. Colloid Interface Sci.* 2001, 239, 587–590.

- [52] Duffy, E., Mitev, D. P., Nesterenko, P. N., Kazarian, A. A., Paull, B., *Electrophoresis* 2014, *35*, 1864–1872.
- [53] Tekrony, A., Cramb, D., *Can. J. Chem.* 2016, *94*, 430–435.
- [54] Voracova, I., Kleparnik, K., Liskova, M., Foret, F., *Electrophoresis* 2015, *36*, 867–874.
- [55] Fichtner, A., Jalil, A., Pyell, U., *Langmuir* 2017, *33*, 2325–2339.
- [56] Pyell, U., Jalil, A. H., Pfeiffer, C., Pelaz, B., Parak, W. J., *J. Colloid Interface Sci.* 2015, *450*, 288–300.
- [57] Pyell, U., Jalil, A. H., Urban, D. A., Pfeiffer, C., Pelaz, B., Parak, W. J., *J. Colloid Interface Sci.* 2015, *457*, 131–140.
- [58] Qu, H., Linder, S. W., Mudalige, T. K., *Anal. Bioanal. Chem.* 2017, *409*, 979–988.
- [59] Vanorman, B. B., McIntire, G. L., *Abstr. Pap. Am. Chem. Soc.* 1990, *199*, 113–IAEC.
- [60] Vanorman, B. B., McIntire, G. L., *Am. Lab.* 1990, *22*, 66–67.
- [61] McCormick, R. M., *J. Liq. Chromatogr.* 1991, *14*, 939–952.
- [62] Hwang, W. M., Lee, C. Y., Boo, D. W., Choi, J. G., *Bull. Korean Chem. Soc.* 2003, *24*, 684–686.
- [63] Yang, Y., Mu, J., Jiang, L., *Chin. Sci. Bull.* 2005, *50*, 1591–1594.
- [64] Lo, C. K., Paa, M. C., Xiao, D., Choi, M. M. F., *Anal. Chem.* 2008, *80*, 2439–2446.
- [65] Du, K., Ma, H. L., Muralidharan, S., *Abstr. Pap. Am. Chem. Soc.* 2006, *231*.
- [66] Vanifatova, N. G., Spivakov, B. Y., Mattusch, J., Wennrich, R., *Talanta* 2003, *59*, 345–353.
- [67] Eckhoff, D. A., Stuart, J. N., Sutin, J. D. B., Sweedler, J. V., Gratton, E., *J. Chem. Phys.* 2006, *125*, 081103.
- [68] Petersen, S. L., Ballou, N. E., *Anal. Chem.* 1992, *64*, 1676–1681.
- [69] Radko, S. P., Stastna, M., Chrmbach, A., *Electrophoresis* 2000, *21*, 3583–3592.
- [70] Ducatte, G. R., Ballou, N. E., Quang, C. Y., Petersen, S. L., *J. Microcolumn Sep.* 1996, *8*, 403–412.
- [71] Quang, C., Petersen, S. L., Ducatte, G. R., Ballou, N. E., *J. Chromatogr. A* 1996, *732*, 377–384.
- [72] Wei, G. T., Wang, C. R. C., Liu, F. K., Chang, S. S., *J. Chin. Chem. Soc.* 1998, *45*, 47–52.
- [73] Vanifatova, N. G., Spivakov, B. Y., Mattusch, J., Wennrich, R., *J. Chromatogr. A* 2000, *898*, 257–263.
- [74] Duffy, C. F., McEathron, A. A., Arriaga, E. A., *Electrophoresis* 2002, *23*, 2040–2047.
- [75] Schnabel, U., Fischer, C. H., Kennidler, E., *J. Microcolumn Sep.* 1997, *9*, 529–534.
- [76] Ivanov, M. R., Bednar, H. R., Haes, A. J., *ACS Nano* 2009, *3*, 386–394.
- [77] Turkevich, J., Stevenson, P. C., Hillier, J., *Dis. Farad. Soc.* 1951, *11*, 55–75.
- [78] Murphy, C. J., San, T. K., Gole, A. M., Orendorff, C. J., Gao, J. X., Gou, L., Hunyadi, S. E., Li, T., *J. Phys. Chem. B* 2005, *109*, 13857–13870.
- [79] Daniel, M. C., Astruc, D., *Chem. Rev.* 2004, *104*, 293–346.
- [80] Pileni, M. P., *Nat. Mater.* 2003, *2*, 145–150.
- [81] Scott, R. W. J., Wilson, O. M., Crooks, R. M., *J. Phys. Chem. B* 2005, *109*, 692–704.
- [82] Sharma, V. K., Yngard, R. A., Lin, Y., *Adv. Colloid Interface Sci.* 2009, *145*, 83–96.
- [83] Peng, Z. M., Yang, H., *Nano Today* 2009, *4*, 143–164.
- [84] Ahmadi, T. S., Wang, Z. L., Green, T. C., Henglein, A., ElSayed, M. A., *Science* 1996, *272*, 1924–1926.
- [85] Cheong, S. S., Watt, J. D., Tilley, R. D., *Nanoscale* 2010, *2*, 2045–2053.
- [86] Kim, S. W., Park, J., Jang, Y., Chung, Y., Hwang, S., Hyeon, T., Kim, Y. W., *Nano Lett.* 2003, *3*, 1289–1291.
- [87] Teranishi, T., Miyake, M., *Chem. Mat.* 1998, *10*, 594–600.
- [88] Hoefelmeyer, J. D., Niesz, K., Somorjai, G. A., Tilley, T. D., *Nano Lett.* 2005, *5*, 435–438.
- [89] Mu, X. D., Meng, J. Q., Li, Z. C., Kou, Y., *J. Am. Chem. Soc.* 2005, *127*, 9694–9695.
- [90] Kramer, J., Redel, E., Thomann, R., Janiak, C., *Organometallics* 2008, *27*, 1976–1978.
- [91] Li, C. X., Leong, W. K., Zhong, Z. Y., *J. Organomet. Chem.* 2009, *694*, 2315–2318.
- [92] Reetz, M. T., Lopez, M., Grunert, W., Vogel, W., Mahlendorf, F., *J. Phys. Chem. B* 2003, *107*, 7414–7419.
- [93] Liu, F. K., Wei, G. T., *Anal. Chim. Acta* 2004, *510*, 77–83.
- [94] Liu, F. K., Ko, F. H., Huang, P. W., Wu, C. H., Chu, T. C., *J. Chromatogr. A* 2005, *1062*, 139–145.
- [95] Liu, F. K., Ko, F. H., *Chem. Lett.* 2004, *33*, 902–903.
- [96] Liu, F. K., Tsai, M. H., Hsu, Y. C., Chu, T. C., *J. Chromatogr. A* 2006, *1133*, 340–346.
- [97] Liu, F. K., Lin, Y. Y., Wu, C. H., *Anal. Chim. Acta* 2005, *528*, 249–254.
- [98] Lin, K. H., Chu, T. C., Liu, F. K., *J. Chromatogr. A* 2007, *1167*, 314–321.
- [99] Liu, F. K., *J. Chromatogr. A* 2007, *1167*, 231–235.
- [100] Liu, F. K., *Anal. Chim. Acta* 2011, *694*, 167–173.
- [101] Qu, H. O., Mudalige, T. K., Linder, S. W., *Anal. Chem.* 2014, *86*, 11620–11627.
- [102] Pallotta, A., Boudier, A., Leroy, P., Clarot, I., *J. Chromatogr. A* 2016, *1461*, 179–184.
- [103] Matczuk, M., Aleksenko, S. S., Matysik, F. M., Jarosz, M., Timerbaev, A. R., *Electrophoresis* 2015, *36*, 1158–1163.
- [104] Franze, B., Engelhard, C., *Anal. Chem.* 2014, *86*, 5713–5720.
- [105] Qu, H. O., Mudalige, T. K., Linder, S. W., *J. Chromatogr. A* 2016, *1429*, 348–353.
- [106] Baharifar, H., Fakhari, A. R., Ziyadi, H., Oghabian, M. A., Amani, A., Faridi-Majidi, R., *J. Iran Chem. Soc.* 2014, *11*, 279–284.
- [107] d’Orlye, F., Varenne, A., Gareil, P., *Electrophoresis* 2008, *29*, 3768–3778.
- [108] Vanifatova, N. G., Spivakov, B. Y., Mattusch, J., Franck, U., Wennrich, R., *Talanta* 2005, *66*, 605–610.
- [109] d’Orlye, F., Varenne, A., Gareil, P., *J. Chromatogr. A* 2008, *1204*, 226–232.
- [110] Petr, J., Teste, B., Descroix, S., Siaugue, J. M., Gareil, P., Varenne, A., *Electrophoresis* 2010, *31*, 2754–2761.

- [111] d'Orlye, F., Varenne, A., Georgelin, T., Siaugue, J. M., Teste, B., Descroix, S., Gareil, P., *Electrophoresis* 2009, **30**, 2572–2582.
- [112] Lopez-Leon, T., Carvalho, E. L. S., Seijo, B., Ortega-Vinuesa, J. L., Bastos-Gonzalez, D., *J. Colloid Interface Sci.* 2005, **283**, 344–351.
- [113] Sarkar, S., Guibal, E., Quignard, F., SenGupta, A. K., *J. Nanopart. Res.* 2012, **14**, 1–24.
- [114] Zitka, O., Sobrova, P., Adam, V., Hubalek, J., Provaznik, I., Zizkova, V., Kizek, R., *Chem. Listy* 2013, **107**, 24–29.
- [115] Abdel-Haq, H., Bossu, E., *J. Chromatogr. A* 2012, **1257**, 125–130.
- [116] Sakakibara, A., Kitagawa, S., Tsuda, T., *Electrophoresis* 2004, **25**, 1817–1822.
- [117] Ermolina, I., Morgan, H., *J. Colloid Interface Sci.* 2005, **285**, 419–428.
- [118] Kobayashi, M., *Colloid Polym. Sci.* 2008, **286**, 935–940.
- [119] Chassagne, C., Ibanez, M., *Pure Appl. Chem.* 2013, **85**, 41–51.
- [120] Chassagne, C., Ibanez, M., *Colloid Surf. A-Physicochem. Eng. Asp.* 2014, **440**, 208–216.
- [121] Kobayashi, M., Sasaki, A., *Colloid Surf. A-Physicochem. Eng. Asp.* 2014, **440**, 74–78.
- [122] Adelantado, C., Rodriguez-Farinas, N., Martin-Doimeadios, R. C. R., Zougagh, M., Rios, A., *Anal. Chim. Acta* 2016, **923**, 82–88.
- [123] Riley, K. R., Liu, S., Yu, G., Libby, K., Cubicciotti, R., Colyer, C. L., *J. Chromatogr. A* 2016, **1463**, 169–175.
- [124] Medintz, I. L., Uyeda, H. T., Goldman, E. R., Mattoussi, H., *Nat. Mater.* 2005, **4**, 435–446.
- [125] Michalet, X., Pinaud, F. F., Bentolila, L. A., Tsay, J. M., Doose, S., Li, J. J., Sundaresan, G., Wu, A. M., Gambhir, S. S., Weiss, S., *Science* 2005, **307**, 538–544.
- [126] Geszke-Moritz, M., Moritz, M., *Mater. Sci. Eng. C-Mater. Biol. Appl.* 2013, **33**, 1008–1021.
- [127] Valizadeh, A., Mikaeili, H., Samiei, M., Farkhani, S. M., Zarghami, N., Kouhi, M., Akbarzadeh, A., Davaran, S., *Nanoscale Res. Lett.* 2012, **7**, 1–14.
- [128] Drbohlavova, J., Adam, V., Kizek, R., Hubalek, J., *Int. J. Mol. Sci.* 2009, **10**, 656–673.
- [129] Morris-Cohen, A. J., Malicki, M., Peterson, M. D., Slavin, J. W. J., Weiss, E. A., *Chem. Mat.* 2013, **25**, 1155–1165.
- [130] Kadkhodazadeh, S., *Micron* 2013, **44**, 75–92.
- [131] Riley, E. A., Hess, C. M., Reid, P. J., *Int. J. Mol. Sci.* 2012, **13**, 12487–12518.
- [132] Petryayeva, E., Algar, W. R., Medintz, I. L., *Appl. Spectrosc.* 2013, **67**, 215–252.
- [133] Wang, Y. C., Hu, R., Lin, G. M., Roy, I., Yong, K. T., *ACS Appl. Mater. Interfaces* 2013, **5**, 2786–2799.
- [134] Song, X. T., Li, L., Chan, H. F., Fang, N. H., Ren, J. C., *Electrophoresis* 2006, **27**, 1341–1346.
- [135] Clarot, I., Wolpert, C., Morosini, V., Schneider, R., Balan, L., Diez, L., Leroy, P., *Curr. Nanosci.* 2009, **5**, 154–159.
- [136] Pereira, M., Lai, E. P. C., Hollebone, B., *Electrophoresis* 2007, **28**, 2874–2881.
- [137] Carrillo-Carrion, C., Moliner-Martinez, Y., Simonet, B. M., Valcarcel, M., *Anal. Chem.* 2011, **83**, 2807–2813.
- [138] Oszwaldowski, S., Zawistowska-Gibula, K., Roberts, K. P., *Anal. Bioanal. Chem.* 2011, **399**, 2831–2842.
- [139] Oszwaldowski, S., Zawistowska-Gibula, K., Roberts, K. P., *Cent. Eur. J. Chem* 2011, **9**, 572–584.
- [140] Stanisavljevic, M., Janu, L., Smerkova, K., Krizkova, S., Pizurova, N., Ryvolova, M., Adam, V., Hubalek, J., Kizek, R., *Chromatographia* 2013, **76**, 335–343.
- [141] Ryvolova, M., Chomoucka, J., Janu, L., Drbohlavova, J., Adam, V., Hubalek, J., Kizek, R., *Electrophoresis* 2011, **32**, 1619–1622.
- [142] Geim, A. K., Novoselov, K. S., *Nat. Mater.* 2007, **6**, 183–191.
- [143] Muller, M. B., Quirino, J. P., Nesterenko, P. N., Haddad, P. R., Gambhir, S., Li, D., Wallace, G. G., *J. Chromatogr. A* 2010, **1217**, 7593–7597.
- [144] Zhao, J. J., Chen, G. F., Zhang, W., Li, P., Wang, L., Yue, Q. L., Wang, H. S., Dong, R. X., Yan, X. L., Liu, J. F., *Anal. Chem.* 2011, **83**, 9100–9106.
- [145] Buhl, M., Hirsch, A., *Chem. Rev.* 2001, **101**, 1153–1183.
- [146] Bakry, R., Vallant, R. M., Najam-UI-Haq, M., Rainer, M., Szabo, Z., Huck, C. W., Bonn, G. K., *Int. J. Nanomed.* 2007, **2**, 639–649.
- [147] Iijima, S., *Nature* 1991, **354**, 56–58.
- [148] Yang, W. R., Ratinac, K. R., Ringer, S. P., Thordarson, P., Gooding, J. J., Braet, F., *Angew. Chem.-Int. Edit.* 2010, **49**, 2114–2138.
- [149] Lim, S. Y., Shen, W., Gao, Z. Q., *Chem. Soc. Rev.* 2015, **44**, 362–381.
- [150] Doorn, S. K., Strano, M. S., O'Connell, M. J., Haroz, E. H., Rialon, K. L., Hauge, R. H., Smalley, R. E., *J. Phys. Chem. B* 2003, **107**, 6063–6069.
- [151] Yamamoto, T., Murakami, Y., Motoyanagi, J., Fukushima, T., Maruyama, S., Kato, M., *Anal. Chem.* 2009, **81**, 7336–7341.
- [152] Doorn, S. K., Fields, R. E., Hu, H., Hamon, M. A., Haddon, R. C., Selegue, J. P., Majidi, V., *J. Am. Chem. Soc.* 2002, **124**, 3169–3174.
- [153] Suarez, B., Simonet, B. M., Cardenas, S., Valcarcel, M., *J. Chromatogr. A* 2006, **1128**, 282–289.
- [154] Lopez-Pastor, M., Dominguez-Vidal, A., Ayora-Canada, M. J., Simonet, B. M., Lendl, B., Valcarcel, M., *Anal. Chem.* 2008, **80**, 2672–2679.
- [155] Xiao, H., Zou, H. F., Pan, C. S., Jiang, X. G., Le, X. C., Yang, L., *Anal. Chim. Acta* 2006, **580**, 194–199.
- [156] Xiao, H., Yang, L. S., Zou, H. F., Yang, L., Le, X. C., *Anal. Bioanal. Chem.* 2007, **387**, 119–126.
- [157] Du, A. W., Stenzel, M. H., *Biomacromolecules* 2014, **15**, 1097–1114.
- [158] Lohcharoenkal, W., Wang, L. Y., Chen, Y. C., Rojanasakul, Y., *Biomed Res. Int.* 2014, **2013**, 1–12.
- [159] Twibanire, J. D. K., Grindley, T. B., *Polymers* 2014, **6**, 179–213.
- [160] Hamidi, M., Shahbazi, M. A., Rostamizadeh, K., *Macromol. Biosci.* 2012, **12**, 144–164.
- [161] Srinivas, R., Samanta, S., Chaudhuri, A., *Chem. Soc. Rev.* 2009, **38**, 3326–3338.
- [162] Khripin, C. Y., Manohar, S., Zheng, M., Jagota, A., *J. Phys. Chem. C* 2009, **113**, 13616–13621.

- [163] Su, H. L., Kao, W. C., Lee, C. Y., Chuang, S. C., Hsieh, Y. Z., *J. Chromatogr. A* 2010, **1217**, 4471–4475.
- [164] Astefanei, A., Nunez, O., Galceran, M. T., *Anal. Bioanal. Chem.* 2012, **404**, 307–313.
- [165] Wu, Y. Y., Remcho, V. T., *Talanta* 2016, **161**, 854–859.
- [166] Liu, M. J., Frechet, J. M. J., *Pharm. Sci. Technol. Today* 1999, **2**, 393–401.
- [167] Gillies, E. R., Frechet, J. M. J., *Drug Discov. Today* 2005, **10**, 35–43.
- [168] Dufes, C., Uchegbu, I. F., Schatzlein, A. G., *Adv. Drug Deliv. Rev.* 2005, **57**, 2177–2202.
- [169] Gao, Y., Gao, G., He, Y., Liu, T. L., Qi, R., *Mini-Rev. Med. Chem.* 2008, **8**, 889–900.
- [170] Astruc, D., Chardac, F., *Chem. Rev.* 2001, **101**, 2991–3023.
- [171] Reek, J. N. H., Arevalo, S., Van Heerbeek, R., Kamer, P. C. J., Van Leeuwen, P., *Adv. Catal.* 2006, **49**, 71–151.
- [172] Ghobril, C., Lamanna, G., Kueny-Stotz, M., Garofalo, A., Billotey, C., Felder-Flesch, D., *New J. Chem.* 2012, **36**, 310–323.
- [173] Menjoge, A. R., Kannan, R. M., Tomalia, D. A., *Drug Discov. Today* 2010, **15**, 171–185.
- [174] Mintzer, M. A., Grinstaff, M. W., *Chem. Soc. Rev.* 2011, **40**, 173–190.
- [175] Stockigt, D., Lohmer, G., Belder, D., *Rapid Commun. Mass Spectrom.* 1996, **10**, 521–526.
- [176] Ebber, A., Vaher, M., Peterson, J., Lopp, M., *J. Chromatogr. A* 2002, **949**, 351–358.
- [177] Shi, X. Y., Orszagh, I., Baker, J. R., Balogh, L., *Abstr. Pap. Am. Chem. Soc.* 2003, **226**, U114–U114.
- [178] Sedlakova, P., Svobodova, J., Miksik, I., Tomas, H., *J. Chromatogr. B* 2006, **841**, 135–139.
- [179] Leriche, E. D., Maire, F., Gossel, M. C., Lange, C. M., Loutelier-Bourhis, C., *Rapid Commun. Mass Spectrom.* 2012, **26**, 1718–1724.
- [180] Shi, X. Y., Majoros, I. J., Patri, A. K., Bi, X. D., Islam, M. T., Desai, A., Ganser, T. R., Baker, J. R., *Analyst* 2006, **131**, 374–381.
- [181] Lalwani, S., Venditto, V. J., Chouai, A., Rivera, G. E., Shaunak, S., Simanek, E. E., *Macromolecules* 2009, **42**, 3152–3161.
- [182] Vetterlein, K., Buche, K., Hildebrand, M., Scriba, G. K. E., Lehmann, J., *Electrophoresis* 2006, **27**, 2400–2412.
- [183] Shi, X. Y., Patri, A. K., Lesniak, W., Islam, M. T., Zhang, C. X., Baker, J. R., Balogh, L. P., *Electrophoresis* 2005, **26**, 2960–2967.
- [184] Shi, X. Y., Majoros, I. J., Baker, J. R., *Mol. Pharm.* 2005, **2**, 278–294.
- [185] Mosca, M., Ceglie, A., Ambrosone, L., *Chem. Phys. Lipids* 2011, **164**, 158–165.
- [186] Hauska, G. A., Prince, R. C., *FEBS Lett.* 1974, **41**, 35–39.
- [187] Rigaud, J. L., Levy, D., *Methods Enzymol* 2003, **372**, 65–86.
- [188] Drummond, D. C., Meyer, O., Hong, K. L., Kirpotin, D. B., Papahadjopoulos, D., *Pharmacol. Rev.* 1999, **51**, 691–743.
- [189] Koltover, I., Salditt, T., Radler, J. O., Safinya, C. R., *Science* 1998, **281**, 78–81.
- [190] Marques, E. F., Regev, O., Khan, A., Miguel, M. D., Lindman, B., *J. Phys. Chem. B* 1998, **102**, 6746–6758.
- [191] Roberts, M. A., LocascioBrown, L., MacCrehan, W. A., Durst, R. A., *Anal. Chem.* 1996, **68**, 3434–3440.
- [192] Tsukagoshi, K., Akasaka, H., Nakajima, R., Hara, T., *Chem. Lett.* 1996, **6**, 467–468.
- [193] Tsukagoshi, K., Okumura, Y., Nakajima, R., *J. Chromatogr. A* 1998, **813**, 402–407.
- [194] Duffy, C. F., Gafoor, S., Richards, D. P., Admadzadeh, H., O’Kennedy, R., Arriaga, E. A., *Anal. Chem.* 2001, **73**, 1855–1861.
- [195] Kawakami, K., Nishihara, Y., Hirano, K., *J. Colloid Interface Sci.* 1998, **206**, 177–180.
- [196] Radko, S. P., Stastna, M., Chrmbach, A., *Anal. Chem.* 2000, **72**, 5955–5960.
- [197] Radko, S. P., Stastna, M., Chrmbach, A., *J. Chromatogr. B* 2001, **761**, 69–75.
- [198] Wiedmer, S. K., Hautala, J., Holopainen, J. M., Kinnunen, P. K. J., Riekkola, M. L., *Electrophoresis* 2001, **22**, 1305–1313.
- [199] Flor, S., Estevez, P., Tripodi, V., Julia Legaspi, M., Mammarella, C., Lucangioli, S., *Curr. Anal. Chem.* 2014, **10**, 241–247.
- [200] Griese, N., Blaschke, G., Boos, J., Hempel, G., *J. Chromatogr. A* 2002, **979**, 379–388.
- [201] Perjesi, P., Kim, T., Zharikova, A. D., Li, X. X., Ramesh, T., Ramasubbu, J., Prokai, L., *J. Pharm. Biomed. Anal.* 2003, **31**, 929–935.
- [202] Quaglia, M. G., Barbato, F., Fanali, S., Santucci, E., Donati, E., Carafa, M., Marianecchi, C., *J. Pharm. Biomed. Anal.* 2005, **37**, 73–79.
- [203] Ostergaard, J., Jorgensen, L., Thomsen, A. E., Larsen, S. W., Larsen, C., Jensen, H., *Electrophoresis* 2008, **29**, 3320–3324.
- [204] Franzen, U., Jorgensen, L., Larsen, C., Heegaard, N. H. H., Ostergaard, J., *Electrophoresis* 2009, **30**, 2711–2719.
- [205] Franzen, U., Nguyen, T., Vermehren, C., Gammelgaard, B., Ostergaard, J., *J. Pharm. Biomed. Anal.* 2011, **55**, 16–22.
- [206] Franzen, U., Vermehren, C., Jensen, H., Ostergaard, J., *Electrophoresis* 2011, **32**, 738–748.
- [207] Kim, H. S., Wainer, I. W., *J. Pharm. Biomed. Anal.* 2010, **52**, 372–376.
- [208] Nguyen, T., Ostergaard, J., Sturup, S., Gammelgaard, B., *Anal. Bioanal. Chem.* 2012, **402**, 2131–2139.
- [209] Franzen, U., Ostergaard, J., *J. Chromatogr. A* 2012, **1267**, 32–44.
- [210] McKeon, J., Khaledi, M. G., *J. Chromatogr. A* 2003, **1004**, 39–46.
- [211] Malek, A. H., Khaledi, M. G., *Electrophoresis* 2003, **24**, 1054–1062.
- [212] Phayre, A. N., Farfano, H. M. V., Hayes, M. A., *Langmuir* 2002, **18**, 6499–6503.
- [213] Bilek, G., Kremser, L., Blaas, D., Kenndler, E., *Electrophoresis* 2006, **27**, 3999–4007.

- [214] Colton, I. J., Carbeck, J. D., Rao, J., Whitesides, G. M., *Electrophoresis* 1998, 19, 367–382.
- [215] Shimura, K., Kasai, K., *Anal. Biochem.* 1997, 251, 1–16.
- [216] Guijt-van Duijn, R. M., Frank, J., van Dedem, G. W. K., Baltussen, E., *Electrophoresis* 2000, 21, 3905–3918.
- [217] Gayton-Ely, M., Pappas, T., Holland, L., *Anal. Bioanal. Chem.* 2005, 382, 570–580.
- [218] Heegaard, N. H. H., Nissen, M. H., Chen, D. D. Y., *Electrophoresis* 2002, 23, 815–822.
- [219] Wang, F. H., Yoshitake, T., Kim, D. K., Muhammed, M., Bjelke, O., Kehr, J., *J. Nanopart. Res.* 2003, 5, 137–146.
- [220] Xie, M. Y., Guo, Z. P., Chen, Y., *Chem. J. Chin. Univ.-Chin.* 2010, 31, 2162–2166.
- [221] Li, N., Zeng, S., He, L., Zhong, W. W., *Anal. Chem.* 2010, 82, 7460–7466.
- [222] Kohl, Y., Oostingh, G. J., Sossalla, A., Duschl, A., von Briesen, H., Thielecke, H., *Nanoscale Res. Lett.* 2011, 6, 505.
- [223] Zhao, S. L., Ji, X. W., Lin, P. T., Liu, Y. M., *Anal. Biochem.* 2011, 411, 88–93.
- [224] Qiao, J., Qi, L., Yan, H. J., Li, Y. P., Mu, X. Y., *Electrophoresis* 2013, 34, 409–416.
- [225] Xie, H. Y., Wang, Z. R., Kong, W. J., Wang, L., Fu, Z. F., *Analyst* 2013, 138, 1107–1113.
- [226] Adachi, K., Noda, N., Nakashige, M., Tsuneda, S., Kanagawa, T., *J. Chromatogr. A* 2006, 1109, 127–131.
- [227] Cao, W., Chen, L., Fu, Y. J., Tan, Z. Y., Qu, B., *J. Sep. Sci.* 2011, 34, 939–946.
- [228] Helle, A., Hirsjadri, S., Peltonen, L., Hirvonen, J., Wiedmer, S. K., *J. Chromatogr. A* 2008, 1178, 248–255.
- [229] Yang, L., Tucker, I. G., Ostergaard, J., *J. Pharm. Biomed. Anal.* 2011, 56, 553–559.
- [230] Blazkova, I., Nguyen, H. V., Dostalova, S., Kopel, P., Stanisavljevic, M., Vaculovicova, M., Stiborova, M., Eckschlager, T., Kizek, R., Adam, V., *Int. J. Mol. Sci.* 2013, 14, 13391–13402.
- [231] Brambilla, D., Verpillot, R., Taverna, M., De Kimpe, L., Le Droumaguet, B., Nicolas, J., Canovi, M., Gobbi, M., Mantegazza, F., Salmona, M., Nicolas, V., Scheper, W., Couvreur, P., Andrieux, K., *Anal. Chem.* 2010, 82, 10083–10089.
- [232] Sobrova, P., Ryvolova, M., Adam, V., Kizek, R., *Electrophoresis* 2012, 33, 3644–3652.
- [233] Aleksenko, S. S., Shmykov, A. Y., Oszwaldowski, S., Timerbaev, A. R., *Metallomics* 2012, 4, 1141–1148.
- [234] Kuo, Y. C., Shih, K. H., Yang, J. T., *Electrophoresis* 2010, 31, 315–323.
- [235] Musile, G., Cenci, L., Andreetto, E., Ambrosi, E., Tagliaro, F., Bossi, A. M., *Anal. Bioanal. Chem.* 2016, 408, 3435–3443.
- [236] Sapsford, K. E., Berti, L., Medintz, I. L., *Angew. Chem.-Int. Edit.* 2006, 45, 4562–4588.
- [237] Li, Y. Q., Wang, J. H., Zhang, H. L., Yang, J., Guan, L. Y., Chen, H., Luo, Q. M., Zhao, Y. D., *Biosens. Bioelectron.* 2010, 25, 1283–1289.
- [238] Wang, J. H., Xia, J., *Anal. Chem.* 2011, 83, 6323–6329.
- [239] Wang, J. H., Li, J. Y., Li, J. C., Wang, C. L., Qiu, L., Jiang, P. J., *Nanomed.-Nanotechnol. Biol. Med.* 2016, 12, 515–515.
- [240] Celiz, M. D., Colon, L. A., Watson, D. F., Aga, D. S., *Environ. Sci. Technol.* 2011, 45, 2917–2924.
- [241] Xu, L. F., Hao, J. J., Yi, T., Xu, Y. Y., Niu, X. Y., Ren, C. L., Chen, H. L., Chen, X. G., *Electrophoresis* 2015, 36, 859–866.
- [242] Huang, X. Y., Weng, J. F., Sang, F. M., Song, X. T., Cao, C. X., Ren, J. C., *J. Chromatogr. A* 2006, 1113, 251–254.
- [243] Vicente, G., Colon, L. A., *Anal. Chem.* 2008, 80, 1988–1994.
- [244] Kleparnik, K., Voracova, I., Liskova, M., Prikryl, J., Hezinova, V., Foret, F., *Electrophoresis* 2011, 32, 1217–1223.
- [245] Wang, J. H., Li, J. C., Wang, J. P., Liu, L., Li, J. P., Qin, H. F., Ding, S. M., Fu, M. L., Ji, J. L., Jiang, P. J., Qiu, L., *J. Sep. Sci.* 2016, 39, 1785–1791.
- [246] Wang, J. H., Li, J. Y., Li, J. C., Qin, Y. Q., Wang, C. L., Qiu, L., Jiang, P. J., *Electrophoresis* 2015, 36, 1523–1528.
- [247] Wang, J. H., Li, J. Y., Li, J. C., Wang, C. L., Qiu, L., Jiang, P. J., *Nanomed.-Nanotechnol. Biol. Med.* 2016, 12, 514–514.
- [248] Wang, J. H., Zhang, C. C., Liu, L., Kalesh, K. A., Qiu, L., Ding, S. M., Fu, M. L., Gao, L. Q., Jiang, P. J., *Electrophoresis* 2016, 37, 2156–2162.
- [249] Wang, J. H., Qin, Y. Q., Qin, H. F., Liu, L., Ding, S. M., Teng, Y. W., Ji, J. L., Qiu, L., Jiang, P. J., *Electrophoresis* 2016, 37, 2163–2169.
- [250] Wang, J. J., Huang, X. Y., Zan, F., Guo, C. G., Cao, C. X., Ren, J. C., *Electrophoresis* 2012, 33, 1987–1995.
- [251] Liskova, M., Voracova, I., Kleparnik, K., Hezinova, V., Prikryl, J., Foret, F., *Anal. Bioanal. Chem.* 2011, 400, 369–379.
- [252] Shao, L. W., Dong, C. Q., Huang, X. Y., Ren, J. C., *Chin. Chem. Lett.* 2008, 19, 707–710.
- [253] Shi, C., Huang, X. Y., Dong, C. Q., Chen, H. J., Ren, J. C., *Chin. Chem. Lett.* 2009, 20, 1119–1122.
- [254] Janu, L., Stanisavljevic, M., Krizkova, S., Sobrova, P., Vaculovicova, M., Kizek, R., Adam, V., *Electrophoresis* 2013, 34, 2725–2732.
- [255] Poudyal, N., Chaubey, G. S., Rong, C. B., Liu, J. P., *J. Appl. Phys.* 2009, 105, 07A749.
- [256] Du, X., He, J. H., *Langmuir* 2010, 26, 10057–10062.
- [257] Bai, G. Y., Wang, Y. J., Nichifor, M., Bastos, M., *Langmuir* 2013, 29, 13258–13268.
- [258] Malik, H., Stephenson, K. J., Bahr, D. F., Field, D. P., *J. Mater. Sci.* 2011, 46, 3119–3126.

Article 10

Adam V, Vaculovicova M. CE and nanomaterials – Part II: Nanomaterials in CE.
Electrophoresis 2017 Oct;38(19):2405-2430.

Vojtech Adam^{1,2}
Marketa Vaculovicova^{1,2} 

¹Department of Chemistry and Biochemistry, Mendel University in Brno, Brno, Czech Republic

²Central European Institute of Technology, Brno University of Technology, Brno, Czech Republic

Received March 6, 2017

Revised July 4, 2017

Accepted July 5, 2017

Review

CE and nanomaterials – Part II: Nanomaterials in CE

The scope of this two-part review is to summarize publications dealing with CE and nanomaterials together. This topic can be viewed from two broad perspectives, and this article is trying to highlight these two approaches: (i) CE of nanomaterials, and (ii) nanomaterials in CE. The second part aims at summarization of publications dealing with application of nanomaterials for enhancement of CE performance either in terms of increasing the separation resolution or for improvement of the detection. To increase the resolution, nanomaterials are employed as either surface modification of the capillary wall forming open tubular column or as additives to the separation electrolyte resulting in a pseudostationary phase. Moreover, nanomaterials have proven to be very beneficial for increasing also the sensitivity of detection employed in CE or even they enable the detection (e.g., fluorescent tags of nonfluorescent molecules).

Keywords:

Carbon nanotubes / Graphene / Quantum dots

DOI 10.1002/elps.201700098

1 Introduction

In the majority of scientific areas including proteomics, pharmaceutical, biological, biochemical, medical, forensic, and/or environmental, the analytes are present in low amounts and in complex biological matrixes and therefore a sample purification and pre-treatment is required. However, besides the pre-treatment procedure a powerful separation technique coupled to the effective detection method is often essential. Currently, capillary-based separation techniques including capillary/nanoliquid chromatography (capillary/nanoliquid chromatography (CEC), and CE are key analytical techniques providing sufficient separation power combined with low consumption of valuable samples and rapid analyses times especially in the microfluidic format [1].

Low sensitivity belongs to the main drawbacks of CE-UV/Vis, which is the most common method in CE. It is associated with both the short optical path-length of the capillary used as a detection cell and the small sample volumes injected. These limitations can be overcome either by increasing amount of the analyte using preconcentration processes, by selection of the more sensitive method (e.g. laser-induced fluorescence, mass spectrometry, etc.), or by the enhancing the signal by labeling with particular tag (optical or electrochemical).

This part of the paper is dedicated to employment of nanomaterials (NMs) to improve the performance of CE in terms of (i) increase of resolution by using nanoparticles as electrolyte additives or capillary wall coatings and (ii) lowering

the limit of detection by improving of both optical as well as electrochemical detection.

Numerous reviews have been published dealing with application of CE for analysis of nanomaterials as well as application of nanomaterials for improvement of CE performance. However, the present article is providing a comprehensive summary highlighting the mutual benefits of these two areas (CE and nanomaterials) to each other.

2 Improvement of CE separation

Several parameters are commonly used to evaluate separation performance, including resolution, number of theoretical plates, and migration time reproducibility.

The degree of separation of two analytes of interest is defined as the resolution (R_s) and can be influenced by modifying the electrophoretic mobility of the analytes and the electro-osmotic mobility induced in the capillary as well as by increasing the efficiency for the band of each analyte according to the equation

$$R_s = \sqrt{N \frac{\mu_{elA} - \mu_{elB}}{4(\mu_{av} + \mu_{EOF})}} \quad (1)$$

where N is the number of theoretical plates, μ_{elA} and μ_{elB} are the respective electrophoretic mobilities of the analytes, μ_{av} is the mean electrophoretic mobility of analytes A and B, and μ_{EOF} is the mobility of the electro-osmotic flow.

It follows from the fundamentals of CE that each analyte migrates through the capillary as an independent zone according to its electrophoretic mobility. Under ideal conditions, analyte zone broadening occurs only by molecular

Correspondence: Dr. Marketa Vaculovicova, Department of Chemistry and Biochemistry, Mendel University in Brno, Czech Republic
Fax: +420-5-4521-2044
E-mail: marketa.vaculovicova@mendelu.cz

Colour Online: See the article online to view Figs. 1, 3–5 and 7 in colour.

diffusion of the solute along the capillary. In this ideal case, the efficiency of the zone, which is expressed as the number of theoretical plates (N), is given by

$$N = \frac{(\mu_{el} - \mu_{EOF}) V l}{2DL} \quad (2)$$

where μ_{el} is the electrophoretic mobility of the analyte, μ_{EOF} is the mobility of electro-osmotic flow, L is the total length of the capillary, V is the applied voltage, and l is the effective length of the capillary.

However, in reality, other phenomena can also contribute significantly to band dispersion, including sample adsorption onto the capillary wall, mismatched conductivity between the sample and buffer, heat dissipation, detector cell size, un-leveled buffer reservoirs, and length of the injection plug [2].

Significantly improved separation with higher efficiency and selectivity and better reproducibility can be achieved by influencing the factors listed above. Due to their large surface-to-volume ratios and favorable surface chemistry, nanomaterials can be used advantageously in this application. Nanomaterials could be used either to create an inner surface coating in permanent or dynamic mode for open-tubular capillary electrochromatography (OT-CEC) or as a pseudostationary phase added to the background electrolyte and used with the partial filling or continuous filling method. A schematic summary of approaches for the application of NMs in separation improvement is given in Fig. 1. The stationary and pseudostationary phases can be created from a broad range of nanomaterials, such as polymers, gold and silica nanoparticles (NPs), fullerenes and carbon nanotubes. This topic has been well discussed in reviews by Kist and Mandaji [3] and Lin et al. [4] and the subject was later reviewed by Nilsson et al. [5]. A review article published by Sebestik et al. [6] focused on biomedical applications of peptide dendrimers and their analogs and summarizes a number of papers that address various types of dendrimers, their characterization via CE, and their application as a pseudostationary phase and dynamic capillary coating. Carbon nanomaterials also play a key role in this field, as shown in a review that addressed applications of carbon nanotubes in CE, capillary electrochromatography, and microchip electrophoresis [7].

A review of applications that use nanomaterials as stationary and pseudostationary phases was published in 2011 by Duan et al. [8] and this paper demonstrates the

advantages of NMs for applications not only in CE but also in gas and liquid chromatography. In addition, as shown in the work of Nilsson et al. [9], NMs are beneficial for the separation of small molecules and also macromolecules, including proteins. Furthermore, nanomaterials can be applied in the large field of electrochromatographic analysis referred to as enantioseparation [10–21]. NMs are suited to modification with chiral selectors and use as enantioselective agents for pseudostationary phases. Enantioselective nanomaterials are expected to interact with every enantiomer, forming locally chiral structures according to their different interaction mechanisms (e.g., electrostatic, dipole–dipole, hydrophobic, attractive and repulsive interactions, and hydrogen bonding). Cyclodextrins are one of the most commonly used groups of enantioselectors, and it is therefore not surprising that a number of studies have used combinations of NMs and cyclodextrins. The applications of chemically modified gold nanoparticles (AuNPs) using cyclodextrins as chiral selectors for enantioseparation based on pseudostationary phase-CEC (PSP-CEC) are presented by Yang et al. [22]. Dinitrophenyl-labeled amino acid enantiomers (DL-Val, Leu, Glu, and Asp) and drug enantiomers (RS-chlorpheniramine, zopiclone, and carvedilol) were analyzed using modified AuNPs as the chiral selectors. The results were promising and reached a theoretical plate number greater than 10^5 [22]. Cyclodextrin was further used as a modifier of multi-walled carbon nanotubes (MWCNTs) in addition to polystyrene, TiO_2 and Al_2O_3 nanoparticles to enhance the enantioseparation of clenbuterol [21]. Successful clenbuterol enantioseparation was also achieved using MWCNTs modified with cyclodextrin as a chiral selector.

2.1 NMs as pseudostationary phases

Electrokinetic chromatography is a mode of CE that uses a carrier to transport the analyte to the detector. Due to the electro-osmotic flow (EOF), neutral molecules can also reach the detection point, however no separation of such molecules can be achieved. With the use of a particular carrier (pseudostationary phase), the analyte can be partitioned between the aqueous phase of the BGE and the pseudostationary phase of the carrier. Such partitioning differs for

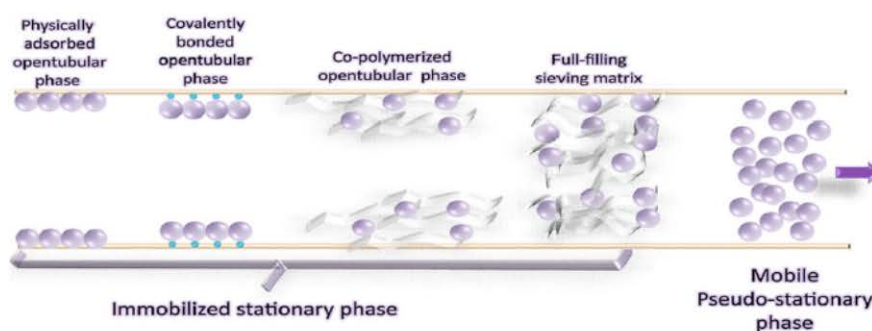


Figure 1. Approaches for separation performance enhancement by nms.

each analyte and is given by the distribution coefficient K , defined as

$$K = \frac{c_{ps}}{c_s} \quad (3)$$

where c_{ps} and c_s are the molar concentrations of analyte in the pseudostationary phase and in solution, respectively.

The variety of pseudostationary phases is wide and includes surfactants, polymers, dendrimers and (probably the most widely used) micelles [23].

The main advantage of this type of CE lies in the fact that the phase is being continuously replaced during the analysis, and thus, repeatable conditions are maintained for each analysis. As a result, carryover and cross-contamination effects are eliminated, which improves the analysis of samples in complex biological matrices. Another benefit is that no column packing or frits are required in these arrangements. In contrast, the presence of the pseudostationary phase in the entire volume of the capillary might negatively influence detection, especially the optical one. Furthermore, highly reproducible synthesis of the nanomaterials is needed and that too could become an issue.

2.1.1 Nanoparticles

The simplicity of functionalizing silica nanoparticles ensures their broad application in this area of analysis. Surface-functionalized silica nanoparticles have been successfully used for the separation of charged and neutral compounds [24], glucose oligomer derivatives and nucleic acid bases [25], and cyclodextrin functionalization has been used for chiral separation [26–28].

Due to the advantageous behavior of silica nanoparticles, these materials were used with biologically active amines for CE with laser-induced fluorescent detection (CE-LIF) [29], and these authors successfully tested formic acid enriched by silica nanoparticles as a background electrolyte (BGE). An increasing concentration of the particles resulted in increased EOF, which accelerated the analysis. Decreasing electrophoretic mobilities with increasing silica nanoparticles concentration indicated interactions between the analytes and the silica NPs. The method was sufficiently sensitive and robust for use in analyzing urine samples. All three tested analytes, i.e., tryptamine, 5-hydroxytryptamine, and tryptophan, were found and determined [29]. The positive effect of silica nanoparticles as a pseudostationary phase was additionally proposed for simultaneous determination of the quinolone family members lomefloxacin, sparfloxacin, fleroxacin, norfloxacin, ofloxacin, gatifloxacin, and pazufloxacin [30] as well as organic acids [31]. Silica nanoparticles can be modified as well, as shown by Yan et al. [32]. Those authors used a silica-based nanoparticles with surface-bound octanoyl-aminopropyl moieties and applied them for the separation of aromatic acids. However, the concentration of the particles was relatively high (1.0 mg/mL), which could be an issue in the use of the isolated fractions for further analysis.

Aromatic acids are a popular analyte for testing of modified silica nanoparticles used as pseudostationary phase [33]. A laboratory-made instrument and aminopropyl-modified silica nanoparticles were used in that work. In addition to achieving good separation results, the authors calculated the average theoretical plate number obtained, and this value exceeded 5.0×10^4 theoretical plates per meter.

A systematic comparison of diamine-modified and amine-modified silica nanoparticles was published by Hui and Ma [34] in 2011. The results indicated that even slight structural changes in the functional groups of the nanoparticles have pronounced effects on the interactions between the pseudostationary phase and the analytes. Among other analytes, protein separation also has been presented in this mode [35]. The combination of poly(ethylene oxide) with silica NPs in a buffer at pH 2.37 enabled detection limits from 2 to 45 ppm with relative deviations of the migration times ranging from 2.1 to 3.4%.

NPs made from metals and metal oxides such as titanium, yttrium or ytterbium oxide, and gold have proven to be highly effective buffer additives. Pharmaceutical application of TiO₂ nanoparticle-enhanced CE separation was demonstrated in a work by Zhou et al. [36], who presented determination of the frequently applied antihypertensive P-blocking compounds atenolol, metoprolol, terbutaline, and propranolol in pharmaceutical tablets. Detection limits at the level of micrograms per milliliter were reported. Yttrium and ytterbium oxide nanoparticles (YNP and YbNP, respectively) were later used to separate DNA fragments ranging in size from 100 to 9000 bp, [37] as shown in Fig. 2. Similar sieving power was observed for both YNP and YbNP matrices, most likely due to the similar sizes of the nanoparticles, and this resulted in the formation of comparable sieving networks for DNA separation. Separation of steroids was also improved by the addition of metal nanoparticles in a work by Liu and Chang [38]. Thiol-capped gold nanoparticles were used, and all of the tested steroids were separated well. Limit-of-detection values ranged from 11.8 to 16.4 µg/L. Gold nanoparticles can also be used as an additive in the separation of DNA [39–42]. The authors of studies in this area used poly(ethylene oxide) (PEO) for this purpose, and the capillary was dynamically coated with polyvinylpyrrolidone to prevent interaction of the capillary wall with DNA. Rapid and high-resolution DNA separations were achieved using different PEO solutions containing gold nanoparticles ranging in diameter from 3.5 to 56 nm. Separation of DNA fragments (from 8 to 2176 base pairs) was accomplished in 5 minutes. The potential of high-throughput DNA analysis using the suggested method is increased mainly due to the automatic replacement of the sieving matrices given by the low viscosity. In 2011, a detailed study of varying plug lengths of nanoparticle pseudostationary phase during CE analysis was published by Subramaniam et al. [43]. Gold nanoparticles functionalized with 11-mercaptoundecanoic acid were used as an additive in the pseudostationary phase plug, and dopamine, epinephrine, pyrocatechol, L-3,4-dihydroxyphenylalanine, glutathione, and uric acid were used as analytes due to their biological

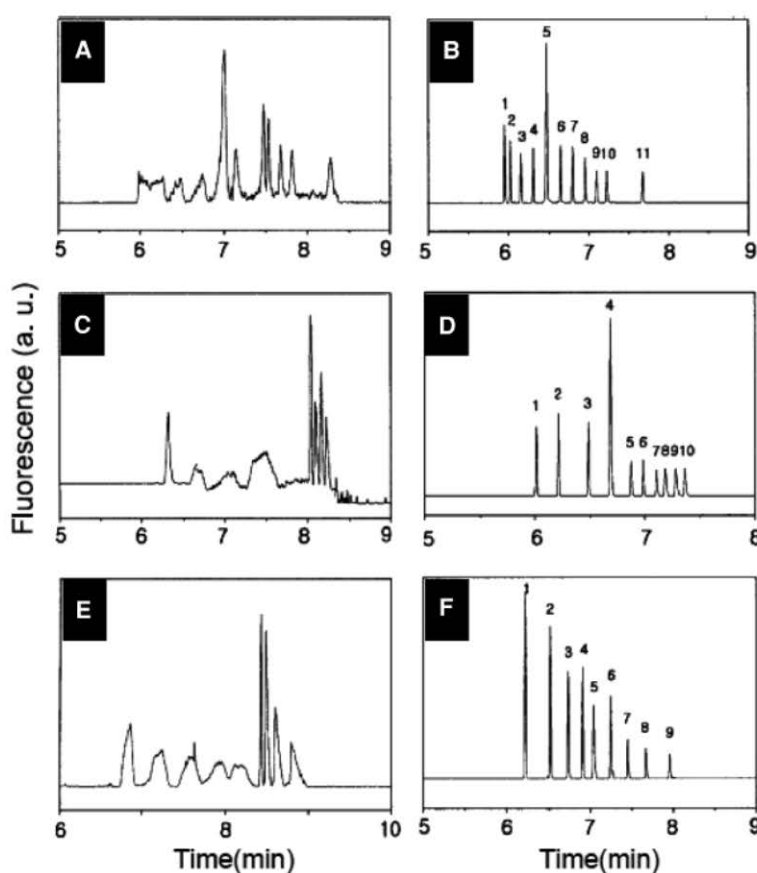


Figure 2. Separation of 100 bp DNA step ladder using (A) 0.10% poly(ethylene oxide) (PEO) only and (B) 0.02% yttrium oxide nanoparticle (YNP) and 0.10% PEO; peak assignment: 1 = 100 bp, 2 = 200 bp, 3 = 300 bp, 4 = 400 bp, 5 = 500 bp, 6 = 600 bp, 7 = 700 bp, 8 = 800 bp, 9 = 900 bp, 10 = 1000 bp, 11 = 1500 bp. Separation of 500 bp DNA ladder using (C) 0.02% PEO only and (D) 0.02% YNP and 0.02% PEO. Separation of 1 kbp DNA ladder using (E) 0.02% PEO only and (F) 0.02% YNP and 0.02% PEO; peak assignment: 1 = 1000 bp, 2 = 2000 bp, 3 = 3000 bp, 4 = 4000 bp, 5 = 5000 bp, 6 = 6000 bp, 7 = 7000 bp, 8 = 8000 bp, and 9 = 9000 bp. Reprinted with permission from [37].

importance. Behavioral differences were observed in the analytes that correlated with the charge of the analyte.

Hydrophobic interactions have been used for protein analysis to take advantage of the benefits of lipid-based liquid crystalline nanoparticles [44]. Latex NPs have also been employed as a pseudostationary phase, as shown in the works of Palmer et al. [45, 46] and Breadmore et al. [47].

In these articles, the authors show that the presence of NPs in the separation has a minimal effect on subsequent UV detection as well as on ESI-MS detection. This observation is in agreement with earlier findings by Viberg et al. [48]. The impact of the presence of NPs in mass spectrometry detection was later investigated in greater detail by Malstrom et al. [49]. Parameters including background electrolyte, sheath liquid ion strength, organic modifier content, nebulizer gas pressure, and concentration of nanoparticles in the electrolyte were examined. Even the lowest pressure investigated was sufficient to guide the nanoparticle flow away from the mass spectrometer inlet. Additionally, no significant effect of the ion strength of either the BGE or the sheath liquid on the separation of a series of dialkyl phthalates was observed, and the presence of NPs had no impact on the ionization efficiency.

An interesting approach that should not be omitted is the use of molecular imprinting technology to create multiple-target predetermined nanoparticles, as shown in a work by Spiegel et al. [50]. (S)-ropivacaine and (S)-propranolol were studied as templates, and the relative amounts of these two templates strongly affected the affinity of the multiply templated nanoparticles for the predetermined targets.

2.1.2 Carbon nanomaterials

A summary of developments in capillary electrokinetic chromatography using carbon nanoparticles was published in 2009 by Moliner-Martinez et al. [51]. That paper summarized the types of carbon NMs, the requirements for their application as a pseudostationary phase, and the mechanisms of their interactions with analytes. CNTs are probably the NMs that are most commonly used as a pseudostationary phase. However, in general, CNTs are insoluble in most common solvents, and thus, functionalized CNTs must be used to enable the interaction and/or adsorption of analytes via the polar groups and van der Waals forces of functionalized NPs. Moreover, although the combination of sodium dodecyl sulfate

(SDS) micellar electrokinetic chromatography with the addition of C-60 fullerenes significantly improved the CE separation of polycyclic aromatic hydrocarbons [52], the application of carbon nanotubes is generally far more widespread than the use of fullerenes or graphenes [53].

In view of these facts, carbon nanotubes are preferred when using nanomaterials as a pseudostationary phase. Carboxylic single-wall carbon nanotubes (c-SWCNTs) have been used for separation of homologues of caffeine and theobromine [54]. Reaching a critical concentration of c-SWCNTs was found to lead to significant changes during the separation. The authors proposed that the network formed by c-SWCNTs provides a different mechanism of separation compared with SDS micelles. Furthermore, Jimenez-Soto et al. [55] described, for the first time, the use of single-walled carbon nanohorns (SWNHs) as a pseudostationary phase. The authors took advantage of such features of this material as its conical-end termination, formation of spherical assemblies, dahlia flower-like superstructure, and easy functionalization. The authors showed that carboxylation and subsequent immobilization of carboxylated SWNHs in a fused silica capillary was helpful for obtaining repeatable and stable pseudostationary phases. The phase was successfully tested to separate water-soluble vitamins.

MWCNTs – especially their functionalization – have also attracted attention. Nitric, sulfuric, and hydrochloric acids have been used to increase their hydrophilicity, and MWCNTs functionalized in this way have been used for the separation of non-steroidal anti-inflammatory drugs [56]. Subunits of functionalized MWCNTs and borate buffer at pH 10 were satisfactory for the separation of six non-steroidal anti-inflammatory drugs and for the analysis of a spiked urine sample [56]. Xiong et al. [57] showed enhanced separation of purine and pyrimidine bases using carboxylic MWCNTs. The authors directed their attention to adenine (A), hypoxanthine (HX), 8-azaadenine (8-AA), thymine (T), cytosine (C), uracil (U) and guanine (G). The calibration curves were linear within two orders of magnitude at the level of $\mu\text{g/mL}$ for the compounds of interest, with detection limits down to units of $\mu\text{g/mL}$ [57]. MWCNTs can also be used for separating alkaloids [58], lipids [59] or DNA fragments [60]. As expected, the concentration of MWCNTs must be varied according to the size of the fragment of interest to achieve the required resolution. As shown by the separation of the 2-Log DNA ladder, even a concentration of MWCNTs below the threshold for CNT-network formation was sufficient. However, for larger DNA fragments, the concentration had to be increased above the threshold value [60]. An example of the use of carbon nanotubes as a buffer additive for separation improvement is shown in Fig. 3.

2.1.3 Liposomes and dendrimers

Lipids appear to be good materials for such purposes. Nilsson et al. [61] showed how anionic and cationic lipid-based liquid crystalline nanoparticles can be used for protein

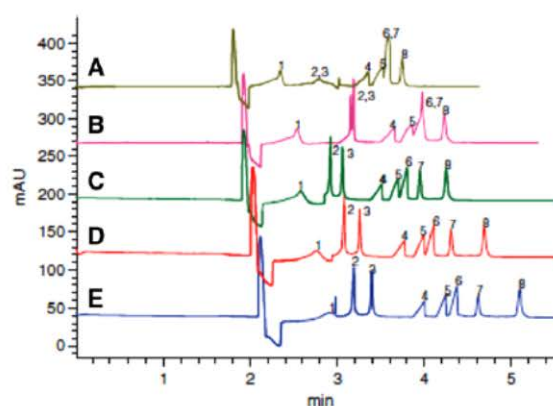


Figure 3. Influence of surfactant-coated single-walled carbon nanotube (SC-SWCNT) concentrations on the separation of eight analytes using microemulsion electrokinetic chromatography: (A) without SC-SWCNTs, (B) 1.5 mg/L SC-SWCNTs, (C) 3.0 mg/L SC-SWCNTs, (D) 4.5 mg/L SC-SWCNTs, and (E) 6.0 mg/L SC-SWCNTs. Microemulsion buffers: 0.5% (57 mM) w/v ethyl acetate, 0.6% (30 mM) w/v lauric acid, 4.0% (666 mM) w/v propanol, 50 mM Tris solution of pH 9.0, and 0–6.0 mg/L SC-SWCNTs additives. Other operating conditions: Analyte concentration, 0.07 mg/mL; capillary length, 40 cm total (31.5 cm effective length); 50 μm inside diameter; temperature, 30°C; voltage, 23 kV; injection, 50 mbar, 3 s; detection, 200 nm; analytes: (1) epicatechin, (2) epigallocatechin gallate, (3) epicatechin gallate, (4) caffeic acid, (5) gallic acid, (6) protocatechuic acid, (7) quercetin, and (8) kaempferol. Reprinted with permission from [204].

separation. Porous liquid crystalline lipid-based nanoparticles have also been used in the miniaturized electroseparation of green fluorescent protein [62]. In contrast to conventional liquid chromatography, a lipid-based phase minimizes the carryover effect and time-consuming column regeneration. Protein and peptide separation using liposome-based pseudostationary phases was at the center of interest for Corradini et al. [63, 64], who studied the application of 1-palmitoyl-2-oleoyl-sn-glycero-3-phosphocholine and its properties in this area with modification of the separation procedure.

Carbosilane dendrimers with interior carbon-silicon bonds and negative charges on the dendrimer surface with carboxylic acid as functional groups have been used as nano-additives to separate soybean and olive-seed proteins [65]. Different dendrimer generations (G1, G2, and G3) and concentrations (0.01–1.0% m/v) were tested. The highest dendrimer generation G3 at 0.1% (m/v) allowed for the observation of the best protein profiles of soybean and olive seeds. This result can be considered a new but not yet fully understood approach for protein profiling [65].

2.2 NMs in open-tubular capillary electrochromatography

Capillary electrochromatography (CEC) is a valuable member of the family of capillary electromigration techniques that use

electrophoretic migration to significantly improve chromatographic performance. As early as 1952, Moulde and Synge [66] applied an electrical field to achieve thin layer chromatography separations, but the first application of an electrical field to column chromatography was reported by Pretorius et al. [67] in 1974. Renewed interest in the technique arose during the 1990s [68–72].

CEC takes significant advantage of a flow profile that approximately corresponds to plug flow for an electrically driven system compared with the parabolic profile for pressure-driven flow. This property results in a significant reduction of the A term in the van Deemter equation and provides a large increase in chromatographic efficiency [72].

The apparent mobility for a charged analyte in OT-CEC is influenced not only by its electrophoretic mobility but also by its partitioning interaction and the EOF [73]. Similar to pressure-driven techniques, in CEC, the behavior of analyte in the column also can be expressed as a capacity factor that incorporates both the electrophoretic and chromatographic separation mechanisms. In CEC, k'_{CEC} can be expressed as

$$k'_{\text{CEC}} = \frac{k' - \mu_{\text{el}}/\mu_{\text{EOF}}}{1 + \mu_{\text{el}}/\mu_{\text{EOF}}} \quad (4)$$

where k' is the capacity factor of the analyte and the column operated in a pressure-driven mode. The parameters μ_{el} and μ_{EOF} are the electrophoretic mobility of the analyte and EOF, respectively.

Selectivity is controlled by tailoring the immobilized stationary phase, and in combination with benefits from the electrophoretically driven migration, the power of CEC is increased. As summarized recently in the review by Hu et al. [74], nanoparticles might be employed in CEC in an open tubular arrangement and also as a modification of monolithic columns. The use of open tubular columns that offer easy preparation procedures, a variety of surface chemistries, and compatibility with smaller diameter capillaries increases the benefits of this method even further. Examples of scanning electron micrographs of capillaries with immobilized nanomaterial on the inner wall are shown in Fig. 4. Smaller internal diameters compared with those commonly used in CE are required in OT-CEC to enable efficient solute diffusion to the surface of the stationary phase. Since the first OT-CEC column reported by Tsuda et al. [75] and the first use of a monolayer silica surface functionalized by octadecylsilane, numerous innovative approaches have been presented to increase the stationary phase area of OT-CEC columns [76].

OT-CEC often suffers from problems of low sample capacity and high phase ratio. Several options appear to be useful in improving this situation, such as etching the capillary and coating the capillary with porous layers and monoliths. Selected attempts to use nanoparticle-driven filling of capillaries have been made, but these also have certain limitations [77,78]. Additionally, deposition of nanoparticle phases has been used to overcome the previously mentioned problems. One essential drawback is the often tedious coating

procedure that is required to achieve a stable nanoparticle coating [5], but a great development in this field (as described below) could overcome this obstacle.

2.2.1 Nanoparticles as OT columns

AuNPs constitute one of the largest groups of nanomaterial-based stationary phases in OT-CEC [11, 14, 79–94]. Coating of the inner surface with gold nanoparticles has been shown to improve the resolution and plate numbers of the solutes, although other types of nanoparticles such as polystyrene [95, 96], titanium oxide [97–99], zirconium oxide [100], and silica [29, 101, 102] have been used to improve CE separation as well.

Another important group of nanoparticles that has proven to be highly effective as a stationary phase in capillary electrochromatography is the group of latex nanoparticles [103–107]. These materials were used either as a preconcentration segment with an in-line connection to an uncoated capillary or as a separation enhancing element.

In cases of protein separation, polystyrene NPs coated with such alpha,omega-diamines as ethylenediamine and 1,10-diaminodecane have been used for capillary coating, and in less than 7 minutes, separation was achieved with efficiencies of up to 1 900 000 theoretical plates per meter [95]. Later, TiO₂ nanoparticles were demonstrated for protein separation (conalbumin, apotransferrin ovalbumin, and bovine serum albumin) [97, 98] using phosphate buffer (40 mM) and an applied voltage of 15 kV, although a separation efficiency of only 10 000 plates/m was achieved. Because the relevance of post-translation modifications is increasing, the analysis of glycosylated proteins is also gaining importance. Up to 14 peaks for glycoisomers of ovalbumin were observed using borate buffer (40 mM, pH 9.0) and a capillary coated with ZrO₂ nanoparticles [100]. Cinchonidine nanocrystals also appear to show promise for the field of OT-CEC [108].

Even if not necessarily apparent from the number of published papers, from the viewpoint of their potential, magnetic particles appear to be of great importance for OT-CEC. A coating of magnetic nanoparticles as a stationary phase is introduced using an external magnetic force to fix the magnetic nanoparticles. An advantage of this coating is the simplicity of regeneration by application of the magnetic field. Magnetic field intensity together with the concentration and flow rate of a nanoparticle suspension were investigated by Zhu et al. [109] to achieve a simple and stable preparation. Compared with conventional open-tubular capillary column, this new system based on magnetic particles showed faster separation speed and higher column efficiency due to the larger surface area of the nanoparticles. This approach offers great potential for development of methods for analysis of complex samples because the magnetic coating can effectively prolong the column life by expediently replacing the stationary phase to eliminate column contami-

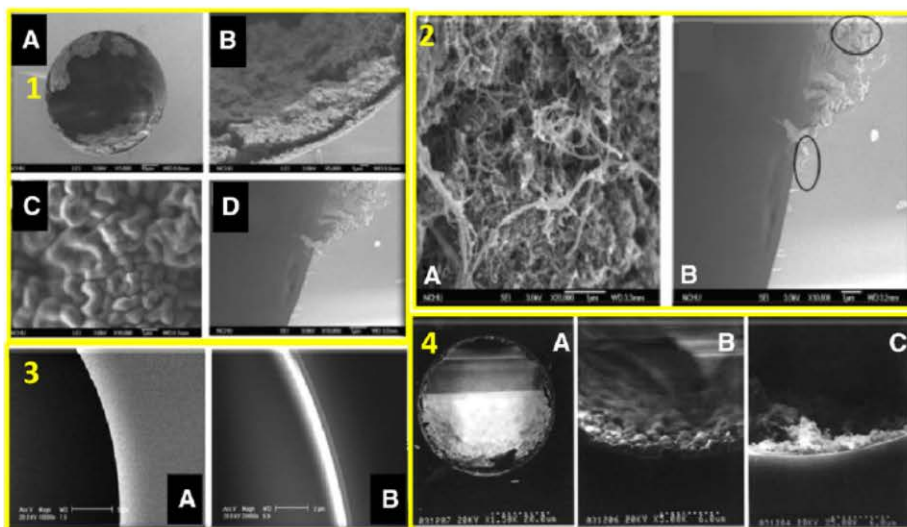


Figure 4. Scanning electron micrographs of various nanomaterials immobilized on the capillary wall. (1) Scanning electron micrograph images of prepared CNT-polymer composites. (A) Mono-(2-(methacryloyloxy)ethyl) succinate carbon nanotubes (MES-CNTs) coated on the capillary wall; (B) five-fold magnification of (A); (C) MES-CNTs formed on aluminum foil; (D) butyl methacrylate carbon nanotubes (BMA-CNTs) coated on capillary wall. Reprinted with permission from ref.205 (2) SEM images of (A) BMA-CNTs composite at 20 000 \times magnification, and (B) as a coating on a capillary wall at 10 000 \times magnification. The voltage used was 3.0 kV. Reprinted with permission from [114] (3) Scanning electron micrographs of (A) bare fused-silica capillary column, and (B) capillary column modified with octadecylamine-capped AuNPs. Reprinted with permission from [84] (4) Scanning electron micrographs of a TiO₂ NP-coated column. (A) Cross-section of the column prepared by two-cycle coating procedures. (B) Edge of the column prepared using two coating procedures. (C) Edge of the column prepared using a single coating procedure. Reprinted with permission from [99].

nation or irreversible adsorption. A model mixture of organic acids was used to evaluate the OT-CEC system. The relative column efficiency determined for anthranilic acid reached 220 000 plates/m. These authors also noted good repeatability of migration times, which was confirmed by another paper in which core/shell magnetic nanoparticles modified with amino and C-18 functional groups were used [110]. The results showed that the EOF gradually decreased with the increasing amount of core/shell magnetic nanoparticles modified by amino and C-18 functional groups in the mixed stationary phases and that the direction of EOF was eventually reversed. These results encouraged the authors to analyze a complex sample of *Rhizoma gastrodiae* extract. Another group of researchers also developed a chip-based platform using β -cyclodextrin (β -CD) conjugated graphene oxide magnetic nanocomposites (GO/Fe₃O₄ NCs) as a stationary phase. [17] Not only do the resultant GO/Fe₃O₄/ β -CD NCs have the magnetism of Fe₃O₄ NPs that make them easily manipulated by an external magnetic field, they also have a larger surface area that can incorporate many more chiral selector molecules. To prove the concept, successful baseline separation of tryptophan enantiomers was achieved in less than 50 s with a resolution factor of 1.65 using a separation length of 37 mm coupled with in-column amperometric detection [17]. In proteomic research, the potential of magnetic particle OT columns could also be exploited, as shown in a work by Wang et al. [111].

2.2.2 Carbon nanomaterials as OT columns

CNTs can be coupled to an inner capillary surface either by covalent or non-covalent bonding. In general, non-covalent methods are simpler, whereas covalent methods provide stronger and more stable coatings. Non-covalent methods are based on the physical adsorption of CNTs in a pretreated capillary. Polymers such as poly(diallyldimethylammonium) chloride and vinylbenzyl chloride combined with ethylene dimethacrylate or proteins such as albumin have been used for the precoating step [112].

Covalent bonding of c-MWCNTs is possible after silanization and coupling with glutaraldehyde on the inner surface of the capillary [112]. In addition, copolymerization of MWCNTs on the surface of the capillary with methacrylate can also be used for covalent bonding [113, 114]. Chen [115] took an approach involving hydrosilylation of nonacidic or acid-treated MWNTs with a silica-hydride capillary.

A combination of single-drop microextraction (SDME) and open tubular capillary electrochromatography with carbon nanotubes as the stationary phase has been used for the detection of illicit drugs in horse urine at low concentrations [116]. Although coating of the capillary allowed for separation of the analytes with high resolution, less band broadening, and without distortion of the baseline, the interactions between the analytes and the MWNTs resulted in an increased migration time and likely the front tailing effect.

The behavior of CNTs also depends greatly on the orientation of discrete fibers. A randomly arranged CNT structure is the most widely used, but stationary phases that use aligned carbon nanotubes offer several benefits to separation. Such phases have been used for electrochromatographic chip separations [117]. Patterned growth of nanotubes in a specific location of the channel has been performed using a solid phase Fe-Al catalyst as well as a vapor-deposited ferrocene catalyst. The chip was successfully tested to isolate a glycosylated protein using concanavalin A immobilized onto the nanotube bed. Moreover, immobilization of the CNTs enabled the application of a notably high electrical field strength, thereby eliminating bubble formation [118].

In addition, relatively new members of the family of carbon nanomaterials, i.e., graphene and graphene oxide (GO), are becoming possible options for OT-CEC stationary phase [119]. GO nanosheets can be immobilized onto the capillary wall using 3-aminopropyltriethoxymethyl silane as a coupling agent [120]. Graphene-coated columns can also be fabricated via hydrazine reduction of a GO-modified column. It was shown that graphene-coated columns exhibited a pH-dependent EOF from anode to cathode in the pH range of 3–9, whereas graphene oxide-coated columns provided a constant EOF. From the viewpoint of separation properties, good separation of the tested neutral analytes on the graphene oxide column was achieved based on a typical reversed-phase behavior. In contrast, the graphene column showed poor separation performance because of the strong π - π stacking and hydrophobic interactions between graphene and polyaromatic hydrocarbons [120]. Despite the fact that graphene was considered a less suitable stationary phase in the previously cited paper, Liu et al. [121] applied graphene as a novel stationary phase in OT-CEC, and their results showed a greatly improved separation due to the greatly enhanced surface area. The proposed OT column exhibited good run-to-run repeatability and excellent stability for at least 2 weeks of usage totaling approximately 200 runs.

2.2.3 Liposomes and dendrimers as OT columns

Applications of liposomes as pseudostationary phases or carriers in electrokinetic chromatography have been reviewed [122], and the review includes chromatographic use of liposomal bilayers as stationary phases attached to the capillary wall.

The immobilization procedure has changed over time from coating with a positively charged polymer followed by negatively charged liposomes [123] through a simple flushing liposome suspension [124–126] to even more complicated procedures [127, 128]. The coating steps can include (i) epoxydiol coating, (ii) activation with 2,2,2-trifluoroethanesulfonyl chloride, and (iii) liposome coupling. The effectiveness of this coating was demonstrated by investigating the effect of the pH of BGE on the EOF and the separation of neutral compounds. The intra- and inter-capillary variations in EOF were 4.02% RSD ($n = 30$) and 6.72% RSD ($n = 4$), respectively [127].

The presence of certain ions might also affect the coating, as shown in the case of calcium [129]. In addition, immobilized dendrimers could diminish the interaction of positively charged analytes with the capillary wall [130], which subsequently also displays enantioselective properties, as shown in work of Shou et al. [131].

The approaches to development of stationary phases that use nms as well as the number of theoretical plates and the theoretical plate heights are summarized in Table 1.

3 Detection enhancement

3.1 Optical detection using nms

Among the optical detection modes, laser-induced fluorescence detection remains (and most likely will remain) the most sensitive of detection techniques following chemical separation, and its most valuable benefits include outstandingly low detection limits (10^{-13} M) [137] with good detection selectivity in cases of sample analysis with rather complex matrices. At the same time, this selectivity could be viewed as a disadvantage because the vast majority of analytes lacks the required fluorescent properties, and therefore, a type of derivatization via fluorescent label is needed.

In discussing optical detection in connection with NMs, quantum dots (QDs) should be especially highlighted due to their application as a fluorescent label in laser-induced fluorescence (LIF) detection [138–141]. An indirect method of laser-induced fluorescence detection using CdTe QDs has been demonstrated and enabled determination of propylparaben, sodium dehydroacetate, sorbic acid, benzoic acid, and sodium propionate in food with detection limits in the range of tenths of mg/L [142]. Additionally, determination of pesticide residues in vegetables [143, 144] and quinolone antibiotic residues in foods [145] by indirect QDs-LIF has been described. An alternative approach was applied by Chen and Fung, [146], who presented LIF detection using immobilized QDs to determine such organophosphate pesticides as mevinphos, phosalone, methidathion, and diazinon in vegetable samples. The method was shown to have detection limits in the range of tens of $\mu\text{g}/\text{kg}$.

Forster/fluorescence resonance energy transfer (FRET) is an effective method to investigate intramolecular structural changes [147] and intermolecular interactions [148] of molecules using fluorescent properties of particular fluorescent tags while taking advantage of the energy transfer between acceptor and emitter or emitter and quencher, respectively. In this case, using the tunable properties of QDs provides broad flexibility for experimental procedures. The energy transfer often occurs between QD and organic dye or between QD and QD, although a QD and another nanoparticle, such as an AuNP also can be used [149].

Besides photoluminescence detection, chemiluminescence (CL) and electrochemiluminescence (ECL) detection are also areas in which NMs are offering their abilities. CL detection is based on the production of electromagnetic

Table 1. Summary of approaches to immobilized nanomaterial-based open tubular stationary phases

| Stationary phase type | Coating procedure | Analyte, number of theoretical plates/meter (theoretical plate height) | Detection | CE conditions: BGE, voltage | Ref. |
|--|---|--|---|--|-------|
| Carbon nanomaterials MWNTs carbon nanomaterials | (1) Introduction of amino group by 2% v/v APTES (2) 10% v/v glutaraldehyde (3) c-MWNT flushing | Chloramphenicol, 5087 (112 μm) Piperacillin, 25830 (22 μm) Cloxacillin, 36692 (15.5 μm) Ampicillin, 46719 (12.2 μm) penicillin G, 41 847 (13.6 μm) amoxicillin, 77140 (7.4 μm) ketoprofen, 61175 (9.3 μm) flurbiprofen, 56815 (10 μm) | UV detection 214 nm@ | 40 mM boric acid: pH 9, 15 kV | [112] |
| MWCNTs | Growth in the channel by chemical vapor deposition method | Trp-Tpr, ~50,000 (0.2 μm) | UV detection 230 and 270 nm | 1 mM MES: pH 6 | [117] |
| MWNTs | (1) Introduction of amino group by 2% v/v APTES (2) 10% v/v glutaraldehyde (3) c-MWNT flushing | Melatonin, N/A (N/A) | UV detection 254 nm | 40 mM sodium tetraborate: pH 9.30, 15 kV | [132] |
| MWNTs | (1) Capillary etching by ammonium hydrogen difluoride in methanol at 400°C for 4 h, (2) Silanization by 1.0 M TES in dioxane for 1.5 h at 90°C, (3) Toluene rinse, (4) Hydrosilylation reaction with MWNTs | Thymidine, 570 000 (0.96 μm) Thymine, 540 000 (1 μm) Adenosine, 210 000 (2.6 μm) Cytidine, 310 000 (1.8 μm) Guanosine, 220 000 (2.5 μm) Uridine, 250 000 (2.2 μm) | UV detection 214 nm for DMSO, 254 nm for nucleosides and thymine, 355 nm for tetra cyclines | 30 mM borate buffer: pH 9.55, 10 kV | [115] |
| MWNTs | (1) Filling with 2,2-diphenyl-1-picrylhydrazyl, γ -MAPS and MeOH (2) Filling with monomer solution: BMA, ethylene dimethacrylate, acid-treated MWNTs, 2,20-azo-bis-isobutyronitrile, 1-propanol, 1,4-butanediol, and H ₂ O | Phenolic acids, 3 000–43 000 (120–8.3 μm) Flavonoids, 3 100–1 600 000 (121–0.02 μm) Nucleosides, 3 100–28 000 (159–17.7 μm) Nucleobases, 3 700–40 000 (171–15.9 μm) | UV detection 214 nm for DMSO, 254 nm for nucleobases nucleosides, 280 nm for flavonoids and phenolic acids | Nucleobases and nucleosides: borate buffer, 50 mM, pH 9.0, 12 kV Flavonoids: 10 mM borate buffer, pH 9.5, 10 kV Phenolic acids: 30 mM borate buffer, pH 9.0, 7 kV | [114] |

(Continued)

Table 1. Continued

| Stationary phase type | Coating procedure | Analyte, number of theoretical plates/meter (theoretical plate height) | Detection | CE conditions: BGE, voltage | Ref. |
|------------------------------|--|---|---|--|-------|
| MWNTs | (1) Filling with 2,2-diphenyl-1-picryl-hydrazyl, g-MAPS, and MeOH, standing at room temperature for 24 h (2) Rinsing with polymerization solution: MAA, Bis-acrylamide, acid-treated MWNTs, TEMED, ammonium persulfate, and borate buffer | Benzene derivatives, 25 000–130 000 (18–3.5 μm) Flavonoids, 170 000–480 000 (2.4–0.8 μm) Tetracyclines, 40 000–92 000 (10–4.3 μm) | UV detection 214 nm for DMSO, and benzene derivatives, 280 nm for flavonoids, 355 nm for tetracyclines | Benzene derivatives: 50 mM borate buffer, pH 8.6, 10 kV Flavonoids: 150 mM borate buffer, pH 8.8 with 10% ACN, 10 kV Tetracyclines: 50 mM phosphate buffer, pH 2.9, 10 kV | [113] |
| MWCNTs | Chemical vapor deposition method | Coumarin dyes, ~1600 (14–18 μm) | LIF 375 nm/420 nm | 50 mM ammonium acetate buffer (pH 7.0) with 90% acetonitrile | [118] |
| Metal nanoparticles AuNPs | AuNPs and 0.02% (wt) PDADMAC flushing for 30 min | o-aminophenol, ~37000 (2 μm) | Gold-coated screen printed carbon electrode (+0.8 V) LIF | 20 mM acetate buffer, pH 5.0, 2 kV 1.5% PEO in Tris–borate buffer, (pH 9.0), 0.8 kV | [91] |
| AuNPs | PVP, PEO and AuNPs flushing | 8 to 2176 bp DNA fragments N/A (N/A) | ex 543.6 nm | | [133] |

(Continued)

Table 1. Continued

| Stationary phase type | Coating procedure | Analyte, number of theoretical plates/meter (theoretical plate height) | Detection | CE conditions: BGE, voltage | Ref. |
|-----------------------|---|--|------------------------|---|------|
| AuNPs | (1) Flushing 1% APTMS solution for 1 h, standing overnight (2) Annealing at 100°C for 24 h 3) flushing with AuNPs and left to stand for 1 h | Testosterone (four layers coating), 168 100 (4.5 μm) progesterone (two layers coating), 34 700 (21.6 μm) testosterone propionate (two-layer coating), 9600 (78 μm) | UV detection 247 nm | 25% (v/v) ACN/75% (v/v) 10 mM Tris, pH 9.5, 25 kV | [80] |
| AuNPs | (1) Solution of ODA Au-NPs in chloroform standing for 5 min (2) ODA-Au-NPs standing for 30 min (3) Injection of ODA-Au-NPs repeated 3 times | Testosterone, 189 000 (3.2 μm) Progesterone, 155 000 (3.9 μm) testosterone propionate, 87 800 (6.8 μm) | UV detection 200 nm | 45 mM phosphate buffer, pH 7.0, 70% v/v MeOH, 25 kV | [84] |
| AuNPs | (1) Filling with MPTMS/MeOH (1:4, v/v), standing for 24 h (2) Filling with BSA-AuNPs conjugate, standing for 24 h | FITC-labeled ephedrine and norephedrine isomers, N/A (N/A) | LIF ex. 473 nm | 0.050 M Tris/0.125 M boric acid/3.50 M urea at a pH of 9.0 590 V/cm | [11] |
| AuNPs | (1) Filling with 0.59 μm AuNP for 60 min (2) Rinsing with BGE for 10 min | Phend, N/A(N/A), o- and p-aminobenzoic acids, N/A (N/A), m-aminobenzoic acid, N/A (N/A) | UV detection 214 nm | 5 mM phosphate buffer pH 5.3 and 0.236 μm AuNP, 15 kV | [94] |
| AuNPs | (1) Modification with a cationic layer of PDADMAC and an anionic layer of PSS, (2) Rinsing with AuNP, standing for 30 min | Naphthalene, 46 900 (12.8 μm) Biphenyl, 18 700 (32 μm) | UV detection 214 nm | MeOH–10 mM phosphate buffer, pH 7, 20 kV | [83] |

(Continued)

Table 1. Continued

| Stationary phase type | Coating procedure | Analyte, number of theoretical plates/meter (theoretical plate height) | Detection | CE conditions: BGE, voltage | Ref. |
|--|--|---|------------------------|---|-------|
| AuNPs | (1) Sequential filling and flushing with PDDA solution (2% w/w) containing 0.1 M NaCl for 1 h (2) Flushing with cyclodextrin-AuNPs solution for 1 h | Zopiclone, 140 000 (3.6 μm), Tropicamide, 100 000 (5 μm) Chlorpheniramine, 120 000 (4.2 μm) | UV detection 214 nm | 12.5 mM phosphate buffer pH 3.300 V/cm | [14] |
| AuNPs | Cellulose-AuNPs composite flushing | Transferrin, 325 000 (1.4 μm), Chymotrypsinogen, 289 000 (1.6 μm), RNase A, 261 000 (1.8 μm) cytochrome c, 166 000 (2.8 μm) trypsin inhibitor, 152 000 (3.1 μm) lysozyme, 149 000 (3.2 μm) | UV detection 210 nm | pH 8.3, 12 kV | [134] |
| AuNPs | Reduction of HAuCl ₄ by dopamine with concurrent polymerization of polydopamine | Benzene, 28 106 (N/A) Methylbenzene, N/A (N/A) Ethylbenzene, N/A (N/A) Propylbenzene, N/A (N/A) n-butylbenzene, N/A (N/A) | UV detection 200 nm | a cetonitrile–20 mM CH ₃ COONa (12/88, v/v), pH 6.0, 20 kV | [135] |
| Fe ₃ O ₄ -COOH NPs | electrostatic self-assembly coating of positively charged poly(diallyldimethylammonium chloride) modified capillaries | bovine serum albumin, 81 600 (4.5 μm); conalbumine, 17 100 (21.6 μm); β -lactoglobulin, 192 000 (1.9 μm) | UV detection 214 nm | 40 mM phosphate buffer, pH 8.5, 20 kV | [111] |
| TiO ₂ NPs | (1) Addition of PEG 8000 dropwise to the TiO ₂ colloidal suspension with stirring, concentrating under vacuum at 50°C (2) Filling with resultant material for 10 min, reacting at 150°C for 24 h | Angiotensin-type peptides, 16 000–98 000 (43.8–7.1 μm) | UV detection 214 nm | 40 mM phosphate buffer, 15 kV | [99] |

(Continued)

Table 1. Continued

| Stationary phase type | Coating procedure | Analyte, number of theoretical plates/meter (theoretical plate height) | Detection | CE conditions: BGE, voltage | Ref. |
|-----------------------|--|--|------------------------------|--|-------|
| TiO ₂ NPs | (1) Flushing with NPs for 10 min (2) Reacting at 150°C for 24 h | Conalbumin, α-po-transferrin, ovalbumin, bovine serum albumin Main peak of ovalbumin in egg white was, ~ 10 000 (70 μm) | UV detection 214 nm | 40 mM phosphate buffer, pH 8.0, 15 kV | [97] |
| TiO ₂ NPs | liquid phase deposition process of TiO ₂ on polydopamine coated capillary | Conalbumin A, 9 130 (31.7 μm), α-Lacalbumin, 40 500 (7.2 μm), β-Lactoglobulin A, 133 000 (2.2 μm), β-Lactoglobulin B, 109 000 (2.7 μm), Bovine serum albumin, 10 200 (28.4 μm) | UV detection 214 nm | 40 mM phosphate (pH 9.0), 20 kV | |
| Silica and Al NPs | (1) γ-Methacryloxypropyltrimethoxysilane activation (2) Flushing with acrylamide (3.5%) solution with K ₂ S ₂ O ₈ and N,N,N',N'-tetramethylethylenediamine | 500 bp DNA step ladder N/A (N/A) | LIF 543.6 nm | 90 mM Tris, 90 mM borate, and 2 mM EDTA, pH 8.4, 100–300 V/cm | [136] |
| ZrO ₂ NPs | (1) Filling with the zirconia sol for 10 min (2) Heating at 350°C for 5, 8 and 24 h | Iron-binding and phosphorylated proteins, N/A (N/A) | UV detection 210 nm | isoforms of BSA: 10 mM phosphate buffer, pH 8, 15 kV glycoisoforms of OVA: 40 mM borate buffer pH 9 | [100] |
| Liposomes | (1) Coating with positively charged derivatized agarose, (2) Liposome flushing for 5 min at 25°C | Acetophenone, N/A (N/A) Propiophenone, N/A (N/A) Butyrophenone, N/A (N/A) Valerophenone, N/A (N/A) Hexanophenone, N/A (N/A) | UV-Vis diode array detection | phosphate buffer, pH 7.4, I = 0.02 M, 285 V/cm | [123] |

(Continued)

Table 1. Continued

| Stationary phase type | Coating procedure | Analyte, number of theoretical plates/meter (theoretical plate height) | Detection | CE conditions: BGE, voltage | Ref. |
|-----------------------|--|--|--------------------------------|--|-------|
| Liposomes | Rinsing with 3 mM liposome solution for 10 min, standing for 15 min | Aldosterone, N/A (N/A) Androstenedione, N/A (N/A) Testosterone, N/A (N/A) 17 α -hydroxyprogesterone, progesterone, | UV detection 245 nm | 40 mM HEPES pH 7.4, 20 kV | [125] |
| Liposomes | Rinsing for 10 min with 3 mM liposome solution, standing for 15 min | Phenol, <i>p</i> -cresol, 2,6-dimethylphenol, eugenol, 38 000–153 000 plates (15.8–3.9 μ m) | UV detection 214 nm | 20 mM HEPES at pH 7.4, 20 kV | [129] |
| Liposomes | (1) 10-min rinsing with 0.5 M HNO ₃ for 15 min with water (2) Phospholipid coating for 10 min with liposomes in BGE solution standing for 15 min | 2,4-dichlorobenzoic acid, N/A (N/A) 2,6-dimethoxybenzoic acid, N/A (N/A) 3,5-dinitrobenzoic acid N/A (N/A) 2,4-dihydroxybenzoic acid, N/A Phenethylamine, N/A (N/A), Atenolol, N/A (N/A), Practolol, N/A (N/A) Imidazole, N/A (N/A), Phenol, N/A (N/A), 2,6-dimethylphenol, N/A (N/A), Eugenol, N/A (N/A), 3,4-dichlorophenol, N/A (N/A), Progesterone N/A (N/A) | UV detection 214 and 254 nm | 20 mM HEPES pH 7.4, 20 kV | [126] |
| Liposomes | (1) Epoxy-diol coating, (2) Activation with 2,2,2-trifluoroethanesulfonyl chloride | Hydrocortisone, 71 220 (5.4 μ m), Androstenedione, 62 150 (6.1 μ m), Testosterone, 34 065 (11.3 μ m), progesterone 7255 (63 μ m) | UV detection 214 nm | 25 mM HEPES buffer (pH 7.40), 15 kV, 25°C | [127] |

(Continued)

Table 1. Continued

| Stationary phase type | Coating procedure | Analyte, number of theoretical plates/meter (theoretical plate height) | Detection | CE conditions: BGE, voltage | Ref. |
|-----------------------|---|--|------------------------|---------------------------------------|-------|
| Liposomes | <p>(1) Physical adsorption method: Rinsing with BGE for 10 min, with a liposome solution for 10 min, standing for 15 min</p> <p>(2) Covalent coupling method: Epoxy-diol coating in which a solution of 20% GPTMS in dry toluene was pumped, standing for 5 h at 110°C, rinsing with toluene and water, flushing with 0.1 M HCl, standing overnight at room temperature, activation with triethylamine, epoxy-diol-coated capillary washed with acetone–water (9:1, v/v) and dry acetone in sequence, followed by a mixed solution of 17 mL triethylamine in dry acetone and 34 mL pyridine pumped</p> <p>(3) Avidin–biotin binding method: Treating with APS (10%) for 5 min, heating at 95°C for 30 min, rinsing w/ glutaraldehyde solution (2%) in 50 mM phosphate (pH 7.0) for 30 min flushing by avidin in 50 mM phosphate for 30 min, rinsing with Tris–HCl buffer (0.5 M, pH 7.5) filling with the biotinylated liposome solution, standing for 30 min</p> | Hydrocortisone, N/A (N/A), Androstenedione, N/A (N/A), Testosterone, N/A (N/A), Progesterone, N/A (N/A) | UV detection 214 nm | 25 mM HEPES buffer (pH 7.4), 15 kV | [128] |
| Dendrimers | | Adenine, Adenosine, 6-Furfurylamino-purine, 165 000 (3.3 μm) | UV detection 254 nm | 40 mM phosphate buffer, 16 kV | [130] |
| Dendrimers | <p>(1) Rinsing with dichloromethane for 10 min</p> <p>(2) Filling with 10% G1P solution in dichloromethane, standing at 35°C for 4 h</p> <p>(3) Purging with methylene dichloride and DMF for 10 min</p> <p>(4) Filling with 5% β-CD solution in DMF and keeping at 110°C for 10 h.</p> | Chlor-Trimeton enantiomers, 31 534–246 857 (17.6–2.2 μm) | UV detection 214 nm | 40 mM phosphate buffer, 16 kV | [131] |

*Coating methods usually contain capillary treatment with hydroxide or acid for surface activation; this procedure and the final rinsing for unreacted compounds removal were left out for spatial reasons.

ACN – Acetonitrile; APTES, APS – (3-Aminopropyl)triethoxysilane; APTMS – (3-Aminopropyl)trimethoxysilane; AuNPs – Gold nanoparticles; BMA – Butylmethacrylate; BGE – Background electrolyte; BSA – Bovine serum albumin; DMF – Dimethylformamide; DMSO – Dimethyl sulfoxide; FITC – Fluorescein isothiocyanate; G1P – carbosilane dendrimers first generation; HEPES – N-(2-Hydroxyethyl)piperazine-N'-(2-ethanesulfonic acid); LIF – Laser-induced fluorescence; MES – 2-(N-morpholino)ethanesulfonic acid; MPTMS – (3-Mercaptopropyl)trimethoxysilane; MWNTs – Multi-walled carbon nanotubes; N/A – not available; NPs – Nanoparticles; ODA – Octadecylamine; PDAA – Poly(diallyldimethylammonium chloride); PDADMAC – Poly(diallyldimethylammonium chloride); PEG – Polyethylene glycol; PEO – Polyethylene oxide; β-CD – Beta-cyclodextrin; γ-MAPS – gamma-methacryloxypropyltrimethoxysilane.

radiation when a chemical reaction excites an electron that either luminesces or transfers the energy to another molecule that subsequently emits the light. The attractiveness of the CL method can be seen in the absence of undesired background signals, better sensitivity, and wide linear dynamic range. Furthermore, because no excitation sources and optical filters are required, the entire instrumentation is simple, robust, inexpensive, and amenable to automation. In these systems, metal NPs can participate as catalysts, reductants, fluorophores, or acceptors of energy. Metal nanoparticles, including gold, silver, platinum, semiconductors, and magnetic types, provide beneficial properties for CL detection [150]. A luminol–H₂O₂ system catalyzed by gold nanoparticles has been proven to enhance the detection signal due to the catalysis of gold nanoparticles, which facilitated the radical generation and electron-transfer processes taking place on the surface of the gold nanoparticles [151, 152], and moreover, the inhibition of signal caused by OH, NH₂ and SH groups made it applicable for the determination of such compounds. Later, an application for determining uric acid in human serum samples was demonstrated for diagnostics of various diseases (including diabetes) associated with alterations in production of uric acid [153]. In addition to gold nanoparticles, zirconia nanoparticles have also been utilized to enhance the copper (II)-catalyzed signal of a luminol–H₂O₂ system [154], and the determination of heme proteins in complex matrices was described using this method. The detection limits were improved by 10- to 22-fold compared with the conventional method. Quantum dot-enhanced chemiluminescence detection for simultaneous determination of dopamine and epinephrine was presented by Zhao et al. [155]. CdTe QDs were added to the running buffer of CE to catalyze the post-column CL reaction between luminol and hydrogen peroxide. The analytes were detected indirectly in terms of the decrease in the CL signal. The detection limits achieved for dopamine and epinephrine were 2.3×10^{-8} M and 9.3×10^{-9} M, respectively.

ECL is a special case of chemiluminescence that involves excitation of electrons by a reaction occurring at the electrode surface. Therefore, ECL is a combination of chemiluminescence and electrochemistry and thus leverages the advantages of both methods, such as sensitivity, wide dynamic range, stability, and simplicity. However, the geometrical arrangement is more instrumentally challenging due to the end-capillary type of detection. Although a luminol-based ECL system was first used in CE-ECL, current CE-ECL applications are almost exclusively based on the ECL system of Ru(bpy)₃²⁺ and its derivatives [156]. General review articles dedicated to the application of nanomaterials in ECL detection have been published [157–159]. Applications of gold nanoparticles have been shown to lead to a 100-fold decrease in the detection limit when used for the detection of pentoxifyverine [160], roxithromycin [161], propranolol and acebutolol [162], thus achieving detection limits in the nanomolar range. In addition to gold NPs, the use of carbon nanotubes also has been described in the form of an electrically heated Ru(bpy)₃²⁺/multiwall carbon-nanotube paste electrode [163]. This system

was applied to separate and detect acephate and dimethoate, and the results indicated that this system coupled with a heated modified electrode could provide high sensitivity, a wide linear range, a satisfactory linear relationship, and excellent reproducibility.

It should be noted that possibilities also exist for the use of certain less traditional systems involving NPs, including Raman spectrometry. Prikryl et al. [164] developed a photodeposition method for silver nanoparticles induced by a laser inside a fused-silica capillary. Good properties for surface-enhanced Raman scattering were achieved, which was beneficial for both separation and detection. The entire system was successfully tested in an analysis of rhodamines, although certain specific applications and testing of possible interferences are still waiting to be explored.

3.2 Electrochemical detection using NMs

Electrochemical detection in CE can be performed in three modes: potentiometric, conductometric and amperometric. Conductometric and potentiometric detectors provide a bulk property response with good sensitivity. By contrast, amperometric detection is selective and can be tuned to the analyte of interest. One of the main differences of this approach versus the optical detection modes is the fact that electrochemical detection is mostly performed by off-column, end-capillary, destructive means. To overcome these limitations, interest in contactless conductometric detection has been growing steadily over the past decade [165–168].

The application of nanomaterials for electrochemical detection encompasses a notably broad area. Due to their electrochemical properties, nanomaterials have been applied for electrochemical analysis of numerous analytes, including nucleic acids [169–171], proteins [172, 173], secondary metabolites [174, 175], and metals [176]. The important functions provided by nanoparticles include the immobilization of biomolecules, catalysis of electrochemical reactions, enhancement of electron transfer between electrode surfaces and proteins, labeling of biomolecules, and even participation as a reactant [177]. In addition to the relatively low costs of electrochemical detection compared with those of optical instrumentation, other advantages such as the possibility of miniaturization and in-field applications are important. Due to the great breadth of this area, it is not surprising that reviews have been published. Pumera and Escarpa [178] summarized the different approaches for constructing nanomaterial-based detectors for conventional CE and microchip electrophoresis and mostly focused on three main types of nanomaterials, i.e., carbon nanotubes, nanoparticles, and nanorods, in various designs. Examples of scanning electron micrographs of electrodes modified by various nanomaterials are shown in Fig. 5. The advantages and disadvantages of the selected detectors have been discussed. From the materials viewpoint, reviews by Chen [179] and Martin [180] were focused on carbon. That review was directed at CNTs and boron-doped diamond and covered CNT-based electrochemical detectors in

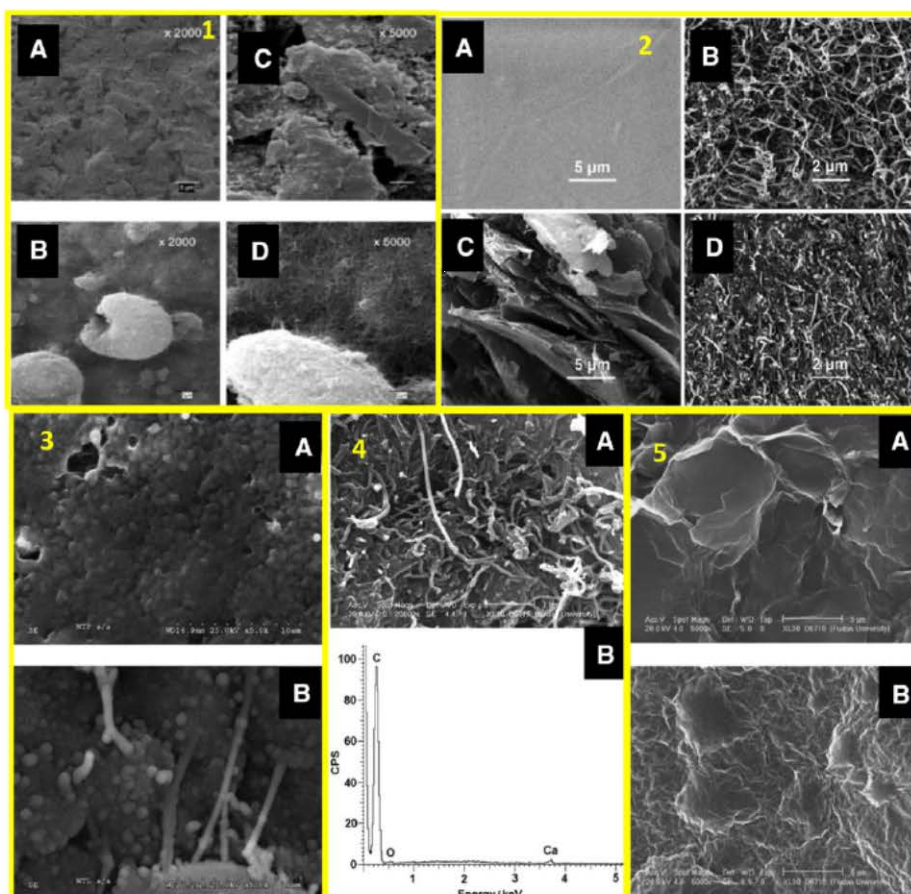


Figure 5. Scanning electron micrographs of various nanomaterial-modified electrode surfaces used for electrochemical detection in CE. (1) SEM micrographs of bare SPE electrode (A) and CNTs dispersed on the SPE electrode surface (B). Reprinted with permission from [185] (2) SEM images of the surfaces of (A) pure PMMA sheet, (B) pure CNTs and cross sections of (C) graphite/PMMA and (D) CNT/PMMA composites. Conditions: Acceleration voltage, 20 kV; magnification, 5000 \times (A, C), 10 000 \times (B, D). Reprinted with permission from [188] (3) SEM images of carbon nanotube paste electrodes prepared with (A) short and (B) long carbon nanotubes. Composition: 55.0% (w/w) carbon nanotubes and 45.0% (w/w) mineral oil. Magnification: 5000 \times . Reprinted with permission from [181] (4) (A) SEM image and (B) energy dispersive spectroscopy results for the CNT–alginate composite on a carbon disk electrode. Conditions for SEM: acceleration voltage: 20 kV; magnification: 20 000 \times . Reprinted with permission from [187] (5) SEM images of (A) pristine graphene and (B) a graphene/poly(urea-formaldehyde) composite. Conditions: Acceleration voltage, 20 kV; magnification, 5000 \times . Reprinted with permission from [193].

microchip CE, CNT-based electrochemical detectors in conventional CE, boron-doped diamond electrochemical detectors in microchip CE, and boron-doped diamond electrochemical detectors in conventional CE.

Based on the previously mentioned facts, it is clear that various carbon modifications play the main role in this field of CE detector development. Carbon paste electrodes modified with carbon nanotubes are at one of the foci of these developments. Chicharro et al. [181] have shown carbon nanotube paste electrodes prepared with short (1–5 μm) and long carbon nanotubes (5–20 μm) of 20–50 nm diameter to be highly useful as detectors in flow injection analysis and CE. Those authors found that electrodes prepared with long carbon nanotubes provided less noisy and more reproducible signals

for 3,4-dihydroxyphenylacetic acid, ascorbic acid, dopamine, norepinephrine, and epinephrine and also achieved lower detection limits. Xu et al. [182] confirmed these promising results using a carbon nanofiber paste electrode that exhibited good repeatability and long-term stability, and under optimized conditions, the beta blockers sotalol, alprenolol, and atenolol could be detected at tens of nm. The suggested method was also applied to determine the three beta blockers in spiked urine samples and achieved satisfactory assay results. The carbon paste electrode can also be modified with a metal oxide, as demonstrated by Cheng et al. [183], who used a nanonickel oxide-modified carbon paste electrode for the determination of carbohydrates. Under the selected optimum conditions, the three carbohydrates

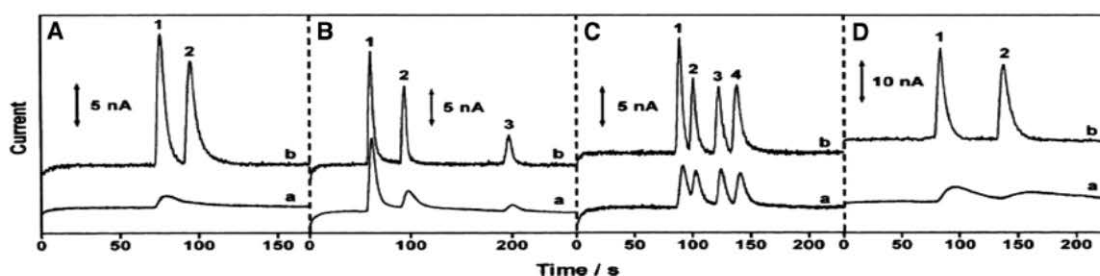


Figure 6. Electropherograms for (A) hydrazines; (B) dopamine, catechol, and ascorbic acid; (C) phenols; and (D) purines on (a) bare and (b) CNT-modified screen-printed carbon electrodes. Sample A: (1) 100 μM hydrazine, and (2) 200 μM dimethylhydrazine. Sample B: (1) 100 μM dopamine, (2) 100 μM catechol, and (3) 100 μM ascorbic acid. Sample C: (1) 100 μM phenol, (2) 100 μM 2-chlorophenol, (3) 200 μM 2,4-dichlorophenol, and (4) 200 μM 2,3-dichlorophenol. Sample D: (1) 200 μM guanine and (2) 200 μM xanthine. Conditions: (A) Run buffer, phosphate buffer (20 mM, pH 7.5), (B) 20 mM MES(2-(N-morpholino)ethanesulfonic acid, pH 6.5), (C) 10 mM borate/20 mM phosphate buffer (pH 8.0), and (D) 5 mM borate/10 mM phosphate buffer (pH 8.0). Separation voltage: (A) +1000 V and (B–D) +1500 V; injection voltage: (A) +1000 V, (B, C) +1500 V, and (D) +2000 V; detection potential: (A) +0.6 V, (B) +0.7 V, (C) +0.9 V, and (D) +0.8 V (versus Ag/AgCl wire). Reprinted with permission from [184] Copyright 2004 American Chemical Society.

of glucose, sucrose and fructose could be perfectly separated within 20 min.

MWCNTs were mixed with epoxy to fabricate a microdisk electrode used as a detector in a specially designed miniaturized CE–amperometric detection system for the separation and detection of several bioactive thiols [184]. The great advantage of this approach was its rapidity, which can be appreciated via the fact that the thiols of interest (homocysteine, cysteine, glutathione, and N-acetylcysteine) were detected within 130 s using phosphate buffer as a BGE. The end-channel CNT amperometric detector offers favorable signal-to-noise characteristics at a relatively low potential (0.8 V) for detection of thiol compounds.

The potential of MWCNTs was confirmed by Crevillen et al. [185], who reported the development of carbon nanotube disposable detectors in microchip CE for determination of water-soluble vitamins. The authors tested a glassy carbon electrode and screen-printed electrode modified with MWCNTs. The screen-printed electrode provided better analytical performance for vitamin analysis (detecting pyridoxine, ascorbic acid, and folic acid).

Another type of electrode, i.e., a gold one, was modified with SWCNTs [186]. The modified gold electrode displayed greatly improved sensitivity and separation resolution compared with the bare gold electrode, thus reflecting the electrocatalytic activity of SWCNTs. The SWCNT/Au electrode exhibits low background noise levels and was found suitable for determining aminophenols and neurotransmitters.

Wei et al. [187] published a paper describing the development and application of a novel carbon-nanotube-alginate composite-modified electrode as a sensitive amperometric detector for CE. The performance of this CNT-based detector was demonstrated by separation and detection of five caffeic acid derivatives. Carbon nanotubes also can be modified by poly(methyl methacrylate) to create a CNT/PMMA electrode as a sensitive amperometric detector for microchip CE, and this design was applied for detection of phenolic

pollutants and purities [188]. The preparation of CNT/copper composite electrodes based on co-mixing CNT and Cu powders within mineral oil has been described as well [189]. The published results suggest that the CNT/Cu composite electrode detector displays enhanced sensitivity compared with detectors based on copper or CNTs alone. This result could be related to specific properties of copper on the surfaces of the various types of electrodes [190–192]. One can conclude that significant improvements in the performance of a CE microchip with an electrochemical detector are observed using a CNT-modified working electrode. The CNT-modified electrode allows CE amperometric detection at significantly lower operating potentials and yields substantially enhanced signal-to-noise characteristics [184], as shown in Fig. 6.

Another published report describes the fabrication and application of a novel graphene/poly(urea-formaldehyde) composite-modified platinum disk electrode as a sensitive amperometric detector for CE. To demonstrate its feasibility and performance, this disk electrode was coupled with CE for separation and detection of salidroside and tyrosol in *Rhodiola rosea*, a traditional Chinese medicinal plant [193]. A summary of detection approaches based on application of nms is given in Table 2.

4 Conclusion and future perspective

Since its discovery, electrophoresis has benefited from the presence of various types of media, such as paper or gel, which offer additional means of separation. In addition, since the separations were transferred to capillary and microfluidic formats, the addition of a “stationary phase”, sieving media or pseudostationary phase has broadened the portfolio of applications. This advance enabled the development of several members of the family of electrophoretic methods, including capillary electrochromatography or capillary micellar electrokinetic chromatography.

Table 2. Summary of detection methods that use nms

| NPs | Detection mode | Detection detail | Analytes | LOD | Ref. |
|-----------------------------|---------------------------|---|---|--|-------|
| <i>Carbon Nanomaterials</i> | | | | | |
| MWCNTs | Amperometric | CNT-modified screen printed electrode | Hydrazines, dopamine, catechol, ascorbic acid, phenols, purines | 6.9 μM for dopamine 7.9 μM for catechol | [184] |
| MWCNTs | Amperometric | CNT-copper composite | glucitol, glucose, gluconic acid, and glucuronic acid, arginine, histidine, glycine | 20 μM for glucose and 25 μM for gluconic acid | [189] |
| MWCNTs | Amperometric | CNT-copper wire electrode | homocysteine, cysteine, glutathione, N-acetylcysteine | 0.75–3.3 μM | [184] |
| MWCNTs | Voltammetric | Paste electrode | dopac, ascorbic acid, dopamine, norepinephrine, epinephrine | 0.9–24 μM | [181] |
| SWCNTs | Amperometric | CNT-gold electrode | p-aminophenol, o-aminophenol, dopamine | 106 mM for p-aminophenol 0.011 μM | [186] |
| MWCNTs | Amperometric | - | 2,6-dimethylphenol, phenol, 2-naphthol, 4-chlorophenol, pentachlorophenol, 2,4-chlorophenol, 3-nitrophenol, 4-nitrophenol | | [188] |
| MWCNTs | Electro-chemiluminescence | Ru(bpy) ₃ ²⁺ / MWCNTs paste electrode | Tri-n-propylamine | 5 nm | [163] |
| MWCNTs | Amperometric | CNT-alginate composite | protocatechuic aldehyde, salvanolic acid A, salvanolic acid B, caffeic acid, protocatechuic acid | 0.18–3.45 μM | [187] |
| MWCNTs | Amperometric | Glassy carbon electrode and screen-printed electrode | pyridoxine, ascorbic acid, folic acid | 8–11 μM | [185] |
| MWCNTs | Amperometric | CNT-poly(ethylene terephthalate) | 5,7-dihydroxychromone, luteolin | 0.093 for 5,7-dihydroxychromone 0.10 μM for luteolin | [194] |

(Continued)

Table 2. Continued

| NPs | Detection mode | Detection detail | Analytes | LOD | Ref. |
|--|--|---|---|--|-------|
| graphene | Amperometric | Graphene/poly(ureaformaldehyde) composite | Salidroside, tyrosol | 0.24 μM for salidroside 0.28 μM for tyrosol | [193] |
| graphene-based nms | Amperometric | Graphene microparticles and graphene oxide electrode | dopamine, catechol, 2,4,6-trinitrotoluene, 2,4-dinitrotoluene, 1,3-dinitrobenzene | - | [195] |
| <i>Quantum dots</i> QD-streptavidin | LIF | 473/525 nm | conjugation between QD-mouse monoclonal anti-human IgM and human IgM | 14.2 nm | [196] |
| CdSe/ZnS and CdTe QDs | FRET | 420/532, 632 nm | conjugation between mouse IgG and goat anti-mouse IgG | - | [148] |
| CdTe/CdS QDs | LIF (QDs coated capillary) | 473/532 nm | organophosphorus pesticides | 50–180 $\mu\text{g}/\text{kg}$ | [146] |
| CdTe-MPA QDs | LIF | 473/568 nm | Acrylamide | 0.1 mg/kg | [138] |
| CdSe/ZnS QDs | Distance dependence of metal-enhanced fluorescence | 420/474 nm | DNA fragments | 19.6 pg | [149] |
| AuNPs | LIF | 488/610 nm | conjugation of QD-anti-ovalbumin with ovalbumin | - | [197] |
| CdTe-MPA QDs | LIF | Indirect LIF detection | thiamethoxam, acetamiprid, imidacloprid residues | 0.009–0.05 mg/kg | [143] |
| CdTe QDs | LIF | Indirect LIF detection, 488/520 nm | loxacin, enrofloxacin, ciprofloxacin, lomefloxacin, and norfloxacin | 0.003–0.008 mg/kg | [145] |
| CdTe-TGA QDs | LIF | Fluorescence of QD-IgG-Cy5 probe is quenched by protein A 420/612, 670 nm | protein A | - | [141] |
| CdSe/ZnS-GSH QDs | FRET | | | | |

(Continued)

Table 2. Continued

| NPs | Detection mode | Detection detail | Analytes | LOD | Ref. |
|----------------------------|---------------------------|--|--|-----------|-------|
| <i>Metal nanoparticles</i> | | | | | |
| AuNPs | Electro-chemiluminescence | Tris(2,2'-bipyridyl) ruthenium(II) (Ru(bpy) ₃ ²⁺) | roxithromycin | 84 nm | [161] |
| AuNPs | Chemiluminescence | Reaction between luminol and hydrogen peroxide | uric acid | 0.046 μM | [153] |
| AuNPs | ICP-MS | - | albumin | 0.5 pM | [198] |
| AuNPs | Electrochemiluminescence | Oxidation of substrate (OAP) with H ₂ O ₂ catalyzed by HRP | DNA fragments | 9.3 pM | [199] |
| AuNPs | Chemiluminescence | AuNPs-catalyzed CL reaction of luminol and hydrogen peroxide | AuNPs-goat-anti-human IgG interaction with human IgG | 7.1 pM | [200] |
| AuNPs | Chemiluminescence | Reaction between luminol and hydrogen peroxide | thrombin | 13.5 fM | [201] |
| AuNPs | Chemiluminescence | Reaction between luminol and hydrogen peroxide catalyzed by antibody-AuNP-G-quadruplex/hemin probe | CA19-9 | 0.016U/mL | [202] |
| PNPs | Amperometric | PtNPs-carbon fiber micro-disk electrode | ascorbic acid | 0.5 μM | [203] |

AuNPs – Gold nanoparticles; CA19-9 – Cancer Antigen 19-9; CL – Chemiluminescence; CNT – Carbon nanotubes; FRET – Förster resonance energy transfer; GSH – Glutathione; HRP – Horseradish peroxidase; ICP-MS – Inductively coupled plasma mass spectrometry; IgG – Immunoglobulin G; IgM – Immunoglobulin M; LIF – Laser-induced fluorescence detection; MPA – 3-Mercaptopropionic acid; MWCNTs – Multi-walled carbon nanotubes; NPs – Nanoparticles; nms – Nanomaterials; OAP – o-aminophenol; QD – Quantum Dots; SWCNTs – Single-walled carbon nanotubes; TGA – Thioglycolic acid.

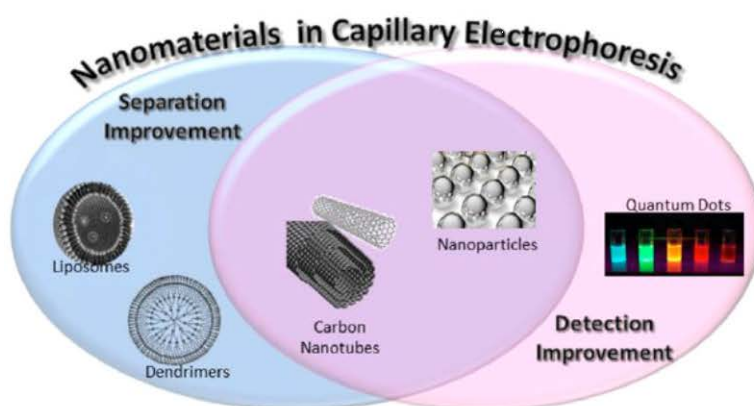


Figure 7. Schematic classification of nanomaterials according to their application in improving a particular CE performance parameter.

Especially in these electrophoretic techniques, the application of nanomaterials provides additional interactions with the sample components and therefore improves the separation performance.

Despite the great advantages provided by the family of electromigration techniques, these methods also display weaknesses that include robustness and repeatability of measurements, which, with the sole exception of the case of DNA sequencers, constitute obstacles to the use of capillary electrophoretic techniques in clinical practice. The use of nanomaterials in electromigration methods offers new perspectives in the field of clinical use because these advanced materials can lower detection limits while simultaneously enhancing separation effectiveness. The combination of the miniaturization potential of CE with the abilities of NMs to improve the overall performance might increase the possibility of development and practical application of a portable and cost-effective device that is applicable in point-of-care areas suitable for personalized diagnostics.

From the viewpoint of CE, we have shown that NMs such as liposomes and dendrimers are able to improve the separation step of CE analysis, and QDs can significantly improve the detection step. Even though, several members of the nanomaterial family, in particular carbon nanotubes and metal nanoparticles, can improve both of these steps (Fig. 7). At the same time, CE represents a group of effective techniques for nm characterization, evaluation, and observation. In this paper, we have demonstrated that nanoparticles have various natures and that nanoparticles, carbon nanomaterials, liposomes, and dendrimers can be characterized by CE in terms of one or more parameters, such as their size, surface chemistry, and interaction abilities. Such symbiosis of CE and nms is beneficial for analytical chemists and material scientists as well as biochemists and molecular biologists because it leads to the development of new, more effective and more sensitive methods.

In our opinion, it is highly improbable that nanomaterials will completely replace such well-established approaches as organic dyes for fluorescent labeling. Nevertheless, nanomaterials offer new possibilities and options for a wide range of

applications. The electrochemical detection modes especially benefit from applications of nms that enable increasingly sensitive detection. Moreover, in combination with advances in microfluidics, the separation power of electrophoretic analysis, which is further enhanced by nanomaterial-based stationary and pseudostationary phases, promises increasingly effective analyses of complex biological samples.

Financial support was provided by Grant agency of Czech Republic (GACR 16–23647Y) and project CEITEC 2020 (LQ1601) with financial support from the Ministry of Education, Youth and Sports of the Czech Republic under the National Sustainability Programme II.

The authors have declared no conflict of interest.

5 References

- [1] Pumera, M., *Chem. Commun.* 2011, 47, 5671–5680.
- [2] Huang, X. H., Coleman, W. F., Zare, R. N., 1989, 480, 95–110.
- [3] Kist, T. B. L., Mandaji, M., *Electrophoresis* 2004, 25, 3492–3497.
- [4] Lin, Y. W., Huang, M. F., Chang, H. T., *Electrophoresis* 2005, 26, 320–330.
- [5] Nilsson, C., Birnbaum, S., Nilsson, S., *J. Chromatogr. A* 2007, 1168, 212–224.
- [6] Sebestik, J., Niederhafner, P., Jezek, J., *Amino Acids* 2011, 40, 301–370.
- [7] Pauwels, J., Van Schepdael, A., *Cent. Eur. J. Chem.* 2012, 10, 785–801.
- [8] Duan, A. H., Xie, S. M., Yuan, L. M., *Trac-Trends Anal. Chem.* 2011, 30, 484–491.
- [9] Nilsson, C., Birnbaum, S., Nilsson, S., *Electrophoresis* 2011, 32, 1141–1147.
- [10] Chang, C. L., Wang, X., Bai, Y., Liu, H. W., *Trac-Trends Anal. Chem.* 2012, 39, 195–206.
- [11] Li, H. F., Zeng, H. L., Chen, Z. F., Lin, J. M., *Electrophoresis* 2009, 30, 1022–1029.

- [12] Moliner-Martinez, Y., Cardenas, S., Valcarcel, M., *Electrophoresis* 2007, 28, 2573–2579.
- [13] Geng, L., Bo, T., Liu, H. W., Li, N., Liu, F., Li, K., Gu, J. L., Fu, R. N., *Chromatographia* 2004, 59, 65–70.
- [14] Li, M., Liu, X., Jiang, F. Y., Guo, L. P., Yang, L., *J. Chromatogr. A* 2011, 1218, 3725–3729.
- [15] Chen, X., Rao, J. A., Wang, J., Gooding, J. J., Zou, G., Zhang, Q. J., *Chem. Commun.* 2011, 47, 10317–10319.
- [16] Lu, J. Y., Ye, F. G., Zhang, A. Z., Wei, Z., Peng, Y., Zhao, S. L., *J. Sep. Sci.* 2011, 34, 2329–2336.
- [17] Liang, R. P., Liu, C. M., Meng, X. Y., Wang, J. W., Qiu, J. D., *J. Chromatogr. A* 2012, 1266, 95–102.
- [18] Stefan-van Staden, R. I., Bokretsiion, R. G., *Anal. Methods* 2012, 4, 1492–1497.
- [19] Su, H. Y., Zheng, Q. L., Li, H. B., *J. Mater. Chem.* 2012, 22, 6546–6548.
- [20] Na, N., Hu, Y. P., Ouyang, J., Baeyens, W. R. G., Delanghe, J. R., De Beer, T., *Anal. Chim. Acta* 2004, 527, 139–147.
- [21] Na, N., Hu, Y. P., Jin, O. Y., Baeyens, W. R. G., Delanghe, J. R., Taes, Y. E. C., Xie, M. X., Chen, H. Y., Yang, Y. P., *Talanta* 2006, 69, 866–872.
- [22] Yang, L., Chen, C. J., Liu, X., Shi, J., Wang, G. A., Zhu, L. D., Guo, L. P., Glennon, J. D., Scully, N. M., Doherty, B. E., *Electrophoresis* 2010, 31, 1697–1705.
- [23] Quirino, J. P., Terabe, S., *J. Chromatogr. A* 1999, 856, 465–482.
- [24] Li, H., Ding, G. S., Chen, J., Tang, A. N., *J. Chromatogr. A* 2010, 1217, 7448–7454.
- [25] Takeda, Y., Hayashi, Y., Utamura, N., Takamoto, C., Kinoshita, M., Yamamoto, S., Hayakawa, T., Suzuki, S., *J. Chromatogr. A* 2016, 1427, 170–176.
- [26] Guo, Y., Qin, W., 2014, 35, 3549–3555.
- [27] Sun, W., Dong, Y., Cui, H., Zhao, H., He, Y., Ding, Y., Li, X., Yuan, Z., 2014, 77, 821–828.
- [28] Gong, Z.-S., Duan, L.-P., Tang, A.-N., 2015, 182, 1297–1304.
- [29] Kuo, I. T., Huang, Y. F., Chang, H. T., *Electrophoresis* 2005, 26, 2643–2651.
- [30] Wang, Y. Q., Baeyens, W. R. G., Huang, C. G., Fei, G. T., He, L., Ouyang, J., *Talanta* 2009, 77, 1667–1674.
- [31] Liu, F. J., Ding, G. S., Tang, A. N., *Food Chem.* 2014, 145, 109–114.
- [32] Yan, X. H., Ding, G. S., Li, H., Tang, A. N., *Electrophoresis* 2011, 32, 1357–1363.
- [33] Liu, D. N., Wang, J., Guo, Y. G., Yuan, R. J., Wang, H. F., Bao, J. J., *Electrophoresis* 2008, 29, 863–870.
- [34] Hui, L. J., Ma, Y., *Chromatographia* 2011, 73, 507–515.
- [35] Qin, W. D., *Electrophoresis* 2007, 28, 3017–3023.
- [36] Zhou, S. S., Wang, Y. Q., De Beer, T., Baeyens, W. R. G., Fei, G. T., Dilinuer, M., Ouyang, J., *Electrophoresis* 2008, 29, 2321–2329.
- [37] Kwon, H., Kim, Y., *Bull. Korean Chem. Soc.* 2009, 30, 297–301.
- [38] Liu, F. K., Chang, Y. C., *Chromatographia* 2010, 72, 1129–1135.
- [39] Chiou, S. H., Huang, M. F., Chang, H. T., *Electrophoresis* 2004, 25, 2186–2192.
- [40] Huang, M. F., Huang, C. C., Chang, H. T., *Electrophoresis* 2003, 24, 2896–2902.
- [41] Chen, Y. L., Shih, C. J., Ferrance, J., Chang, Y. S., Chang, J. G., Wu, S. M., *J. Chromatogr. A* 2009, 1216, 1206–1212.
- [42] Huang, M. F., Kuo, Y. C., Huang, C. C., Chang, H. T., *Anal. Chem.* 2004, 76, 192–196.
- [43] Subramaniam, V., Griffith, L., Haes, A. J., *Analyst* 2011, 136, 3469–3477.
- [44] Nilsson, C., Becker, K., Harwigsson, I., Bulow, L., Birnbaum, S., Nilsson, S., *Anal. Chem.* 2009, 81, 315–321.
- [45] Palmer, C. P., Hilder, E. F., Quirino, J. P., Haddad, P. R., *Anal. Chem.* 2010, 82, 4046–4054.
- [46] Palmer, C. P., Keeffer, A., Hilder, E. F., Haddad, P. R., *Electrophoresis* 2011, 32, 588–594.
- [47] Breadmore, M. C., Macka, M., Haddad, P. R., 1999, 20, 1987–1992.
- [48] Viberg, P., Jornten-Karlsson, M., Petersson, P., Spegel, P., Nilsson, S., *Anal. Chem.* 2002, 74, 4595–4601.
- [49] Malmstrom, D., Axen, J., Bergquist, J., Viberg, P., Spegel, P., *Electrophoresis* 2011, 32, 261–267.
- [50] Spegel, P., Schweitz, L., Nilsson, S., *Anal. Chem.* 2003, 75, 6608–6613.
- [51] Moliner-Martinez, Y., Cardenas, S., Simonet, B. M., Valcarcel, M., *Electrophoresis* 2009, 30, 169–175.
- [52] Treubig, J. M., Brown, P. R., *J. Chromatogr. A* 2000, 873, 257–267.
- [53] Sun, Y. M., Bi, Q., Zhang, X. L., Wang, L. T., Zhang, X., Dong, S. Q., Zhao, L., *Anal. Biochem.* 2016, 500, 38–44.
- [54] Wang, Z. H., Luo, G. A., Chen, J. F., Xiao, S. F., Wang, Y. M., *Electrophoresis* 2003, 24, 4181–4188.
- [55] Jimenez-Soto, J. M., Moliner-Martinez, Y., Cardenas, S., Valcarcel, M., *Electrophoresis* 2010, 31, 1681–1688.
- [56] Huang, Y. J., Wang, G. R., Huang, K. P., Hsieh, Y. F., Liu, C. Y., *Electrophoresis* 2009, 30, 3964–3970.
- [57] Xiong, X., Ouyang, J., Baeyens, W. R. G., Delanghe, J. R., Shen, X. M., Yang, Y. P., *Electrophoresis* 2006, 27, 3243–3253.
- [58] Hou, J. Y., Li, G., Wei, Y. Q., Lu, H., Jiang, C., Zhou, X. T., Meng, F. Y., Cao, J., Liu, J. X., *J. Chromatogr. A* 2014, 1343, 174–181.
- [59] Su, M.-Y., Chen, Y.-Y., Yang, J.-Y., Lin, Y.-S., Lin, Y.-W., Liu, M.-Y., 2014, 35, 978–985.
- [60] Xu, Y., Li, S. F. Y., *Electrophoresis* 2006, 27, 4025–4028.
- [61] Nilsson, C., Harwigsson, I., Birnbaum, S., Nilsson, S., *Electrophoresis* 2010, 31, 1773–1779.
- [62] Ohlsson, P., Ordeig, O., Nilsson, C., Harwigsson, I., Kutter, J. P., Nilsson, S., *Electrophoresis* 2010, 31, 3696–3702.
- [63] Corradini, D., Mancini, G., Bello, C., *Chromatographia* 2004, 60, S125–S132.
- [64] Corradini, D., Mancinia, G., Bello, C., *J. Chromatogr. A* 2004, 1051, 103–110.

- [65] Montealegre, C., Rasines, B., Gomez, R., de la Mata, F. J., Garcia-Ruiz, C., Marina, M. L., *J. Chromatogr. A* 2012, **1234**, 16–21.
- [66] Mould, D. L., Syngé, R. L. M., 1952, **77**, 964–969.
- [67] Pretorius, V., Hopkins, B. J., Schieke, J. D., 1974, **99**, 23–30.
- [68] Altria, K. D., *J. Chromatogr. A* 1999, **856**, 443–463.
- [69] Cikalo, M. G., Bartle, K. D., Robson, M. M., Myers, P., Euerby, M. R., *Analyst* 1998, **123**, 87R–102R.
- [70] Colon, L. A., Reynolds, K. J., Alicea-Maldonado, R., Fermier, A. M., *Electrophoresis* 1997, **18**, 2162–2174.
- [71] Dermaux, A., Sandra, P., *Electrophoresis* 1999, **20**, 3027–3065.
- [72] Robson, M. M., Cikalo, M. G., Myers, P., Euerby, M. R., Bartle, K. D., *J. Microcolumn Sep.* 1997, **9**, 357–372.
- [73] Kapnissi-Christodoulou, C. P., Zhu, X. F., Warner, I. M., *Electrophoresis* 2003, **24**, 3917–3934.
- [74] Hu, W., Hong, T., Gao, X., Ji, Y., 2014, **61**, 29–39.
- [75] Tsuda, T., Nomura, K., Nakagawa, G., 1982, **248**, 241–247.
- [76] Guihen, E., Glennon, J. D., *J. Chromatogr. A* 2004, **1044**, 67–81.
- [77] Nilsson, C., Viberg, P., Spegel, P., Jornten-Karlsson, M., Petersson, P., Nilsson, S., *Anal. Chem.* 2006, **78**, 6088–6095.
- [78] Spegel, P., Viberg, P., Carlstedt, J., Petersson, P., Jornten-Karlsson, M., *J. Chromatogr. A* 2007, **1154**, 379–385.
- [79] Hamer, M., Yone, A., Rezzano, I., *Electrophoresis* 2012, **33**, 334–339.
- [80] Liu, F. K., Hsu, Y. T., Wu, C. H., *J. Chromatogr. A* 2005, **1083**, 205–214.
- [81] Miksik, I., Lacinova, K., Zmatlikova, Z., Sedlakova, P., Kral, V., Sykora, D., Rezanka, P., Kasicka, V., *J. Sep. Sci.* 2012, **35**, 994–1002.
- [82] O'Mahony, T., Owens, V. P., Murrhy, J. P., Guihen, E., Holmes, J. D., Glennon, J. D., *J. Chromatogr. A* 2003, **1004**, 181–193.
- [83] Qu, Q. S., Liu, D. P., Mangelings, D., Yang, C., Hu, X. Y., *J. Chromatogr. A* 2010, **1217**, 6588–6594.
- [84] Qu, Q. S., Zhang, X. X., Shen, M., Liu, Y., Hu, X. Y., Yang, G. J., Wang, C. Y., Zhang, Y. K., Yan, C., *Electrophoresis* 2008, **29**, 901–909.
- [85] Rezanka, P., Navratilova, K., Zvatora, P., Sykora, D., Matejka, P., Miksik, I., Kasicka, V., Kral, V., *J. Nanopart. Res.* 2011, **13**, 5947–5957.
- [86] Yang, L., Guihen, E., Glennon, J. D., *J. Sep. Sci.* 2005, **28**, 757–766.
- [87] Yang, L., Guihen, E., Holmes, J. D., Loughran, M., O'Sullivan, G. P., Glennon, J. D., *Anal. Chem.* 2005, **77**, 1840–1846.
- [88] Neiman, B., Grushka, E., Lev, O., *Anal. Chem.* 2001, **73**, 5220–5227.
- [89] Zheng, J. W., Zhu, Z. H., Chen, H. F., Liu, Z. F., *Langmuir* 2000, **16**, 4409–4412.
- [90] Wang, H. Y., Knobel, G., Wilson, W. B., Calimag-Williams, K., Campiglia, A. D., *Electrophoresis* 2011, **32**, 720–727.
- [91] Pumera, M., Wang, J., Grushka, E., Polsky, R., *Anal. Chem.* 2001, **73**, 5625–5628.
- [92] Yu, C. J., Su, C. L., Tseng, W. L., *Anal. Chem.* 2006, **78**, 8004–8010.
- [93] Liu, Q., Yao, L. H., Shen, Q. P., Nie, Z., Guo, M. L., Yao, S. Z., *Chem.-Eur. J.* 2009, **15**, 12828–12836.
- [94] Yan, H. T., Li, T., Guo, Y. L., *Chin. J. Chem.* 2009, **27**, 759–762.
- [95] Kleindienst, G., Huber, C. G., Gjerde, D. T., Yengoyan, L., Bonn, G. K., *Electrophoresis* 1998, **19**, 262–269.
- [96] Wang, D. M., Song, X. J., Duan, Y., Xu, L., Zhou, J., Duan, H. Q., *Electrophoresis* 2013, **34**, 1339–1342.
- [97] Hsieh, Y. L., Chen, T. H., Liu, C. Y., *Electrophoresis* 2006, **27**, 4288–4294.
- [98] Li, T., Xu, Y., Feng, Y. Q., *J. Liq. Chromatogr. Relat. Technol.* 2009, **32**, 2484–2498.
- [99] Hsieh, Y. L., Chen, T. H., Liu, C. P., Liu, C. Y., *Electrophoresis* 2005, **26**, 4089–4097.
- [100] Lee, C. H., Huang, B. Y., Chen, Y. C., Liu, C. P., Liu, C. Y., *Analyst* 2011, **136**, 1481–1487.
- [101] Ohno, T., Matsuda, T., Suzuki, H., Fujimoto, M., *Adv. Powder Technol.* 2006, **17**, 167–179.
- [102] Dong, X. L., Wu, R. A., Dong, J., Wu, M. H., Zhu, Y., Zou, H. F., *Electrophoresis* 2008, **29**, 3933–3940.
- [103] Diao, X. F., Zhang, F. F., Yang, B. C., Liang, X. M., Ke, Y. X., Chu, X. G., *J. Chromatogr. A* 2012, **1267**, 127–130.
- [104] Liu, Z., Wu, R., Zou, H. F., 2002, **23**, 3954–3972.
- [105] Zhang, S. S., Macka, M., Haddad, P. R., 2006, **27**, 1069–1077.
- [106] Guo, Y., Meng, L., Zhang, Y., Tang, W., Zhang, W., Xia, Y., Ban, F., Wu, N., Zhang, S., 2013, **942**, 151–157.
- [107] Zhang, Y., Yang, L., Tian, X., Guo, Y., Tang, W., Yu, A., Zhang, W., Sun, B., Zhang, S., 2015, **70**, 885–891.
- [108] Kitagawa, F., Sudaki, H., Sueyoshi, K., Otsuka, K., *Anal. Sci.* 2013, **29**, 107–112.
- [109] Zhu, Y. X., Zhou, C. R., Qin, S. S., Ren, Z. Y., Zhang, L. Y., Fu, H. G., Zhang, W. B., 2012, **33**, 340–347.
- [110] Zhang, L. Y., Zhu, Y. X., Zhang, W. B., *Acta Chim. Sin.* 2013, **71**, 62–68.
- [111] Wang, W., Xiao, X., Chen, J., Jia, L., 2015, **1411**, 92–100.
- [112] Sombra, L., Moliner-Martinez, Y., Cardenas, S., Valcarcel, M., *Electrophoresis* 2008, **29**, 3850–3857.
- [113] Chen, J. L., Hsieh, K. H., *Electrophoresis* 2010, **31**, 3937–3948.
- [114] Chen, J. L., Lu, T. L., Lin, Y. C., *Electrophoresis* 2010, **31**, 3217–3226.
- [115] Chen, J. L., *J. Chromatogr. A* 2010, **1217**, 715–721.
- [116] Stege, P. W., Lapierre, A. V., Martinez, L. D., Messina, G. A., Sombra, L. L., *Talanta* 2011, **86**, 278–283.
- [117] Goswami, S., Bajwa, N., Asuri, P., Ci, L. J., Ajayan, P. M., Cramer, S. M., *Chromatographia* 2009, **69**, 473–480.
- [118] Mogensen, K. B., Chen, M., Molhave, K., Boggild, P., Kutter, J. P., *Lab Chip* 2011, **11**, 2116–2118.

- [119] Yu, B., Shu, X., Cong, H. L., Chen, X., Liu, H. W., Yuan, H., Chi, M., *J. Chromatogr. A* 2016, **1437**, 226–233.
- [120] Qu, Q. S., Gu, C. H., Hu, X. Y., *Anal. Chem.* 2012, **84**, 8880–8890.
- [121] Liu, X., Liu, X. L., Li, M., Guo, L. P., Yang, L., *J. Chromatogr. A* 2013, **1277**, 93–97.
- [122] Bilek, G., Kremser, L., Blaas, D., Kenndler, E., *J. Chromatogr. B* 2006, **841**, 38–51.
- [123] Ornskov, E., Ullsten, S., Soderberg, L., Markides, K. E., Folestad, S., *Electrophoresis* 2002, **23**, 3381–3384.
- [124] Manetto, G., Bellini, M. S., Deyl, Z., *J. Chromatogr. A* 2003, **990**, 281–289.
- [125] Hautala, J. T., Linden, M. V., Wiedmer, S. K., Ryhanen, S. J., Saily, M. J., Kinnunen, P. K. J., Riekkola, M. L., *J. Chromatogr. A* 2003, **1004**, 81–90.
- [126] Wiedmer, S. K., Jussila, M., Hakala, R. M. S., Pystynen, K. H., Riekkola, M. L., *Electrophoresis* 2005, **26**, 1920–1927.
- [127] Mei, J., Xu, J. R., Xiao, Y. X., Liao, X. Y., Qiu, G. F., Feng, Y. Q., *Electrophoresis* 2008, **29**, 3825–3833.
- [128] Mei, J., Tian, Y. P., He, W., Xiao, Y. X., Wei, J. A., Feng, Y. Q., *J. Chromatogr. A* 2010, **1217**, 6979–6986.
- [129] Hautala, J. T., Wiedmer, S. K., Riekkola, M. L., *Anal. Bioanal. Chem.* 2004, **378**, 1769–1776.
- [130] Shou, C. Q., Xing, X. X., Kang, J. F., Zhang, Z. L., Song, N. J., Pan, S., *Chin. J. Anal. Chem.* 2008, **36**, 167–171.
- [131] Shou, C. Q., Kang, J. F., Song, N. J., *Chin. J. Anal. Chem.* 2008, **36**, 297–300.
- [132] Stage, P. W., Sombra, L. L., Messina, G., Martinez, L. D., Silya, M. F., *Electrophoresis* 2010, **31**, 2242–2248.
- [133] Lin, Y. W., Huang, M. J., Chang, H. T., *J. Chromatogr. A* 2003, **1014**, 47–55.
- [134] You, J., Zhao, L. G., Wang, G. W., Zhou, H. T., Zhou, J. P., Zhang, L. N., *J. Chromatogr. A* 2014, **1343**, 160–166.
- [135] Li, X. J., Fu, Q. F., Zhang, Q. H., Jiang, X. M., Yang, F. Q., Wei, W. L., Xia, Z. N., *Anal. Methods* 2015, **7**, 8227–8234.
- [136] Back, S. K., Kang, C., Kim, Y., *Bull. Korean Chem. Soc.* 2006, **27**, 133–136.
- [137] Swinney, K., Bornhop, D. J., *Electrophoresis* 2000, **21**, 1239–1250.
- [138] Chen, Q. D., Zhao, W. F., Fung, Y. S., *Electrophoresis* 2011, **32**, 1252–1257.
- [139] Bai, Y., Du, F. Y., Yang, Y. Y., Liu, H. W., *J. Sep. Sci.* 2011, **34**, 2893–2900.
- [140] Guo, D. S., Chen, G. H., Tong, M. Z., Wu, C. Q., Fang, R., Yi, L. X., *Chin. J. Anal. Chem.* 2012, **40**, 1379–1384.
- [141] Qiu, L., Bi, Y. H., Wang, C. L., Li, J. Y., Guo, P. L., Li, J. C., He, W. J., Wang, J. H., Jiang, P. J., *Int. J. Mol. Sci.* 2014, **15**, 1804–1811.
- [142] Guo, D.-S., Chen, G.-H., Tong, M.-Z., Wu, C.-Q., Fang, R., Yi, L.-X., 2012, **40**, 1379–1384.
- [143] Chen, G. H., Sun, J., Dai, Y. J., Dong, M., *Electrophoresis* 2012, **33**, 2192–2196.
- [144] Tang, T. T., Deng, J. J., Zhang, M., Shi, G. Y., Zhou, T. S., *Talanta* 2016, **146**, 55–61.
- [145] Meng, H. L., Chen, G. H., Guo, X., Chen, P., Cai, Q. H., Tian, Y. F., *Anal. Bioanal. Chem.* 2014, **406**, 3201–3208.
- [146] Chen, Q. D., Fung, Y. S., *Electrophoresis* 2010, **31**, 3107–3114.
- [147] Zhang, C. Y., Johnson, L. W., *Anal. Chem.* 2006, **78**, 5532–5537.
- [148] Li, Y. Q., Wang, J. H., Zhang, H. L., Yang, J., Guan, L. Y., Chen, H., Luo, Q. M., Zhao, Y. D., *Biosens. Bioelectron.* 2010, **25**, 1283–1289.
- [149] Li, Y. Q., Guan, L. Y., Zhang, H. L., Chen, J., Lin, S., Ma, Z. Y., Zhao, Y. D., *Anal. Chem.* 2011, **83**, 4103–4109.
- [150] Giokas, D. L., Vlessidis, A. G., Tsogas, G. Z., Evmiridis, N. P., *Trac-Trends Anal. Chem.* 2010, **29**, 1113–1126.
- [151] Zhang, Z. F., Cui, H., Lai, C. Z., Liu, L. J., *Anal. Chem.* 2005, **77**, 3324–3329.
- [152] Jiang, J., Zhao, S. L., Huang, Y., Qin, G. X., Ye, F. G., *J. Chromatogr. A* 2013, **1282**, 161–166.
- [153] Zhao, S. L., Lan, X. H., Liu, Y. M., *Electrophoresis* 2009, **30**, 2676–2680.
- [154] Liu, Q. C., Wu, J. Q., Tian, J., Zhang, C. L., Gao, J. J., Latep, N., Ge, Y., Qin, W. D., *Talanta* 2012, **97**, 193–198.
- [155] Zhao, Y., Zhao, S., Huang, J., Ye, F., 2011, **85**, 2650–2654.
- [156] Guo, L. H., Fu, F., Chen, G. N., *Anal. Bioanal. Chem.* 2011, **399**, 3323–3343.
- [157] Qi, H. L., Peng, Y., Gao, Q., Zhang, C. X., *Sensors* 2009, **9**, 674–695.
- [158] Huang, H. P., Li, J. J., Zhu, J. J., *Anal. Methods* 2011, **3**, 33–42.
- [159] Bertocello, P., Forster, R. J., *Biosens. Bioelectron.* 2009, **24**, 3191–3200.
- [160] Liu, Y. J., Pan, W., Liu, Q., Yao, S. Z., 2005, **26**, 4468–4477.
- [161] Wang, J. W., Yang, Z. M., Wang, X. X., Yang, N. J., *Talanta* 2008, **76**, 85–90.
- [162] Duan, H. B., Cao, J. T., Wang, H., Liu, Y. M., *RSC Adv.* 2016, **6**, 45533–45539.
- [163] Chen, Y., Lin, Z., Chen, J., Sun, J., Zhang, L., Chen, G., *J. Chromatogr. A* 2007, **1172**, 84–91.
- [164] Prikryl, J., Kleparnik, K., Foret, F., *J. Chromatogr. A* 2012, **1226**, 43–47.
- [165] Elbashir, A. A., Aboul-Enein, H. Y., 2010, **24**, 1038–1044.
- [166] Elbashir, A. A., Aboul-Enein, H. Y., 2012, **26**, 990–1000.
- [167] Kuban, P., Hauser, P. C., 2004, **16**, 2009–2021.
- [168] Zemann, A. J., 2003, **24**, 2125–2137.
- [169] Erdem, A., *Talanta* 2007, **74**, 318–325.
- [170] Liu, X. G., Cheng, Z. Q., Fan, H., Ai, S. Y., Han, R. X., *Electrochim. Acta* 2011, **56**, 6266–6270.
- [171] Mao, X., Liu, G. D., *J. Biomed. Nanotechnol.* 2008, **4**, 419–431.
- [172] Rusling, J. F., *Chem. Rec.* 2012, **12**, 164–176.
- [173] Rusling, J. F., Sotzing, G., Papadimitrakopoulou, F., *Bioelectrochemistry* 2009, **76**, 189–194.
- [174] de Andres, F., Zougagh, M., Castaneda, G., Rios, A., *J. Chromatogr. A* 2008, **1212**, 54–60.
- [175] Songa, E. A., Waryo, T., Jahed, N., Baker, P. G. L., Kgarebe, B. V., Iwuoha, E. I., *Electroanalysis* 2009, **21**, 671–674.

- [176] Aragay, G., Merkoci, A., *Electrochim. Acta* 2012, **84**, 49–61.
- [177] Luo, X. L., Morrin, A., Killard, A. J., Smyth, M. R., *Electroanalysis* 2006, **18**, 319–326.
- [178] Pumera, M., Escarpa, A., *Electrophoresis* 2009, **30**, 3315–3323.
- [179] Chen, G., *Talanta* 2007, **74**, 326–332.
- [180] Martin, A., Lopez, M. A., Gonzalez, M. C., Escarpa, A., *Electrophoresis* 2015, **36**, 179–194.
- [181] Chicharro, M., Sanchez, A., Bermejo, E., Zapardiel, A., Rubianes, M. D., Rivas, G. A., *Anal. Chim. Acta* 2005, **543**, 84–91.
- [182] Xu, L., Guo, Q. H., Yu, H., Huang, J. S., You, T. Y., *Talanta* 2012, **97**, 462–467.
- [183] Cheng, X., Zhang, S., Zhang, H. Y., Wang, Q. J., He, P. G., Fang, Y. Z., *Food Chem.* 2008, **106**, 830–835.
- [184] Chen, G., Zhang, L. Y., Wang, J., *Talanta* 2004, **64**, 1018–1023.
- [185] Crevillen, A. G., Pumera, M., Gonzalez, M. C., Escarpa, A., *Electrophoresis* 2008, **29**, 2997–3004.
- [186] Pumera, M., Llopis, X., Merkoci, A., Alegret, S., *Microchim. Acta* 2006, **152**, 261–265.
- [187] Wei, B. G., Wang, J., Chen, Z., Chen, G., *Chem.-Eur. J.* 2008, **14**, 9779–9785.
- [188] Yao, X., Wu, H. X., Wang, J., Qu, S., Chen, G., *Chem.-Eur. J.* 2007, **13**, 846–853.
- [189] Wang, J., Chen, G., Wang, M., Chatrathi, M. P., *Analyst* 2004, **129**, 512–515.
- [190] Chomoucka, J., Drbohlavova, J., Masarik, M., Ryvolova, M., Huska, D., Prasek, J., Horna, A., Trnkova, L., Provaznik, I., Adam, V., Hubalek, J., Kizek, R., 2012, **9**, 746–783.
- [191] Jelen, F., Yosypchuk, B., Kourilova, A., Novotny, L., Palecek, E., *Anal. Chem.* 2002, **74**, 4788–4793.
- [192] Navratil, R., Pilarova, I., Jelen, F., Trnkova, L., *Int. J. Electrochem. Sci.* 2013, **8**, 4397–4408.
- [193] Chen, B., Zhang, L. Y., Chen, G., *Electrophoresis* 2011, **32**, 870–876.
- [194] Sheng, S. J., Zhang, L. Y., Chen, G., *Food Chem.* 2014, **145**, 555–561.
- [195] Chua, C. K., Ambrosi, A., Pumera, M., *Electrochem. Commun.* 2011, **13**, 517–519.
- [196] Feng, H. T., Law, W. S., Yu, L., Li, S. F. Y., *J. Chromatogr. A* 2007, **1156**, 75–79.
- [197] Kleparnik, K., Voracova, I., Liskova, M., Prikryi, J., Hezinovala, V., Foret, F., *Electrophoresis* 2011, **32**, 1217–1223.
- [198] Liu, J. M., Li, Y., Jiang, Y., Yan, X. P., *J. Proteome Res.* 2010, **9**, 3545–3550.
- [199] Cao, W., Chen, L., Fu, Y. J., Tan, Z. Y., Qu, B., *J. Sep. Sci.* 2011, **34**, 939–946.
- [200] Liu, Y. M., Mei, L., Liu, L. J., Peng, L. F., Chen, Y. H., Rei, S. W., *Anal. Chem.* 2011, **83**, 1137–1143.
- [201] Liu, Y. M., Liu, Y. Y., Zhou, M., Huang, K. J., Cao, J. T., Wang, H., Chen, Y. H., *J. Chromatogr. A* 2014, **1340**, 128–133.
- [202] Shi, M., Zhao, S. L., Huang, Y., Zhao, L. M., Liu, Y. M., *Talanta* 2014, **124**, 14–20.
- [203] Wang, X. L., Li, L. J., Li, Z. Y., Wang, J., Fu, H. Y., Chen, Z. Z., *J. Electroanal. Chem.* 2014, **712**, 139–145.
- [204] Cao, J., Dun, W. L., Qu, H. B., *Electrophoresis* 2011, **32**, 408–413.
- [205] Chen, J. L., Lin, Y. C., *Electrophoresis* 2010, **31**, 3949–3958.

Article 11

Nejdl L, Zitka J, Mravec F, Milosavljevic V, Zitka O, Kopel P, Adam V, Vaculovicova M.

Real-time monitoring of the UV-induced formation of quantum dots on a milliliter, microliter, and nanoliter scale. *Microchim Acta* 2017;184(5):1489-1497.

Real-time monitoring of the UV-induced formation of quantum dots on a milliliter, microliter, and nanoliter scale

Lukas Nejdil^{1,2} · Jan Zitka^{1,2} · Filip Mravec³ · Vedran Milosavljevic^{1,2} · Ondrej Zitka^{1,2} · Pavel Kopel^{1,2} · Vojtech Adam^{1,2} · Marketa Vaculovicova^{1,2}

Received: 28 November 2016 / Accepted: 19 February 2017 / Published online: 3 March 2017
© Springer-Verlag Wien 2017

Abstract The authors report on a systematic study on the low-cost, low-temperature, and fast synthesis of water soluble quantum dots (QDs) stabilized by mercaptosuccinic acid by UV irradiation. The effects of UV irradiation (at 254 nm and 250 nm) and temperature on the precursors (Cd:Se, Cd:Te, Cd, Zn:S, Zn:Se and Zn) are described. Best results are achieved with a mixture of precursors containing cadmium, selenium and MSA where a 10-min irradiation with 254-nm light gives CdSe QDs with a quantum yield of 13.5%. The authors also describe the preparation and monitoring of the formation of QDs in sub-mg, sub- μ g and sub-ng quantities, the smallest concentration being 258 pg in volume of 4 nL. The growth of the QDs can be monitored in real time by absorption, fluorescence and dynamic light scattering. The solutions of the particles also are characterized by fluorescence correlation spectroscopy and detected by LED-induced fluorescence. The preparation of such QDs by UV radiation is simple, easily controllable, and inexpensive. Conceivably, it can be integrated with lab-on-chip, micro total analysis systems or other instrumentation.

Keywords Nanocrystal · Capillary electrophoresis · Irradiation · Fluorescence

Introduction

Fluorescent nanoparticles with a size range of units or tens of nanometers, better known as quantum dots (QDs), possess unique properties [1]. Their optical and semiconductor properties are tunable by changing the size, shape, spatial arrangement, conductivity, and surface modification (i.e. conjugation with ligands) [2] QDs have been applied in (bio)sensors, in biosciences such as in vivo imaging, drug delivery and diagnostic, or in vitro labeling of molecules, cells and tissues [3, 4]. Due to their small size they not only retain properties of the material from which they originate, but also adopt new features related to their size [5]. For biological applications, nanocrystals of CdSe, CdSe/ZnS, CdTe, CdTe/CdS are the most widely used [6]. However, potential toxicity of heavy metals attracted a great attention to safety concerns for health and environment [7]. For this reason, QDs made from less toxic materials, such as zinc [8] and carbon [9] were developed. The photo-physical properties, which make QDs interesting compared to classic organic dyes include very narrow emission spectra, broad absorption spectra, long fluorescence lifetime, high quantum yield, high molar extinction coefficient, large effective Stokes shift, and high stability against photobleaching [10]. Generally, the techniques for synthesis of different nanoparticle types are categorized either as a top-down or bottom-up approach [11, 12]. Top-down (physical) methods includes different types of lithographic techniques (laser, ion and X-ray) or etching and grinding [13–18]. Among the more popular methods belongs bottom-up (chemical) approach. Usually it is a synthesis of the nanoparticles in non-aqueous solvents (organometallic synthesis)

Electronic supplementary material The online version of this article (doi:10.1007/s00604-017-2149-8) contains supplementary material, which is available to authorized users.

✉ Marketa Vaculovicova
marketa.vaculovicova@mendelu.cz

¹ Department of Chemistry and Biochemistry, Mendel University in Brno, Zemedelska 1, 613 00 Brno, CZ, Czech Republic

² Central European Institute of Technology, Brno University of Technology, Purkynova 123 3058/10, -612 00 Brno, CZ, Czech Republic

³ Materials Research Centre, Faculty of Chemistry, Brno University of Technology, Purkynova 118, 612 00 Brno, Czech Republic

along with toxic instable precursors at high temperatures [19, 20]. Due to the complexity of these procedures, alternative method using aqueous solvents were developed [21, 22]. Both variants (non-aqueous or aqueous solvents) lead to formation of nanocrystals in the presence of stabilizing ligands, which prevent aggregation of QDs in the reaction medium. The bottom-up processes include a variety of methods such as microwave-assisted technique, ultrasonic-assisted technique [23], photochemicals-assisted technique [24], high temperature technique and biosynthesis (in microorganisms [25], animals [26], plant [27], fungi and actinomycete [28, 29]). Another option is the interaction with UV light. Earlier, number of nanoparticles able to interact with UV radiation was described including TiO₂ nanorods [30], ZnO nanoparticles [31] and others [32]. The processes of photoactivation, photoenhancement or photobrightening were intensively studied, e.g. Guo-Yu Lan et al. in his work described a photo-assisted synthesis of highly fluorescent ZnSe QDs in aqueous solution stabilized with mercaptosuccinic acid (MSA) [33]. Uematsu et al. dealt with photoetching of CdTe nanocrystals [34], Shang Yazhuo et al. synthesized gold nanoparticles by reduction of HAuCl₄ under UV irradiation [35], Kao Mahalio et al. presented the synthesis of indium nitride nano- and microstructures by UV-assisted procedure [36].

The study is focused primarily on investigation of low cost, low temperature, and fast synthesis of water soluble QDs stabilized by MSA by UV irradiation, where the optimal conditions are found. Moreover, the use three methods for synthesis of QDs were compared and their pros and cons are discussed.

Experimental section

Chemicals

Working solutions (buffers and standard solutions) were prepared daily by diluting the stock solutions. Standards and other chemicals were purchased from Sigma-Aldrich (St. Louis, MO, USA) in ACS purity unless noted otherwise.

Synthesis of quantum dots by UV

3 mL of prepared solution (precursors) was taken in a 4 mL quartz cuvette (Hellma GmbH & Co. KG, Müllheim, Germany) and irradiated by UV ($\lambda_{em} = 254$ nm) transilluminator (Vilber Lourmat, Marne-la-Vallée Cedex, France). The sample area of 20 × 20 cm was illuminated by 6 UV emitting tubes with power of 15 W each. The intensity of UV radiation incoming to the quartz cuvette was recorded by optical power meter (PM100D, sensor SV120VC, Thorlabs Inc., Newton, NJ, USA). Based on these measurements the intensity of incoming UV energy into the sample was determined as $E = 0.14 \text{ mW} \cdot \text{mm}^{-2}$.

Fluorescence and absorbance analysis

Fluorescence was acquired by multifunctional microplate reader Tecan Infinite 200 M PRO (TECAN, Switzerland). Wavelength of 250 nm was used for excitation and the fluorescence scan was measured within the range from 300 to 700 nm using 2-nm steps. The detector gain was set to 80. The samples (50 μL) were placed in UV-transparent 96 well microplate with flat bottom by CoStar (Corning, USA). Absorption spectra were recorded under the same conditions in the range 240–600 nm. All measurements were performed at 25 °C controlled by Tecan Infinite 200 PRO (TECAN, Switzerland).

Particle size and zeta-potential analysis

Zetasizer MALVERN, Malvern Instruments Ltd. Worcestershire WR14 1XZ, United Kingdom was used.

Particle size assessment (dynamic light scattering)

The particle size measurements were performed considering a refraction index of the dispersive phase of 3.00 and 1.33 for the dispersive environment. The absorption coefficient in both cases was 10^{-3} . The measuring temperature was set at a constant value of 25 °C, while the viscosity was 0.8872 cP. For each measurement, disposable cuvettes type ZEN 0040, were used, containing 40 μL of sample. The equilibration time was 120 s, at a measurement angle of 173° backscatter and pH of solution was 9. All measurements were triplicate and the data was expressed as the average value.

Zeta potential assessment

The particle size measurements were performed considering the same refraction index, pH and absorption coefficient as described in particle size measurements. Furthermore, the parameters such as, temperature and viscosity were the same as in particle size measurements. Calculations considered the diminishing of particles concentration based Smoluchowsky model, with a $F(\kappa a)$ of 1.50 and an equilibrating time of 120 s. For the measurements, a disposable cell DTS1070 was employed. In each case, the number of runs varied between 20 and 40. The measurements were carried out in triplicates and were performed under the automatic setting of attenuation and voltage selection.

Determination of quantum yields (QY)

The quantum yields were determined by analysis of emission maxima with the excitation at 250 (ZnS, ZnSe and Zn) or 380 nm (CdSe, CdTe and Cd). The absorbance was analyzed using the same excitation wavelength. The quantum yields

were calculated on the basis of integration of absorption and emission value. Absolute values were calculated using the standard samples (quinine sulfate), with known fluorescence QY value, according to the following Eq. [37]:

$$\Phi_X = \Phi_{ST} \left(\frac{\text{Grad}_X}{\text{Grad}_{ST}} \right) \left(\frac{\eta_K^2}{\eta_{ST}^2} \right) \quad (1)$$

where the subscripts *ST* and *X* denote standard and test, respectively, Φ is the fluorescence quantum yield ($\Phi_{ST} = 0.54$), *Grad* the gradient from the plot of integrated fluorescence intensity vs. absorbance ($\text{Grad}_{ST} = 80,000,000$, and η the refractive index of the solvent (1.33).

Capillary electrophoresis with LED-induced fluorescence (CE-LED-IF) detection

CdSe QDs were analyzed by CE (PACE MDQ, Beckman Coulter, USA) with blue LED ($\lambda_{em} = 380$ nm) as an excitation source. Unmodified fused silica capillary with internal diameter of 75 μm and with the total length of 64.5 cm (14 cm to a special window for optical fiber and 54 cm to detector window) was used. Optical fiber (diameter 910 μm Core Multimode, High-OH for 250–1200 nm, Thorlabs Inc., USA) was focused to a capillary in the special window and connected with the UV LED with ball lens, $\lambda_{em} = 250$ nm, 1 mW (Thorlabs Inc., USA). Hydrodynamic injection by 5 psi for 5 s was employed. As pretreatment the separation voltage 20 kV and waiting time of 0, 5, 10, 15, 20, 25 and 30 min (for synthesis of QDs in special window) was used and after that 30 kV separation voltage was applied. 20 mM sodium borate buffer pH 9 was used as a separation electrolyte.

Results and discussion

Temperature testing of precursors

For biological applications, nanocrystals of CdSe, CdTe, ZnS, ZnSe are usually used [6, 38, 39]. For these reasons these common precursors (Cd:Se, Cd:Te, Zn:S, Zn:Se, Zn, Cd in combination with and without reducing agent, Note: utilization of the reduction agent is noticed by a label “red”) with MSA as a capping agent were tested. First, the temperature dependent behavior was monitored (25, 35, 45, 55, 65, 75, 85 and 95 °C, samples were incubated at each temperature for 30 min). In this experiment, twelve aliquots of precursors were prepared. These aliquots contained various combinations of precursors, as described in Supplementary material. Samples (1 mL) were heated and afterwards cooled to the temperature of 25 °C, the samples were immediately analyzed. Absorption spectra in range 230–600 nm and emission

spectra ($\lambda_{ex} = 250$ nm and $\lambda_{em} = 380$ to 800 nm) were recorded (data not shown). If the fluorescence was observed, the QY was calculated (Table S1). For most studied precursors, QY below 1% was observed. An exception was the sample labelled as CdTe red, which exhibited a significant increase in QY, increasing with temperature. Increasing the temperature caused a bathochromic shift of the emission spectrum (λ_{em} max = 494 nm (35 °C), 498 nm (45 °C), 506 nm (55 °C), 516 nm (65 °C), 520 nm (75 °C), 528 nm (85 °C), and 534 nm (95 °C)). The highest QY was achieved at 95 °C (λ_{em} max = 534 nm, QY = 20.1%).

UV ($\lambda_{em} = 254$ nm) synthesis of QDs from precursors by transilluminator

In the next step, the influence of UV irradiation ($\lambda = 254$ nm) on formation of QDs from precursors was tested. The samples (3 mL) were pipetted in to the quartz cuvette and placed to the center of the illumination area of the UV transilluminator and irradiated in time (0, 10, 20 and 30 min). The temperature inside transilluminator increased from 25 to 35 °C (depending on the time of irradiation). For all investigated samples, interaction with UV light was observed. The values of λ_{em} maxima and QY are summarized in Table S2. The lowest QY (≤ 1) was recorded after 10-min irradiation in case of ZnS, ZnS red (Note: utilization of the reduction agent is noticed by a label “red”) and ZnSe. Longer intervals of irradiation (20 and 30 min) caused a fluorescence loss in ZnS and ZnS red. For ZnSe, QY $\leq 1\%$ was observed for all times of irradiation. On the other hand, the best result was achieved in case of CdSe. At all times of irradiation, QY of 13.4% was observed. For all investigated samples, a bathochromic shift of the emission maxima was observed depending on the duration of illumination.

Formation of CdSe - QDs from precursors monitored by spectroscopic techniques

Based on previous experiments, precursor solution composed of Cd and Se was chosen for fluorescence and spectrophotometric analysis. Precursors (3 mL) were pipetted into the quartz cuvette and placed in the center of UV transilluminator (emission spectrum of UV lamps, Fig. 1a) and irradiated for 0–60 min. In five-minute intervals, 50 μL aliquots were taken and absorption spectra were measured (240–600 nm), Fig. 1b. It is shown that increasing the illumination time caused an increase in the intensity and a shift of the absorption maximum of CdSe QDs, Fig. 1c. Absorption maximum of CdSe QDs after 5 min irradiation was $\lambda_{max} = 324$ nm. After another 55 min was shifted for about 54 nm ($\lambda_{max} = 378$ nm).

Subsequently, the emission maxima of these samples were measured ($\lambda_{ex} = 250$ nm a $\lambda_{em} = 330$ –700 nm), Fig. 1d. An increase in the emission intensity was

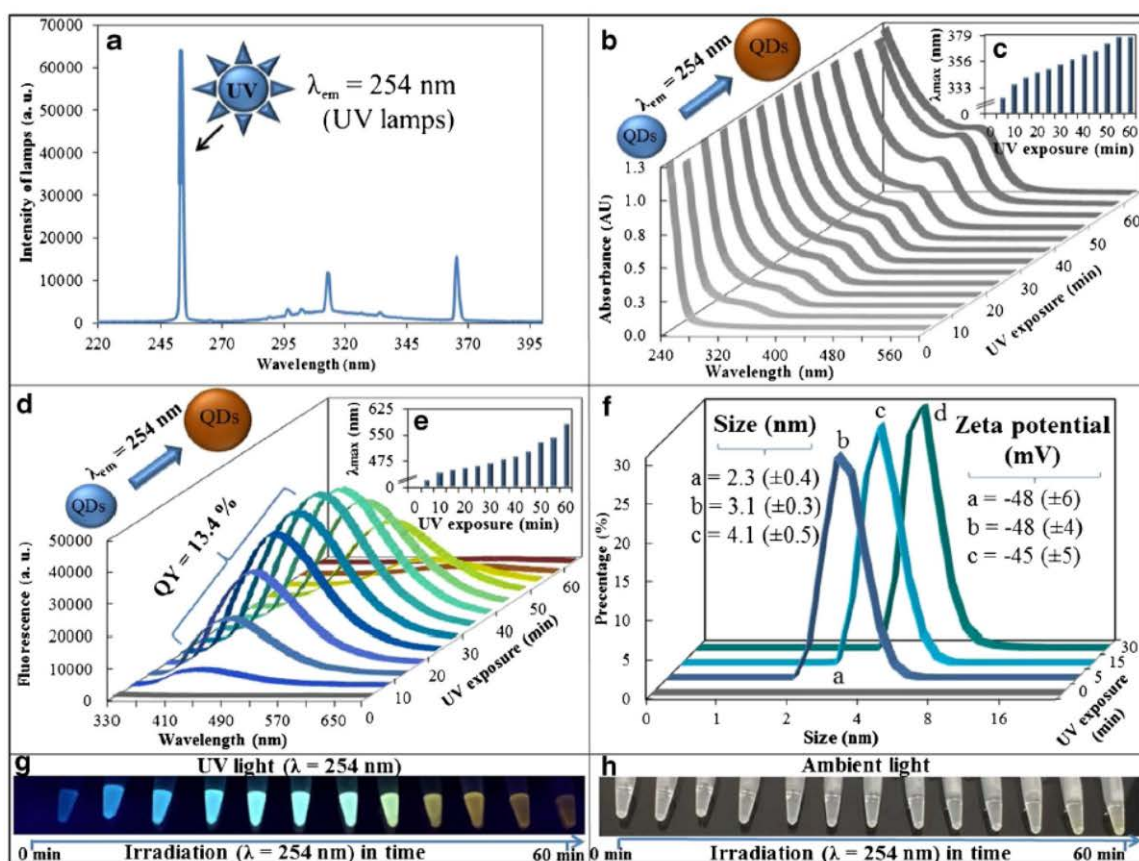


Fig. 1 Spectral analysis of UV-formed QDs **a** Emission spectrum of UV tubes in the transilluminator, **b** Absorption spectra of CdSe QDs (240–600 nm) obtained after illumination of precursors (0–60 min) by UV light (spectrum shown in **1a**), **c** Absorbance maximum shift dependent on illumination time, **d** Fluorescence emission spectra (330–700 nm)

dependent on illumination time (0–60 min), **e** Emission maximum shift dependent on illumination time, **f** Particle size distribution and zeta potentials of the UV-formed QDs, **g** Photographs of the UV-formed QDs under UV illumination, **h** Photographs of the UV-formed QDs under ambient light

observed during first 30 min of illumination, however in the time interval 35–60 min of illumination, the fluorescence intensity decreased. In addition, the emission spectrum exhibited a bathochromic shift as shown in Fig. 1e. After 5 min of illumination, the emission maximum was $\lambda_{em\ max} = 420$ nm, but after 60 min, the maximum increased for 158 nm to 578 nm. The presented results confirm that the UV illumination causes formation of the fluorescent nanocrystals ($[Cd(CH_3CO_2)_2 + Na_2Se \rightarrow CdSe\downarrow + 2Na(CH_3CO_2)]$), stabilized by the MSA via the thiol group, demonstrated by the red shift of the absorption and emission spectra. The chemical principle of this observation was explained elsewhere [40], stating that the thiol groups are photo-oxidized by the application of the UV light forming disulfide bridges in the molecules of the capping agents. These molecules are afterwards dissolved by the surrounding aqueous solution and released from the particle

surface. The exposed hydrophobic surface of the particle causes subsequent aggregation of the crystals resulting in the increased particle size and therefore the red shift in the spectra.

Using the dynamic light scattering technique the increasing particle size dependent on the time of illumination was confirmed (Fig. 1f). It was observed that after 5-min illumination, QDs with the size of $2.3 (\pm 0.4)$ nm and zeta potential of $-48 (\pm 6)$ mV were formed and after 15-min illumination, the size and increased to $3.1 (\pm 0.3)$ nm. Finally, the illumination for 30 min caused the formation of nanoparticles with the size of $4.1 (\pm 0.4)$ nm and zeta potential of $-45 (\pm 5)$ mV. From the values of zeta potential, the stability of the colloidal solution is commonly evaluated. The results suggested that the solution resulting by the UV light illumination was stable, because the solution with zeta potential of value above 30 mV or -30 mV is generally considered non-aggregating and stable [41]. The photographs of the QD solutions in UV and ambient light are shown in Fig. 1g, h, respectively.

Fluorescence lifetime and concentration of CdTe – QDs as a function of the duration of UV exposure

In this experiment, conventional fluorescence correlation spectroscopy (fluorescence correlation spectroscopy measurement is described in Supplementary material.) was modified as shown in Fig. 2a. The solution of Cd:Se precursors (15 μ L) was pipetted on quartz glass (Fig. 2a – a) and on the top of this sample UV LED ($\lambda_{em} = 250$ nm, 1 mW), Fig. 2a – b was placed. After turning on the UV LED, the QDs started to be formed and observed in the confocal volume (Fig. 2a – c) as schematically shown in Fig. 2a – d. This process was recorded in real time by microscope objective with water immersion (Fig. 2a – e) and excitation laser ($\lambda_{em} = 367$ nm and 1 MHz repetition). Finally, beam continued through the optical elements (50 μ m pinhole and longpass emission filter, Fig. 2a – f, g) to the detector, Fig. 2a – h.

FCS is based on monitoring of the variations in the intensity of fluorescence of substances diffusing through a very small volume (1 fL) observed. Temporal fluctuations of the intensity of fluorescence are recorded and analyzed using the autocorrelation function $G(\tau)$. The correlation curves were

fitted to the equation, see in supplementary material. In this manner, CdSe QDs synthesis from precursors was recorded in real time, as evidenced in Fig. 2b. According to the time of occurrence of individual CdSe - QDs the genesis of QDs may be subdivided into five parts QDs 1–5. Each part is characterized by the length of interval (QDs 1 = 270 s, QDs 2 = 269 s, QDs 3 = 207 s, QDs 4 = 101 s and QDs 5 = 39 s). Thanks to the deconvolution of the temporal waveform can be the intervals studied in separately. The measured decay curves are found best represented by a tetraexponential diffusion analysis function of the form $I(t) = a_1 \exp(-x/\tau_1) + a_2 \exp(-x/\tau_2) + a_3 \exp(-x/\tau_3) + a_4 \exp(-x/\tau_4)$, where τ_1, τ_2, τ_3 and τ_4 are the lifetime components and a_1, a_2, a_3 and a_4 are the corresponding amplitudes. The lifetime components $\tau_1 - \tau_4$, average lifetime of components τ , average amplitudes a and approximated concentration c , estimated using $\tau = (\tau_1 + \tau_2 + \tau_3 + \tau_4)/4$, $a = (a_1 + a_2 + a_3 + a_4)/4$ and approx. $c = \frac{N}{V_{eff} N_{av}}$ are in detail collected in Table S3. From the values in the table is clear that the longer the time of UV irradiation the new quantum dots are detected, which resulted in increasing average length lifetime τ . From the initial 40 ns (interval QDs 1) the time decay was growing up to 112.2 ns (2.8 times), interval

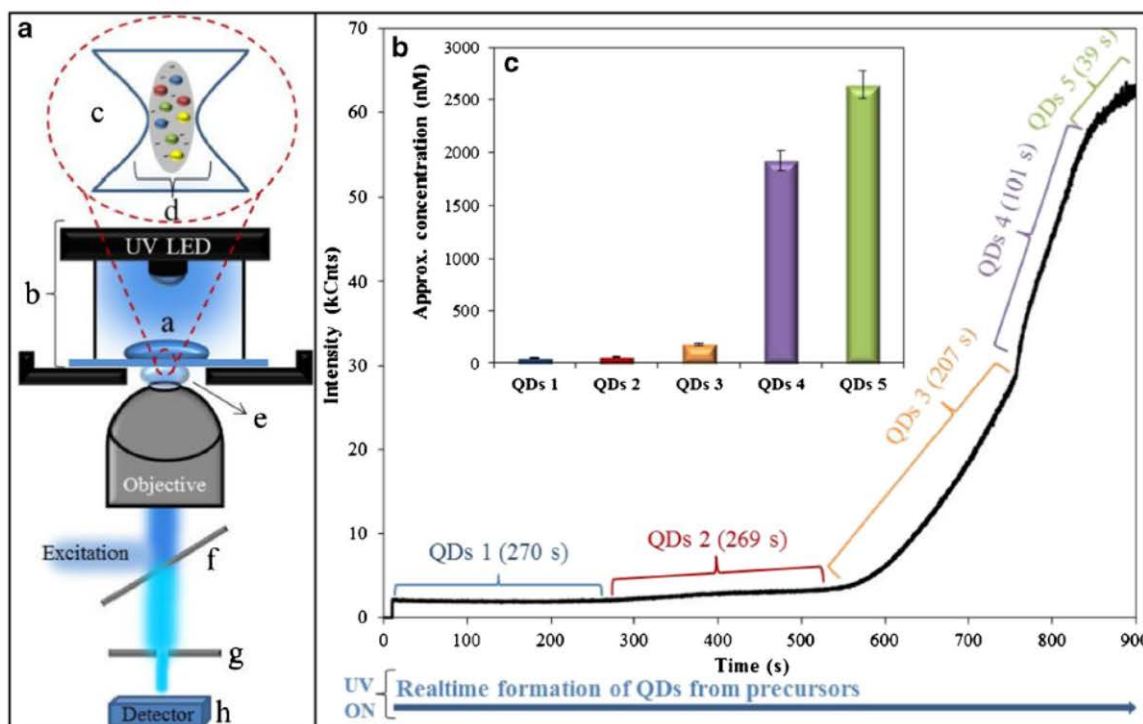


Fig. 2 a Schematic representation of the UV LED modified FCS a) 15 μ L drop of precursors (Cd:Se) on quartz glass, b) UV LED ($\lambda_{em} = 250$ nm), c) idealized confocal volume, d) schematic representation of the QDs formation in a confocal volume, e) lens with water immersion, f, g) laser ($\lambda_{em} = 367$ nm, 1 MHz repetition), optical

elements (50 μ m pinhole and longpass emission filter) and h) detector. b Formation of CdSe QDs from precursors (Cd:Se) recorded in real time (0–15 min). c Approximated concentration of CdSe QDs generated during the UV irradiation

QDs 5. With increasing time, decay is directly proportional to increasing average lifetime amplitude α . Besides increasing τ and α there were also noted increasing concentrations of CdSe QDs, Fig. 2c. The sharp increase in the concentration of CdSe QDs was mainly reflected in the tenth minute after UV irradiation. The fluorescent intensity depends on the concentration of the fluorophore; however, the lifetime of the fluorophore is independent of concentration.

In-capillary formation of CdSe QDs

Finally, the work was focused on the direct synthesis of CdSe QDs in nanoliter scale (in capillary). For these purposes, the standard CE instrument was used with a little modification as shown in the schematic drawing, Fig. 3a. For the synthesis of CdSe QDs, the UV LED was used. It was connected to the capillary by optical fiber, Fig. 3a – a. The capillary pathway was partially modified by its local direction out of the cooling tube, Fig. 3a – b. An optical fiber was focused into the exposed capillary, where a special window was made (Fig. 3a – c). The QDs precursors were hydrodynamically injected (5 psi for 5 s) into the capillary and the procedure was stopped for 0, 5, 10, 15, 20, 25 and 30 min (to ensure the formation of QDs in special window, Fig. 3a – d). Subsequently, separation voltage of 30 kV was applied and formed CdSe QDs (Fig. 3a – e) migrated to the detection window, Fig. 3a – f.

First, CdSe QDs prepared by UV synthesis in a milliliter scale (using the transilluminator) were analyzed by CE-LIF. As shown in the electropherograms in Fig. 3b, Bright fluorescent signals were observed and their intensity was increasing with increasing time of UV illumination. Moreover, this effective separation technique showed that the solution was a mixture of different nanoparticles (various particle sizes) formed during the illumination process. For demonstration, four most distinct signals were labelled (QDs1 – QDs 4). There were probably more components present in the mixture; however, it was not the aim of the study to separate the mixture completely. The dependence of the peak heights on the illumination time is summarized in Fig. 3c and it is shown that the peak with migration time of 7 min is exhibiting the highest fluorescence intensity, reaching even fluorescence intensity over the detector range. However, it is shown that with increasing the illumination time, also other fluorescent signal started to be observed, which, as it is believed, belong to the QDs with higher particle sizes or to the QD aggregates.

Finally, the in-capillary formation of QDs by UV light was tested, which can be applied in microfluidic devices to significantly decrease the amount of chemicals used and meeting the requirements of green chemistry/analysis.

As describe above, the optical fiber guiding the UV light from the UV LED was focused into the special window made at the injection end of the capillary (14 cm from the start).

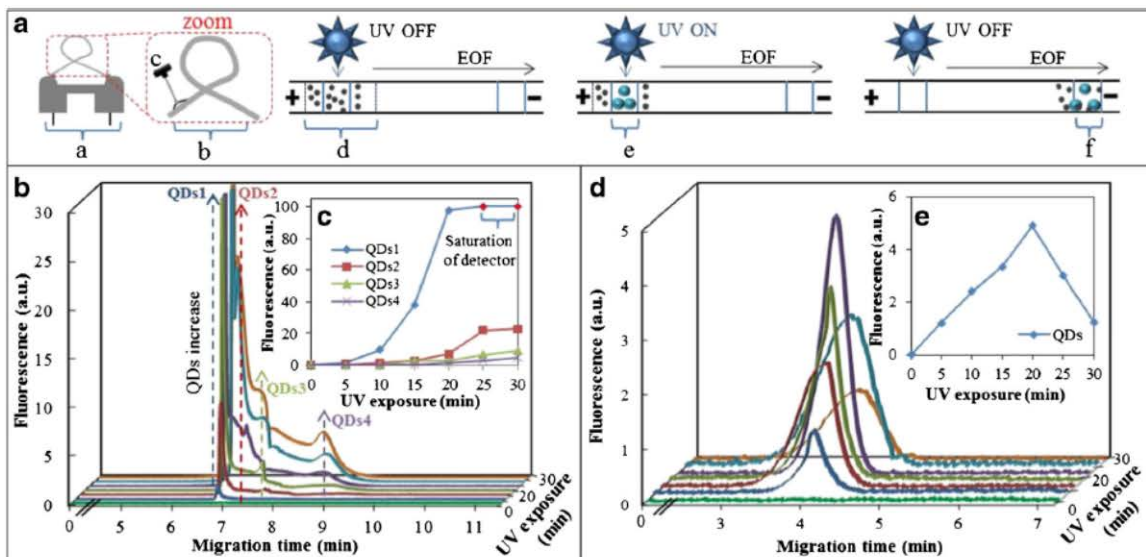


Fig. 3 a Scheme of modified capillary pathway and special window position, a) conventional capillary cartridge with the capillary inside the cooling tube, b) capillary directed out of the cooling tube, c) UV LED ($\lambda_{em} = 250$ nm) connected to the optical fiber focusing the light into the capillary, d) zone of QD precursors injected into the capillary UV LED off, e) formation of QDs using UV LED on, f) CE separation of formed QDs and LED-LIF detection by 380 nm LED

excitation. b Electropherograms of CdSe QDs formed by UV illumination in transilluminator (0–30 min) c Dependence of UV light illumination time on peak heights of four main fluorescent signals (QDs1– QDs4). d Electropherograms of CdSe QDs formed after in-capillary UV LED illumination (0–30 min). e Dependence of UV light illumination time on peak heights – in-capillary QD formation

Subsequently, the solution of precursors was hydrodynamically injected into the capillary and illuminated for 5, 10, 15 or 20 min. After the illumination time, the CE separation started and the formed QDs were conventionally detected. The electropherograms are shown in Fig. 3d. The fluorescent signals were observed with maximum in migration time of 4.3 min. The lower migration time compared to Fig. 3b is given by the shortened effective capillary length. In addition, the fluorescence intensity was lower due to the lower optical power of the UV LED. However, the signal-to-noise ratio was satisfactory. It has to be noted that the maximum fluorescence intensity in this arrangement was reached after 20 min of illumination and with increasing time, the intensity decreased significantly. On the other hand, only one signal is observed suggesting lower polydispersity of the QDs prepared by this technique.

In general, it can be stated that in situ (or flow through) synthesis of QDs by elevated temperature [42, 43] is convenient and effective; however for some, mostly biological, applications, the excessive heating may interfere the process in the fluidic device (e.g. protein denaturation, cell damage etc.). For these purposes, the in-line formation of QDs for automated, low-volume synthesis by UV light irradiation is advantageous. The UV light may be focused in the extremely low volume and the powerful lasers may be used, which increases the effectivity of the proposed method. Afterwards, the in-capillary interactions may take place without the need of interaction by the operator.

Quantification of CdSe QDs formed by UV light

Using three different optical arrangements, QDs formed by UV light illumination in three different volumes (3 mL,

15 μL , 4 nL) were observed and the amount of QDs formed was investigated. To quantify this amount, a sufficient amount of QDs powder was prepared by UV illumination (irradiation of the 21 mL of precursor's solution (CdSe)). The solution was filtered through Amicons Ultra 0.5 mL 3 K Centrifugal Filters and dried overnight at 50 $^{\circ}\text{C}$. The powder was resuspended in 5 mM borate buffer pH 9 to create the calibration curve.

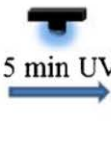
The concentration of QDs formed during large-volume (3 mL), middle-volume (15 μL) and low-volume (4 nL) synthesis was determined as 88 $\mu\text{g}\cdot\text{mL}^{-1}$, 31.6 $\mu\text{g}\cdot\text{mL}^{-1}$ and 64.5 $\mu\text{g}\cdot\text{mL}^{-1}$, respectively. The higher concentration of QDs formed in capillary format (4 nL) was caused by higher radiation power because maximum of the light from the UV LED was focused into the capillary volume by optical fiber while in case of 15 μL drop, the light was distributed in a much larger area.

The absolute amount in the given volume (Fig. 4) calculated for each method demonstrates the possibility of the capillary-based methods to monitor the formation of very low amounts of QDs, which can be further transferred by electric field.

Conclusion

Even though the quantum dots will not probably replace conventional fluorescent labels based on organic fluorophores, they have several significant benefits (e.g. tuneability of optical properties and simplicity of synthesis compared to organic dyes) and therefore they will find their place in the family of fluorescent tracers.

Fig. 4 Schematic representation of UV synthesis of CdSe QDs by a large-volume (3 mL) b middle-volume (15 μL), c low-volume (4 nL)

| | | | |
|---|--|---|--|
| a Quartz cuvette  |  5 min UV 3 mL | Concentration of QDs in 3 ml 88 $\mu\text{g}\cdot\text{mL}^{-1}$ | total amount of QDs 264 μg |
| b Confocal volume  |  5 min UV 15 μL | Concentration of QDs in 15 μL 31.6 $\mu\text{g}\cdot\text{mL}^{-1}$ | total amount of QDs 476 ng |
| c Capillary 4 nL  |  5 min UV | Concentration of QDs in 4 nL 64.5 $\mu\text{g}\cdot\text{mL}^{-1}$ | total amount of QDs 258 pg |

Based on a systematic study formation of QDs by UV light illumination from the most commonly used precursors, CdSe nanoparticles exhibited the best optical properties such as QY (13.4%). The formation of QDs was observed in milliliter (quartz cuvette), microliter (solution drop), and nanoliter (in-capillary) scale by spectrophotometry, fluorescence correlation spectroscopy and capillary electrophoresis with LED-IF detection, respectively.

The biggest advantage of formation of QDs by UV light is in the possibility of synthesis of QDs in very small volumes (nanoliters), which meets not only the requirements on green chemistry (low consumption of chemicals) but also can be easily integrated into the lab-on-chip, micro-total-analysis microfluidic devices or other methods.

For some applications, the QY of the UV-synthesized QDs may be insufficient. However, the flow-through method of synthesis requiring extremely low amount of precursors in combination with sensitive detection (i.e. laser-induced fluorescence or electrochemical detection) may be beneficial for certain analytical purposes.

Acknowledgements Financial support was provided by Grant agency of Czech Republic (GACR 16-23647Y) and project CEITEC 2020 (LQ1601) with financial support from the Ministry of Education, Youth and Sports of the Czech Republic under the National Sustainability Programme II.

Compliance with ethical standards The author(s) declare that they have no competing interests.

References

- Kilina SV, Tamukong PK, Kilin DS (2016) Surface chemistry of semiconducting quantum dots: theoretical perspectives. *Accounts Chem Res* 49:2127–2135
- Singh G, Fisch M, Kumar S (2016) Emissivity and electrooptical properties of semiconducting quantum dots/rods and liquid crystal composites: a review. *Rep Prog Phys* 79
- Zhou J, Yang Y, Zhang CY (2015) Toward biocompatible semiconductor quantum dots: from biosynthesis and Bioconjugation to biomedical application. *Chem Rev* 115:11669–11717
- Lim SY, Shen W, Gao ZQ (2015) Carbon quantum dots and their applications. *Chem Soc Rev* 44:362–381
- Alivisatos AP (1996) Semiconductor clusters, nanocrystals, and quantum dots. *Science* 271:933–937
- Reimann SM, Manninen M (2002) Electronic structure of quantum dots. *Rev Mod Phys* 74:1283–1342
- Lin P, Chen JW, Chang LW, Wu JP, Redding L, Chang H, Yeh TK, Yang CS, Tsai MH, Wang HJ, Kuo YC, Yang RSH (2008) Computational and ultrastructural toxicology of a nanoparticle, quantum dot 705, in mice. *Environ Sci Technol* 42:6264–6270
- Tan L, Rang CC, Xu SY, Tang YW (2013) Selective room temperature phosphorescence sensing of target protein using Mn-doped ZnS QDs-embedded molecularly imprinted polymer. *Biosens Bioelectron* 48:216–223
- LeCroy GE, Yang ST, Yang F, Liu YM, Fernando KAS, Bunker CE, Hu Y, Luo PG, Sun YP (2016) Functionalized carbon nanoparticles: syntheses and applications in optical bioimaging and energy conversion. *Coord Chem Rev* 320:66–81
- Galian RE, de la Guardia M (2009) The use of quantum dots in organic chemistry. *Trac-Trends Anal Chem* 28:279–291
- Wang YL, Xia YN (2004) Bottom-up and top-down approaches to the synthesis of monodispersed spherical colloids of low melting-point metals. *Nano Lett* 4:2047–2050
- Ghosh B, Shirahata N (2014) Colloidal silicon quantum dots: synthesis and luminescence tuning from the near-UV to the near-IR range. *Sci Technol Adv Mater* 15(1):014207
- Erdem T, Soran-Erdem Z, Hernandez-Martinez PL, Sharma VK, Akcali H, Akcali I, Gaponik N, Eychmuller A, Demir HV (2015) Sweet plasmonics: sucrose macrocrystals of metal nanoparticles. *Nano Res* 8:860–869
- Koch CC (2003) Top-down synthesis of nanostructured materials: mechanical and thermal processing methods. *Rev Adv Mater Sci* 5:91–99
- Amendola V, Meneghetti M, Granozzi G, Agnoli S, Polizzi S, Riello P, Boscaini A, Anselmi C, Fracasso G, Colombatti M, Innocenti C, Gatteschi D, Sangregorio C (2011) Top-down synthesis of multifunctional iron oxide nanoparticles for macrophage labelling and manipulation. *J Mater Chem* 21:3803–3813
- Bertino MF, Gadipalli RR, Martin LA, Heckman B, Leventis N, Guha S, Katsoudas J, Divan R, Mancini DC (2008) 236th National Meeting of the American-Chemical-Society, Philadelphia, PA, Aug 17–21, 2008. Published in: Abstracts of papers of the American Chemical Society, Vol. 236
- Wu JZ, Ho PC (2006) Evaluation of the in vitro activity and in vivo bioavailability of realgar nanoparticles prepared by cryo-grinding. *Eur J Pharm Sci* 29:35–44
- Zeng HB, Cai WP, Liu PS, Xu XX, Zhou HJ, Klingshirn C, Kalt H (2008) ZnO-based hollow nanoparticles by selective etching: elimination and reconstruction of metal-semiconductor interface, improvement of blue emission and photocatalysis. *ACS Nano* 2:1661–1670
- Murray CB, Norris DJ, Bawendi MG (1993) Synthesis and characterization of nearly monodisperse CdA (E = S, Se, Te) semiconductor nanocrystallites. *J Am Chem Soc* 115:8706–8715
- Peng ZA, Peng XG (2001) Formation of high-quality CdTe, CdSe, and CdS nanocrystals using CdO as precursor. *J Am Chem Soc* 123:183–184
- Rogach AL, Katsikas L, Komowski A, Su DS, Eychmuller A, Weller H (1996) Synthesis and characterization of thiol-stabilized CdTe nanocrystals. *Ber Bunsen-Ges Phys Chem Chem Phys* 100:1772–1778
- Talapin DV, Rogach AL, Shevchenko EV, Kornowski A, Haase M, Weller H (2002) Dynamic distribution of growth rates within the ensembles of colloidal II-VI and III-V semiconductor nanocrystals as a factor governing their photoluminescence efficiency. *J Am Chem Soc* 124:5782–5790
- Zhu YL, Li CS, Xu Y, Wang DF (2014) Ultrasonic-assisted synthesis of aqueous CdTe/CdS QDs in salt water bath heating. *J Alloy Compd* 608:141–147
- Lin YW, Hsieh MM, Liu CP, Chang HT (2005) Photoassisted synthesis of CdSe and core-shell CdSe/CdS quantum dots. *Langmuir* 21:728–734
- Li XQ, Xu HZ, Chen ZS, Chen GF (2011) Biosynthesis of nanoparticles by microorganisms and their applications. *J Nanomater*. doi:10.1155/2011/270974
- Kominkova M, Michalek P, Moulick A, Nemcova B, Zitka O, Kopel P, Beklova M, Adam V, Kizek R (2014) Biosynthesis of quantum dots (CdTe) and its effect on *Eisenia fetida* and *Escherichia coli*. *Chromatographia* 77:1441–1449
- Borovaya MN, Naumenko AP, Matvieieva NA, Blume YB, Yemets AI (2014) Biosynthesis of luminescent CdS quantum dots using plant hairy root culture. *Nanoscale Res Lett* 9. doi:10.1186/1556-276X-9-686
- Ahmad A, Mukherjee P, Senapati S, Mandal D, Khan MI, Kumar R, Sastry M (2003) Extracellular biosynthesis of silver

- nanoparticles using the fungus *Fusarium oxysporum*. *Colloid Surf B-Biointerfaces* 28:313–318
29. Sastry M, Ahmad A, Khan MI, Kumar R (2003) Biosynthesis of metal nanoparticles using fungi and actinomycete. *Curr Sci* 85:162–170
 30. Kandiel TA, Dillert R, Feldhoff A, Bahnemann DW (2010) Direct synthesis of Photocatalytically active rutile TiO₂ nanorods partly decorated with Anatase nanoparticles. *J Phys Chem C* 114:4909–4915
 31. Liu XJ, Pan LK, Zhao QF, Lv T, Zhu G, Chen TQ, Lu T, Sun Z, Sun CQ (2012) UV-assisted photocatalytic synthesis of ZnO-reduced graphene oxide composites with enhanced photocatalytic activity in reduction of Cr(VI). *Chem Eng J* 183:238–243
 32. Adegboyega NF, Sharma VK, Cizmas L, Sayes CM (2016) UV light induces Ag nanoparticle formation: roles of natural organic matter, iron, and oxygen. *Environ Chem Lett* 14:353–357
 33. Lan GY, Lin YW, Huang YF, Chang HT (2007) Photo-assisted synthesis of highly fluorescent ZnSe(S) quantum dots in aqueous solution. *J Mater Chem* 17:2661–2666
 34. Uematsu T, Kitajima H, Kohma T, Torimoto T, Tachibana Y, Kuwabata S (2009) Tuning of the fluorescence wavelength of CdTe quantum dots with 2 nm resolution by size-selective photoetching. *Nanotechnology* 20(21):215302
 35. Shang YZ, Min CZ, Hu J, Wang TM, Liu HL, Hu Y (2013) Synthesis of gold nanoparticles by reduction of HAuCl₄ under UV irradiation. *Solid State Sci* 15:17–23
 36. Kao M, Erasmus RM, Moloto N, Coville NJ, Mhlanga SD (2015) UV-assisted synthesis of indium nitride nano and microstructures. *J Mater Chem A* 3:5962–5970
 37. Krizkova S, Dostalova S, Michalek P, Nejdil L, Kominkova M, Milosavljevic V, Moulick A, Vaculovicova M, Kopel P, Adam V, Kizek R (2015) SDS-PAGE as a tool for hydrodynamic diameter-dependent separation of quantum dots. *Chromatographia* 78:785–793
 38. Samanta A, Deng ZT, Liu Y (2012) Aqueous synthesis of glutathione-capped CdTe/CdS/ZnS and CdTe/CdSe/ZnS Core/Shell/Shell nanocrystal Heterostructures. *Langmuir* 28:8205–8215
 39. Chan WCW, Maxwell DJ, Gao XH, Bailey RE, Han MY, Nie SM (2002) Luminescent quantum dots for multiplexed biological detection and imaging. *Curr Opin Biotechnol* 13:40–46
 40. Carrillo-Carrion C, Cardenas S, Simonet BM, Valcarcel M (2009) Quantum dots luminescence enhancement due to illumination with UV/Vis light. *Chem Commun* 45(35):5214–5226
 41. Kirby BJ, Hasselbrink EF (2004) Zeta potential of microfluidic substrates: 1. Theory, experimental techniques, and effects on separations. *Electrophoresis* 25:187–202
 42. Chakrabarty A, Marre S, Landis RF, Rotello VM, Maitra U, Del Guerzo A, Aymonier C (2015) Continuous synthesis of high quality CdSe quantum dots in supercritical fluids. *J Mater Chem C* 3:7561–7566
 43. Nightingale AM, Krishnadasan SH, Berhanu D, Niu X, Drury C, McIntyre R, Valsami-Jones E, deMello JC (2011) A stable droplet reactor for high temperature nanocrystal synthesis. *Lab Chip* 11:1221–1227